

**Water quality assessment and characterisation of
chlorophyll-*a* variability related to river discharges,
within the south-eastern Bay of Biscay:**

**Evaluation and development of chlorophyll-*a*
algorithms for MODIS and MERIS imagery**



PhD THESIS

Water quality assessment and characterisation of chlorophyll-*a*
variability related to river discharges, within the southeastern

Bay of Biscay:

Evaluation and development of chlorophyll-*a* algorithms for
MODIS and MERIS imagery

Specialty

MARINE ENVIRONMENT AND RESOURCES

Presented by

Stéfani Novoa Gautier

Thesis director

Dr. Guillem Chust Peters

Department of Zoology and Animal Cell Biology

Year 2012

azti

eman ta zabal zazu



Universidad
del País Vasco

Euskal Herriko
Unibertsitatea



ACKNOWLEDGEMENTS

First, I would like to thank my thesis director Dr. Guillem Chust. It has been an honour to be his first PhD student. I appreciate all his contributions of time and ideas, to make my PhD experience stimulating and productive. This thesis would not have been possible without his help, support and patience.

I gratefully acknowledge the funding sources that made my PhD possible. I was funded by Fundación de Centros Tecnológicos Iñaki Goenaga.

I would also like to thank the organisations that made this research possible:

- The AZTI-Tecnalia Research Centre
- The University of the Basque Country (Universidad del País Vasco/Euskal Herriko Unibersitatea)
- The Basque Government for the Aquitania-Euskadi cooperation funds.
- The Basque Water Agency (URA)
- The European Union for the Structural Funds Programme INTERREG IVa (LOREA project: Littoral, Ocean and River in Euskadi-Aquitaine).
- The European Space Agency for the MERIS images.
- The NASA for the MODIS images.
- Ifremer, for the OC5 satellite products

Especial thanks to all the people that help me during these four years of thesis, especially:

- Dr. Jean-Marie Froidefond for all the help provided, for teaching me about spectral measurements and remote sensing in general, and for all the data he provided us and helped us acquire.
- Dr. Caroline Petus for all the guidance, time and help with the articles and the data whenever I needed it, even from far away.

- Dr. Francis Gohin for his useful comments and ideas. Thanks for assisting me with the satellite products and the IDL programs and revising the manuscript.

- Dr. David Doxaran for his thorough and constructive revision of the manuscript.

- Dr. Angel Borja, Dr. Javier Franco, Yolanda Sagarminaga, Dr. Marta Revilla for their constructive comments, ideas and corrections.

- Dr. SeungHyun Son for his help with IDL programming.

- All the researchers, technicians and employees at AZTI-Tecnalia that helped me with the acquisition, analysis and interpretation of the data, or anything else needed to achieve this goal.

- The researchers at the University of the Basque Country, Emma Orive and Sergio Seoane for their help with phytoplankton pigments.

- Ionan Marigómez (University of the Basque Country) for giving me this opportunity.

- Michael Collins (School of Ocean and Earth Science, University of Southampton and AZTI-Tecnalia) for his useful comments and corrections.

Muchas gracias a todos los becarios de AZTI y a los estudiantes del Master MER por la ayuda y el apoyo prestado desde el comienzo de esta aventura. Gracias Usua, Leire, Maria M., Maria B., Natalia, Nerea, Marta P., Irati L., Eneko, Mikel, Ernesto y a todos los becarios de Sukarrieta y de Pasaia.

Gracias Iñaki por todo tu apoyo durante los momentos más difíciles.

Ale, gracias por animarme siempre con todo.

Muchas gracias a mi familia y amigos. Papá, Mamá, Hervé, gracias por estar ahí.

Gracias a todos los que me habéis apoyado y ayudado a lo largo este camino. Aunque sólo pueda mencionar a algunos aquí, no lo habría conseguido sin todos vosotros.

It would not have been possible to write this doctoral thesis without the help and support of the kind people around me, to only some of whom it is possible to give particular mention here.

PUBLICATIONS

The work performed during this thesis has produced four articles that were published in international scientific journals.

Novoa, S., G. Chust, Y. Sagarminaga; M. Revilla, A. Borja. 2012. Water quality assessment using satellite-derived chlorophyll-*a* within the European directives, in the southeastern Bay of Biscay. *Marine Pollution Bulletin*. Doi:10.1016/j.marpolbul.2012.01.020.

Novoa, S., G. Chust, J.M. Froidefond, C. Petus, J. Franco, E. Orive, S. Seoane, A. Borja. 2012. Water quality monitoring in Basque coastal areas using a local chlorophyll-*a* algorithm and MERIS images. *Journal of Applied Remote sensing* 6, 063519. Doi: 10.1117/1.JRS.6.063519.

Novoa, S., G. Chust, V. Valencia, J.M. Froidefond, D. Morichon. 2011. Estimation of chlorophyll-*a* concentration in waters over the continental shelf of the Bay of Biscay: a comparison of remote sensing algorithms. *International Journal of Remote Sensing* 32(23): 8349-8371.

Novoa, S. G. Chust, J.M. Froidefond. 2009. Optical measurements of ocean colour with the field-based High-Resolution Fibre Optic Spectrometer (HR4000CG) for remote sensing applications. *Revista de Investigación Marina (RIM)* 16).

INDEX

RESUMEN	9
SUMMARY	15
GENERAL INTRODUCTION	17
1. Problematic.....	18
2. Optical properties of the water.....	21
3. Oceanic and coastal water bodies classification.....	27
4. Satellite Remote Sensing.....	28
5. Approaches to derive water constituents	31
6. Hypothesis and objectives	34
7. Structure of the thesis.....	36
GENERAL CHARACTERISATION OF THE BAY OF BISCAY AND THE AREA OF STUDY.....	39
1. Geographical and physiographic characteristics.....	41
2. Water bodies	42
3. Water circulation	43
4. Physico-chemical characteristics.	45
5. Phytoplankton.....	48
RESULTS	51
Chapter I. Optical measurements of ocean colour with the field-based High- Resolution Fiber Optic Spectrometer (HR4000CG) for remote sensing applications	53
1. Introduction	54
1.1. Objectives.....	54
2. Materials and Methods.....	55
2.1. Estimation of remote sensing reflectance.....	55
2.2. Instrumentation and platform	56
2.3. Laboratory experiments	58
2.4. Field measurements	61
2.5. Comparison between HR4000CG and TriOS measurements	61
3. Results.....	62
3.1. Laboratory experiments	62

3.2. Field measurements	64
4. Discussion	67
Chapter II. Estimation of chlorophyll-<i>a</i> concentration in waters over the continental shelf of the Bay of Biscay: a comparison of remote sensing algorithms.	71
1. Introduction	72
1.1. Objectives.....	72
2. Materials and Methods.....	73
2.1. Oceanographic survey.....	73
2.2. Chlorophyll- <i>a</i> estimation	74
2.3. MERIS image.....	75
3. Results.....	77
4. Discussion	84
4.1. Radiometric measurement procedure	84
4.2. Estimation of chlorophyll- <i>a</i>	84
Chapter III. Water quality monitoring in Basque coastal areas using a local chlorophyll-<i>a</i> algorithm and MERIS images	89
1. Introduction	90
1.1. Objectives.....	90
2. Materials and Methods.....	91
2.1. Oceanographic Surveys and Measurements	91
2.2. Optical Measurements	92
2.3. Phytoplankton groups and pigments.....	93
2.4. Water mass classification.....	94
2.5. Chlorophyll- <i>a</i> algorithm development	95
2.6. Evaluation of the local algorithm performance	95
2.7. Algorithm comparison.....	96
2.8. MERIS imagery	98
3. Results.....	99
3.1. Description of biophysical measurements	99
3.2. Water mass classification.....	99
3.3. Radiometric <i>in situ</i> measurements	101
3.4. Phytoplankton groups and pigments.....	103
3.5. Chlorophyll- <i>a</i> estimation and mapping.....	104
3.6. Comparison of chlorophyll- <i>a</i> algorithms	107
3.7. Application to MERIS imagery.....	109

4. Discussion	110
4.1. Water mass classification.....	110
4.2. Chlorophyll- <i>a</i> estimation	113
4.3. Evaluation of algorithm performance	114
4.4. Application to MERIS imagery.....	117
Chapter IV. Water quality assessment using MODIS satellite-derived chlorophyll-<i>a</i> within the European directives, in the southeastern Bay of Biscay	119
1. Introduction	120
1.1 Objectives.....	120
2. Materials and Methods.....	121
2.1. Basque Littoral Monitoring Network	121
2.2. <i>In situ</i> dataset	123
2.3. MODIS Imagery.....	124
2.4. Chlorophyll- <i>a</i> algorithms.....	125
2.5. 90 th Percentile Calculation	127
2.6. Algorithm evaluation	127
2.7. Quality status classification	129
3. Results.....	129
3.1. Spectrophotometry versus CTD fluorescence.....	129
3.2. Satellite versus <i>in situ</i> data	130
3.3. Chlorophyll- <i>a</i> annual cycle	131
3.4. Ecological quality classification using satellite images.....	134
4. Discussion	136
4.1. <i>In situ</i> -Satellite match-ups	137
4.2. Chlorophyll- <i>a</i> annual cycle	138
4.3. Ecological quality classification using satellite images.....	140
4.4. Combination of <i>in situ</i> and satellite data for water quality assessment.....	140
Chapter V. Chlorophyll-<i>a</i> variability within Basque coastal waters and the Bay of Biscay	143
1. Introduction	144
1.1. Objectives.....	145
2. Materials and Methods.....	145
2.1. <i>In situ</i> dataset	145
2.2. Satellite data	146
2.3. Daily data analysis	146
2.4. Seasonal analysis.....	147

2.5. Inter-annual analysis	148
2.6. Spatial analysis	148
2.7. Cluster and Principal Component Analysis	149
3. Results	150
3.1. Daily variability	150
3.2. Seasonal variability	152
3.3. Inter-annual variability	159
3.4. Unsupervised classification and principal component analysis	163
4. Discussion	164
4.1. Daily variability	164
4.2. Seasonal variability	165
4.3. Inter-annual variability	164
4.4. Unsupervised classification and principal component analysis	168
GENERAL DISCUSSION	169
1. Radiometric measurements	171
2. Chlorophyll- <i>a</i> algorithms	172
3. MERIS and MODIS imagery	173
4. Variability of water constituents	174
5. Sources of error	175
5.1. Influences of optical water constituents on algorithms	175
5.2. Atmospheric correction	176
5.3. <i>In situ</i> vs. satellite measurements	177
6. Further research	178
6.1. Combination of Algorithms I and II	178
6.2. Algorithm adjustment	179
6.3. Merging images	179
6.4. Data applications	180
7. Towards a better assessment of water quality with satellite imagery	180
7.1. Phytoplankton discrimination	180
7.2. Collaboration projects	181
7.3. New challenges	182
CONCLUSIONS	183
A protocol for radiometric measurements	184
Development of chlorophyll- <i>a</i> algorithms	185
Application to water quality assessment	187
Chlorophyll- <i>a</i> variability	187

REFERENCES..... 191
APPENDIX 209

RESUMEN

La implementación de las directivas europeas Marco del Agua (Water Framework Directive) y la Estrategia Marina (Marine Strategy Framework Directive), implican un incremento del monitoreo de la calidad del agua, dentro de los límites de las aguas costeras y de la zona económica exclusiva europea. La teledetección es el único método que permite obtener observaciones frecuentes y sinópticas de áreas extensas. Por ello, los datos del "color del agua" son utilizados cada vez más, como una herramienta para evaluar la calidad del agua, estimando la concentración de diferentes constituyentes del agua, como por ejemplo la concentración de clorofila-*a*, considerada como un indicador de la biomasa del fitoplancton y de la eutrofización del agua. Los dos sensores elegidos para este estudio, MODIS y MERIS, proporcionan información satelital diaria y global, a una resolución media (1 km x 1 km), además de mapas de clorofila-*a* derivados de dicha información. Sin embargo, los algoritmos utilizados a nivel global en aguas oceánicas (o de caso 1), se muestran imprecisos para determinar la concentración de clorofila en aguas ópticamente más complejas, debido a la presencia de material en suspensión y/o materia orgánica disuelta, como es el caso de las aguas costeras o también llamadas aguas de caso 2. Los constituyentes del agua en estas zonas son afectados por fenómenos locales y presentan, en general, características regionales. Por ello, una de los métodos utilizados para determinar la concentración de clorofila en aguas de caso 2 con mayor exactitud, es la parametrización de algoritmos empíricos locales. Otras aproximaciones emplean, por ejemplo, algoritmos analíticos, semi-analíticos o de redes neuronales, pero los algoritmos empíricos, los cuales han sido elegidos para este estudio, tienen la ventaja de ser matemáticamente más simples que los anteriores. Son fáciles y rápidos de aplicar y se desarrollan a partir de medidas realizadas en el campo, siendo por ello, de alcance regional o local. Además, para poder determinar la concentración de clorofila con precisión, es necesario estudiar los factores que afectan la variabilidad de este elemento en la zona de estudio. Los principales objetivos de esta tesis son:

1) seleccionar el algoritmo de clorofila-*a*, aplicado a imágenes de MODIS y MERIS, más adecuado para evaluar la calidad del agua en la plataforma continental del País Vasco, y

2) estudiar la variabilidad de la clorofila-*a* entre 2005 y 2010 con respecto a las descargas de los ríos en la misma área de estudio, utilizando mapas de clorofila-*a* producidos con el algoritmo que proporcione la mayor precisión, para poder establecer relaciones entre las descargas fluviales y el fitoplancton.

En primer lugar, se ha evaluado la precisión con la que los distintos algoritmos más empleados en la literatura, determinan la concentración de clorofila-*a*. Por lo tanto, ha sido necesario realizar medidas de campo y, para ello, desarrollar un protocolo y adaptar unas plataformas para la medida en alta mar de la radiancia solar y la radiancia emergente del agua, para calcular así la reflectancia de teledetección. El capítulo I del apartado de los resultados, describe los experimentos realizados en el laboratorio y en el campo para poner a punto el protocolo y poder obtener medidas de campo con el espectroradiómetro Ocean Optics HR4000CG.

En el capítulo II, se describe como dicho protocolo se puso a prueba durante una campaña de 20 días en el golfo de Vizcaya, entre el 5 y el 25 de mayo del 2008. Se muestrearon un total de 68 estaciones, donde se realizaron medidas radiométricas, y se tomaron muestras de agua para posteriormente determinar en el laboratorio las concentraciones de clorofila-*a*, sólidos en suspensión y materia orgánica disuelta. Las plataformas desarrolladas permitieron realizar medidas espectrales en la superficie del agua, de una forma rápida y consistente, puesto que el sensor se ajusta en la posición correcta y su estabilidad está garantizada por su diseño. En general, las firmas espectrales obtenidas durante la campaña corresponden con las que se encuentran en la literatura científica y su similitud con los espectros proporcionados por el espectroradiómetro TriOS permiten concluir que el protocolo y las plataformas desarrolladas para el HR4000CG, son apropiados para realizar medidas espectrales en alta mar. Las relaciones empíricas entre las medidas biogeoquímicas y espectrales tomadas durante la campaña permitieron la validación de algoritmos utilizados comúnmente para medir

la concentración de clorofila en aguas oceánicas. Asimismo, las medidas realizadas permitieron desarrollar algoritmos empíricos para el Golfo de Vizcaya, uno para el sensor MERIS y el otro para el sensor MODIS. Las comparaciones con los algoritmos validados muestran que los algoritmos desarrollados funcionan mejor en esta zona.

En el capítulo III se utilizaron las medidas realizadas con el espectroradiómetro TriOS, debido, en primer lugar, a la disponibilidad de este aparato en la campaña realizada en aguas costeras del País Vasco, y en segundo lugar, debido a su mayor precisión en este tipo de aguas. La mayor variabilidad encontrada en estas aguas, en lo referente a su composición y a la hidrodinámica de las plumas de los ríos, hace que una mayor precisión sea necesaria en este medio, la cual es aportada por el TriOS. Esto se debe a que este aparato mide la radiancia solar y la radiancia emergente del agua simultáneamente, y no con un intervalo máximo de 10 minutos como en el caso del HR4000CG. Estas medidas se han utilizado para desarrollar un algoritmo específico para las aguas costeras del país vasco, aplicado a imágenes de MERIS y MODIS. Además, una clasificación de las masas con análisis discriminante de los datos hidrológicos es comparada con la clasificación realizada con un "cluster" de los datos espectrales, resultando en una correspondencia del 80%. Se concluye que este algoritmo funciona mejor que los demás algoritmos evaluados (Gitelson, MERIS OC5, OC4Ev6, Carder) para los productos de MERIS. Se confirma también que el algoritmo no se ve afectado por los 23 pigmentos auxiliares identificados (correspondientes a 56 especies de fitoplancton) en las concentraciones medidas durante la campaña, ni por sólidos en suspensión hasta una concentración de 6.6 g.m^{-3} . Así, este algoritmo se puede aplicar en aguas costeras con concentraciones de clorofila entre 0.1 y 9.57 mg.m^{-3} . Por otro lado, la exactitud con la que el algoritmo local, aplicado a las imágenes de MODIS, determina la clorofila-*a*, es ligeramente menor a la del algoritmo OC5, como se muestra en el capítulo IV.

En el capítulo IV, el algoritmo local desarrollado, el algoritmo OC5 aplicado a MODIS y el algoritmo global OC3M, son validados con datos *in situ* de clorofila estimada por fluorimetría. Estos datos fueron obtenidos durante las campañas de la red de calidad llevadas a cabo entre 2005 y 2010 en las aguas costeras y continentales del País Vasco.

Se compararon los algoritmos entre sí y se validaron de dos formas diferentes: 1) haciendo coincidir las mediadas *in situ* de clorofila con las medidas tomadas por el satélite en las mismas localizaciones con un intervalo máximo de 3 horas; y 2) calculando el percentil 90 de cada mes del año para las imágenes obtenidas durante el periodo 2005-2010 y comparándolo con la misma medida calculada durante el mismo periodo, con las medidas cuatrimestrales de clorofila-*a* tomadas *in situ*. Se compararon los ciclos anuales de la clorofila para las 4 masas de agua en las cuales se dividen las aguas del País Vasco, utilizando los valores del percentil 90. En general, el OC5 proporcionó un mejor resultado. Un mapa de clorofila realizado con los valores de percentil 90 con el OC5 de todas las imágenes existentes entre 2005 y 2010, fue utilizado para evaluar el estado de la calidad del agua. Según la directiva Marco, la calidad del agua se puede dividir en 5 categorías o estados: "Muy bueno", "Bueno", "Aceptable", "Deficiente", "Malo" correspondientes a los siguientes rangos de concentración de clorofila-*a* para las aguas del país vasco (percentil 90): $\leq 3.5 \text{ mg.m}^{-3}$, $3.5- 7 \text{ mg.m}^{-3}$, $7-10 \text{ mg.m}^{-3}$, $10-14 \text{ mg.m}^{-3}$ y $\geq 14 \text{ mg.m}^{-3}$. Por lo tanto, se le otorgó a cada pixel del mapa de percentil 90, su correspondiente estado según su concentración de clorofila-*a*. Así, se obtuvo un mapa con el estado de la calidad del agua por cada píxel. El estado final de cada masa de agua se obtuvo al promediar el valor de todos los píxeles dentro de la masa del agua. Se obtuvo el mismo estado de la calidad del agua con los datos *in situ* que con los datos satelitales para todas las masas de agua, es decir "Muy bueno". Esto sugiere que un uso complementario de ambas metodologías, sería una buena solución para obtener una evaluación eficiente de la calidad de las aguas costeras utilizando la clorofila-*a*, sin un muestreo exhaustivo de la zona, reduciendo así el esfuerzo y el coste del monitoreo de campo.

En el capítulo V, se describe la variabilidad espacial y temporal de la clorofila-*a* en relación con las descargas de los ríos del País Vasco. El estudio de esta variabilidad es crucial para una evaluación adecuada de la calidad del agua, puesto que establece relaciones entre la clorofila (fitoplancton) y los sólidos en suspensión (luz para la fotosíntesis). En general, se observa un aumento de la concentración de clorofila-*a* uno o dos días después de un episodio de lluvias en las zonas costeras del país vasco, cerca de las

desembocaduras del Nervión y del Adour. Sin embargo, no hay un registro anterior que permita decir que este incremento tan rápido de la clorofila-*a* después del aporte de nutrientes al ecosistema marino, se deba a floraciones algales causadas por nutrientes fluviales. Por lo tanto, la clorofila-*a* medida por el satélite podría ser debida al fitoplancton de origen terrestre, estuárico o bentónico que es transportado y resuspendido por las aguas fluviales y la acción de las olas (tensión de fondo) y del viento (turbulencia) en la costa, producida por las tormentas. Así mismo, se podría deber a una sobrestimación por los algoritmos satelitales de la clorofila, debido a la presencia de una gran cantidad de sólidos en suspensión, descargados por los ríos o bien puestos en resuspensión por los efectos de las tormentas (viento y olas). Por otra parte, los patrones de variabilidad estacional de la clorofila-*a* son diferentes en las desembocaduras del Adour y del Nervión, y se distinguen a su vez de los patrones observados en aguas oceánicas. En el caso del Adour, las concentraciones de clorofila-*a* más altas se registran a finales de otoño y principios de primavera, principalmente entre abril y junio, los meses con los niveles de descargas fluviales más altos. En el caso del Nervión, el ciclo es similar al de las aguas oceánicas, en las que se observan floraciones de fitoplancton en primavera y a finales de otoño. Sin embargo, se observa un pico de clorofila-*a* en junio en aguas de la desembocadura del Nervión, que no se advierte en aguas oceánicas. Finalmente, el análisis de la variabilidad inter-anual muestra una leve disminución de la concentración de clorofila-*a* (determinada a partir de datos de satélite) en el 2005 y el 2010 en las desembocaduras del Nervión y del Adour, y un ligero aumento en aguas oceánicas. La clasificación insupervisada realizada, confirma que en la actualidad el fitoplancton está en buen estado ecológico y que el riesgo de eutrofización es bajo en las aguas costeras del país vasco.

En conclusión, los resultados presentados en esta tesis, aportan un conocimiento científico importante con respecto al uso de la teledetección como herramienta para determinar la concentración de clorofila-*a* con los sensores MERIS y MODIS, en aguas del País Vasco y del golfo de Vizcaya. El método desarrollado, por el cual se combinan las medidas *in situ* y de satélite de la clorofila-*a*, es un método eficaz para la evaluación de la calidad del agua en las áreas protegidas por las directivas europeas Marco del

Agua y Estrategia Marina. Además, esta tesis aporta información sustancial acerca de la variabilidad espacial y temporal de la clorofila-*a* en la zona de estudio durante el periodo 2005 y 2010, a partir de datos satelitales. Sin embargo, aún se registran inexactitudes en la determinación de clorofila-*a* en los casos de altas descargas fluviales. Por lo tanto, la siguiente etapa de este trabajo consistiría en analizar en mayor profundidad los procesos y los factores que afectan la variabilidad de la clorofila-*a* en áreas costeras con sensores remotos, así como la mejora de la estimación mediante satélite de este pigmento en dichas áreas. Asimismo, los datos espectrales y biogeoquímicos recopilados y analizados en esta tesis, pueden ser utilizados no sólo para calibrar y validar futuros sensores remotos, pero también pueden ser útiles para validarlos o "forzar" modelos biogeoquímicos, pudiéndose así estudiar más a fondo la dinámica de los elementos que afectan la calidad del agua en las costas del País vasco.

SUMMARY

The implementation of water quality European Water Framework (WFD) and Marine Strategy Directives (MSFD) requires an intensification of water quality monitoring, within the limits of the Exclusive Economic Zone. Remote sensing technologies can provide a valuable tool for frequent, synoptic, water-quality observations, over large areas. Hence, ocean colour data is used increasingly as a tool to assess water quality, by estimating the concentration of the water constituents, such as chlorophyll-*a* (a proxy of the eutrophication risk). Both MODIS and MERIS, the satellite sensors selected for this study, provide global and daily ocean information and satellite-derived chlorophyll-*a* maps at a medium resolution (1 km x 1 km). However, algorithms designed for assessments at global scales for these sensors are less accurate locally, due to the variability of optically-active in-water constituents. Hence, regionally parameterized empirical algorithms are useful to cope with the inaccuracies produced. Additionally, to improve the water quality assessment in Basque coastal waters, the effect of river discharges needs to be studied, as it is one of the major factors affecting phytoplankton growth in this region.

The main objectives of this thesis are:

- 1) to select the most suitable chlorophyll-*a* algorithms applied to MERIS and MODIS satellite images to assess the water quality in the Basque coastal and offshore waters (southeastern corner of the Bay of Biscay); and
- 2) to study the variability of chlorophyll-*a* with respect to river discharges into the same area, between 2005 and 2010.

To address these objectives, four regional empirical algorithms for MERIS and MODIS were developed with spectral and biogeochemical data acquired *in situ*. Two were developed for the entire Bay of Biscay with spectral measurements acquired with the OceanOptics spectrometer and biogeochemical data. A protocol and a specific platform were developed in this study especially for this spectrometer. Another two algorithms were developed with spectral data obtained with the TriOS spectrometer, as it provided improved results for the coastal waters than the OceanOptics spectrometer. The optical data was acquired during oceanographic surveys in the area of study. The influ-

ence of suspended matter, phytoplankton species and pigment content, on the algorithms developed was explored. These algorithms were validated with *in situ* data and were compared to well-established global and regional chlorophyll-*a* algorithms. The algorithms developed in this study generally improved the estimation of chlorophyll-*a* in Basque coastal waters. However, the OC5 algorithm was considered more suitable for the ecological water quality assessment of the study area, as it corresponded most accurately with *in situ* measurements. A 90th percentile chlorophyll-*a* map was generated with this algorithm to apply the classification scheme required by the Directives. The water quality status assessment obtained using both, *in situ* and satellite data, resulted in high quality status for all the water bodies. Hence, remote sensing is suited for the quality assessment and water body classification, when a densification of the monitoring network is needed to comply with European marine policies. A complementary use of both methodologies provides an efficient assessment of the water quality, within European Directives. Finally, daily MODIS imagery permitted the characterisation of the variability of chlorophyll-*a* in the Basque coast and the Bay of Biscay at a daily, seasonal and inter-annual scale. The seasonal chlorophyll-*a* cycle differs slightly in coastal waters, compared to the offshore waters, especially those areas affected by high river discharges (such as the Adour). The spring chlorophyll-*a* peak in March, in the offshore waters, is shifted to May in the nearby area influenced by the Adour. The unsupervised classification performed confirms that, at present, phytoplankton is at good status and eutrophication risk is low in the Basque coastal waters.

This thesis is the first study that provides scientific knowledge on the assessment of water quality, using remote sensing and chlorophyll-*a*, in Basque coastal and offshore water bodies. It provides also important spectral and biogeochemical information on the water bodies of the area, which will be valuable in future studies.

GENERAL INTRODUCTION

GENERAL INTRODUCTION

1. Problematic

Coastal waters are among the most productive natural systems on earth. They occupy 15% of the globe, provide 90% of the commercial fisheries, 25% global biological productivity and 80% of the marine biodiversity. Since the majority of the human population lives within 60 km of the coast, the quality of coastal waters and estuaries is increasingly threatened by anthropogenic activities, such as population growth, urbanization, maritime traffic, fishing, aquaculture, primary production exploitations and tourism, among others. Rivers are the primary link between the land and the ocean systems, and serve as the primary channel for the delivery of significant amounts of dissolved and particulate materials from terrestrial environments to the ocean. The development of anthropogenic activities produces discharges that pollute and weaken ecosystems, and increases the vulnerability of these environments.

In order to respond to this problematic, the Water Framework directive (2000/60/EC) and the European Marine Strategy Framework Directive (MSFD, 2008/56/EC) were published. The first directive was created to protect and manage estuarine and coastal waters up to one nautical mile offshore, and aims to reach good ecological status of all European water masses by 2015. This Directive (WFD; 2000/60/EC) establishes a framework for *“the protection of all waters (including inland surface waters, transitional (estuarine) waters, coastal waters and groundwater) which: (i) prevents further deterioration, protects and enhances the status of water resources; (ii) promotes sustainable water use; (iii) aims at enhancing protection and improvement of the aquatic environment through specific measures for the progressive reduction of discharges; (iv) ensures the progressive reduction of pollution of groundwater and prevents its further pollution; and (v) contributes to mitigating effects of floods and droughts.”* The WFD requires member states to assess the ecological quality status of water bodies, based upon the status of the biological, hydromorphological and physico-chemical quality elements, in relation to reference conditions (i.e. without anthropogenic pressure). The biological parameters have especial importance and include the phytoplankton composition and abundance, the frequency and the intensity of blooms and their effect on water transparency. The hydromorphological elements consider the freshwater inputs, dominant current direc-

tions and wave exposition. The physico-chemical components comprise water transparency, temperature, salinity, oxygen, nutrient concentration and a number of specific pollutants (Devlin et al. 2007).

However, analyses performed in Europe identified an inadequate institutional framework for the management of the sea, since a lack of coordination occurs between a number of regional strategies or conventions (Borja 2006). The MSFD was articulated to approach this problem, with the main objective of protecting and/or restoring the European seas, and “to promote the sustainable use of the seas and conserve marine ecosystems”. As the WFD, this directive establishes a framework for the development of marine strategies designed to reach good environmental status in the marine environment, but extended to the year 2020 instead of 2015. At the present time, the WFD considers a small part of European waters (19.8%, as stated by Borja (2005), and the MSFD will overlap with the WFD (1 nautical mile, from the baseline) and extend it to 200 nautical miles seaward, including the water column, the sea bed and its sub-surface geology. This directive searches a coordinated and integrated assessment of sea environmental status following the ecosystem approach, in addition to the principles adopted by the WFD. The assessment must be performed at a level of Eco-regions or sub-regions (Borja et al. 2011), namely the Bay of Biscay within the North East Atlantic Ocean (Borja 2006). Hence, the aim of both directives is the achievement of good quality status of European waters, from the baseline until 200 nautical miles seaward. This extension of the monitoring area reveals the need of monitoring methodologies to meet the directives’ requirements. The application of these two directives will require an intense and continuous monitoring of water constituents.

One of the biological water constituents to be assessed is phytoplankton biomass (Devlin et al. 2007; Domingues et al. 2008; Revilla et al. 2009), estimated through chlorophyll-*a* (hereinafter referred to as chl-*a*) concentration. This parameter is a good indicator of the eutrophication risk, which is considered as one of the major environmental problems across Europe (Bøgestrand et al. 2005). Eutrophication is caused by the input of large quantities of anthropogenic nutrients (mainly nitrate and phosphate) to the aquatic ecosystems (Nixon 1995). These contributions enhance phytoplankton growth and cause a disturbance of the balance of organisms in the water as

well as a decrease of water quality (i.e., reduction of dissolved oxygen, increase of organic matter and turbidity).

Within the Bay of Biscay, Basque coastal waters (Figure 1) are directly influenced by river freshwater discharges (Stoichev *et al.*, 2004, Morichon and Dailloux, 2006, Ferrer *et al.*, 2009) that affect coastal ecosystems and water properties. Methods to evaluate the quality of coastal waters in relation to WFD, started to develop early in 2000. These methods used *in situ* measurements of chl-*a* to derive phytoplankton biomass to calculate an integrated index that classified the quality status into five distinct categories (from “High” to “Poor”), matching the WFD typology classification. The evaluation of the eutrophication risk was established through the calculation of the 90th percentile (P90) of chl-*a*, integrated in a selected water mass over time (Revilla *et al.* 2009).

In situ methods employed for water quality assessment can present time and physical constraints. Only a limited number of sampling points can be performed, making it difficult to capture the range and variability of coastal processes and constituents. In addition, the mixing between fresh and oceanic water creates complex physical, chemical and biological processes that are difficult to understand, causing the existing measurement methodologies to have significant logistical, technical, and economic challenges and constraints.

Satellite sensors provide the most effective means for frequent, synoptic, water-quality observations over large areas (Miller *et al.* 2005). Hence, “ocean colour” imagery is increasingly used as a tool to complete data sets collected by traditional means (Hellweger *et al.* 2004; Gohin *et al.* 2008). Optical satellite sensors such as SeaWiFS (Sea-viewing Wide Field-of-view Sensor), MODIS (Moderate-Resolution Imaging Spectroradiometer) and MERIS (MEdium Resolution Imaging Spectrometer) already provide global and daily ocean information*. Remote sensing of ocean colour makes it possible to acquire information on the distribution of chlorophyll and other constituents over large areas of the oceans in short periods. There are many potential applications of ocean colour data. Satellite-derived products are a key data source to study the distribution pattern of organisms and nutrients (Guillaud *et al.* 2008) and fishery research (e.g., Zainuddin *et al.* 2006). Also, the study of spatial and temporal variability of phytoplankton blooms (Holmhansen *et al.* 2004; Navarro and Ruiz 2006; Radiarta

and Saitoh 2008), red tide identification or harmful algal blooms monitoring (Miller et al. 2005, Stumpf and Tomlinson 2005, Chapter 12), river plume or upwelling assessments (Doxaran et al. 2002; Patti et al. 2008; Petus et al. 2010), global productivity analyses (Platt et al. 1988; Sathyendranath et al. 1995; Lohrenz et al. 1997; IOCCG 2006) and oil spill detection (Chust and Sagarminaga 2007).

In coastal or estuarine (named case 2), global chl-*a* algorithms used for oceanic or "clear" waters show inaccuracies (IOCCG 2000). This is because in clear waters the optical properties can be modelled as a function of chl-*a*, whereas in optically-complex waters (such as coastal), the optical properties are affected not only by phytoplankton and associated substances, but also by other suspended and dissolved substances. These substances vary independently of phytoplankton and may make a significant contribution to the water optical properties. Therefore, the adjustment of existing global and regional chl-*a* algorithms or the development of new ones for a specific area, are usually performed to improve the chl-*a* estimation in regional coastal areas (IOCCG, 2000). Field determinations of the water-leaving radiance signal have been employed to derive empirical relationships between the variables of interest (i.e. phytoplankton, suspended matter or colour dissolved organic matter) and *in situ* optical measurement (Froidefond et al. 2002, Ouillon and Petrenko 2005, Dall'olmo et al 2005, Petus et al. 2009). These empirical relationships are used then to derive algorithms, by means of spectral band ratios and combinations. While different methodological approaches (i.e. models, neural networks) are used to accurately estimate water constituents in coastal waters, these empirical algorithms have the advantage of being mathematically simple and robust, and can be implemented very rapidly (Sathyendranath *et al.* 1994), but they have to be locally parameterised. The accurate estimation of water constituents with remote sensors could considerably facilitate the application of the WFD and MSFD (Gohin et al. 2008). For instance, satellite imagery can be employed to provide an intensive and extensive assessment of water quality of coastal waters and be a useful tool for monitoring purposes (Brando and Dekker 2003; Hellweger et al. 2004; Gohin et al. 2008). It can be used as well to understand the dynamics of chlorophyll-*a* in relation to river inputs and anthropogenic pressures (Signoret et al. 2006; Wysocki et al. 2006; Werdell et al. 2009).

2. Optical properties of the water

The "colour" of the ocean is determined by the interactions of light with the water (Figure 1 and 2). When light hits the surface of the water, the different colours can be absorbed, transmitted, scattered, or reflected in differing intensities. Remote sensors resolve the water components based on spectral appearance: i.e. the colour shifts from blue to green, when the amount of dissolved or suspended constituents in the water increases.

Remote sensing of ocean colour can be defined as a derivation of the spectral surface water-leaving upward radiance, L_w , in the direction of the sensor and at wavelength λ , from the top-of-atmosphere radiance $L_{TOA}(\lambda)$. The water-leaving radiance, L_w , results from the interaction of the downward irradiance E_d (radiant flux per unit surface area), having penetrated the sea surface, with the different optically-active water constituents. The retrieval of water components involves the estimation of the remote sensing reflectance optical parameter R_{rs} . It is defined as the ratio of water-leaving radiance L_w measured above the water surface, to the incident downwelling irradiance E_d just above the water surface. R_{rs} is expressed as (Mobley 1999):

$$R_{rs}(\lambda, \theta, \varphi) = \frac{L_w(\lambda, \theta, \varphi)}{E_d(\lambda, 0^+)} \quad (\text{eq.1})$$

where the arguments θ and φ indicate that the upwelling radiance can vary with the viewing angle.

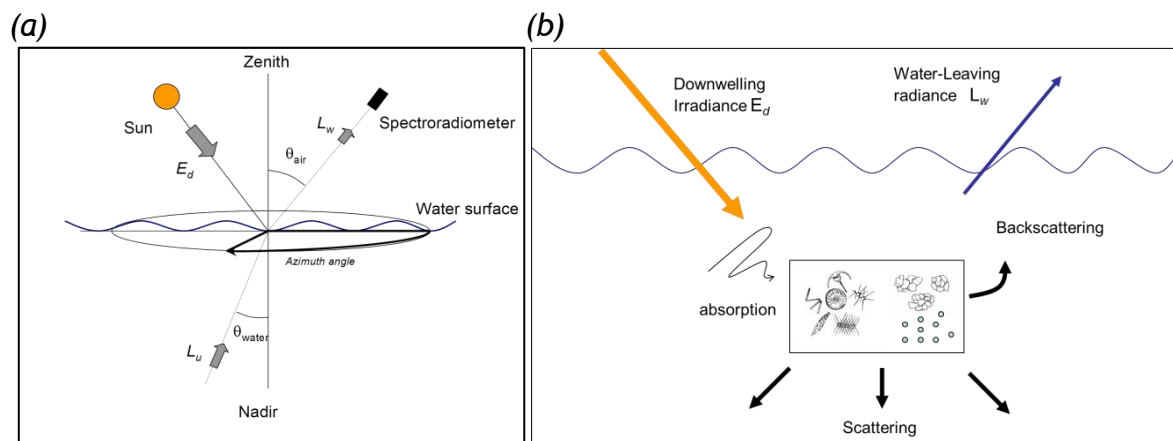


Figure 1. Ocean colour physics. (a) Apparent optical properties (AOPs): downwelling irradiance and water-leaving radiance. (b) Inherent optical properties (IOPs): absorption, backscatter and scatter. Adapted from Doxaran (2002).

R_{rs} is an apparent optical property (Figure 1(a)). This type of properties depends both on the medium and on the geometric structure of the radiance distribution, and displays enough regular features and stability to be useful descriptors of a water body. Inherent optical properties (IOPs), such as absorption and scattering, are properties of the medium and do not depend on the ambient light field (Figure 1(b)). That is, a volume of water has well defined inherent properties whether or not there is any light there to be absorbed or scattered. The emission, absorption, and scattering of radiation are also known as radiative processes. The radiative transfer equation states that as a beam of radiation travels, it loses energy to absorption, gains energy by emission, and redistributes energy by scattering (Sathyendranath and Platt 1997).

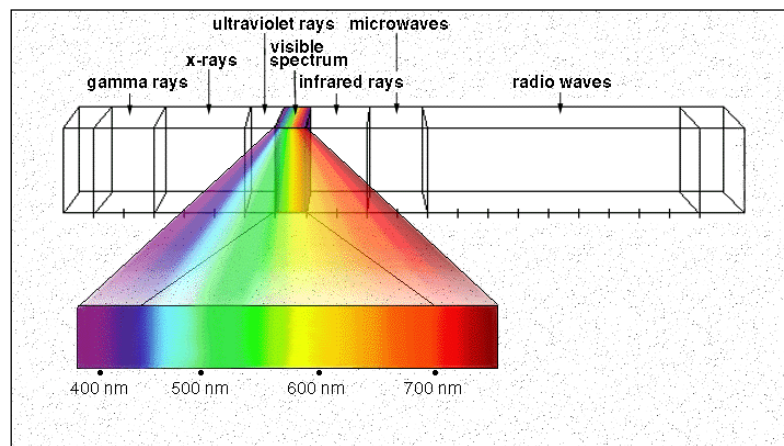


Figure 2. Colours and wavelengths of the light Spectrum.

In order to determine the relationships between apparent (reflectance) and inherent optical properties, the simulation of the radiative transfer processes in the ocean is necessary. One of the most common approaches employed is the Monte Carlo simulation of photon propagation through aquatic media. This method was developed by Plass and Kattawa (1968) and was applied by numerous studies (e.g., Gordon et al. 1975; Morel and Gentili 1991, 1993; Sathyendranath and Platt 1998). Despite some differences, in general, all the studies concluded that the reflectance of sea surface (R) can be expressed as the ratio between the back-scattering (b_b) and the absorption coefficient (a):

$$R(0) = f \frac{b_b}{(a+b_b)} \quad (\text{eq. 2})$$

Where f is a variable that depends on the solar zenith angle, the optical properties of the water and the wavelength (Morel and Gentili 1991, 1993). In case 1 wa-

ters, where $b_b \ll a$ the equation can be $R = f b_b/a$, while in case 2 the first form is used, since the backscattering coefficient cannot be neglected in the presence of inorganic particles.

Remote sensing reflectance is related to the inherent properties through the following equation:

$$R_{rs}(0^-) = 0.54 \frac{f}{Q} \times \frac{b_b}{(a+b_b)} [\text{sr}^{-1}] \quad (\text{eq. 3})$$

Where 0.54 is the coefficient that considers the effects of the air-water inter-phase (transmittance, reflexion and refraction, Mobley 1994) and Q links both diffuse reflectance (R) and remote sensing reflectance (R_{rs}), with the following equation:

$$Q(\lambda, \theta, \varphi) = \frac{R(\lambda, 0^-)}{R_{rs}(\lambda, \theta, \varphi)} [\text{sr}] \quad (\text{eq. 4})$$

Hence, the colour of the water is established by the scattering and absorption of visible light by pure water, together with inorganic and organic, particulate and dissolved material present in the medium. From an optical perspective, three main components affect the properties of water bodies (see Figure 3): 1) phytoplankton and other microscopic organisms; 2) non-algal particles or suspended particulate matter (SPM); 3) yellow substances or coloured dissolved organic matter (CDOM), which includes also detrital particulate material (IOCCG 2000).



Figure 3. Diagrammatic representation of "Case 1" and "Case 2" waters, extracted from Prieur and Sathyendranath (1981).

The bulk optical properties are the inherent optical properties that represent the combined effects of water and all its constituents. The specific inherent optical properties of a medium are the inherent optical properties of individual constituents of that medium, per unit concentration of the constituent. Thus, the bulk absorption coefficient of seawater (a) includes the absorption of the water itself (a_w), phytoplankton (a_p), yellow substances or CDOM (a_y) and inorganic suspended matter (a_s). It is defined as (IOCCG 2000):

$$a = a_w + Pa_p^* + Ya_y^* + Ss_s^* \quad (\text{eq. 5})$$

Where P, Y and S stand for the phytoplankton, CDOM and suspended matter concentrations, and the asterisks stand for the specific coefficients.

Likewise, the backscattering coefficient can be divided into three components:

$$b_b = b_{bw} + b_{bp}^* + Sb_{bs}^* \quad (\text{eq. 6})$$

This equation (eq.6) does not consider that CDOM contributes significantly to the bulk backscatter, but an additional term can be added in case this component needs to be considered.

The ocean colour signal in coastal or estuarine waters is defined by the particular wavelength dependencies of water components, since all the apparent, inherent, bulk and specific optical properties of water are wavelength dependent.

Figures 4 and 5 show some examples of reflectance spectra for different chl- a levels and absorbance coefficient spectra of chl- a auxiliary phytoplankton pigments measured in the laboratory (Bidigare et al. 1990; Schalles 2006) and chl- a spectra measured in the Atlantic region (Babin et al. 2003a). Examples of the equations used to estimate specific inherent optical coefficients of water components are defined in table A1 of the appendix.

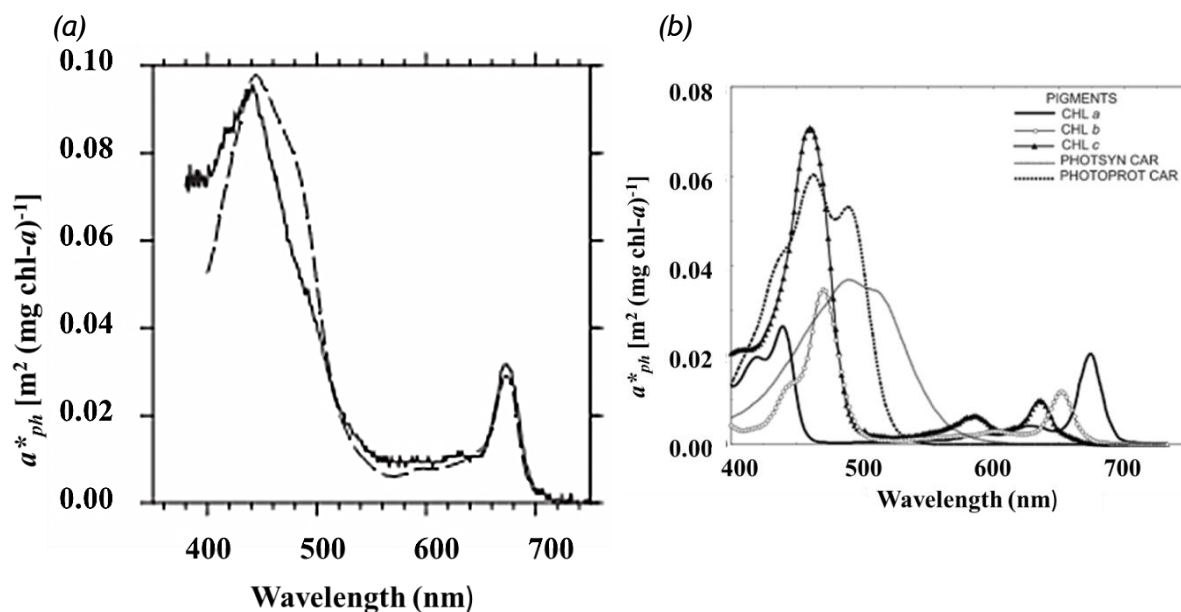


Figure 4. (a) Examples of phytoplankton absorption spectra (solid lines) for the Atlantic region. The spectra derived from the statistics of Bricaud et al. (1995) are shown as dashed lines, and the measured spectra by Babin et al. (2003a) are shown as solid lines. (b) Specific absorption coefficients for the major phytoplankton pigments: chl *a*, *b*, *c* = chlorophylls *a*, *b*, and *c*, Psyn Car = photosynthetically active carotenoids, Pprot Car = photoprotective carotenoids. Figure extracted from (Schalles 2006), data extracted from (Bidigare et al. 1990).

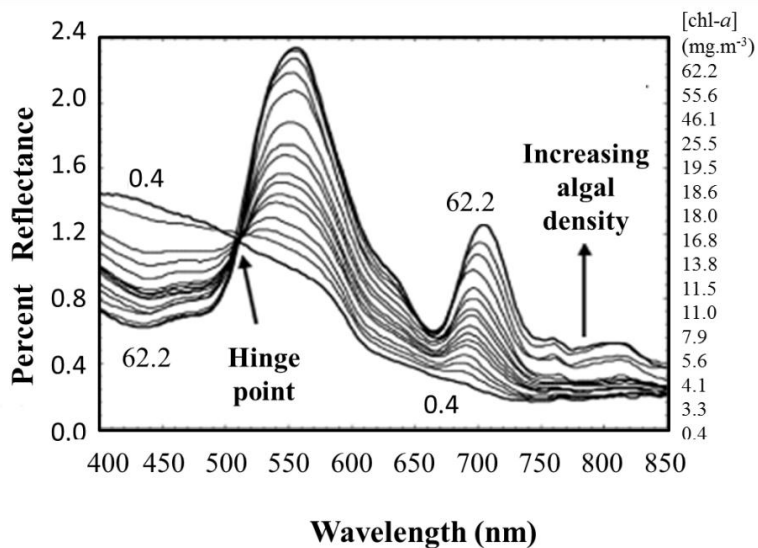


Figure 5. Graded series of reflectance spectra for different chl-*a* levels for an experiment performed by Schalles et al. (1997) (extracted from Schalles 2006).

3. Oceanic and coastal water bodies classification

A marine water classification was first introduced by Morel and Prieur (1977), which partitioned waters into Case 1, for oceanic or clear waters, and Case 2, for optically-complex water bodies, such as estuarine or coastal. They suggested the use of high or low values of the ratio of pigment concentration to scattering coefficient as a basis for differentiating between Case 1 and Case 2 waters. Nonetheless, their concept has evolved over time and the definition is not standardised (Gordon and Morel 1983; Prieur and Sathyendranath 1981; Morel 1988; Mobley and Stramski 2004, Lee and Hu 2006). In general, and according to the International Ocean Colour Coordinating Group (IOCCG 2000), Case 1 waters are those in which phytoplankton (with their associated and co-varying retinue of material of biological origin) is the main element altering the optical properties of the water. All the optical properties of Case 1 waters can be modelled as a function of chl-*a* concentration. On the other hand, Case 2 waters are affected not only by phytoplankton and associated substances, but also by suspended particulate matter and yellow substances that vary independently of phytoplankton, needing to be considered as independent variables. Chlorophyll absorbs red and blue light and reflects green light. Particles can reflect and absorb light, which reduces the clarity (light transmission) of the water. Dissolved organic matter strongly absorbs blue light, and its presence can interfere with measurements of chlorophyll (Morel and Prieur 1977; Gordon and Morel 1983; Mobley 1994).

The term phytoplankton includes all the planktonic single-celled organisms belonging to the plant kingdom. The concentration of the main phytoplankton pigment, chl-*a* is usually taken as an index of phytoplankton biomass. Nonetheless, it is important to remark the importance of the auxiliary pigments that go with chl-*a*. The pigment composition of a sample can vary with the community structure and the physiological state of the cells (IOCCG 2000). The terms suspended matter or non-algal particles, include all inorganic particulate material that is not included in the phytoplankton component. Several names are attributed to this type of particles, such as Suspended particulate matter (SPM), Total Suspended Matter (TSM), Total Suspended Solids (TSS) or Total, Sediment (TSS). They all, essentially, have the same meaning; in this document, this type of constituent will be referred to as SPM or TSM. The term coloured dissolved organic matter (CDOM) or yellow substances, refers to

the group of organic, dissolved substances, consisting of humic and fulvic acids (Kirk 1994). The CDOM is the light absorbing fraction of dissolved organic carbon (DOC; Rochelle-Newall et al. 1999). DOC is commonly used as a substitute value for CDOM and is included in many water monitoring programs. The estimation of CDOM from DOC is based on the finding that approximately 60% of CDOM consists of carbon, resulting in a positive linear relationship between CDOM and DOC (Corbett 2007). Coastal waters influenced by river discharges exhibit good relationships between CDOM and DOC (Del Castillo, 2007).

4. Satellite Remote Sensing

Ocean colour remote sensing was initiated in 1978 with the launch of the satellite remote sensor “Coastal Zone Color Scanner” or CZCS. This sensor provided frequent and synoptic images until 1986 and made the scientific community aware of the necessity of observing the colour of the ocean from space. Hence, spatial agencies from all over the world started and planned to launch remote sensors on board satellites with that purpose. Table 1 shows a list of past, present and future launches of ocean colour sensors.

For the present study, two remote sensors were selected because of their adequate spectral channels for the estimation of chl-*a* (Morel 2006; Table 1): (i) the Moderate Resolution Imaging Spectroradiometer (MODIS), and (ii) the Medium resolution Imaging Spectroradiometer (MERIS). MODIS imagery was selected due to its high image frequency since 2002 and its easy image access provided by NASA free of charge. MERIS imagery was selected as full resolution (FR) images (300 m x 300 m) are available every 2-3 days, since 2002. The FR images are appropriate for coastal studies. Table 2 shows the main band characteristics of these two satellites.

The description of the algorithms used for the satellite image processing and detailed information on these two remote sensors will be provided in succeeding chapters. Below are explained the procedures applied in general to ocean colour satellite imagery in order to obtain concentrations of water constituents with remote sensing.

The “ocean colour” instruments on board satellites perform radiance measurements of the ocean-atmospheric system. These radiance measurements are per-

formed at different wavelengths between the visible and the infrared wavelengths and need to be compared and calibrated against measurements made on the ground, to establish the link between sensor output signal (voltage, digital numbers) and absolute physical values at sensor input. The calibration of earth observation data is critical to reliably attribute detected changes observed in satellite data to real environmental changes occurring at ground level. Without calibration it is not possible to exclude the influence of other factors such as instrument error or influences of the atmosphere.

Most sensors transport autonomic calibration systems or are calibrated against stable natural or artificial sites on the surface of the Earth. Remote sensors such as SeaWiFs, MODIS and MERIS are regularly calibrated (Barnes and Zalewski 2003). Physical measurements made by a sensor and of the derived geophysical variables are then validated. Subsequently, a verification of the link between measurements in orbit and measurements made on ground (sensor validation) as well as verification of models, algorithms, derived parameters and data products (algorithm validation) needs to be performed. The validation is essential to understand and quantify the quality and accuracy of data products (Mueller et al. 2003). Vicarious calibrations consist of comparisons between water-leaving radiances or reflectances at the sea level and those derived from satellite measurements, after proper atmospheric corrections.

Table 1. List of the historical, current and future scheduled ocean colour remote sensors in alphabetical order (source http://www.ioccg.org/sensors_ioccg.html).

	Sensor	Agency	Satellite	Dates	Swath (Km)	Spatial resolution (m)	Num. of Bands	Spectral Coverage (nm)
Historical	CZCS	NASA (USA)	Nimbus-7 (USA)	1978 - 1986	1556	825	6	433-12,500
	CMODIS	CNSA (China)	SZ-3 (China)	2002 - 2002	650-700	400	34	403-12,500
	COCTS	CNSA (China)	HY-1A(China)	2002 -2004	1400/500	1100/250	10/4	402-12,500/ 420-890
	GLI	NASDA (Japan)	ADEOS-II (Japan)	2002 - 2003	1600	250/1000	36	375-12,500
	MMRS	CONAE (Argentina)	SAC-C (Argentina)	2000 - 2009	360	175	5	480-1700
	MOS	DLR (Germany)	IRS P3 (India)	1996 - 2004	200	825	18	408-1600
	OCI	NEC (Japan)	ROCSAT-1(Taiwan)	1999 - 2004	690	825	6	433-12,500
	OCTS	NASDA (Japan)	ADEOS (Japan)	1996 - 1997	1400	700	12	402-12,500
	OSMI	KARI (Korea)	KOMPSAT-1 (Korea)	1999 - 2008	800	850	6	400-900
	POLDER	CNES (France)	ADEOS (Japan)	1996 - 1997	2400	6000	9	443-910
	POLDER-2	CNES (France)	ADEOS-II (Japan)	2002 - 2003	2400	6000	9	443-910
	SeaWiFS	NASA (USA)	OrbView-2 (USA)	1997 - 2011	2806	1100	8	402-885
Current	COCTS	CNSA (China)	HY-1B (China)	2007	1400/ 500	1100/250	10/4	402-12,500/ 433-695
	GOCI	KARI/KORDI (South Korea)	COMS (South Korea)	2010	2500	500	8	400-865
	HICO	ONR and DOD (USA)	JEM-EF (Japan)	2009	50,000	100	124	380-1000
	MERIS	ESA (Europe)	ENVSAT (Europe)	2002	1150	300/120	15	412-1050
	MODIS-Aqua	NASA (USA)	Aqua (EOS-PM1) (USA)	2002	2330	250/500/100	36	405-14,385
	MODIS-Terra	NASA (USA)	Terra (USA)	1999	2330	250/500/100	36	405-14,385
	OCM	ISRO (India)	IRS-P4 (India)	1999	1420	360/4000	8	402-885
	OCM-2	ISRO (India)	Oceansat-2 (India)	2009	1420	360/4000	8	400-900
	POLDER-3	CNES (France)	Parasol (France)	2004	2100	6000	9	443-1020
Scheduled launches	COCTS	CNSA (Japan)	HY-1C/D (China)	2014	2900/1000	1100/250	10/10	402-12,500/ 433-885
	COCTS	CNSA (Japan)	HY-1E/F (China)	2017	2900/1000	1100/250	10/4	402-12,500/ 433-885
	HIS	DLR (Germany)	EnMAP (Germany)	2013	30	30	228	420-2450
	Multi-spectral	INPE/CONAE (Brasil-Argentina)	SABIA-MAR (Brasil-Argentina)	2015	200/2200	200/1100	16	380-11,800
	OC Scanner	ROSCOSMOS (Russia)	Meteor-3M(3) (Russia)	2015	3000/800	1000/80	8/6	402-885/ 433-885
	OLCI	ESA/EUMETSAT (Europe)	GMES-Sentinel 3A (Europe)	2013	1270	300/1200	21	400-1020
	OLCI	ESA/EUMETSAT (Europe)	GMES-Sentinel 3B (Europe)	2017	1265	260	21	390-1040
	SGLI	JAXA (Japan)	GCOM-C (Japan)	2014	1150/1400	250/1000	19	374-12,500
	VIIRS	NOAA (USA)	NPP (USA)	2011	3000	370/740	22	402-11,800
VIIRS	NOAA/NASA (USA)	JPSS-1 (USA)	2015	3000	370/740	22	402-11,800	

Table 2. Band information and usage for MODIS and MERIS (table adapted from Morel 2006 and IOCCG 1998).

MODIS	MERIS	Information retrieved
Channels (Central wavelength [nm])		
412.5	412.5	Gelbstoff (CDOM) Detection
443	442.5	Phytoplankton absorption maximum
488	490	Phytoplankton absorption
531	510	Hinge point for Reflectance
551	560	Phytoplankton absorption minimum
667	665	Baseline for fluorescence detection
678	681.25	Chlorophyll- <i>a</i> fluorescence detection
	709	Baseline for fluorescence detection
748	779	Aerosol detection/quantification
869.5	870	Aerosol detection/quantification

Such validations are used to test the performance of the sensor, but also the quality of the atmospheric correction (IOCCG 1998). Algorithm validation allows for the verification and improvement of the algorithms used (e.g. for atmospheric correction and chl-*a* concentration). To achieve this, conventional, ground-based observations are required using calibrated and traceable field instrumentation and associated methods (IOCCG 1998).

Over 89-90% of the total visible radiance received by a satellite sensor pointing at the ocean is due to atmospheric scattering of solar radiation (i.e. aerosols) or specular reflection (the mirror-like reflection of light) by ocean's surface; only 10-20% of the signal comes from the ocean (Muller-karger et al. 2005). This contamination needs to be removed, since it can be a source of error when the remote sensing surface radiance or reflectance values are used to quantify water constituents (e.g. chl-*a* concentration as well as suspended and dissolved particles). Atmospheric correction procedures have to assess these atmospheric optical properties accurately and precisely in order to compute what would have been the ocean-colour signal in the absence of the atmosphere (IOCCG 2010). Hence, this step in the processing of satellite imagery is very important because errors at this stage can lead to inaccurate estimations of water constituents.

Two general steps are required to obtain quantitative estimates of water constituents from calibrated radiances measured by a satellite sensor. The first is removal of the colour of the atmosphere (atmospheric correction). The second is the derivation of water properties based on water-leaving radiance or surface reflectance estimates. The overall accuracy of retrieved water leaving radiance and constituents thus rely on the performance of the atmospheric correction and in-water algorithms (Muller-Karger et al. 2005).

5. Approaches to derive water constituents

The aim of ocean colour remote sensing is to remotely derive concentrations of seawater constituents, such as dissolved organic matter, suspended sediments, and particularly, chlorophyll concentration in the surface layer (Clarke et al. 1970), based on the water-leaving radiance. The overall accuracy of retrieved water leaving radiance and constituents depends on the performance of the atmospheric correction and in-water algorithms. The water colour interpretation can be approached with different methods (Gordon and Morel 1983):

1) The empirical approach. It entails the establishment of statistical relationships between the water-leaving radiance (L_w) and the concentration of the water constituents (e.g. chl-*a*, SPM). These relationships are made based upon *in situ* measurements of the substance and simultaneous measurement of the radiance or reflectance at different wavelengths. For example, the most common relationship to estimate chl-*a*, makes use of the “colour ratio”, where ratio radiance or reflectance values between different wavelengths is linearly regressed against chl-*a* concentration. The presence of phytoplankton highly decreases the reflectance in the blue region of the spectrum, while it does not significantly affect the green reflectance. Hence, ratios of two reflectance values are used as a way to deal with the variability and the uncertainty affecting the absolute reflectance and water-leaving radiance values (O’Reilly et al. 1998). In Case 2 waters, algorithms based on one ratio, estimate chl-*a* with relatively low accuracy, so multiple colour ratios are used to include a wider range of variability or to assess specific spectral features (Hoge and Swift 1986). This type of algorithms is named empirical.

2) The analytical approach. It involves the determination of the optical substances concentration solving the radiative transfer equation (Gordon et al. 1975). This is a complex and difficult method to implement. It is less found in the literature and will not be explained in further detail. When the analytical approach requires approximations or calibrations with empirical coefficients (Carder et al. 1999), the epithet "semi-" is used.

3) The semi-analytical or semi-empirical approach, which is in between the first two methods. In general, this approach uses models to provide values of reflectance ratios based on inherent optical properties (Gordon and Morel 1983; Gordon et al. 1988; Morel and Maritorena 2001). The radiative transfer equation is introduced in the empirical relationships, providing the spectral shape of IOPs of phytoplankton, particulate and dissolved water constituents. They have the advantage of considering the physical and biological causes of the colour variation of the ocean. This approach has been used by numerous models to estimate water constituents in case 1 and case 2 waters (Gordon et al. 1988; Carder et al. 1999; Morel and Maritorena 2001; Gitelson et al. 2008; Yang et al. 2011).

In order to cope with the complexity of case 2 waters, the use of neural network modelling has been recently introduced. MERIS imagery, for instance, uses this method developed by Schiller and Doerffer (1999) to atmospherically correct images over case 2 waters, and accurately estimate chl-*a* in this type of water body. This approach entails the use of models, either empirical or semi-analytical, to train the neural network, and obtain the case 2 products. Table 4 presents some examples of algorithms used to estimate chl-*a* concentration with MODIS and MERIS satellite products.

Table 4. Examples of algorithms employed to estimate chlorophyll-*a* concentration in case 1 and case 2 waters with MODIS and MERIS remote sensors. References: **1:** O'Reilly et al 1998 and Ocean color NASA URL: <http://oceancolor.gsfc.nasa.gov/REPROCESSING/R2009/ocv6/>; **2:** Gohin et al. 2002; **3:** Carder et al. 1999; **4:** Gitelson et al. (2009); **5:** Moses et al. (2007); **6:** Gower et al. (1999) (FLH: Fluorescence Line Height). C= Chlorophyll-*a*

Name	Water type	Satellite	Equation	a0	a1	a2	a3	a4	Ref.
OC3M	Case 1	MODIS	$C = 10^{(a0+a1 \cdot R+a2 \cdot R^2+a3 \cdot R+a4 \cdot R^4)}$ $R = \log_{10}(\max(R_{rs,443} > R_{rs,489}) / R_{rs,550})$	0.242	-2.583	1.706	-0.342	-0.881	1
	Case 1	MODIS	$C = 10^{(a0+a1 \cdot R+a2 \cdot R^2+a3 \cdot R+a4 \cdot R^4)}$ $R = \log_{10}(\max(R_{rs,489} / R_{rs,550}))$	0.248	-2.296	1.405	-3.13	0.648	
	Case 1	MERIS	$C = 10^{(a0+a1 \cdot R+a2 \cdot R^2+a3 \cdot R+a4 \cdot R^4)}$ $R = \log_{10}(\max(R_{rs,489} / R_{rs,560}))$	0.252	-2.15	1.519	-0.77	-0.429	
OC4E	Case1	MERIS	$C = 10^{(a0+a1 \cdot R+a2 \cdot R^2+a3 \cdot R+a4 \cdot R^4)}$ $R = \log_{10}(\max(R_{rs,443} > R_{rs,489} > R_{rs,510} / R_{rs,560}))$	0.326	-2.768	2.441	-1.129	-0.499	2
OC5	Case1/ Case 2	MODIS/ MERIS	C = OC4 band ratio, nLw (412), nLw(555) triplet based on Look-up-table						
Carder	Case 2	MODIS (empirical)	$C = 10^{(a0+a1 \cdot R+a2 \cdot R^2+a3 \cdot R)}$ $R = \log_{10}(R_{rs,489}/510)$	0.282	-2.783	1.863	-2.387		3
	Case 2	MODIS (semi-analytical)	$a_{phl}(675)_{emp} = 0.328 * [10^{-0.191-1.037p25+1.702p35^2-3531p25+1.702p35^2} - 0.008]$ $C = P_0 [a_{phl}(675)]^{P1}$	P0	P1	p 25	p35		
Gitelson Moses	Case 2	MERIS (semi-analytical)	$C = 194.2 \times [R_{rs}^{-1}(\lambda_1) - R_{rs}^{-1}(\lambda_2)] \times R_{rs}^{-1}(\lambda_3)$	56.8	1.03	44.3/555	490/555		4
	Case 2	MERIS (semi-analytical)		λ_1	λ_2	λ_3			
FLH	Case 2	MODIS	FLH= R2-(R3+ (R1-R3)*($\lambda_3 - \lambda_2$)/($\lambda_3 - \lambda_1$))	667	678	743			6
	Case 2	MERIS	R is the radiance at the wavelength λ	680.5	708	753			

6. Hypothesis and objectives

This study emerged from the need of an optical and biogeochemical characterisation of the water masses of the study area, non-existent previously, for the application of remote sensing tools to evaluate water quality. *In situ* measurements including the widest range of water constituents concentrations (i.e. chlorophyll-*a* and suspended matter) had to be performed simultaneously with *in situ* spectral measurements, to validate already existent algorithms for coastal areas and for the development of regional empirical algorithms.

This thesis aimed to answer the following questions:

- Can we improve the assessment of water quality with remote sensing and chlorophyll-*a* algorithms specifically parameterized for the marine waters of the Bay of Biscay, to fulfil the WFD and MSFD requirements?
- Will a regionally parameterised algorithm, developed with *in situ* spectral measurements, improve the estimation of chlorophyll-*a* in the area of study?
- Can we successfully characterise the variability of the chlorophyll-*a*, in relation to river inputs, in the southeastern Bay of Biscay through remote sensing?

6.1. Hypothesis

The implementation of the WFD and MSFD will require an intense, extensive and continuous monitoring of the water quality indicators. Phytoplankton determined from chl-*a* concentration, is considered an indicator of eutrophication, a major environmental issue in Europe. Currently, satellite sensors provide the most effective means for frequent, synoptic, water-quality observations over large areas and represent a potential tool to effectively assess chlorophyll-*a* concentration over coastal and oceanic waters; thus, the areas covered by these two directives. However, algorithms designed to estimate chl-*a* at global scales have been shown to be less accurate in Case 2 waters, due to the presence of water constituents other than phytoplankton. Water constituents are region-specific because of the intrinsic variability of these optically-active substances affected by factors such as river input (e.g. suspended matter type and grain size) and phytoplankton composition.

In this regard, we pose the following hypothesis as a basis for this study: the use of regionally parameterized algorithms will improve the estimation of chlorophyll-*a* in coastal areas, and lead to a more comprehensive assessment of the water quality with this indicator, framed within the WFD and MSFD requirements. It will lead, as well, to an improved characterisation of the variability of chlorophyll-*a* within the Bay of Biscay, especially the southeastern part.

6.2. Objectives

In order to test the previous hypothesis, two main objectives are followed in this thesis:

- 1- Investigate the use of remote sensing as a tool to assess water quality of the Basque coastal areas with sea surface chlorophyll-*a* concentration, comparing established MERIS and MODIS global, regional and locally developed algorithms, to *in situ* measurements.
- 2- Study the spatial and temporal variability of chlorophyll-*a* in the area of study, between 2005 and 2010, in relation to river inputs.

With that aim, several specific objectives were pursued and are listed below:

- I. To acquire *in situ* spectral and biogeochemical measurements, for a subsequent calibration of MERIS and MODIS remote sensing images of the study area and the development of local chlorophyll-*a* algorithms.
- II. To explore the influence of suspended matter, coloured dissolved organic matter, phytoplankton species and pigment content on the retrieval of chlorophyll-*a*, with the algorithms developed.
- III. To compare global, regional and locally developed algorithms with *in situ* chlorophyll-*a* measurements acquired between 2005 and 2010.
- IV. To apply the selected algorithm to assess the ecological status of Basque coastal water bodies using satellite data estimations of chl-*a*.
- V. To study the variability of chlorophyll-*a* in the area of study between 2005 and 2010, in relation to river inputs.

7. Structure of the thesis

Initially, a description of the area of study is presented. The main characteristics of the Bay of Biscay are described to set the framework of study area, i.e. the coastal of area Basque country extended to the 200 nautical miles offshore limit established by the MSFD. Then, information is provided on the hydrodynamics and the rivers discharges that affect the water quality of the study area.

Subsequently, the results of the thesis are presented. This section represents the main body of the thesis and it is organized in five chapters. Each chapter starts with an introduction presenting the context of the chapter, followed by the materials and methods applied and the results obtained, and it finishes with the discussion of the main results. The main subject of each chapter is stated below:

Chapter I describes the development of a platform and an adapted measurement protocol for a field spectroradiometer (HR4000CG), with the purpose of acquiring *in situ* spectral signatures. These measurements are used to estimate remote sensing reflectance for the subsequent spectral characterisation of water bodies, validation and development of empirical algorithms with remote sensing images of the study area. In addition, the basic principles of remote sensing and on the calculation of remote sensing reflectance are described.

The aim of **Chapter II** and **III** is similar: to acquire abundant *in situ* optical and biogeochemical measurements covering a wide range of water constituent concentrations, to i) differentiate with spectral signatures the water masses of the area, knowing their corresponding water constituent concentrations; ii) evaluate the performance of already established algorithms with the *in situ* dataset acquired during the surveys; iii) be able to establish optical-biogeochemical statistical relationships to develop local algorithms and evaluate them. These two chapters are presented separately because part of methodology used and the area of study were different, but also to facilitate the understanding of the results obtained. Empirical algorithms were developed for case 1 (**Chapter II**) and case 2 (**Chapter III**) waters, as the area covered by WFD and WFD includes both types of water masses. The algorithms for case 1 waters were developed with radiance measurements performed with the Ocean Optics HR4000CG. On the other hand, the algorithms for case 2 waters were developed with measurements per-

formed with the TriOS spectrometer. This is because the TriOS instrument was available for the surveys described in **Chapter III** (not available in Chapter's II survey) and because it is better suited for the measurements performed at sea, especially in coastal waters. **Chapter II** includes an exploration of the effect of CDOM and suspended matter on the empirical relationships established. **Chapter III** also contains an analysis of the influence of suspended matter on the algorithm developed and a validation of the local case 2 algorithm is performed, together with an assessment of the effect of pigment content (from different species identified) on the algorithm. The local algorithm developed is compared to established algorithms for case 1 and case 2 waters and to field measurements. It is then applied to MERIS imagery.

Chapter IV is dedicated (i) to the validation and comparison of the local algorithm developed in Chapter III, applied to MODIS bands; and (ii) to the assessment of the ecological status of Basque coastal water masses with satellite data. MODIS imagery was selected for this chapter because it provides a higher frequency of images and was considered more advantageous for operational applications. The algorithm developed for MERIS images in Chapter III was adapted to MODIS bands. Subsequently, the algorithm that predicted chl-*a* with suitable accuracy in coastal areas, was selected and compared to *in situ* data collected during WFD monitoring surveys between 2005-2010. Satellite-*in situ* match-ups and 90th percentile (P90) monthly values are used to perform the selection. Then, the ecological status of the area was assessed with the resulting P90 chlorophyll-*a* maps generated with the algorithm selected.

Chapter V describes the variability of chlorophyll-*a* in the area of study, in regards to the daily, seasonal and inter-annual characteristics of the area and river inputs into the system.

In the final sections, the major findings achieved in this thesis are discussed as a whole, and the main conclusions of the thesis are enumerated.

GENERAL CHARACTERISATION OF THE BAY OF BISCAY AND THE AREA OF STUDY

GENERAL CHARACTERISATION OF THE BAY OF BISCAY AND THE AREA OF STUDY

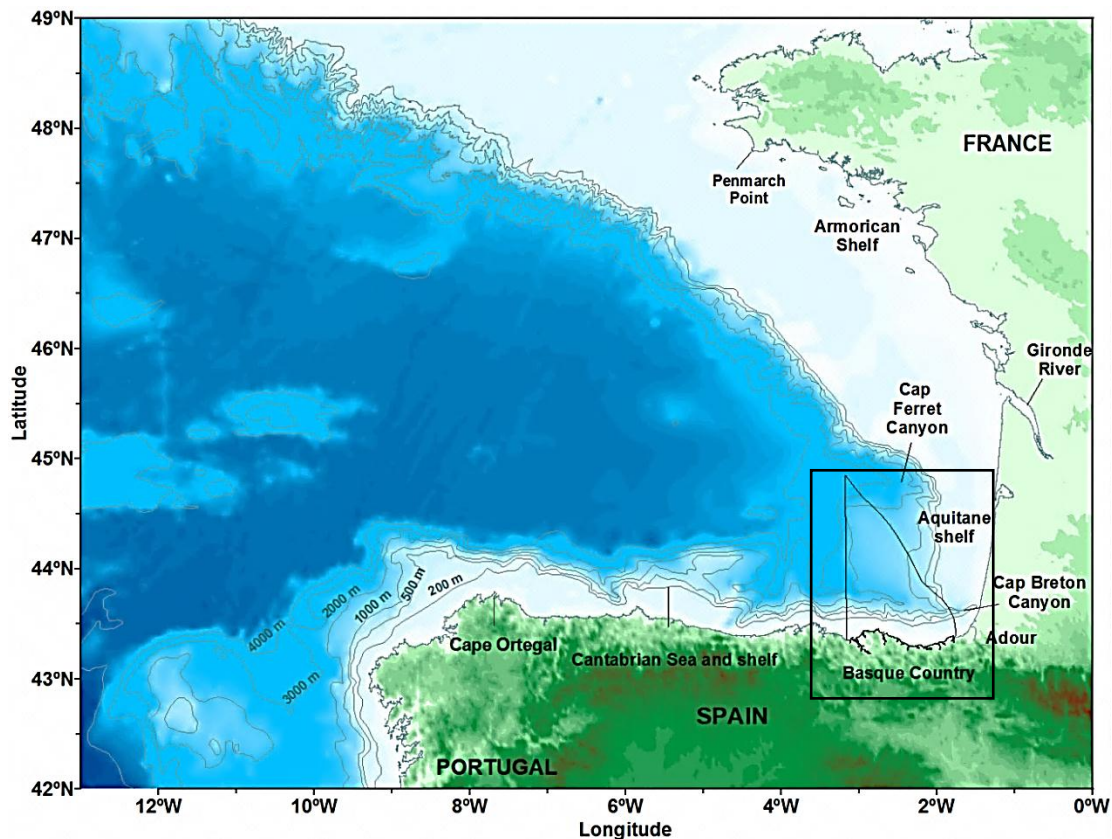


Figure 4. (a) Bay of Biscay map and area limited by the WFD and the MSFD: from the Basque coastline, up to 200 nautical miles offshore, and the French border.

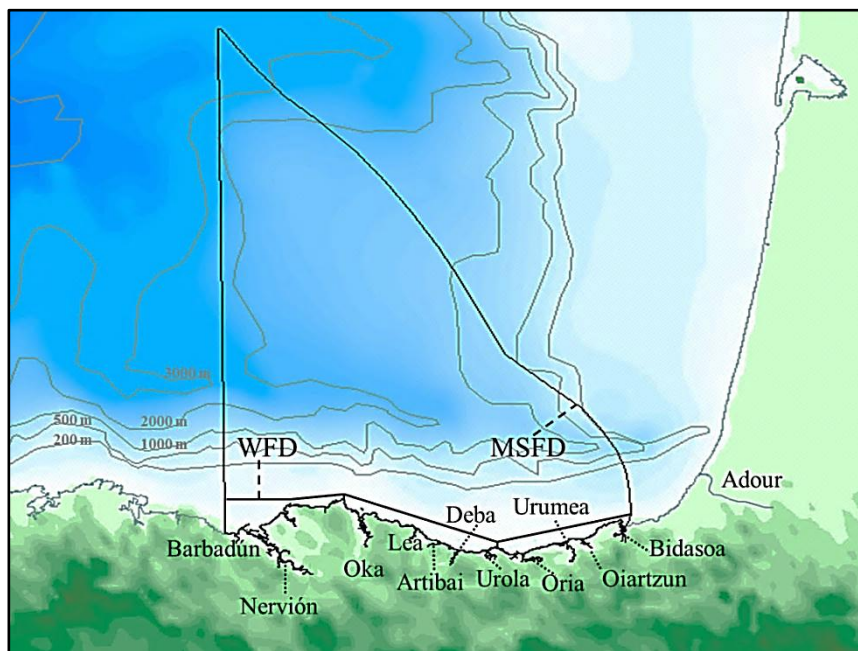


Figure 4. (b) Area of study: Basque coast, limited by the WFD (Water Framework Directive), the MSFD (Marine Strategy Framework Directive) and the French border, and main Basque rivers.

This thesis focuses on the area framed within the limits of the WFD and MSFD, as well as the borders of France and the Basque Country (Figure 4). Nevertheless, the Bay of Biscay has particularities that need to be considered when studying a southeastern part of the bay, the morphology, hydrodynamics and hydrology of the Bay of Biscay are described in this section to contextualise the area of study.

1. Geographical and physiographic characteristics

The Bay of Biscay is a gulf with 245 000 km² of surface, located in the North East Atlantic Ocean. It is limited by the Ortegal Cape (43° 46' N, 7° 52' W) in the northwestern Spanish province of Galicia, and the Penmarch Point (47° 46' N, 4° 22' W) located in Brittany, in northwestern France. The Bay of Biscay possesses specific hydrodynamic and physiographic characteristics due to its exposition to the Atlantic Ocean. There are two distinct areas in the Gulf limited by the bathymetry: the Continental shelf and the Abyssal Plain. The continental shelf extends far into the Gulf, and it can be divided in 3 different areas: the Armorican shelf, the Aquitaine shelf, and the Northern Iberian Peninsula shelf (or Cantabrian shelf). Beyond the continental shelf is the Biscay abyssal plain, at a water depth of 4,500 meters. Bordering the southeastern part of this abyssal plain is the Basque continental shelf, located within the eastern section of Northern Iberian Peninsula shelf (See Figure 4 (a)).

The southeastern part of the Bay of Biscay, has some morphological peculiarities, which influence significantly the water characteristics of the Basque coastal areas. As such, the CapBreton canyon creates a discontinuity between the wide French continental shelf and the narrow but irregular Spanish shelf. Due to this peculiarity, anomalous patterns take place in the area, which are enhanced by meteorological and hydrological aspects, such as the wind-driven transport, the precipitation or river runoff (Valencia et al. 2004). The Cantabrian littoral of the Bay of Biscay has a length of 1500 km. It is an exposed coast mostly composed of cliffs of calcareous rocks with small beaches, bays and estuaries (Díez et al. 2000).

2. Water bodies

The characteristics of the water masses of the Bay of Biscay are associated with the general features of the water masses of the North-Eastern Atlantic Ocean. Howev-

er, the properties of the masses can suffer some changes when entering the bay (Pingree 1973). Five types of water masses were identified in the southeastern part of the bay (Durrieu de Madron et al. 1999).

- In addition to the surface waters, influenced strongly by seasonal variations of the atmospheric regime, which is typical of temperate latitudes, the Upper Waters include the NACW (North Atlantic Central Water). In general, it has temperatures between 10.00°C and 12.20°C, and salinities 35.4 and 35.6 (Valencia et al. 2004).

- The ENAW (Eastern North Atlantic Water). This water mass originates from the subpolar mode water (Harvey 1982) and it is found at a depth of 200-300 meters, with temperatures of 4°C-12°C and salinities between 35.0 and 35.6 (Ríos et al. 1992).

- The MOW (Mediterranean Overflow Water), found at a depth of 700 to 1300 meters, this water mass reaches Bay of Biscay by spreading around shelf of the Gibraltar strait and west- and northward around the northern Iberian Peninsula. The water mass has warmer (11.9 °C) and more saline (35.7) waters than the ENAW.

- The LSW (Labrador Sea Water), which is found at a depth of 2000 m and is characterised by a maximum oxygen concentration at a depth of 1900 m. The salinity of this water mass is masked by the mixing with the overlying MOW.

- The BW (Bottom Water), found below the LSW. This water mass is the result of the mixing between the North Atlantic Deep Water and the Antarctic Bottom Water, it can reach temperatures below 0°C and salinities around 34.9 - 34.65 (Valencia et al. 2004).

3. Water circulation

The Bay of Biscay is mainly characterised by the presence of weak anticyclonic oceanic circulation over the abyssal plain and the presence of eddies (SWODDIES, or slope water oceanic eddies; see Ferrer et al. 2009; Figure 5), which are the result of the interaction between the continental margin current instabilities and the bottom topography (Pingree and Le Cann 1989; Koutsikopoulos and Le Cann 1996; Ferrer et al. 2009). The circulation over the continental shelf is primarily regulated by wind, tides and water density (Koutsikopoulos and Cann 1996).

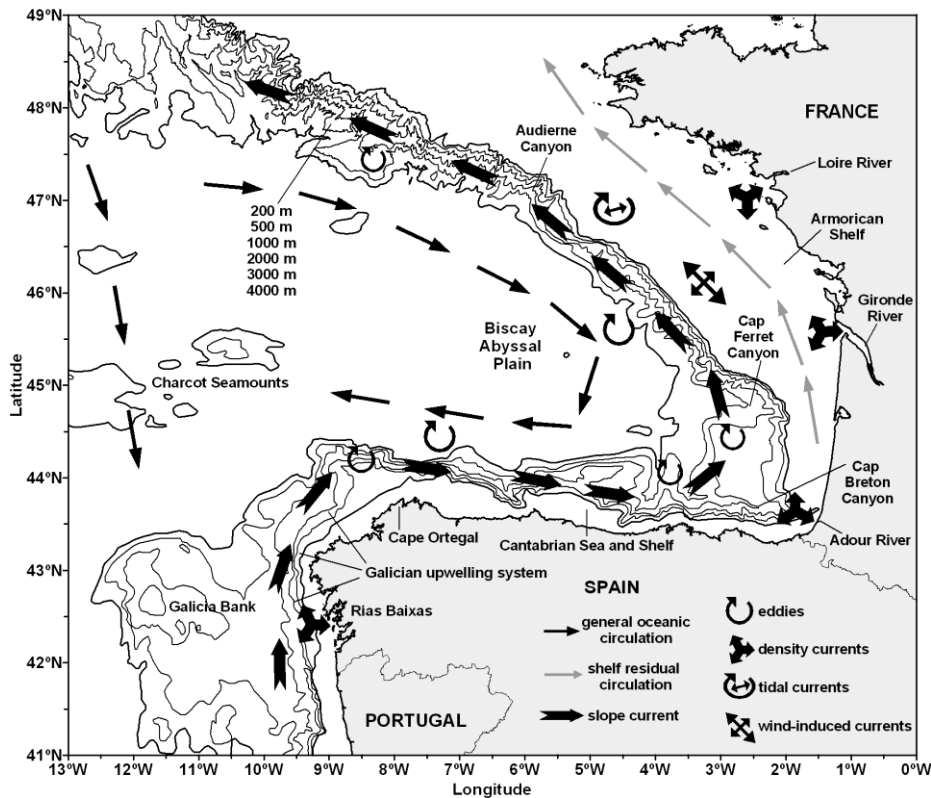


Figure 5. General water circulation over the Bay of Biscay (Source: Ferrer and Caballero, 2011).

Tides are semi-diurnal and their strength is related to the width of the continental shelf, they are strong over the northern Armorican shelf and weak over the southern part of the bay, where density and wind-induced currents mainly control the water mass circulation (Le Cann 1990). Over the French continental shelf, the northwesterly wind stress is dominant during spring and late summer and southwesterly wind stress prevails from autumn to early spring. However, the significant variability of the wind in this area can outweigh on occasions any seasonal trend (Puillat et al. 2006). The shelf waters are characterised by a rapid response to wind stress. The northwesterly winds induce south-southwesterly currents over the French shelf, while the southwesterly winds cause a northwesterly circulation (Puillat et al. 2006). Over the Basque continental shelf, the circulation pattern is more complicated due to the narrowness of the shelf, but, in general, the autumn and winter southerly winds cause a current drift towards the north and east, and the spring and summer northwesterly winds cause the currents to move towards the west-southwest over the Spanish and French Basque continental shelf. Summer winds are similar to spring winds but weaker and more variable, causing an indeterminate direction of currents (Ibañez 1979; Gonzalez et al. 2004; Valencia et al. 2004; Fontán et al. 2009; Ferrer et al. 2009). The upwelling of deep,

cold and nutrient-rich waters in spring and summer characterises the west coast of Spain. However, the upwelling intensity decreases eastwards along the Cantabrian coast, slightly affecting the Basque Coast.

Table 3. Mean annual river flow and river basin area of the Basque corresponding rivers, from east to west. Data was extracted from Uriarte et al. (2004) and Valencia et al. (2004).

River	River Flow ($\text{m}^3 \text{s}^{-1}$)	River basin area (km^2)
Barbadún	2.9	129.6
Nervión	36	1,750
Butrón	4.7	179
Oka	3.6	180
Lea	1.8	79
Artibai	2.5	103.5
Deba	14	502.2
Urola	8	353.3
Oria	26	860.9
Urumea	17	266.2
Oiartzun	4.8	83.4
Bidasoa	29	700
Adour	300	16,880

Density currents have been observed near the Bay's estuaries caused by the interaction between the continental freshwater and the salty marine waters. The main French rivers discharging into the Bay are the Charente ($140 \text{ m}^3 \text{ s}^{-1}$ mean annual flow; Grelie 1933), Vilaine ($68 \text{ m}^3 \text{ s}^{-1}$ mean annual flow; Le Bris and Glémarec 1996) Loire, Gironde ($900 \text{ m}^3 \text{ s}^{-1}$ mean annual flow each; Lavín et al. 2006), and Adour ($300 \text{ m}^3 \text{ s}^{-1}$; Valencia et al. 2004), which can introduce high levels of river runoff inducing significant density currents. The main Cantabrian Rivers are the Pas, Nalon, Navira and Sor and the three Basque rivers Bidasoa, Urola and Nervión (Prego et al. 2007). Basque rivers are of torrential character, with a short time-lag between the rainfall and the subsequent river discharge, which is lower than the French rivers' runoff (e.g. the mean annual flow for all the Basque rivers is approximately $150 \text{ m}^3 \text{ s}^{-1}$). The main mean annual river flow and basin area of Basque rivers (Figure 4 (b)) are shown in table 3. In general, high river flows take place in spring and autumn, while low river flows occur at the end of the summer. The main freshwater influence over the Basque coast comes from the Adour French River. This River has a pluvio-nival regime and, in general, 3 main floods occur during the year: two over winter (November/December and Janu-

ary/February) and one over spring, around April or May (Brière 2005). The freshwater contributions to the Cantabrian coastal zone are typical of oceanic climate, with a rainy period (November-May) and a dry season (June-October).

4. Physico-chemical characteristics

According to Valencia et al. (2004), the shelf waters of the southeastern Bay of Biscay generally show an "overcontinentalisation" because of the strong terrestrial influence on the thermal and hydrological balances. Besides direct land runoff, discharges of large rivers (i.e. dissolved and particulate loads) on the French coast and numerous small rivers of the Basque coast have a high influence on the properties of the coastal waters. The estuaries control the inputs of the coastal areas by trapping suspended material, precipitating dissolved materials and by diluting the concentration of the elements present in river water. Thus, the dynamics and morphology of each estuary regulate the influence of estuarine water components on coastal areas (Valencia et al. 2004).

The thermal regime in the bay is spatially and temporally highly variable, although an annually recurrent thermo-haline front has been detected between November and mid-April (Castaing and Allen 1981). This front limits the dispersion of river freshwater by winds (whose temperature is generally less than 7 °C) originating in the estuaries of the Loire and Gironde and can act as a barrier for the transport of terrigenous suspended matter either resuspended or coming from land (Castaing and Allen 1981). On average Basque coastal water temperatures can range between 12 °C in winter and 22 °C in summer. Hence, there is noticeable seasonality throughout the year, where vertical homogeneity is alternated with stratification periods (Valencia et al. 2004). Maximum nutrient concentrations are observed during the turbulent mixing processes taking place in autumn and winter, as the deep nutrient-rich water masses mix with the nutrient-depleted surface waters. In addition, the increase in freshwater discharges during the cold seasons (Prego and Vergara 1998; Prego et al. 2008), contributes to these nutrient maximum concentrations.

The optical properties on the surface layers of the coastal waters depend upon the materials discharged by river and land runoff, mainly induced by rainfall. After heavy

rainfall, river and land runoff create fronts of highly turbid waters that can extend up to 5 km offshore and reach a depth of 75 m, according to Borja and Valencia (1993). These plumes are composed of low salinity surface waters, and are generally associated with high concentrations of suspended matter, high values of turbidity and attenuation coefficients, and occasionally, with high concentrations of chlorophyll-*a*. In general, the most turbid areas are located close to the coastline, and with increasing distance from the coast and river mouths, there is a decrease in turbidity and transparency. However, around the Cap Breton area, a less transparent water mass is found in the outer shelf, caused by the westward spreading of the Adour river plume, which indirectly affect phytoplankton growth (Valencia et al. 1996). During dry and calm climatic conditions, phytoplankton is one of the main elements affecting the water optical properties (Valencia and Franco 2004).

Several studies have described the nutrient and dissolved oxygen cycles taking place in the Bay of Biscay (Tréguer et al. 1979; Laborde et al. 1999; McCave et al. 2001; Valencia et al. 2004), and describe them as typical from mid-latitude areas. They are affected by the seasonal variations related with the thermal cycle and the alternation between the winter homogeneity and the summer stratification. Their concentration and distribution within the water column is mainly controlled by the succession of phytoplankton populations (Orive et al. 2004). In coastal areas, the nutrient cycle is regulated by river discharges and land runoff, as well as by phytoplankton production fluctuations (Valencia and Franco 2004). There is an increase in nutrient concentration during autumn and winter, due to (i) the upwelling of nutrient-rich deep water caused by the seasonal mixing, (ii) the higher freshwater discharges taking place in the Cantabrian coast during these seasons (Prego et al. 2008).

The rivers draining into the Bay of Biscay deliver about 2.5×10^6 t yr⁻¹ of continental fine sediments, 60% of which is derived from the Gironde estuary (Jouanneau et al. 1999), and 65% is considered to be stored on the shelf. Two kinds of mud fields can be found in the Bay of Biscay: coastal mud and shelf mud belts. Fine-grained material from various terrigenous sources (primarily from the Gironde and Loire rivers) accumulate in the mid-shelf muddy belt, but bioturbation and long-period swells remove and mix the sediments in this area. Uriarte et al. (2004) predicted a total discharge of suspended material of 1.57×10^6 t.yr⁻¹ by Basque rivers into the Cantabrian Sea, an input comparable to that of the Gironde (1.5×10^6 t.yr⁻¹, Probst, 1986). The Adour river discharge

directly influences Basque coastal waters (Stoichev et al. 2004; Morichon and Dailoux 2006; Ferrer et al. 2009). The annual discharge of suspended material has been estimated at $0.25 \times 10^6 \text{ t.yr}^{-1}$ (Maneux et al. 1999). The sedimentation rates are low in the Adour estuary, so most of the sediment inputs from the river are rapidly exported to the ocean (Maneux et al. 1999). These are transported and deposited from east to west along the Adour River mouth and towards Spanish Basque coastal waters, where they are resuspended by wave action at a depth of 100 m (Jouanneau et al. 1999; Figure 6). The Adour runoff variability leads to wide ranges of turbidity and suspended matter in the adjacent coastal waters.



Figure 6. MODIS satellite images in RGB, acquired on 10/03/2007; sources and solid fluxes to the Basque country shelf. Adapted from Jouanneau et al. (2008).

5. Phytoplankton

The annual cycle of phytoplankton in the Bay of Biscay is typical of a temperate sea, i.e. there is a mixing period during winter time followed by a stratification phase in the summer (Longhurst 1998), while phytoplankton blooms occur during the transition periods (spring and autumn). Longhurst (1998) documented four ecological seasons in the Bay: (i) mixed conditions and light limitation in winter, (ii) a nutrient limited spring bloom, (iii) summer stratified conditions with a deep chlorophyll maximum, and (iv) a second bloom when the autumn storms disrupt the summer stratification. Chl-*a* concentrations can reach 16 mg.m^{-3} in transitional waters (Borja et al. 2004; Gohin et al. 2008), 8 mg.m^{-3} in coastal waters (Borja et al. 2004) and 3 mg.m^{-3} in oceanic waters (García-Soto and Pingree 2009).

However, several authors have reported some particularities in the area. Labry et al. (2001) pointed out the occurrence of significant winter blooms within the Gironde plume in the Southeastern part of the Bay. As such, with the increase of light availabil-

ity, phytoplankton grows within the surface layer associated with the haline stratification, during high river flow. In addition, Morin et al. (1991) demonstrated that phytoplankton blooms in frontal zones of south and west Brittany were caused by halostratification. Gohin et al. (2003) confirmed as well, using *in situ* and satellite observations, the existence of winter phytoplankton blooms within large river plumes of the French coast, between 1998 and 2000. Lampert et al. (2002) described the spring blooms taking place on the French continental shelf as pluri-specific and composed mainly by coccolithophores (*Emiliana huxleyi*), diatoms (mainly *Rhizosolenia*) and silicoflagellates. Outside of the bloom area, “green algae” and cryptophytes dominated the phytoplankton, and dinoflagellates were found to be dominant in the outer shelf area of the southern part of the bay (Lampert et al. 2002). Similarly, Guillaud et al. (2008) explained that in the northern part of the Bay, the phytoplankton production only starts in mid-spring due to the winter light limitation caused by suspended sediment fluxes taking place in the Bay. On the other hand, in the center of the bay, diatoms first bloom in late winter at the edge of the central Bay’s river plumes, as they take advantage of the haline stratification caused by the ocean saline water and the rivers’ freshwater, and the seasonal light increase at the end of February (Labry et al. 2001). In spring, the central part of the bay becomes phosphorus-limited and the phytoplankton community competes for nutrients. At that time, diatoms grow thanks to the nutrient enrichment taking place at the river mouths. During summer, the river plumes become nitrogen-limited and small forms of phytoplankton dominate the central area of the shelf, using regenerated nutrients.

In Cantabrian coastal waters, Varela (1996) described the phytoplankton annual cycle as typical of temperate areas, but with some peculiarities as well. The author described three important processes that modify the basic pattern of the phytoplankton cycle: (i) the intrusion of saline waters (Eastern North Atlantic Central Water of subtropical origin; Rios et al. 1992) during winter-spring, which can cause a decrease in the phytoplankton biomass, (ii) the coastal upwelling during summer stratification taking place in the western Cantabrian shelf, which produces an elevation of the subsurface chlorophyll maximum, and (iii) river discharge and water turbidity (Varela 1996; Orive et al. 2004). The phytoplankton species composition in Cantabrian coastal areas during spring is typical of spring blooms, dominated by diatoms (Varela 1996), as described in

other regions of the Bay of Biscay (Tréguer et al. 1979), and the oceanic offshore water bodies are dominated by microflagellates.

RESULTS

Chapter I

Optical measurements of ocean colour with the field-based High-Resolution Fiber Optic Spectrometer (HR4000CG) for remote sensing applications

1. INTRODUCTION

Field spectrometers have been widely employed in the validation of satellite ocean colour data products as a way of establishing measurement uncertainties, assessing their scientific utility, and most importantly, to develop empirical algorithms for the quantitative and qualitative estimation of water constituents. Such efforts require a considerable amount of high quality *in situ* data, processed as consistently as possible. However, obtaining high quality *in situ* optical and biogeochemical data for those purposes can be challenging: other than the difficulty of performing accurate measurement at sea (Froidefond and Ouillon 2005), various other obstacles, such as the corrosiveness of the sea on instruments or the challenge of the measurements at a reasonable cost, can really complicate data acquisition.

Remote sensors, such as SeaWiFS and MODIS, are commonly validated and calibrated with *in situ* measurements performed with field spectrometers, i.e. Marine Optical Buoy program, (MOBY) (Bailey et al. 2008). Dall’Olmo et al. (2003, 2005) and Gitelson et al. (2007, 2008) used reflectance spectra obtained with the Ocean optics USB2000 spectrometer, with a similar methodology to the one exposed in this chapter, to evaluate the extent to which reflectance ratios could be applied to remote sensors to estimate chl-*a* concentration in turbid, Case 2 waters. Froidefond and Ouillon (2005) developed an innovative platform, a mini-catamaran fitted with a TriOS radiance sensor, to perform reflectance measurements at sea. Measurements were performed away from the ship to avoid the hull influence, and the sensor was placed below and above the water surface. They showed it was preferable to perform upwelling radiance measurements below the surface, except for highly turbid waters.

1.1. Objectives

The objective of this chapter was to develop a platform and establish a measurement protocol for the High-Resolution Fibre Optic Spectrometer, HR4000CG, for a subsequent calculation of R_{rs} , with the acquired data. Several experiments were performed in the laboratory and in the field to determine the optimal parameters and conditions for *in situ* reflectance measurements. This approach will permit the validation of remote sensing data products for the Bay of Biscay (coastal and estuarine areas) in the following chapters.

2. MATERIAL AND METHODS

2.1. Estimation of remote sensing reflectance

As previously mentioned, remote sensing reflectance estimation provides an essential connection between imagery from satellite sensors and *in situ* concentrations of water constituents (Gordon and Morel 1983; O'Reilly et al. 1998). R_{rs} is a parameter that indicates the effective reflectance of a body of water when viewed by a remote sensor and is used to derive biophysical parameters such as chl-*a*. It is defined as the ratio of water-leaving radiance L_w measured above the water surface, to the incident downwelling irradiance E_d just above the water surface (eq.1 of the General Introduction, section 2.)

The water-leaving radiance L_w cannot be measured directly with an instrument, instead the upwelling radiance $L_u(\lambda)$ is measured just above (0^+) or just beneath (0^-) the air-water interface. For measurements above the water surface, the radiance measured when the sensor views the sky L_{sky} and the reflected sky radiance when the spectrometer views the sea surface L_u need to be taken into account. These two parameters are related through the reflectance factor ρ , a complex factor that depends on incident light, viewing directions, wavelength, wind speed and cloud coverage (Mobley 1999). Thus, the water-leaving radiance above water surface L_w is equal to $L_u - L_{sky} * \rho$.

When the sensor is placed below the water surface, the conversion of the upwelling radiance into water-leaving radiance is performed by taking into account the variation of the refraction index of water in relation to the air n (1.33 for freshwater and 1.34 for seawater) and the radiance transmittance t (0.98 for a sensor pointing towards the nadir) at the water-air interface (Mobley 1999). Therefore, to obtain water-leaving radiance $L_w(\lambda)$, the upwelling radiance L_u is multiplied by the conversion factor t/n^2 .

The index of refraction changes when the sensor is placed below the water surface since the spectrometer was calibrated for air measurements. In the water, the semi-opening angle (θ_{water}) is different and it is given by the Descartes' law:

$$\theta_{water} = \arcsin[(1/n) * \sin \theta_{air}] \quad (\text{eq. 1.1})$$

The solid angle (angle in three-dimensional space) corresponding to a measurement performed with a 4° semi-opening angle in the air ($\Omega_{\text{IFOV}} = 2\pi (1 - \cos\theta)$), corresponds to 1.53×10^{-2} steradians, whereas in seawater it is of 0.85×10^{-2} and in freshwater of 0.66×10^{-2} . This results in an angle decrease by a factor of 1.796 for seawater (Froidefond and Ouillon 2005) and 1.770 for freshwater. Therefore, this factor multiplied by the t/n^2 factor, results in a multiplication factor of 0.98 for the L_u measurements acquired in both media.

The downwelling radiance L_d is measured directly when the sensor views a Lambertian (the surface radiance is isotropic) Spectralon® plate and is kept pointing in the same direction as for the upwelling radiance. The E_d downwelling irradiance can be then calculated by taking into account the known irradiance reflectance of the Lambertian surface R_g (Labsphere WS-1 Diffuse Reflectance Standard = 0.99) as follows (Doxaran et al. 2002):

$$E_d = \pi \frac{1}{R_g(\lambda)} L_d(\lambda) \quad (\text{eq. 1.2})$$

2.2. Instrumentation and platform

Spectroradiometers are designed to measure the spectral power distributions of illuminants in the visible region of the spectrum. They transform the photon energy resulting from the incident solar beam, into electrical signals.

Radiance measurements were performed using an Ocean Optics High-Resolution Fibre Optic Spectrometer HR4000CG (Ocean Optics Inc., 2001-2006; Figure 1.1 (a)). This device measures radiance (expressed in relative intensity units, i.e., digital counts; (Dall'Olmo et al. 2005) between 200 to 1100 nm in 3648 channels, with a spectral resolution of 0.75 nm (FWHM). The HR4000CG spectrometer is connected to a computer via USB, from which it draws power. Data is stored into a memory chip on the HR4000CG spectrometer and is processed by the Ocean Optics operating software Spectrasuite (www.oceanoptics.com/) (Ocean Optics Inc., Spectrasuite Manual, 1999-2007). The spectrometer is then connected to a Gershun tube, of field-of-view of 8°, by means of a

20 m-long optical fibre. The calibration of the device was performed in the factory, which provided a calibration certification data sheet.

To measure the upwelling radiance (L_w) of water surface on the field, we developed a stainless steel flotation device to mount the sensor (Figure 1.1, (b)), mainly based on the mini-catamaran platform implemented by Froidefond and Ouillon (2005). Its dimensions are of 50 x 50 x 15 cm, and the weight is of 8 kg approximately. The dimensions were chosen in order to minimise its influence on the optical measurements. The symmetrical square shape avoids the anisotropic influence of its shade on the measurements. This device enables the measurements to be taken far from the ship and therefore away from its shade. With this prototype, the Gershun tube is maintained approximately 1-2 cm below the water surface (under calm sea conditions) allowing upwelling radiance measurements below the surface and away from any shade-producing objects, except for the flotation device.

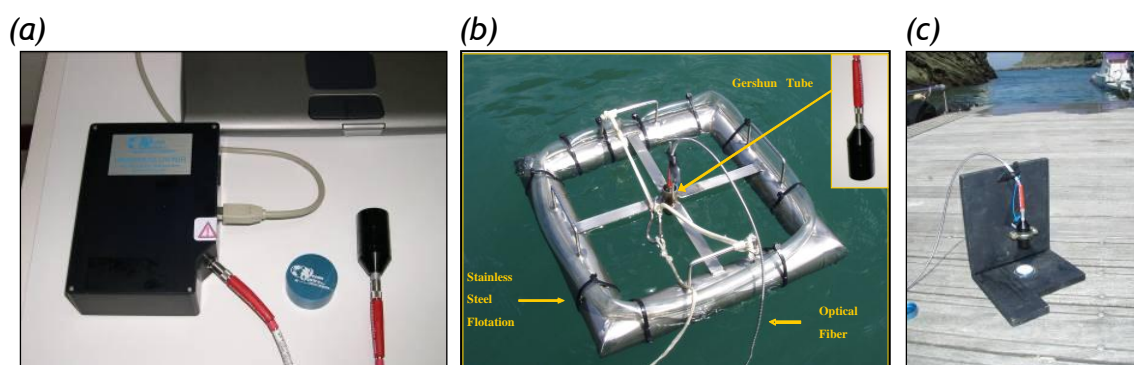


Figure.1.1. (a) Ocean Optics High-Resolution Fibre Optic Spectrometer HR4000C (b) Upwelling radiance measuring platform (L_u); (c) Downwelling radiance measuring platform (L_d).

The downwelling irradiance (L_d) was measured on a Labsphere Spectralon® (www.labsphere.com) target, which was placed on a special stand (Figure.1.1, (c)) designed to measure the irradiance at nadir (90°). The Gershun tube was held pointing directly towards the target (perpendicularly) and the platform was placed facing the sun for the downwelling radiance measurement. The Gershun tube is placed on the platform at a sufficient distance to avoid its own shadow, approximately 6 cm, perpendicularly above the Spectralon target. The measurement is performed with the platform facing the sun.

2.3. Laboratory experiments

a) Above and below water surface

The estimation of water-leaving radiance and the radiative transfer theory have been established by Mobley (1999) and later studies (Mobley et al. 1993; Mobley and Maffione 1997; Maffione et al. 1998; Hoge et al. 2003). The protocol developed by Mobley (1999) for the estimation of R_{rs} at sea has been widely used and even adopted by NASA for the calibration and validation of products (Mueller et al. 2000). This protocol entails the measurements to be performed above the water surface, with a nadir angle of 40° and an azimuth viewing direction of 135° (with an accuracy of $\pm 5^\circ$), in order to minimize the reflection at the sea surface, also referred as sun glint. This phenomenon is the specular reflection of sunlight off the sea surface. Its signal is much greater than the sunlight reflected from below the water surface, affecting the correct acquisition of spectral information concerning in-water constituents. While sun glint distortion in the upwelling radiance measurements above the surface is difficult to correct, this effect can be highly mitigated measuring below the water surface (Froidefond and Ouillon 2005).

For that reason, an experiment was carried out to estimate the difference between measurements performed above and below the water surface, using the protocol established by Froidefond and Ouillon (2005) for the TriOS radiance/irradiance sensors as a reference. Figure 1.2 shows the laboratory setup for the experiment. Upwelling radiance was measured by placing the Gershun tube directly 1 cm above and 1 cm below the water surface, pointing towards the nadir. The experiment was performed in a dark room, with a 100-watt light bulb as the only source of light, which pointed the sensor at a 50° angle (to avoid the shade of the tube). At the bottom of the container filled with water, a white paper was placed to obtain significant radiance intensity.

b) Measurement parameters

In order to establish a sampling protocol for the Ocean Optics spectrometer, several acquisition parameters needed to be adjusted: integration time, averaging of the number of acquired scans, dark correction, and spectral signature smoothing. Measurements were performed below the water surface as shown in the diagram of Figure 1.2.

"Integration time" is the time the sensor monitors incoming light (photons). It is a similar parameter to the shutter speed of a camera. The integration time needs to be adjusted so that the greatest amount of light that is anticipated for the application chosen causes a signal of about 85% of the spectrometer's capability (Ocean Optics Inc., Spectrasuite Manual, 1999-2007). The appropriate integration time has to capture enough light intensity without signal saturation that can occur in high light level applications. Therefore, the light intensity determines the integration time needed to be adjusted in every experiment. Tests performed in the laboratory and on field pre-established an integration time of 0.3 seconds for downwelling radiance measurements (i.e. on Spectralon®) and of 1 second for upwelling radiance measurements (i.e. target, mainly for water surface). These settings were eventually modified in accordance with the specific environmental conditions of each measurement.

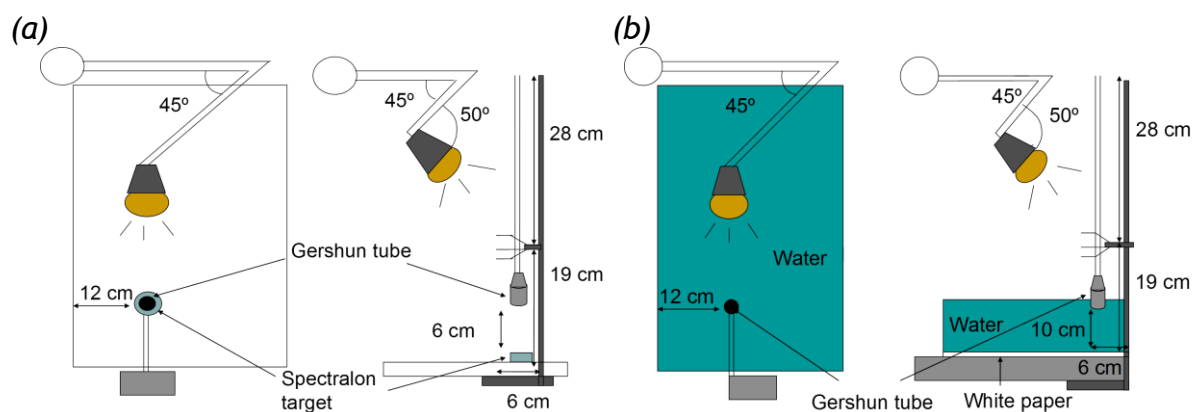


Figure 1.2. Experimental laboratory setup. (a) Downwelling radiance measurement on the Spectralon target. (b) Upwelling radiance measurement on container filled with water.

The discrete spectral acquisitions were stored individually in order to remove spectral observations that are distant from the rest of the spectra (for instance, affected by accidental shades caused by the movement of the vessel). The deviations of each spectrum from the mean spectra were calculated. The percent deviation of each spectrum with respect to the mean with the following equation:

$$\frac{\text{Observed} - \text{Theoretical}}{\text{Observed}} \times 100 \quad (\text{eq. 1.3})$$

The spectra with a deviation higher than 10% were removed.

To obtain accurate spectral radiance data, the inherent noise in the instrument (i.e., background electronic noise caused by the power supply) needs to be removed. With this purpose, in addition to the conventional subtraction of the dark spectrum (measured under dark conditions; Dall’Olmo and Gitelson, 2005) the electric dark correction was applied to both upwelling and downwelling irradiance measurements. This correction enables a dark-level correction during temperature changes caused by the power supply.

Smoothing is an additional way of reducing noise in the data and reveal the important underlying shape of the spectral signature. The simplest form of smoothing is the “moving average” or “moving box”, which substitutes each data value with the average of adjacent channel values. The boxcar smoothing parameter allows setting the width of this averaging box. The greater the smoothing width, the smoother the data and the higher the signal-to-noise ratio (S:N). If the smoothing width is too high, there will be a loss in spectral resolution (Ocean Optics Inc., Spectrasuite Manual, 1999-2007). The same experimental setup as in previous section was used to determine the suitable boxcar width. Intensity of the downwelling and upwelling radiances was measured with nine different boxcar smoothing values: 0, 1, 2, 4, 6, 8, 10, 15, 30. In order to choose the most convenient boxcar smoothing the average intensity difference between closest channels was calculated and was plotted against the boxcar smoothing values. Thus, the intensity value of channel λ_i was subtracted to the value of the adjacent channel λ_j ($=\lambda_i + 0.27$ nm), and successively applied for the 3648 channels measured. The total absolute resulting values were then averaged and plotted against their respective boxcar widths.

The signal strength of field spectrometers may suffer a derivation over time. Hence, a test was performed to determine the difference in intensity between the first and the last measurements, under identical illumination conditions. The same laboratory setup as for previous experiments was used to compare spectra obtained in February 2008 (before performing field measurements) to spectra acquired in April and June 2009. It was believed that one of the terminations of the optical fibre (the one placed in the water, Figure 1.1) could have been deteriorated during the measurements performed at sea, so it was replaced following the indications provided by OceanOptics technicians in July 2009.

2.4. Field measurements

The protocol parameters established with laboratory experiments were tested on the field. One hundred and forty-eight field measurements were performed between March 2008 and June 2009, during several sampling campaigns: 68 over the continental shelf of the Bay of Biscay (5th to the 25th of May, 2009; Bioman survey, described in Chapter II), 11 on surface waters of the Cantabrian Sea (between April 2008 and February 2009), 10 in the Oiartzun river mouth area (between February 2008 and October 2008) and 59 in the Adour river mouth area (between March 2009 and June 2009; Batel-2 survey, described in Chapter III). The protocol parameters were not modified during the field measurement except for areas where the light conditions were rather low (i.e., cloudiness) so the integration time was increased to allow the sensor to capture greater light intensity.

To determine the influence of clouds on measurements performed outdoors, a water container was placed in the same location during completely overcast and clear skies. Measurements were performed under identical conditions (except for the cloud cover) and at the same time of the day (11 GMT) on different days (19/08/2008 and 20/08/2008).

2.5. Comparison between HR4000CG and TriOS measurements

In addition, a spectral comparison was performed on the field between HR4000CG and the TriOS spectroradiometer (URL: www.trios.de) during a survey at the Adour river mouth area (named Batel-2, see Chapter III). The averaged Root Mean Square Error (RMSE) was calculated for 29 simultaneous radiance measurements performed on the field by these two devices. The RMSE was calculated with the following equation (Gohin et al. 2002):

$$\text{RMS} = \sqrt{\frac{\sum_{i=1}^n (V_{est,i} - V_{in\ situ,i})^2}{N}} \quad (\text{eq. 1.4})$$

where, V_{est} is the predicted variable, $V_{in\ situ}$ is the *in situ* measurement, and N is the number of stations.

3. RESULTS

3.1. Laboratory experiments

The radiance measurement above and below the water surface on a white paper placed at the bottom of the water container presented spectral curves with analogous shapes (Figure 1.3). There is an absolute difference of 4.1% in average between 200 and 1100 nm of wavelength. The below surface radiance measurement shows slightly higher mean absolute values; however, the standard deviation of the 20 spectral signatures of each type of measurement reveals an overlap between the two measures (above measurement plus standard deviation and below measurement minus standard deviation). Thus, the difference between above and below surface is not statistically significant. In addition, the Kurskal-Wallis test performed for the spectral region of maximal radiance differences (650 nm) showed a non-significant difference amongst the medians (p -value = 0.14).

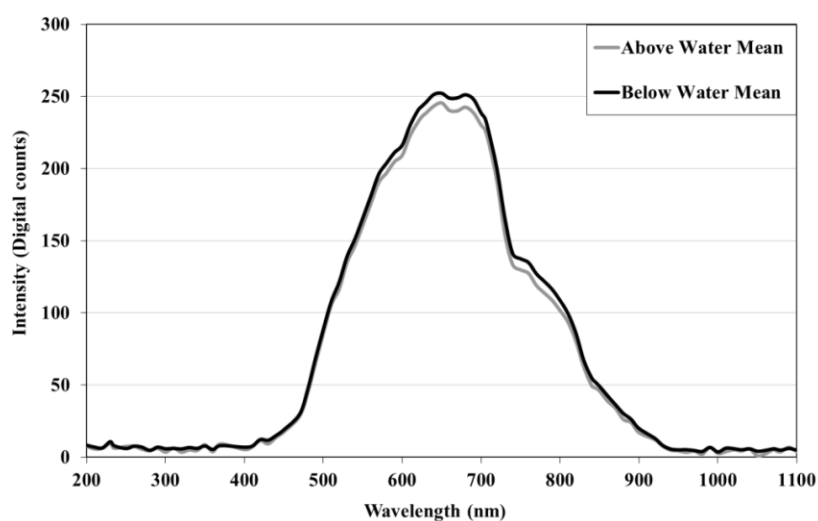


Figure 1.3. Upwelling radiances (in relative intensity units, i.e., digital counts) obtained in the laboratory following the diagram shown in Figure 1.2. The measurements were performed with the radiance sensor placed 1 cm above (blue) and 1 cm below the water surface on a white paper placed underwater. Dotted lines show the mean \pm SD (standard deviation) for the 20 spectral signatures acquired for each type of measurement.

The absolute intensity difference between closest channels was averaged and was plotted against the boxcar smoothing values used (Figure 1.4), to select the

most convenient boxcar smoothing. The values become levelled after a boxcar smoothing of 6 to 8.

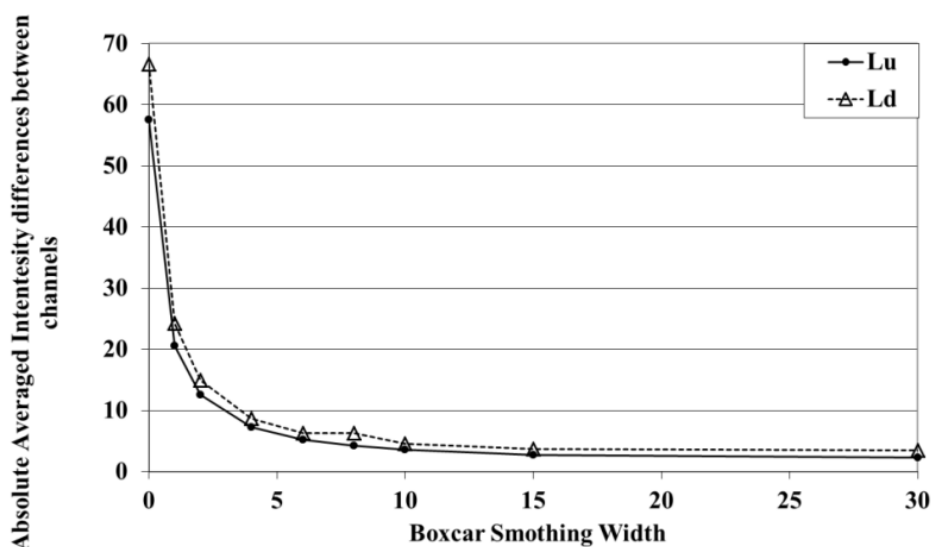


Figure 1.4. Absolute averaged intensity differences between adjacent channels plotted against the smoothing width for Spectralon (L_d) and Upwelling radiance (L_u).

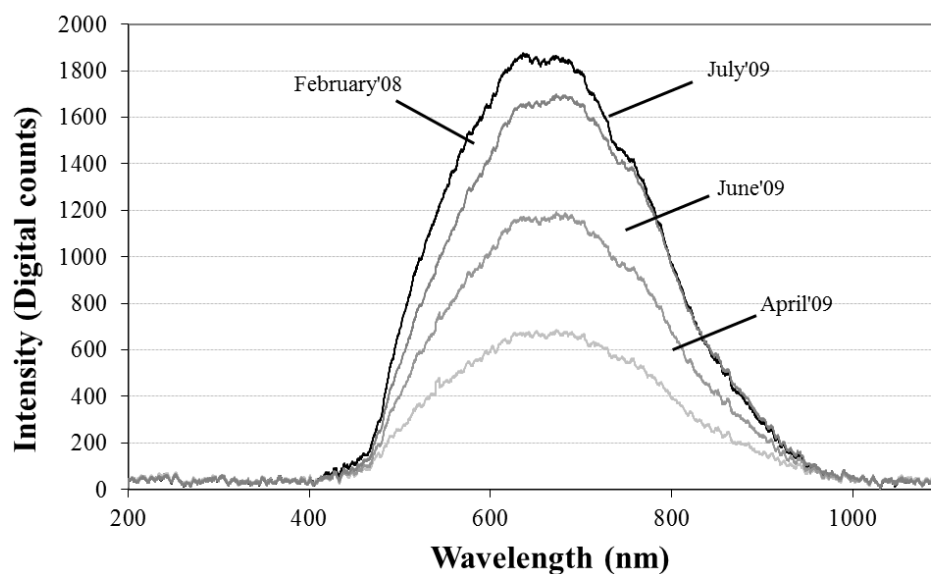


Figure 1.5. Upwelling radiance measurements, in digital counts, obtained in the laboratory in February 2008, before any field measurements were performed, and in April and June 2009, after the sampling campaigns. The radiance obtained, after the optical fibre termination was changed in July 2009, is also represented.

The change of the optical fibre termination showed an improvement on the spectra acquisition signal under identical illumination conditions, higher digital counts were recorded (Figure 1.5). However, not complete recovery of the initial conditions could be reached.

3.2. Field measurements

The stainless steel flotation developed for the measurement of upwelling radiance, performed well under relatively rough sea conditions (2 to 3 meter waves, 10-15 knot winds). It showed good floatability, it was fairly stable, and permitted the measurement of the radiance in a rapid and consistent manner (Figure 1.1 (a)). The downwelling radiance measuring stand worked also well under the same sea conditions, allowing for the acquisition of spectra in a rather fast and consistent way (Figure 1.1 (c)).

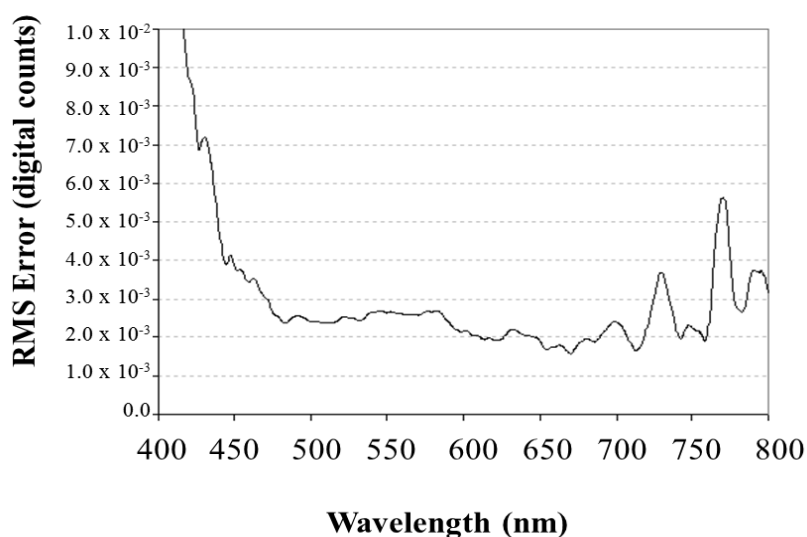


Figure 1.6. Averaged Root Mean Square Error of digital counts, comparing the 29 field measurements performed with the TRIOS and the HR4000CG spectrometers.

During the field measurements, it was noticed that the optical fibre inside the Gershun tube was immersed in the water during the measurements. Hence, the adjustments and test to determine the measurement differences between 1 and 2 cm below the water surface were performed. The results showed that no differences existed in the shape or magnitude of the spectra in most circumstances (Laboratory, turbid and clear waters).

The averaged RMS Error curve (Figure 1.6) for the comparison between the HR4000CG spectrometer and the TriOS, illustrates the increase in error at lower (< 450 nm; RMS Error > 0.003) and higher (>750 nm; RMS Error > 0.003) wavelengths. There is a minimum difference of 1.6×10^{-3} at 675 nm and a maximum difference of above 1×10^{-2} below 400 nm.

Figure 1.7 shows that under clear skies conditions, the reflectance is higher. There is also an increase in noise at lower (<450 nm) and higher (>750 nm) wavelengths. Hence, ideally, measurements should be performed under clear skies conditions.

Spectra measured on the field were noisier than the ones acquired under laboratory conditions. The spectral range considered, was limited to 450-750 nm (Figure 1.8), due to the high noise recorded at wavelengths below and above this range (Figures 1.6, 1.7).

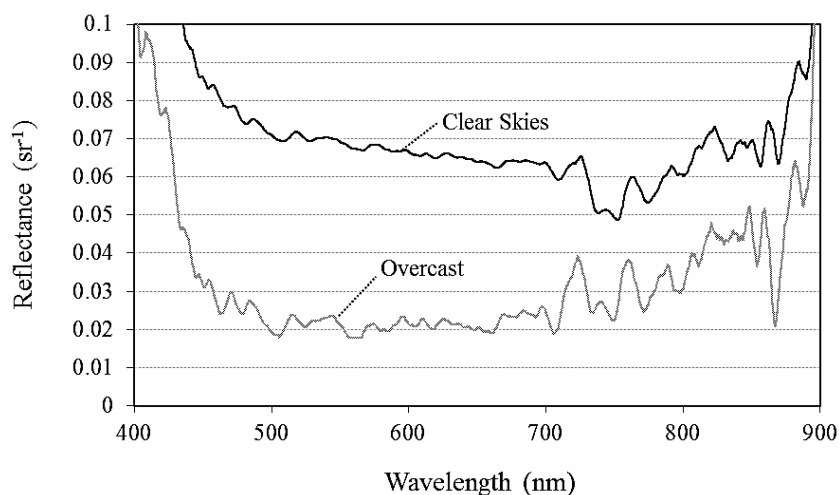


Figure 1.7. Difference in reflectance (sr^{-1}) between measurements performed under clear and covered skies conditions. The measurements were performed in the same location, at the same time of the day (11 GMT), on different days (19th and 20th of August 2008). The only difference was the cloud coverage. An averaging box of 5 nm was applied for display purposes.

Figure 1.8 shows the R_{rs} spectra of a subset of sampling stations, obtained at the seawater surface. Three different types of spectra, corresponding to different water masses, could be distinguished: (1) oceanic waters, (2) plume influenced waters and (3) estuarine waters. The oceanic water spectrum shows a peak emerging in the blue area around 450 nm, which decreases with higher wavelengths. With the increasing influence of river freshwater, a depression can be observed in the blue area of the spectrum around 450 nm, as well as a peak emerging between 500 and 600 nm. With increasing suspended matter input from the river, the highest spectral peak shifted towards higher wavelengths. In addition, a peak of lower magnitude appears around 670 and 700 nm ($0.001\text{-}0.002 \text{ sr}^{-1}$).

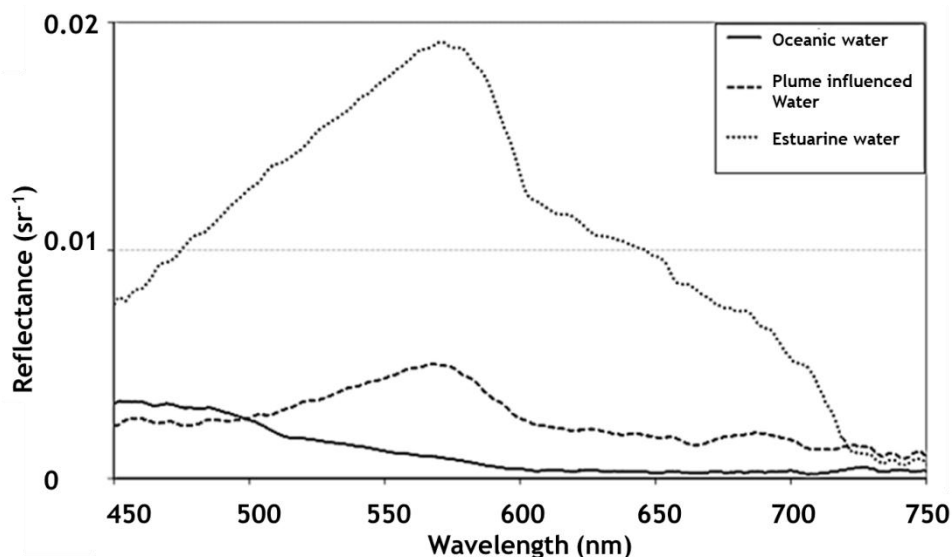


Figure 1.8. Subset of samples showing R_{rs} for three different water types: 1) continental or oceanic waters, 2) plume influenced waters and 3) estuarine waters. These are averaged spectra of R_{rs} measurements performed on the field with a boxcar width of 8 (averaged 8 adjacent channels).







		Turbidity (NTU)		
		Low values	Medium values	High values
Chlorophyll-<i>a</i>	High values	 1.3 NTU 9.5 mg.m ⁻³	na	na
	Medium values	 1.0 NTU 5.0 mg.m ⁻³	 3.8 NTU 3.8 mg.m ⁻³	na
	Low values	 0.01 NTU 0.90 mg.m ⁻³	 5.0 NTU 0.75 mg.m ⁻³	 64.7 NTU na mg.m ⁻³

Figure 1.9. Table relating chl-*a* and turbidity with respect to water colour (the pictures were taken under direct sun light, without clouds nor fog and avoiding sun reflection). Empty cells (na) are due to the absence of water bodies with coincident high values for both chl-*a* and turbidity.



Figure 1.10. Turbid plume caused by the Adour river freshwater (Light colour), close to the river mouth, occurred on the 6th of June 2007 at 3:00 pm.

Figure 1.9 illustrates the colour of the different types of waters, taken with conventional digital photography, an innovative method developed for water quality monitoring (Goddijn-Murphy et al. 2009). The figure shows: i) River freshwater with high turbidity (64 NTU), show a brownish colour. An example of these loaded waters is the Adour river mouth plume appreciated on Figure 1.10. There is a clear difference in colour between river freshwater with high suspended matter load and low chl-*a* concentration (64 NTU; na mg.m⁻³), and coastal water, with low turbidity and chl-*a* content (0.01 NTU; 0.90 mg.m⁻³). None or really low chl-*a* is measured in highly turbid waters, mainly because the presence of suspended sediments does not allow enough sunlight penetration in the water column, for the phytoplankton to photosynthesize. ii) Transitional or plume influenced and coastal waters present a greener colour (Turbidity 1-3.8 NTU, chl-*a* 3.8-5.0 mg.m⁻³) with lower sediment and higher chl-*a* content. iii) Water bodies with low chlorophyll and low turbidity (0.90 mg.m⁻³; 0.01 NTU) concentrations appear blue.

4. DISCUSSION

The main advantages of the upwelling-radiance measuring platform (a stainless steel flotation device) developed include its relative lightness (it can be easily released overboard), its stability (the sensor is maintained at a constant distance just below the water surface, approx. 1-2 cm), and the fact that measurements can be performed at nadir (perpendicular to the water surface). The advantages of the downwelling radi-

ance-measuring platform are also that it allows performing the measurements at a fixed distance from the Spectralon® target and at nadir. Thanks to these two platforms, the *in situ* spectral sampling can be carried out fast and in a consistent manner, since the sensor is easily adjusted to the correct position and its stability is guaranteed by the design.

The good consistency of the R_{rs} derived from the radiance measurements (at sea surface under different meteorological conditions) and the similarity to the reflectance spectral signatures obtained with semi-analytically modelled reflectance spectra (Morel and Maritorena 2001), show that the experimental protocol provides coherent results. That is, there is a correspondence between peaks and depressions in the spectral signatures of surface water containing different concentration of water constituents. The adoption of the below surface measurement method was therefore appropriate and in accordance with Froidefond and Ouillon's conclusions (2005). Even if the measurements performed just below and above the water surface are not identical, they are not statistically different. As Froidefond and Ouillon (2005) explained, the slight difference in raw signal is due to measurements being performed in different media (air and water) and the device being factory calibrated for air measurements. Hence, the conversion factor for below water measurements used when calculating R_{rs} (0.98), takes into account the loss of signal at the passage through the air-water interface and levels off the differences.

With the aim of reducing the signal noise, a boxcar smoothing of 8 nearest channels was selected for measurements performed on the field. This value was considered, from the experiments performed, as a good compromise between the loss of data information and the reduction of noise. However, some data still returned a relatively high amount of background noise in some parts of the spectral signatures so posterior spectral smoothing was performed by passing a 5 nm running mean filter over the entire spectrum (Dall'Olmo et al. 2005). An increase of the boxcar smoothing value was considered while performing measurements at sea; however, it was preferred to acquire the data as raw as possible for its posterior treatment using different approaches (i.e., test different levels of smoothing to find the optimal one). The scans were also kept raw by not averaging them on acquisition to facilitate posterior treatment of the data. Hence, scans that presented a higher deviation than 10% from the mean (of 40

scans) were discarded. If the scans would have been averaged when measured, it would have not been possible to filter the data set and find invalid scans.

Nevertheless, there are still some potential sources of error in the estimation of the R_{rs} with measurements performed *in situ*. Firstly, the self-shading effect of the water-leaving measuring platform could be introducing inaccuracies. Several studies have approached this issue and developed algorithms for the correction of the shade (Leathers et al. 2001; Gordon and Ding 1992; Leathers et al. 2004; Doxaran et al. 2006). These corrections are mainly for cylindrical devices and we considered it was complicated to apply in this case. This platform was inspired by the one developed by Froidefond and Ouillon (2005) and they did not apply any corrections, as it was tailor-made to minimize the influence of self-shading. To cope with the self-shading issue Leathers and Downes (2004) recommendations were followed: the collection of upwelling radiance measurements was avoided at times when self-shading is greatest. For that reason, measurements with this platform should be performed preferably when the sun is at nadir. An intercomparison exercise with the upwelling radiance measured using an in-water profiling radiometer would have been useful to completely validate the adopted methodology. Secondly, the effect of waves could also be introducing errors in the collection of radiance spectra due to the movement of the sensor when placed on the floating platform. Hence, the manual filtering of the spectra is necessary and the measurements need to be performed during calm sea conditions, if possible. Thirdly, as Doxaran et al. (2004) explained, under cloudy or covered sky conditions, shadow effects induced by the structures of the boat, by the person or system holding the radiance sensor, and by the radiance sensor itself, can modify the measured downwelling signal. During clear sky conditions these effects are low, the placement of the lambertian plate facing the sun is sufficient to obtain correct measurements. However, under a diffuse incident light (i.e., cloudy or covered sky) conditions, the light intensity is lower and the shadow effects can produce measurements errors (Doxaran et al. 2004). Even if the downwelling platform built for this study generally followed the recommendations of these authors, the effect of uncontrolled shadows during cloudy days could have still produced measurement errors. Hence, it is recommended to perform measurements under clear sky conditions when possible. Under cloud-covered conditions, it is important to pay special attention to the shadows on the Spectralon target, but also on the upwelling radiance-measuring platform. Finally, the deterioration of the fibre in

contact with seawater, suggests that a sensor compatible with seawater should be used instead of the Gershun tube, to avoid the loss of signal and possible measurements errors. Further optimisation of the measuring protocol and platforms would be useful to reduce the sources of error just mentioned.

Chapter II

Estimation of chlorophyll-*a* concentration in waters over the continental shelf of the Bay of Biscay: a comparison of remote sensing algorithms

INTRODUCTION

Water constituents are region-specific due to the intrinsic variability of optically active substances, such as chl-*a*, suspended matter and CDOM, caused by factors such as river input (e.g. suspended matter type and grain size) and phytoplankton composition (e.g. species; Carder et al. 1999). Algorithms designed for use at global scales by remote sensors such as MODIS and MERIS, have been shown to be less accurate in Case 2 and continental shelf waters (Morel and Prieur 1977), because of this variability (Carder et al. 1991, Darecki and Stramski 2003).

The interpretation of satellite imagery in regional waters can be improved with accurate field determinations of the water-leaving radiance signal (Mobley 1994). Thus, the relationships established between accurate *in situ* optical and biogeochemical data, covering a wide range of water constituent concentrations, are used in the calibration and validation of ocean colour remote sensing data, the regional parameterization of existing algorithms or the development of new algorithms (Doxaran et al. 2002, Froidefond et al. 2002, Ouillon and Petrenko 2005, Gitelson et al. 2008, Petus et al. 2008). These approaches help better assess water quality (IOCCG 2000) by improving the estimation of chl-*a* at a regional scale.

1.1. Objectives

The previous chapter showed that consistent measurements with the protocol and platform developed could be performed consistently. In this chapter, the optical and biogeochemical data, gathered during a survey over the continental shelf of the Bay of Biscay (mentioned in Chapter I) is analysed and used to develop statistical relationships. The objectives of this chapter were to: (i) evaluate the performance of already established algorithms with the *in situ* dataset acquired during the survey; (ii) establish relationships between the *in situ* optical and biogeochemical data acquired, employing band ratios commonly used by global remote sensing chl-*a* algorithms; (iii) Develop empirical algorithms for the Bay of Biscay based on the best correlations obtained in (ii), to apply them to MERIS and MODIS imagery.

2. MATERIALS AND METHODS

2.1. Oceanographic survey

In May 2008, spectral and biogeochemical measurements were performed during a 20-day survey over the continental shelf of the Bay of Biscay (Bioman 2008 survey) on board the “*Investigador*” vessel. The month of May was selected for the experiments because: 1) chl-*a* peaks take place during spring (García-Soto and Pingree 2009); 2) the daylight hours are long (approximately 15 hours), allowing more time for measurements; and 3) there is a higher possibility of cloud-free satellite images (less rain between May and September; Pérez Puebla (2009)).

Sixty-eight stations were sampled, with the aim of obtaining spectral signatures along a chl-*a* gradient. Measurements were undertaken mainly near the sea surface, between 9:00 and 17:00 (GMT), at water depths of between 20 and 1962 meters: hence, within the boundaries of the continental shelf of the Bay of Biscay. Measurements were performed on the side of the ship where no shade was present at the time. Figure 2.1 shows the location of the sampling stations. Around 100 L_d and L_u scans were performed, per station. Thirty-five of the measurements were performed under clear sky conditions with broad sunshine, 12 under completely covered skies and 22 under intermediate conditions (scattered clouds). The water samples were taken at the sea surface, within 10 minutes of the spectral measurements.

At each sampling station, surface temperature (°C) and salinity were measured with a thermosalinometer. Turbidity was also measured *in situ* by nephelometry (Nephelometric Turbidity Units, NTU), with a HANNA portable turbidimeter with a measuring range between 0.01 and 1000 NTU) and an accuracy of $\pm 2\%$ of the measured value. The chl-*a* and Total Suspended Matter (TSM) concentration were measured at the sea surface, by filtration of 1-2 l of water at each station, using Whatman® GF/C filters with a diameter of 47 mm and a porosity of 1.2 μm (as recommended by the UNESCO guide for water quality assessment, (Chapman 1996)). Filters were frozen (-20°C) immediately and taken to the AZTI Marine Research Centre, where chl-*a* was determined by spectrophotometry (following the Jeffrey and Humphrey (1975) protocols) and TSM was estimated by gravimetry (following the APHA-AWWA-WPCF (1989) protocols). In this study, unless specified otherwise, when referring to chl-*a* measured *in situ*, it means it

was determined by spectrophotometry with water samples collected and filtered *in situ*. Filtered water was saved in the refrigerator for later analysis of CDOM in the laboratory, by means of spectrophotometry. The colour of the water samples was estimated against MilliQ distilled water, at a wavelength of 460 nm. Most of the biogeochemical sampling and optical determinations were undertaken quasi-simultaneously. The reflectance measurements were acquired with a HR4000CG spectrometer using the protocol described in the previous chapter.

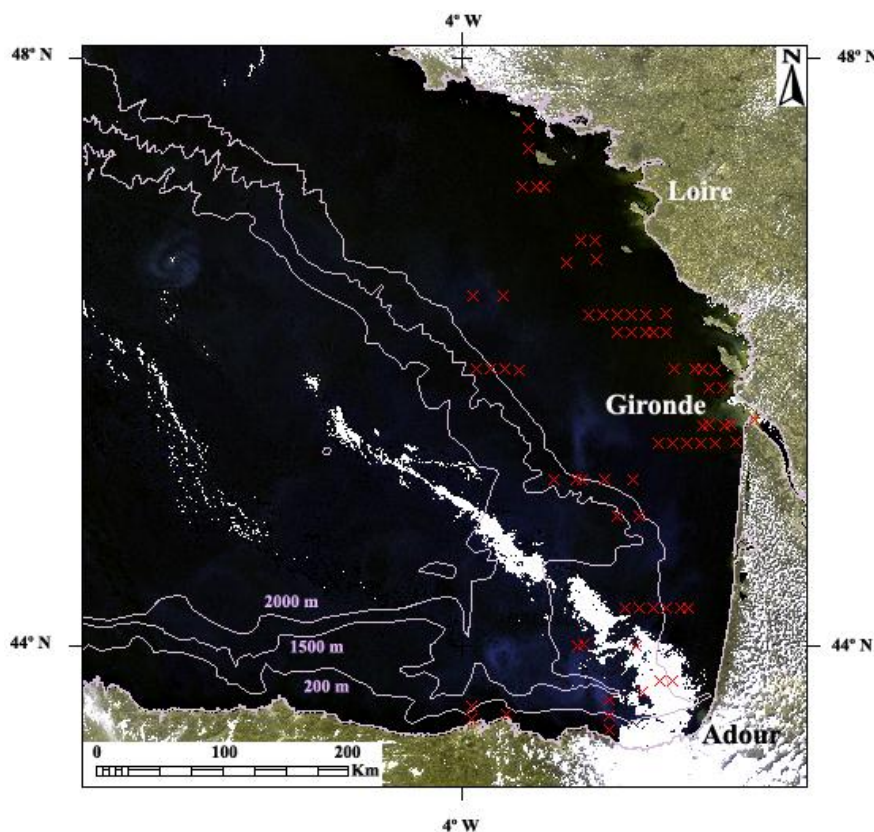


Figure 2.1. MERIS image (RGB composite) acquired on the 20th of May 2008 showing the stations where spectral and hydrological measurements were performed on the continental shelf of the Bay of Biscay.

2.2. Chlorophyll-a estimation

Band ratios between different wavelengths are used in satellite imagery to determine chlorophyll concentrations in open waters (O'Reilly et al. 1998). The presence of phytoplankton highly decreases the reflectance in the blue region of the spectrum, while it does not significantly affect the green reflectance. Hence, ratios of two reflectances, one in the blue and the other in the green, are used as a technique to relate reflectances with in-water constituents. The ratio “blue-to-green” technique, where $R_{rs}(\lambda_1)/R_{rs}(\lambda_2)$ ($\lambda_1 = 443, 490, \text{ and } 510 \text{ nm}$; $\lambda_2 = 550, 555, \text{ and } 560$), is used as a way to

deal with the variability and the uncertainty affecting the absolute reflectance and water-leaving radiance values (O'Reilly et al. 1998). The ratio values systematically decrease with increasing chl-*a*. The OC4 algorithm used for SeaWiFS sensor takes the greater of the three ratios R_{rs443}/R_{rs555} , R_{rs490}/R_{rs555} , R_{rs510}/R_{rs555} values; the MERIS (Medium Resolution Imaging Spectrometer Instrument) algorithm OC4E takes the greatest of the three ratios R_{rs443}/R_{rs560} , R_{rs490}/R_{rs560} , R_{rs510}/R_{rs560} , while MODIS algorithm OC3M uses only the greatest of the two ratios R_{rs443}/R_{rs550} , R_{rs490}/R_{rs550} (O'Reilly et al. 1998). This means that the band ratio is calculated for each pixel in an image to provide an estimate of chl-*a*. The Carder MODIS (chlor_a_3) algorithm, developed by Carder et al. (1999), only uses the R_{rs443}/R_{rs551} and R_{rs488}/R_{rs551} ratio.

The reflectance data measured *in situ* simulating satellite bands, were used to calculate the ratios and establish the statistical relationships. Therefore, log-transformed ratios used in the algorithms were calculated for the Bay of Biscay dataset and compared with log-transformed chl-*a* to determine the relationship between these variables (Table 2.1). In addition to the band ratio calculations, the previously mentioned algorithms were applied to our dataset (Table 2.2), as well as the OC4E algorithm adjusted to our dataset (i.e. our own coefficients for the equation). Using the R program, a model was established between the log-transformed chl-*a*, using the maximum reflectance value for each station. The resulting algorithms were validated with the jackknife resampling procedure (Burnham and Anderson 2002), developed with R language (Venables and Smith 2008). With a data set of n data stations, the jackknife procedure recalculated the model n times, leaving out one station in turn. Each one of the regression models, based on the $n-1$ times station, was then applied to that excluded station in order to produce a predicted water property value for that station. The predictive power of the model was evaluated with the coefficient of determination (r^2_{jac}) between the recorded and the jackknife-estimated water property.

2.3. Satellite images

Images from MERIS and MODIS were selected for this chapter. MERIS is a medium-spectral resolution, imaging spectrometer operating in the solar reflective spectral range. It forms part of the of ESA's environmental research satellite ENVISAT-1. MERIS has a swath width of 1150 km, measuring the solar radiation reflected by the Earth in

15 spectral bands, from about 412.5 nm to 900 nm (ESA 1996: <http://envisat.esa.int/instruments/meris/>). Because of the wide instrument field of view (68.5°), spatial sampling varies in the across track direction, between 0.26 km at nadir and 0.39 km at swath extremities. The spatial resolution over the Bay of Biscay is 300 m \times 300 m. The MERIS overpass time for central Europe is between 9:30 and 11:00 UTC, with a global coverage every 3 days. In this chapter, the Full Resolution image before the reprocessing performed by ESA was employed. The geo-located and atmospherically-corrected (Antoine and Morel 1999, 2011) reflectance MERIS full resolution (FR) product (level 2) was used.

MODIS is a sensor device located aboard the Terra (EOS AM) and Aqua (EOS PM) satellites. Both platforms are scheduled to pass over the south eastern corner of the Bay of Biscay twice daily, in the morning and in the afternoon. MODIS Terra and Aqua (<http://modis.gsfc.nasa.gov/>), acquire data in 36 spectral bands, between 415 and 14,235 nm, with spatial resolutions of 250 m (2 bands), 500-m (5 bands) and 1000-m (29 bands). MODIS Level 1 (Top-of-the-atmosphere Radiances, Calibrated and Geolocated) products were downloaded from the MODIS ftp site* and converted to Level 2 reflectance bands and chl-*a* products, through the SeaDAS** processing chain. The SeaDAS operational atmospheric correction from Gordon and Wang (1994) with NIR iteration was applied in that process.

The images of the corresponding dates to the oceanographic survey were 11 for MERIS and 19 for MODIS, most of them affected by clouds and haze. The MERIS image less affected by clouds, which was acquired on the 20th of May 2008, was selected and downloaded using the Eolisa interactive tool. This image was used to produce a chl-*a* map using the BEAM 4.6 program, available from: <http://www.brockmann-consult.de/beam>. Also, the MODIS image corresponding to the same date was downloaded and used to produce a chl-*a* map with the ENVI software (<http://www.exelisvis.com/>).

There was a maximum time-lag (i.e. absolute time difference between *in situ* and satellite measurements) lower than 3 hours. On the day the image was acquired, 5 stations were sampled. The MERIS bands used were 4 (510 nm) and 5 (560 nm). The reflectance band values were divided by π since the MERIS reflectance is defined as (ESA 2006):

$$\rho_w = \pi \frac{L_w(\lambda)}{E_s(\lambda)} \quad (\text{eq. 2.1})$$

Where E_s , is the downwelling irradiance and L_w the water-leaving radiance (after removal of air-sea interface reflection).

The algorithm with the best correlation between the band ratios and chl-*a*, was represented using the “band math” application of the program. Cloud and land masks, provided by the MERIS and MODIS, level 2 products were applied.

In addition, the reflectance bands of the MODIS and MERIS level 2 products from the 20th of May 2008 were matched-up with *in situ* reflectance measurements. Thus, the remote sensing reflectance bands were compared with the *in situ* measurement acquired at the same location and day. The ratio between the satellite and the *in situ* values was calculated as a way to evaluate the correspondence between *in situ* and satellite reflectance measurements.

3. RESULTS

The 68 stations sampled during the Bioman survey showed temperatures ranging between 15.0 and 17.8 °C, with salinities between 25.3 and 35.7. Water masses influenced by river discharges were colder (15.0 °C) and had lower salinities (25.3), than marine (offshore) water masses. The chl-*a* ranged between 0.10 and 9.00 mg.m⁻³. Most of the samples had concentrations below 4 mg.m⁻³, except for 5 samples. TSM values ranged between 0.68 and 14.15 g.m⁻³, although most recorded values were below 3.00 g.m⁻³ and only a few above. Turbidity ranged between 0.01 and 7.50 NTU, with most of them being below 3 NTU. CDOM data ranged between 0.1 and 1 m⁻¹ (Absorbance at 460 nm), where most recorded absorbances were below 0.4 m⁻¹, except for 8 of the measurements.

Figure 2.2 shows the R_{rs} spectra of a subset of sampling stations, obtained at the sea water surface, during the survey. The spectral range shown in the figure was limited to 450-750 nm, due to the high noise recorded at wavelengths below and above this range, when measurements were performed on the field. Three different types of spectra, corresponding to different water masses, could be distinguished: (1) oceanic

waters (low chl-*a*, low TSM, low CDOM) (2) plume influenced waters (High chl-*a*, medium TSM, high CDOM); and (3) estuarine waters (low chl-*a*, high TSM, high CDOM). The estuarine water spectrum in Figure 2.2 corresponds to the station located inside the Gironde estuary (Figure 2.1), with a salinity of 25.3. The oceanic water spectrum shows a peak emerging in the blue area around 450 nm, which decreases with higher wavelengths. With the increasing influence of river freshwater, a depression can be observed in the blue area of the spectrum around 450 nm, as well as a peak emerging between 500 and 600 nm. Both depressions and peaks are magnified with increasing chl-*a*, TSM and CDOM. With increasing freshwater input from the river, the highest spectral peak shifted towards higher wavelengths. Also, a peak of lower magnitude appears around 670 and 700 nm (0.001-0.002 sr⁻¹).

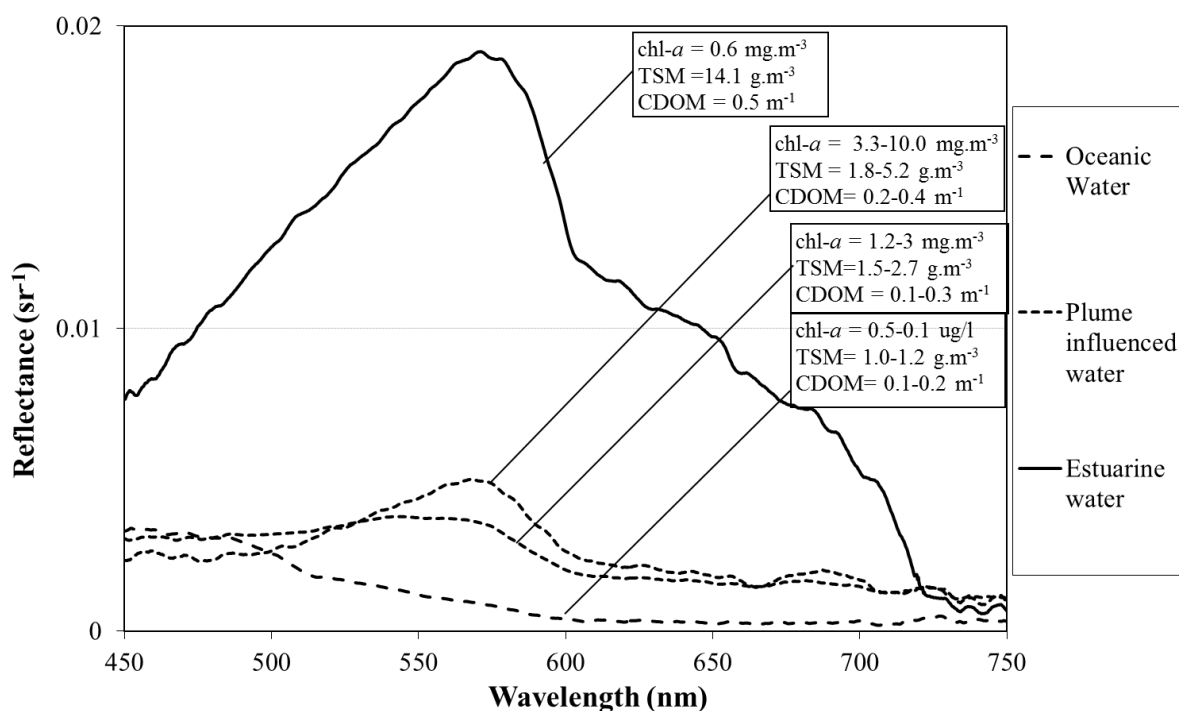


Figure 2.2. Subset of samples showing R_{rs} and corresponding chl-*a*, TSM and CDOM, for the Bay of Biscay, where three main water types can be distinguished spectrally. R_{rs} measurements were performed with a boxcar width of 8 plus an averaging of 10 adjacent channels was performed for display purposes.

The band ratios obtained from the survey data were calculated and correlated to chl-*a* (Table 1). The highest correlation for MERIS bands is obtained between the log-transformed ratio of reflectance values at 510 and 560 nm of wavelength, R_{rs510}/R_{rs560} , and the log-transformed chl-*a* (coefficient of determination $r^2 = 0.76$). The highest correlation with MODIS bands and log-transformed chl-*a* was obtained with

band reflectances at 488 and 551 nm of wavelength. However, when the station with the highest TSM (14.15 g.m^{-3}) is removed from the dataset, the r^2 value increased for all the correlations (r^2 for $R_{rs510}/R_{rs560} = 0.81$; r^2 for $R_{rs488}/R_{rs551} = 0.80$), indicating a negative effect of TSM concentration on the chl-*a* algorithms (Figures 2.3 and 2.4). On the other hand, there is a slight decrease in the r^2 values when the 8 stations with the highest TSM values were removed (Table 1). In addition, when the 8 stations with the highest CDOM values were removed from the dataset ($n = 56$), there is a significant increase in all of the band ratio correlations with chl-*a* (Table 1). Once again, the best correlation was obtained with R_{rs510}/R_{rs560} and R_{rs488}/R_{rs551} ($r^2 = 0.83$; $r^2_{jac} = 0.82$).

Table 2.1. Band ratios and chl-*a* with corresponding r^2 , p -values and Jackknife validation r^2 values.

R_{rs} Band ratio	All data (n=64)			Data without highest CDOM stations (n=56)			Data without highest TSM stations (n=56)		
	r^2 chl- <i>a</i> vs.	p -value	Jackknife validation r^2	r^2 chl- <i>a</i> vs.	p -value	Jackknife validation r^2	r^2 chl- <i>a</i> vs.	p -value	Jackknife validation r^2
	Ratio			Ratio			Ratio		
443/555	0.50	0.00	0.45	0.62	0.00	0.60	0.61	0.00	0.58
490/555	0.39	0.00	0.35	0.44	0.00	0.41	0.37	0.00	0.33
510/555	0.75	$<2.2 \times 10^{-16}$	0.66	0.81	$<2.2 \times 10^{-16}$	0.80	0.74	$<2.2 \times 10^{-16}$	0.72
490/550	0.40	0.00	0.31	0.44	0.00	0.41	0.37	0.00	0.33
443/550	0.49	0.00	0.44	0.62	0.00	0.60	0.58	0.00	0.56
443/560	0.50	0.00	0.41	0.63	0.00	0.61	0.50	0.00	0.44
490/560	0.72	$<2.2 \times 10^{-16}$	0.67	0.81	$<2.2 \times 10^{-16}$	0.80	0.72	0.00	0.71
510/560	0.76	$<2.2 \times 10^{-16}$	0.68	0.83	$<2.2 \times 10^{-16}$	0.82	0.76	$<2.2 \times 10^{-16}$	0.74
443/551	0.69	$<2.2 \times 10^{-16}$	0.44	0.63	0.00	0.61	0.56	0.00	0.53
488/551	0.71	$<2.2 \times 10^{-16}$	0.67	0.80	$<2.2 \times 10^{-16}$	0.79	0.74	$<2.2 \times 10^{-16}$	0.72

Figure 2.3 represents the correlation between the *in situ* and the predicted chl-*a*, using the R_{rs510}/R_{rs560} algorithm (named Local MERIS algorithm I):

Local MERIS Algorithm I:

$$\text{chl-}a = 10^{-1.432R + 0.388}; \text{ where } R = \log_{10}(R_{rs510}/R_{rs560})$$

This algorithm it is compared with the MERIS OC4E algorithm, adjusted to our dataset. The algorithms were calculated with the reflectance value at the central wavelength of the corresponding band. The calculations performed considering the wider bandwidths for SeaWiFS (20 nm), MODIS (20 nm) and MERIS (10 nm), did not improve significantly the resulting r^2 (increased by 0.03), so only the calculations performed with the central wavelengths are shown.

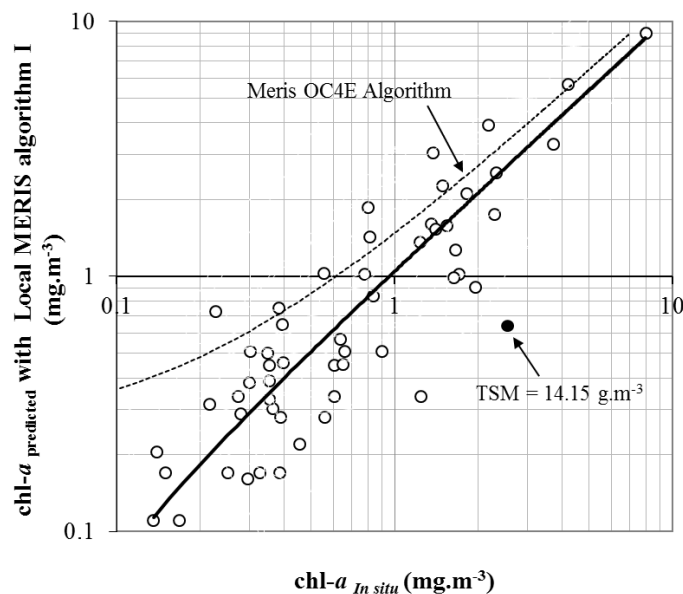


Figure 2.3. Linear regression between the predicted chl-*a* by the Rrs510/Rrs560 band ratio algorithm (Local MERIS algorithm I) and *in situ* chl-*a* (in logarithmic scale). The OC4E algorithm adjusted to our dataset is shown in dashed lines.

The MODIS bands equivalent to the ones used by the MERIS algorithm, the $R_{rs\ 488}$ and $R_{rs\ 551}$ bands, were used to develop a Local Algorithm I to apply to MODIS imagery:

Local MODIS Algorithm I:

$$\text{chl-}a = 10^{-1.32 R + 0.501}; \text{ where } R = \log_{10}(R_{rs\ 488}/R_{rs\ 551})$$

The chl-*a* predicted with this algorithm was compared to *in situ* chl-*a* (Figures 2.4) as well, but the correlation coefficient (r) decreased in comparison with the MERIS algorithm (MODIS: $r = 0.75$ vs. MERIS: $r = 0.8$).

The algorithms tested (OC4, OC3M, OC4E, Carder MODIS) presented lower R^2 values than the $R_{rs\ 510}/R_{rs\ 560}$ and $R_{rs\ 488}/R_{rs\ 551}$ band ratios, with the best of the four being the one obtained with the OC4E algorithm (Table 2.2). Figure 2.5 shows the linear regression between chl-*a* that was estimated using different algorithms and that was measured *in situ* chl-*a*.

Table 2.2. Chl-*a* algorithms for different sensors tested for the Bay of Biscay *in situ* acquired data and resulting jackknife validation r^2 values.

Sensor	Equation	Maximum ratio value (R)	Jackknife validation r^2
MODIS/OC3M	$\text{chl-}a = 10^{(0.2830 - 2.753R + 1.457R^2 - 0.659R^3 - 1.403R^4)}$	$R_{rs}(443;490)/R_{rs}(550)$	0.546
MERIS OC4E	$\text{chl-}a = 10^{(0.368 - 2.814R + 1.456R^2 - 0.768R^3 - 1.292R^4)}$	$R_{rs}(443;490;510)/R_{rs}(560)$	0.587
SeaWiFS/OC4v4	$\text{chl-}a = 10^{(0.366 - 3.067R + 1.930R^2 + 0.649R^3 - 1.532R^4)}$	$R_{rs}(443;490;510)/R_{rs}(555)$	0.558
Carder MODIS (Chlor_a_3)	$\text{chl-}a = 10^{(0.3147 - 2.859R + 2.007R^2 - 1.730R^3)}$	$R_{rs}(443;488)/R_{rs}(551)$	0.582
Adjusted OC4E	$\text{chl-}a = 10^{(-0.215 - 0.2934R + 0.53R^2 + 0.141R^3 + 0.553R^4)}$	$R_{rs}(443;490;510)/R_{rs}(560)$	0.601

These algorithms were applied to the single MERIS image acquired with low cloud coverage (Figure 2.6) during the oceanographic survey (20th of May 2008) and to the MODIS image acquired on the same day. The biggest difference of estimated chl-*a* obtained between the algorithms developed and the chl-*a* measured *in situ*, was of 1 mg.m⁻³ and the smallest of 0.2 mg.m⁻³.

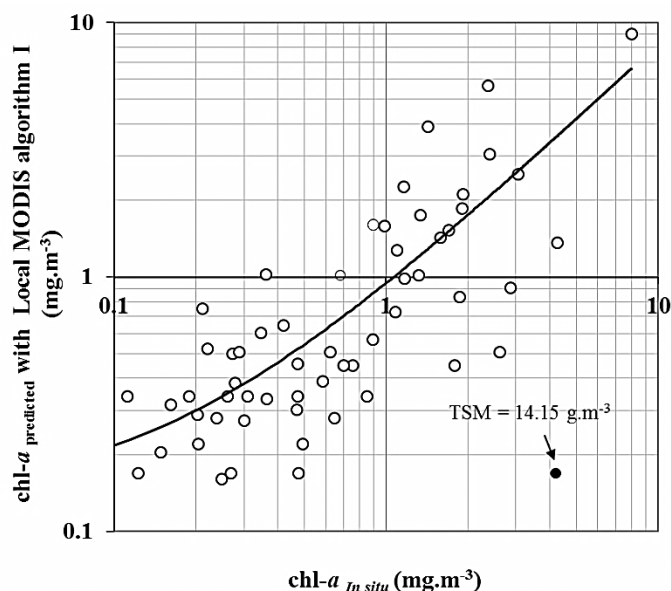


Figure 2.4. Linear regression between the predicted chl-*a* by the R_{rs488}/R_{rs551} band ratio algorithm (Local MODIS algorithm I) and *in situ* chl-*a* (in logarithmic scale).

The chl-*a* maps (2.6 and 2.7) show that the areas with the highest chl-*a* are located close to the French coast and river mouths, corresponding with the brownish coloured water in the RGB image (Figure 2.1).

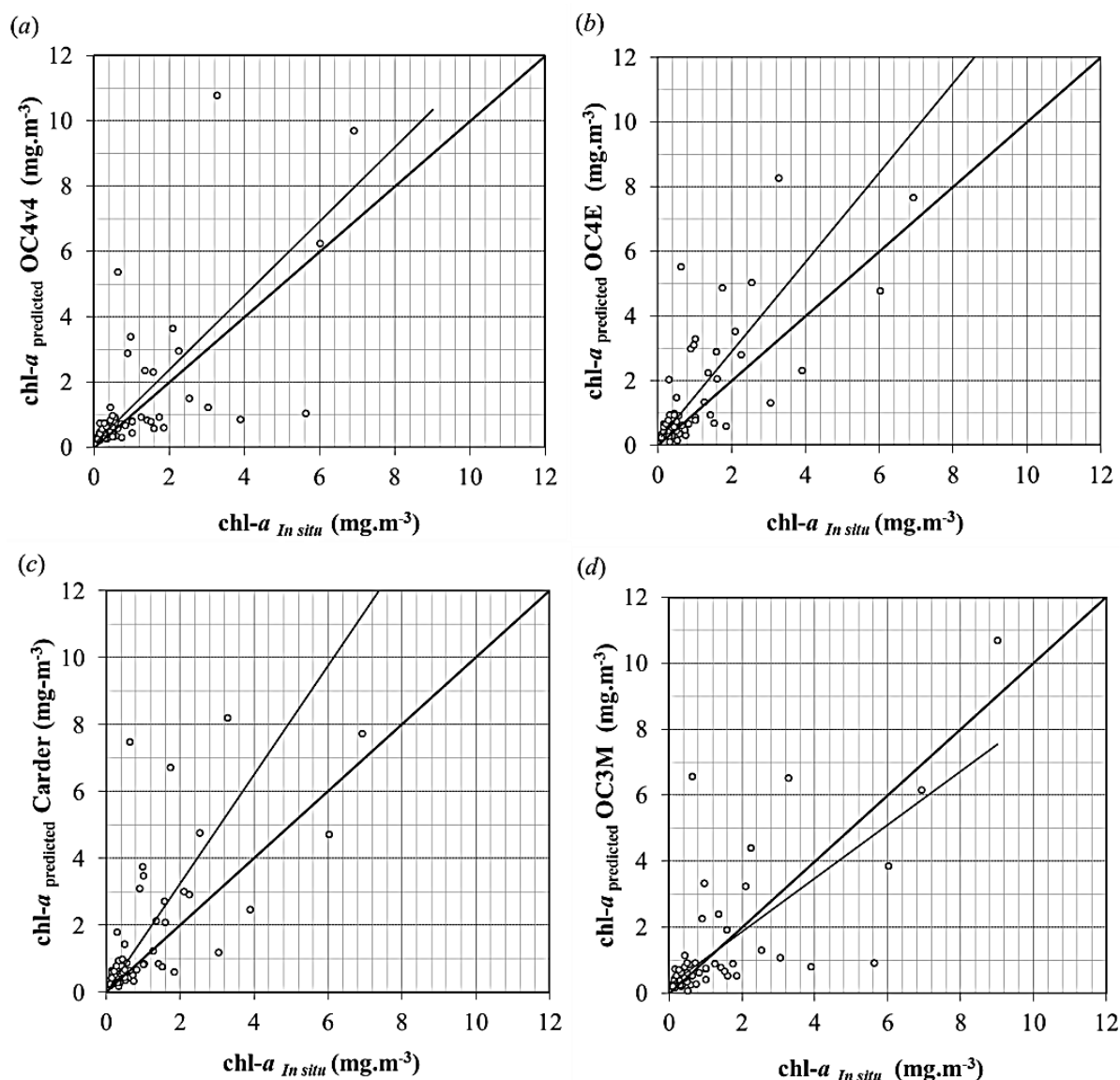


Figure 2.5. Linear regression between *in situ* chl-*a* and algorithm estimated chl-*a*: (a) OC4v4, (b) OC4E, (c) Carder (Chlor_a_3) and (d) OC3M.

Only five match-ups could be performed between *in situ* and satellite reflectance measurements, as only one cloud and flag free MERIS image (for the entire bay) acquired during the survey (20th of May 2008). The ratio between the MERIS reflectance bands 443 nm, 510 nm and 560 nm and the *in situ* reflectances at those same wavelengths were 1.5, 1.6 and 1.2. The ratios between the MODIS bands at wavelengths 443 nm, 488 nm and 551 and the *in situ* reflectances at those same wavelengths were 1.14, 0.94 and 1.02, respectively. The *in situ*-satellite scatterplots are presented in the appendix.

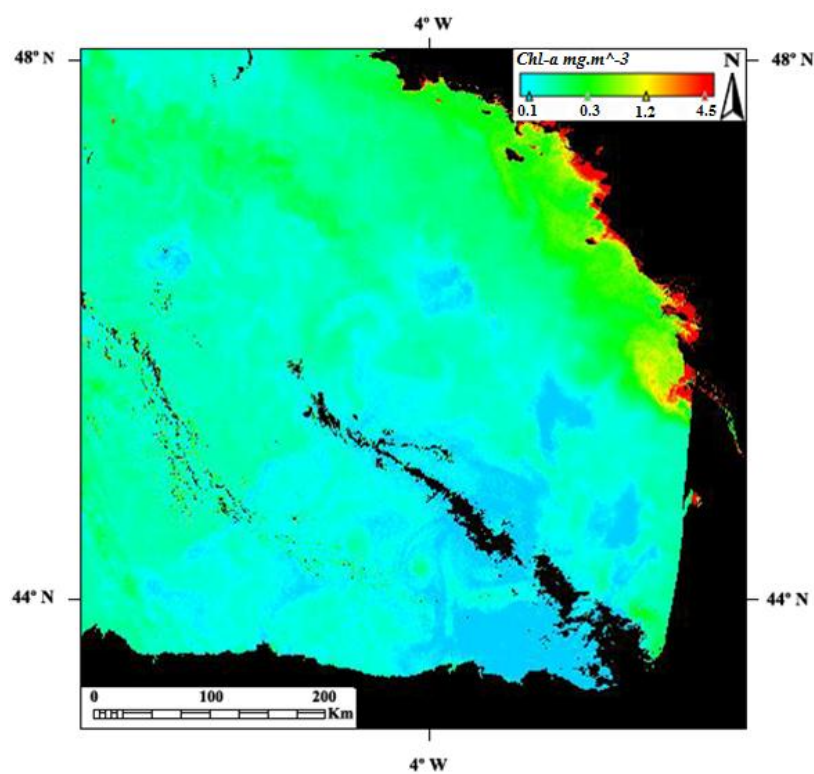


Figure 2.6. Chl-a map generated using a MERIS (FR) image acquired during the survey (20th May 2008) and the linear relationship established between chl-a and the R_{rs510}/R_{rs560} (Local MERIS algorithm I).

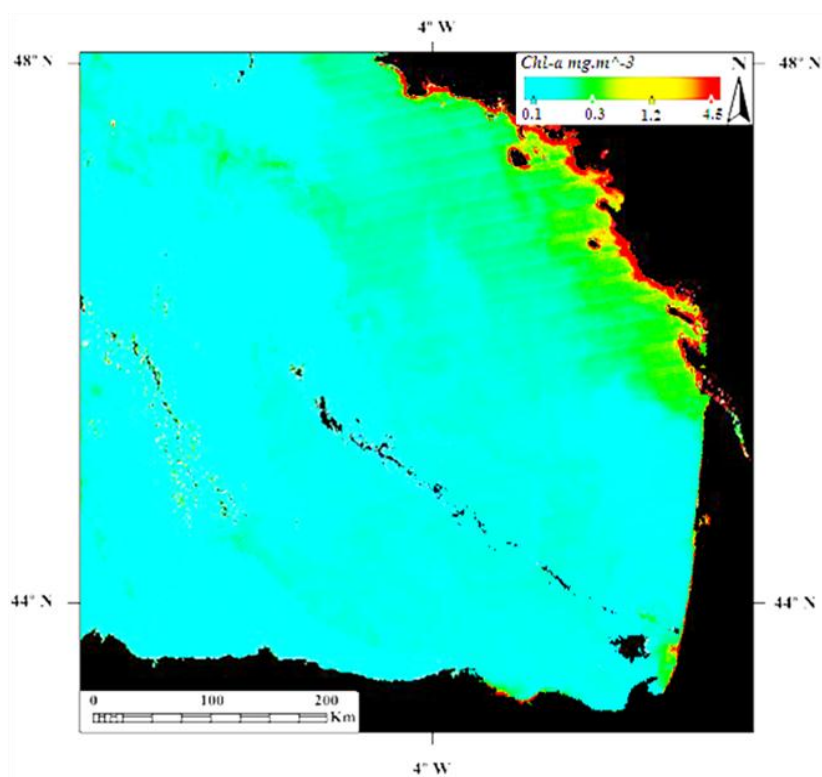


Figure 2.7. Chl-a map generated using a MODIS image acquired during the survey (20th May 2008) and the linear relationship established between chl-a and the R_{rs488}/R_{rs550} (Local MODIS algorithm I).

4. DISCUSSION

4.1. Radiometric measurement procedure

The spectral range of the HR4000CG radiance measurements for this survey was limited to 440-700 nm, due to the high background noise obtained beyond this spectral region on the field measurements. An anomalous peak appears around 430 nm, which cannot exist in nature, i.e. compared to published spectra (Schalles 2006). This is due probably to an instrumental error, as it can be observed in all the reflectance spectra. There is also a peak at 760 nm, which corresponds to the oxygen absorption feature (Schott 1997). The appearance of this peak in reflectance spectra is due to the fact that both radiance and irradiance measurements were not performed simultaneously, as the absorption by atmospheric oxygen should not be seen in aquatic spectra. Most remote sensing chl-*a* algorithms use wavelengths within the 440-700 nm range; therefore, they are not affected by these anomalous peaks. There could also be errors due to the sources mentioned in chapter I, such as the self-shading and/or wave effect. Measurements were performed seeking to minimise uncertainty, and hence error, to the extent possible.

Definite conclusions on the correspondence between *in situ* and satellite reflectance measurements cannot be derived due to the low number of match-ups obtained. Still, the resulting ratios calculated (satellite-*in situ*) denote an overestimation of the MERIS and MODIS bands. This overestimation was observed as well by Wang and other authors, in the IOCCG (2009) report on atmospheric corrections. Simultaneous measurements in the field with other spectrometers, could be used as complementary validation of the radiometric data obtained.

4.2. Estimation of chlorophyll-a

The spectral signatures obtained for the different types of waters coincide with the spectral signature presented by Schalles (2006). For instance, from the water samples collected, a shift of the highest peak towards higher wavelengths (from 500 nm, towards 600 nm) can be noted with increasing river load influence. Interestingly, it has been reported that in sediment laden waters, there is an increase in reflectance that affects the whole of the spectrum (Morel and Bélanger 2006). However, the green part

of the spectrum (510-570 nm) is heightened anomalously, when compared to Case 1 waters with the same chl-*a* (Bricaud and Morel 1987). Spectral signatures acquired during the survey show also a depression increase, with increasing chl-*a* in the blue area of the spectrum (440 nm); this corresponds to the maximum absorption wavelength of chl-*a* (Morel and Prieur 1977, Sathyendranath et al. 1987). In the range near to 560 nm, absorption by chl-*a* is weak so there is a noticeable increase in reflectance, as a result of the increase in backscattering (Morel 2006). In fact, the phytoplankton absorption minimum is considered to be around 550-560 nm, by remote sensors such as SeaWiFS or MODIS (IOCCG 1998).

The analysis of *in situ* spectral signatures and the biogeochemical measurements acquired over the shelf of the Bay of Biscay has revealed a strong relationship between chl-*a* and R_{rs} . The highest correlation values obtained correspond to band ratios used in the SeaWiFS OC4, the MERIS OC4E and the MODIS OC3 algorithms. Hence, a polynomial, potential or exponential fit to these band ratios, with chl-*a*, could be used as an algorithm for the retrieval of chl-*a* in the waters surveyed. In contrast, when validating the dataset with the algorithms used by the remote sensors with the Jackknife procedure, the resulting r^2 values were lower than the ratios (Tables 1 and 2).

The correlation between chl-*a* and the band ratios R_{rs510}/R_{rs560} , R_{rs510}/R_{rs555} , R_{rs490}/R_{rs560} and R_{rs488}/R_{rs551} improves when the station with the highest TSM (Station 42: $14.1 \text{ g}\cdot\text{m}^{-3}$) is removed from the data set, while all others sampling stations presented $\text{TSM} < 5.2 \text{ g}\cdot\text{m}^{-3}$. This pattern suggests the influence of TSM on these correlations. The increase in particulate matter would have caused the ratio-chl-*a* relationship at this station to be different with respect to the other stations. Station 42 was located inside of the Gironde estuary (Le Verdon), where TSM surface concentrations of between 35.0 and $2072.0 \text{ g}\cdot\text{m}^{-3}$ have been reported during summer time (Doxaran et al. 2002). Conversely, when the 8 stations with the highest TSM concentrations ($< 2.8 \text{ g}\cdot\text{m}^{-3}$) were removed, the correlations again decreased ($r^2 = 0.7$, for the R_{rs510}/R_{rs560}). This suggests that there is only the effect of highly turbid waters on the relationship. When the 8 stations with the highest CDOM absorbance ($> 0.4 \text{ m}^{-1}$) were removed from the dataset, there was a significant increase of the r^2 values of all the ratios. The highest relationship was found also with R_{rs510}/R_{rs560} ($r_{jac}^2 = 0.8$); this implies that CDOM is affecting all of the bands considered, i.e. channels between 443 and 560.

Thirty-five stations of our data set had a dominant phytoplankton component (High chl-*a*, low TSM and CDOM), while 29 of the stations were located in waters where chl-*a* was not the dominant constituent (4 stations were discarded). CDOM, in these 29 stations, presents values above 0.4 m^{-1} and 2 stations showed TSM values above 5.0 g.m^{-3} . Considering the IOCCG (2000) optical classification of water bodies, 35 stations would correspond to Case 1 waters and 29 to Case 2. On the other hand, most of the stations with dominant chl-*a* (26) have concentrations of below 1.0 mg.m^{-3} . The relationship derived between stations with chl-*a* lower than 1 mg.m^{-3} and R_{rs510}/R_{rs560} , resulted in an r^2 of 0.4; this suggests that there might be limitations in estimating chl-*a*, based upon reflectance with the spectrometer (field or satellite) in waters with low chl-*a*, as has happened with already-established algorithms (Hooker and McClain 2000). Water bodies where the phytoplankton component is not dominant (TSM or CDOM are dominant), show an even lower relationship with this band ratio ($r^2 = 0.2$).

In areas where phytoplankton dominates the water colour, while the scattering and absorbing components of seawater co-vary with chl-*a*, blue-green band-ratio algorithms are often successful, as phytoplankton absorbs more blue light than green. However, the precision of these algorithms can diminish when environmental conditions differ from those representative of the data set analysed, to derive empirically the covariance relationships (Carder et al. 2003). Thus, chl-*a* absorption by phytoplankton can change depending upon the species, nutrient concentration or lighting conditions. In Case 2 waters, substances that do not co-vary with chl-*a*, change the water optical conditions. This causes inaccuracies in the retrieval of pigment concentration on the basis of satellite imagery (Carder et al. 1991). The variability of in-water constituents, due to environmental changes such as upwelling currents waters or river run-off input, needs to be considered in algorithm parameterisation. Therefore, a large data set needs to be gathered, in order to develop robust empirical algorithms for the continental shelf of the Bay of Biscay, which take into account seasonal and local variations. In particular, chl-*a* algorithms for turbid coastal waters might incorporate the green to red band ratio, as those developed by Dall'Olmo and Gitelson (2005) and Gitelson et al. (2007).

The MERIS RGB image, corresponding to the oceanographic survey, illustrates the influence of coastal areas and river plumes; waters appear greener and darker than oce-

anic waters and the colours match the estimated high chl-*a* (Figure 2.5). The effect of coastal CDOM and TSM could have influenced also the chl-*a* estimation using the algorithm developed here, since it has been found that there is an effect of these parameters on the chl-*a*-ratio relationship.

This is a first approach towards the development of a regionally-parameterized algorithm, on the basis of the field spectrometer spectra and MERIS/MODIS images. In order to reach this objective, it is necessary to use a larger data set together with a more extensive study of the empirical relationships existing between water parameters and ‘apparent optical properties’. On-going research in specific areas (Northern Spain and Adour river mouth) will permit the enlargement of the data set for the development of more robust relationships.

Chapter III

Water quality monitoring in Basque coastal areas using a local chlorophyll-*a* algorithm and MERIS images

1. INTRODUCTION

The results presented in the previous chapter demonstrate that in optically-complex waters, such as coastal (affected by river outflows; Morel and Prieur 1977), the standard and global algorithms used in clear or “oceanic” waters reveal inaccuracies (IOCCG 2000). The input of suspended and dissolved substances by river discharges, alter the colour of the water, significantly affecting accurate chl-*a* estimation. This is because the absorption and backscattering of chl-*a* are affected by particulate and dissolved matter mainly discharged by river runoffs (Carder et al. 1991; Gohin et al. 2005). Further, chl-*a* is not the only absorbing pigment. Both photosynthetic and photoprotecting pigments are also present in algal cells and can affect the retrieval of chl-*a* with satellite imagery (Morel 2006). The pigment composition depends upon species and, for a given species, it can vary considerably with environmental conditions such as light, depth and nutrients. Usually, natural species communities are a mixture of many species, although a single species can proliferate and form blooms temporarily, due to favourable environmental conditions, such as nutrient enrichment. Remote sensing could be a useful tool for phytoplankton bloom mapping since, in many cases, the blooms are associated with increased or decreased brightness emanating from the water bodies, e.g. blooms of *Karenia brevis* (Cannizzaro et al. 2008, 2009), cyanobacteria *Trichodesmium spp.* (Woodruff et al. 1999) and coccolithophores (Siegel et al. 2007).

Hence, a characterisation and classification of the water masses, according to their biogeochemical characteristics, is useful to distinguish the parameters that could be causing retrieval inaccuracies. Such an issue has been studied elsewhere (IOCCG 2000), where the authors state that water constituents are region-specific, while regionally-parameterized empirical algorithms are useful to estimate accurately chl-*a* at a local scale.

1.1. Objectives

Using the Bay of Biscay water masses affected by Basque rivers runoff (Ferrer et al. 2009), as a case study, the objective of this investigation is to improve the local estimation of chl-*a* in coastal waters, using MERIS imagery; this sensor provides suitable spatial resolution (300 x 300 m) for coastal studies within the study area. For this purpose, four specific objectives are addressed: (i) the development of an empirical algo-

rithm, to estimate water surface chl-*a* for the optically-complex Basque coastal waters; (ii) the investigation of the influence of suspended matter, phytoplankton species and pigment content on the algorithm developed for the MERIS imagery; (iii) the comparison of the local algorithm to three ocean colour algorithms (OC4v6 (O'Reilly et al. 1998), Gitelson's MERIS 3 band algorithm (Gitelson et al. 2007), the OC5 (Gohin et al. 2002)), and the Carder empirical algorithm (Carder et al. 1999, 2003) and subsequent validation of all the algorithms with *in situ* data; and (iv) the application of the local algorithm to the MERIS images, for its comparison with an OC5 chl-*a* map.

2. MATERIAL AND METHODS

2.1. Oceanographic Surveys and Measurements

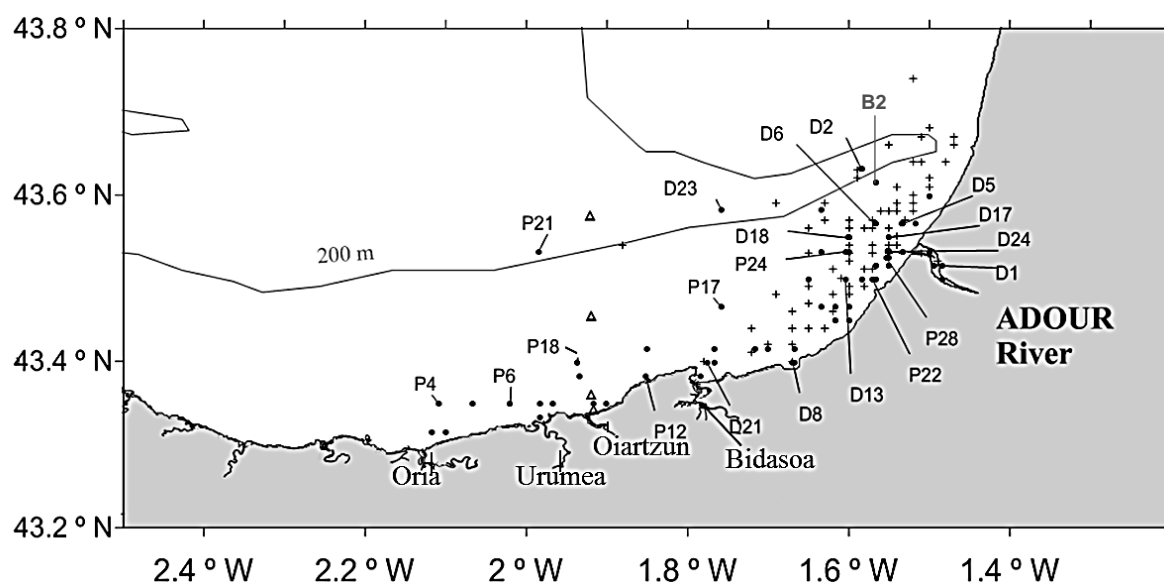


Figure 3.1. Location of the study area within the Bay of Biscay and oceanographic sampling stations of the Batel-1 (crosses +), Batel-2 (black circles ●) and the LQM surveys (triangles Δ). See text for details.

Two oceanographic surveys were undertaken within the study area (Figure 3.1): (i) the Batel-1 in June 2007, obtaining biogeochemical and optical data at 96 stations, as described in (Petus et al. 2010); and (ii) the Batel-2 survey, which was carried out during two different periods, in March-April 2009 and June 2009, when 56 measurements were performed. Additional measurements were performed at 4 stations belonging to the *Basque Littoral Monitoring Network* (LQM) between October 2008 and August 2009. The data from the Batel-2 survey are used to develop the local algorithm and the data from the Batel-1 and the LQM surveys are used to validate the algorithms.

At each station, conductivity, temperature, depth, light transmission and Photosynthetic Active Radiance profiles were obtained, while chl-*a* was estimated from CTD fluorescence, on continuous vertical profiles with a SeaBird 25 CTD. Fluorescence units were calibrated, regularly, against spectrophotometer measurements of chl-*a*, in natural water samples. Niskin bottles were used to obtain surface water samples, analysing: (i) total suspended matter concentrations (TSM), measured by filtration through pre-weighed Whatman GF/F filters, following the methodology detailed in Etcheber et al. (2007); and (ii) chl-*a*, measured by filtration of 1 to 2 l of surface water, at each station, using Whatman GF/C filters. Filters were frozen (-20 °C) immediately and chl-*a* was determined using spectrophotometry (following the Jeffrey and Humphrey protocols; 1975). During the Batel-1 survey, only 15 measurements of chl-*a* were performed with spectrophotometry. This methodology was used to determine chl-*a* concentration at all the stations during the Batel-2 survey and 15 during the Batel-1 survey. Turbidity was measured also *in situ* using nephelometry, in Nephelometric Turbidity Units (NTU). During the Batel-1 survey, dissolved organic carbon (DOC) measurements were performed. Pre-burned GF/F filters at 500 °C (diameter 25 mm, porosity 0.7 µm) and a glass syringe was used to perform the filtrations on board. The filtrated water was kept cold (4 °C) in Pyrex decontaminated flasks and acidified to a pH of 2. The DOC measurements were then performed by catalytic oxydation at high temperatures (Abril et al. 2002) by Etcheber at the Bordeaux 1 University (Petus 2009).

2.2. Optical Measurements

Optical signatures of coastal waters were quantified using Remote Sensing Reflectances (R_{rs}) measured using the TriOS spectroradiometers (see Methodology, in Froidefond and Ouillon (2005) and Petus et al. (2010)). The TriOS instrument was considered to be better suited for the measurements in coastal waters, where the sea water surface (e.g. coastal bathymetry, waves) and constituents' variability (concentration TSM, CDOM) is higher. The uncertainties related to fast changes that can occur on the field (e.g. rocking of the vessel, cloud movement) are reduced with TriOS equipment, as measurement of the downwelling and upwelling radiances are simultaneous; with the HR4000CG an approximate 10 minute lag exists between the two measurements, which could increase the measurement error. The TriOS instrument was made available

for the surveys presented in this chapter, but was not accessible for the previous survey (Chapter II).

Essentially, a minimum of 40 spectral measurements were recorded per sampling site, with a simultaneous data acquisition of an irradiance sensor (Ramses-ACC n°8108), oriented in the zenith direction, and a radiance sensor (Ramses-ARC n°8091) located approximately 2 cm below the water surface. The spectral resolution was 5 nm, between 350 and 950 nm. The R_{rs} was calculated using the equation 1 (see introduction). As the TriOS spectroradiometers are calibrated for measurements in air (Ohde and Siegel 2003), the calculation of $L_w(\lambda, 0^+)$ needs to incorporate both the variation in the refraction index, between the submerged and emerged measurements, and signal transmission through the water-air as interface reduced by the Fresnel reflectance (Froidefond and Ouillon 2005; Gitelson et al. 2008).

$$L_w(\lambda, 0^+) = F \times (t/n^2) \times L_u(\lambda, -2) \quad (\text{eq.3.1})$$

where the factor n is the index of water refraction ($n \approx 1.34$; Gordon and Morel 1983; Gitelson et al. 2008), t is the radiance transmittance ($t \approx 0.98$; Mobley 1994) and F is the immersion factor of the solid angle of the TriOS ($F \approx 1.796$; Ohde and Siegel 2003).

2.3. Phytoplankton groups and pigments

Phytoplankton species counts were incorporated in this study, to identify the species that could be affecting the retrieval of chl-*a*, with the algorithm developed (see below). Water samples were preserved with 1 ml of 25% glutaraldehyde, in 125 ml borosilicate bottles; these were maintained cold (4°C) and in the dark, until their analysis; this was undertaken within 3 months following collection. Standard methods were used for the taxonomic species identification and counting (inverted microscopy and Utermohl). This methodology is explained in more detail in Garmendia et al. (2011).

High Performance Liquid Chromatography pigment (HPLC) analysis was included, to determine the effect of the phytoplankton accessory pigments on the algorithm developed. The methodology followed is explained in more detail in (Zapata et al. 2000). The phytoplankton species and pigment analysis samples were selected based upon

their location, to have them uniformly-distributed throughout the study area, and on their chl-*a* concentration, which was previously determined with spectrophotometry.

2.4 Water mass classification

The coastal areas are influenced by river runoff that discharges suspended matter into the marine water bodies, affecting the correct retrieval of chl-*a* using remote sensors. In order to quantify the input of river freshwater into the marine system and identify the extension of the river plume, a stratification index was used (Sharp et al. 1986). This index defines the difference in salinity throughout the water column, by subtracting the bottom salinity value from the surface value, then dividing it by the depth of the bottom measurement. Such an index was calculated for 67 stations (since no CTD profiles could be performed for 3 of them and the stratification index could not be calculated); this was used to perform a cluster classification of water masses, together with other biogeochemical parameters such as water surface salinity, TSM and chl-*a*. The cluster classification was performed using the Ward's method (squared Euclidean distance), with the "pvclust" library (Suzuki and Shimodaira 2006) of the R programme (Venables and Ripley 2002). This procedure provides an hierarchical cluster, with an "Approximately Unbiased" *p*-value, computed by multiscale bootstrap resampling, and a "Bootstrap Probability" value. The separability of the groups classified with a *p*-value below 0.05 was tested according to its reflectance data, by means of a discriminant analysis. A cross-validation of the water mass groups classified correctly (i.e. using the biogeochemical and the spectral data), was performed to assess the discrimination capacity of spectral data. For this analysis, all the stations were used where chl-*a* spectrophotometric measurements were performed during both the Batel-1 (n=14) and Batel-2 (n=53) surveys and CTD profiles were available. The DOC data was not included in this analysis since this constituent was only measured during the Batel-1 survey.

2.5. Chlorophyll-*a* algorithm development

Several combinations of R_{rs} ratios of *in situ* spectral measurements, equivalent to reflectance bands provided by MERIS (wavelength of bands considered: 412.50, 442.50, 490.00, 510.00, 560.00, 620.00, 665.00, 681.25, 708.75 nm), were initially selected from the literature (O'Reilly et al. 1998; Carder 2004; Gitelson et al. 2007) and linearly regressed against the log-transformed chl-*a*.

The step-wise procedure (package “Mass”, (Venables and Ripley 2002)) was used to select the ratios that contributed significantly (with p -value<0.05) to the estimation of chl- a and to remove co-linearity. The best model obtained was validated using a jack-knife resampling procedure (Burnham and Anderson 2002), developed also with R language. More details on this procedure are provided in Chapter II. The developed algorithm was named “Local MERIS Algorithm II”, but it is referred in this chapter as local algorithm. The chl- a estimated with this algorithm is referred as predicted chl- a .

2.6. Evaluation of the local algorithm performance

The effect of several biophysical parameters on the selected algorithm was tested then using the Root-Mean-Square difference (RMS) with the following equation (Gohin et al. 2002):

$$\text{RMS} = \sqrt{\frac{\sum_{i=1}^n (V_{est,i} - V_{in\ situ,i})^2}{N}} \quad (\text{eq. 3.2})$$

Where, V_{est} is the predicted variable, $V_{in\ situ}$ is the *in situ* measurement, and N is the number of stations. The RMS was computed for the local algorithm, in relation to different concentrations of TSM, followed by concentrations of each estimated pigment. The RMS for the predicted chl- a was plotted against different concentrations of the tested parameter, to detect the effect of different concentration ranges on the algorithm. In the case of phytoplankton pigments, the relative concentration of each pigment to chl- a ($[\text{Pigment}]/[\text{Pigment}+\text{chl-}a]$) was expressed in terms of three different concentration intervals. A Kruskal-Wallis test (Kruskal and Wallis 1952) was performed between pigment groups to determine if the differences in RMS were significant. The data set used for the evaluation of the algorithm performance with respect to TSM, consists of all the stations where chl- a spectrophotometric measurements were collected during both the Batel-1 ($n=15$) and Batel-2 ($n=56$) surveys. Twenty-six and 20 stations respectively, were selected for the pigment and phytoplankton analysis. The DOC data was not included in this analysis since this constituent was only measured during the Batel-1 survey.

2.7. Algorithm comparison

Initially, 84 *in situ* measurements of $R_{rs}(\lambda)$ from the Batel-1 survey and 10 from the LQM, were used to run the four MERIS algorithms, i.e. OC4Ev6, Gitelson, Carder, OC5, and the local algorithm. The resulting chl-*a* estimates were compared with coincident *in situ* values of chl-*a* (measured with CTD fluorescence).

The OC4Ev6 is a fourth-order band algorithm that uses the maximum of three band ratios (see Table 1.1), depending upon the reflectance characteristics of the water type. It was developed firstly by O'Reilly et al. (1998, 2000) for the Sea-Viewing Wide Field-of-View Sensor (SeaWiFS). The version used in this study is the one adapted for the MERIS bands, while the coefficients were extracted from the Ocean color website (<http://oceancolor.gsfc.nasa.gov/>). In the OC4E version 6*, the coefficients were updated using an *in situ* data set from the second version of the NOMAD survey (Werdell and Bailey 2005).

The Gitelson's algorithm (Gitelson et al. 2007, 2008) is a semi-analytical model, containing reflectance in three MERIS spectral bands, in the red and near infra-red range of the spectrum; this is to retrieve chl-*a* concentrations in turbid productive waters (Table 1). This algorithm has been extensively validated for Case 2 waters, with variable chl-*a* concentrations of between 1 and 236 mg m⁻³ and TSM of between 0.2 and 213 g.m⁻³ (Gitelson et al. 2008, 2009).

The OC5 algorithm (Gohin et al. 2002, 2005) is a modified version of the OC4v4; this involves an empirical parameterisation of the 412 and 560 channels, related to the absorption of CDOM and scattering by TSM. The maximum ratio from the OC4 triplets is used to determine chl-*a* concentration. The nLw 412 and nLw 560 are obtained from a Look-up-table (LUT) based on the relationship of chl-*a* and R_{rs} from measurements performed in the English Channel and the Bay of Biscay. This algorithm estimates chl-*a* operationally between 0.2 and 65 mg.m⁻³. The OC5 chl-*a* estimates from R_{rs} were obtained using IDL programming.

The Carder empirical algorithm used in Chapter II was also considered in the comparison exercise (Carder 1999, 2003).

These algorithms are compared to the local algorithm developed during the course of this study, using a Taylor diagram; this shows the statistical results of the validation exercise, between chl-*a* estimated from *in situ* R_{rs} and chl-*a* measured *in situ* for the various algorithms. This type of diagram is useful in providing a general view of the main results, summarising algorithm performance (Taylor 2001).

Table 3.1. Description of satellite algorithms used.

Algorithm	Functional form
OC4Ev6 (O'Reilly et al. 1998, 2000)	$\text{Chl-}a = 10^{(a+bR+cR^2+dR^3+eR^4)}$ $R = \log_{10}\{\max[R_{rs}(443/560), R_{rs}(489/560), R_{rs}(510/560)]\}$ And the coefficients were determined by linear regression: a=0.3273; b=-2.9940; c= 2.7218; d=-1.2259; e=-0.5683
Gitelson (Gitelson et al. 2007)	Algorithm with MERIS bands: $\text{Chl-}a = 194.2 \times [R_{rs}^{-1}(665) - R_{rs}^{-1}(708)] \times R_{rs}(750) + 18.775$
OC5 (Gohin et al. 2002, 2005)	Chl- <i>a</i> = OC4 band ratio, nLw(412), nLw(555) triplet - based on look-up-table
Carder (empirical) (Carder et al. 1999, 2003)	$\text{Chl-}a = 10^{(0.3147-2.859R+2.007R^2+1.730R^3)}$ $R = \log_{10}\{\max[R_{rs}(443/551), R_{rs}(489/551)]\}$ With MERIS bands $R = \log_{10}\{\max[R_{rs}(443/560), R_{rs}(489/560)]\}$
Local algorithm developed with Batel 2 data	$\text{Chl-}a = 10^{\left[1.66-1.09 \times R_{rs}\left(\frac{510}{560}\right)-2.39 \times R_{rs}\left(\frac{708}{681}\right)+1.69 \times R_{rs}\left(\frac{708}{665}\right)\right]}$

The *in situ* chl-*a* observations ("reference" field) are represented on the x-axis of the diagram by their standard deviation (σ_r). The algorithm chl-*a* outputs ("test" field) are represented by points at a radial distance from the origin equal to the deviation of predicted chl-*a* values, and the cosine of the angle between the radial and the x-axis; this is the correlation coefficient between the algorithm-predicted chl-*a* concentration and the *in situ* measured chl-*a*. Then, the centered root-mean-square (RMS) difference between the predicted and observed patterns is proportional to the distance to the point on the x-axis identified as observed. Hence, the position of the algorithm points illustrates, at the same time: the level of correlation with the reference observations; a comparison of the standard deviation reproduced by the algorithm output, with respect to that of the reference field; and the bias between the two fields and the RMS differences.

On the basis of the observed chl-*a* (r) and the chl-*a* predicted (f) by the algorithms, the correlation coefficient (R), the centered RMS difference (E), and the standard de-

viations of the predicted (σ_f) and the observed chl-a concentration (σ_r), have been derived from the following formulae (extracted from: Taylor 2001):

$$R = \frac{\frac{1}{N} \sum_{n=1}^N (f_n - \bar{f})(r_n - \bar{r})}{\sigma_f \sigma_r} \quad (\text{eq. 3.3})$$

$$E^2 = \frac{1}{N} \sum_{n=1}^N [(f_n - \bar{f}) - (r_n - \bar{r})]^2 \quad (\text{eq. 3.4})$$

$$\sigma_f^2 = \frac{1}{N} \sum_{n=1}^N (f_n - \bar{f})^2 \quad (\text{eq. 3.5})$$

$$\sigma_r^2 = \frac{1}{N} \sum_{n=1}^N (r_n - \bar{r})^2 \quad (\text{eq. 3.6})$$

2.8. MERIS imagery

MERIS images full resolution FR (300 x 300 m) and reduced resolution RR (1040 m x 1160m) images were used in this chapter. The only MERIS cloud-free image available for the Batel-1 survey period was acquired on the 5th June, 2007. The geolocated, atmospherically-corrected, reduced resolution (RR) level 2 product was downloaded from the ESA ftp server. The RR product corresponds to the third ESA reprocessing, performed in June 2011. The level 1 FR geolocated product for the same day was also downloaded. Radiometric re-calibration and the atmospheric corrections for case 2 waters (Schroeder et al. 2007; Doerffer 2008) was applied to the FR product with the BEAM-Visat (version 4.9) software.

The MERIS bands selected initially from the literature, then selected by the step-wise procedure and used to generate the chl-a map, were 4 (510 nm), 5 (560 nm), 7 (665 nm), 8 (681) and 9 (708). The chl-a estimated by the developed algorithm was generated with these bands and the BEAM-Visat. The resulting FR and RR chl-a maps were then compared the chl-a map of the same day generated by the OC5 algorithm (Gohin et al. 2002). The OC5 chl-a map was downloaded from Ifremer's ftp server*.

Satellite-*in situ* data match-ups were performed with reflectance spectra and chl-a concentration (measured using fluorescence of the CTD instrument) derived with the

local algorithm, with the FR MERIS product. Satellite and *in situ* measurements with a maximum time lag of 3 hours were used.

Additionally, a k-means cluster analysis was performed using the KM analysis tool** of the Beam-Visat software, to assess the possibility of classifying superficial water masses using the MERIS FR atmospherically-corrected reflectance bands. The bands selected by the algorithm (bands 4, 5, 7-9) in section 2.5 were selected for this analysis. The cluster algorithm classifies the pixels in a scene with a given number of clusters k , in this case the same number of clusters as in section 2.4 and the reflectance bands. First, the algorithm randomly chooses k pixels whose samples define the initial cluster centres. Then it assigns each pixel to the nearest cluster centre as defined by the Euclidean distance and recalculates the cluster centres as the arithmetic means of all samples from all pixels in a cluster. This last step is repeated until the convergence criterion is met, in this case a number of iterations of 100. The classification of the stations sampled within 3 hours of the image acquisition were then compared to the classification of the samples performed using the optical and biogeochemical data (explained in section 2.4).

3. RESULTS

3.1. Description of biophysical measurements

Measurements of salinity, temperature, TSM, turbidity, chl-*a* and stratification index, for the 84 measurements from the Batel-1 survey, ranged from 0.1 to 33.7, 17.0 to 22.2 °C, 0.3 to 145.6g.m⁻³, 0.01 to 188.20 NTU, and 0.11 to 9.57 mg.m⁻³, respectively. More details on the dataset can be found in (Petus et al. 2010). The same biophysical measurements were performed during the Batel-2 survey. Temperature measurements ranged between 12.3 and 20.1 °C. For the Batel-2 surveys, there was a seasonal difference between the two survey periods, with the lowest temperatures being measured in March-April and the highest in June. The average salinity was 32.4 ± 5.1: only four stations showed values below 28 - two were measured in the estuary and two in the river mouth. TSM ranged between <0.1 and 27.5 g.m⁻³, although 90% of the stations sampled had values of below 3 g.m⁻³; the average was 2.2 ± 4.0 g.m⁻³ and only the samples in the estuary showed concentrations greater than 4 g.m⁻³. Turbidity measurements

**<http://www.brockmann-consult.de/beam/doc/help/clusteranalysis/KMeans.html>

ranged between <0.1 and 20.7 NTU, with an average value of below 1.4 ± 3.2 NTU. A high percentage of the measurements (91%) showed turbidity values below 3 NTU; only 3 stations showed values above 5 NTU. Chl-*a* varied between 0.2 and 4.9 mg.m^{-3} while on average, the values were $2.0 \pm 1.2 \text{ mg.m}^{-3}$, with 47% of the measurements being above a concentration of 2 mg.m^{-3} . The DOC varied between 0.1 and 10 mg.m^{-3} .

3.2. Water mass classification

From both of the surveys, 67 stations (i.e. all the stations where chl-*a* was measured with spectrophotometry- 53 from the Batel-1 survey and 14 from the Batel-2 survey) were included in the cluster classification with the biogeochemical data, which provided three main water masses (referred to as I, II, and III). The water constituent concentrations for each type and for the complete dataset used in this water classification are listed in Table 3.2. Type I showed the lowest salinity values (below 28), and the highest TSM (27.7 g.m^{-3}) and turbidity values (20.7 NTU). Surface water chl-*a* for Type I was on average 9 mg.m^{-3} . All of the stations were located inside the estuary, or very close to the river mouth. Type II showed salinities of 32.0 ± 1.7 and the average chl-*a* was the highest of the three types ($3.16 \pm 0.6 \text{ mg.m}^{-3}$). The sampling stations were located close to the river mouth areas, although farther offshore than Type I stations. Type II is associated with clearer water than Type I, but is influenced still by river runoff. Type III had the lowest water constituent concentrations together, in some cases, with a turbidity of 0.3 ± 0.2 NTU. The stations were located farther away from the river mouth areas than the two other types.

Table 3.2. Mean and standard deviation values for the biogeochemical characteristics of the water masses identified by hierarchical clustering and average values, for both the Batel-1 (only the 15 stations with chl-*a* estimated spectrophotometrically) and the Batel-2 survey (TSM: Total Suspended Matter concentration).

Type/ Surveys	Surface Salinity	Temperature (°C)	TSM (g.m^{-3})	Turbidity (NTU)	Chl- <i>a</i> (mg.m^{-3})	Stratification index	DOC (n=15) (mg.m^{-3})	Number of stations
I	22.4 (± 10.8)	18.3 (± 2.6)	7.0 (± 5.1)	2.5 (± 1.5)	9.0 (± 2.1)	0.48 (± 0.38)	3.9 (± 0.6)	8
II	32.0 (± 1.7)	17.2 (± 3.3)	1.5 (± 0.5)	0.9 (± 0.4)	3.2 (± 0.6)	0.10 (± 0.09)	4.2 (± 0.9)	33
III	34.5 (± 0.8)	15.4 (± 3.3)	0.8 (± 0.3)	0.3 (± 0.2)	0.9 (± 0.5)	0.08 (± 0.06)	1.6 (± 1.4)	26
Batel-1 (average)	30.5 (± 2.6)	19.2 (± 1.4)	3.0 (± 2.6)	1.9 (± 1.7)	4.2 (± 3.2)	0.16 (± 0.10)	3.1 (± 1.6)	15
Batel-2 (average)	32.4 (± 5.1)	15.6 (± 3.3)	2.2 (± 4.0)	1.4 (± 3.2)	2.2 (± 1.2)	0.12 (± 0.13)	-	56

Stations with the highest content of TSM and lowest salinity values are concentrated around the river mouth and coastal areas (Type I), while the other two types have variable locations within the study area. The correlation between salinity and TSM for the 15 Batel-1 stations ($r^2=0.64$) and for the Batel-2 dataset ($r^2=0.84$) are both high and significant (p -values=0.005 and 0.0006, respectively); this indicates the river origin of the particles (Figure 3.2, (a)). The high positive correlation between the TSM and turbidity ($r^2=0.99$, p -value=0.01, for Batel-2; and $r^2=0.94$, p -value=0.001, for Batel-1 (see Figure 3.2 (b)), indicates that TSM supplied by river runoff affects the optical properties of the surface waters in the study area.

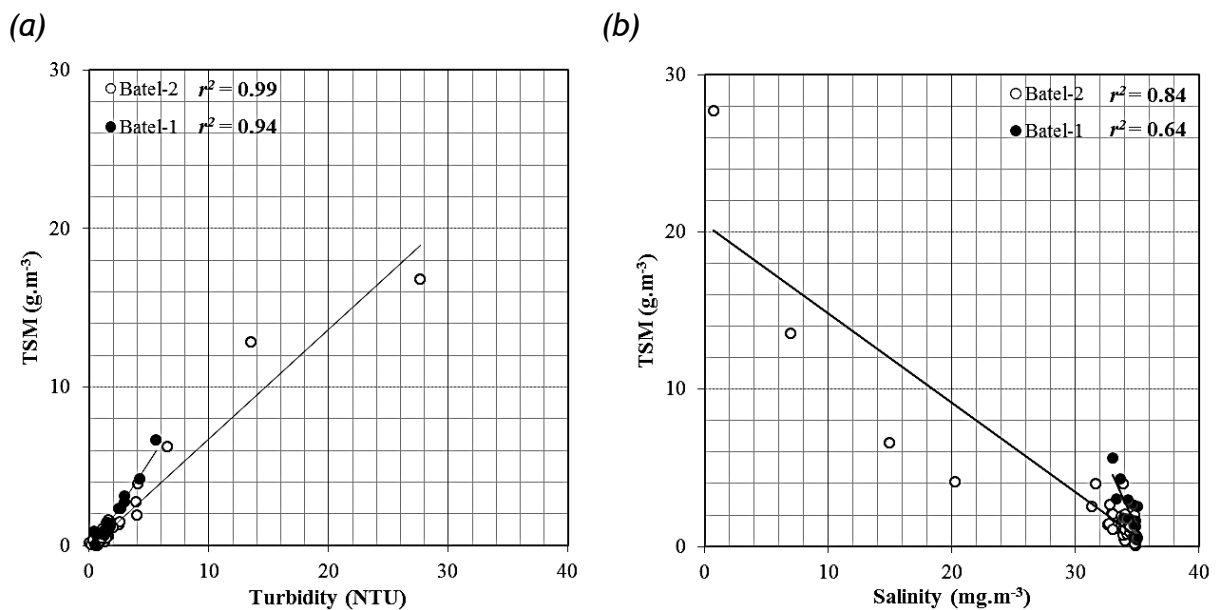


Figure 3.2. Linear regression for both Batel surveys between (a) Total Suspended Matter (TSM) and salinity and (b) TSM and turbidity.

The DOC data was not included in the classification, due to the low number of measurements ($n=14$), but the Batel-1 stations included in the defined classes, were examined. They showed DOC concentrations around 3-5 mg.m⁻³ in water mass Type I and variable concentrations in Type II, between 3 and 6 mg.m⁻³. Stations corresponding to Type III presented variable DOC concentrations as well, between 0.1 and 3.5 mg.m⁻³, similar to those of the other water types.

3.3. Radiometric *in situ* measurements

The three types of water masses were used to perform a discriminant analysis, using the *in situ* reflectance data measured for each station. Seventy averaged spectra (one per station) were acquired during the sampling surveys, with an amplitude variation of

between 1.6×10^{-2} and $3.2 \times 10^{-2} \text{ sr}^{-1}$, for both surveys. Subsequently, for the discriminant analysis, each spectra was assigned its corresponding water Type (I, II, or III) determined by the cluster analysis of the biogeochemical parameters; this resulted in 80% of the cross-validated grouped cases being classified correctly (Table 3). The three stations not used in the biogeochemical classifications were included in this analysis, because of the TSM, salinity and chl-a information they provided. They were all assigned as being Type I, since they all showed high TSM ($\geq 5 \text{ g.m}^{-3}$) and low salinities (≤ 28).

Table 3.3. Cross-validation of the discriminant analysis (based upon spectral data), for the three water types identified by the cluster analysis (based on biogeochemical data).

	Predicted group			Total User's accuracy (%)		
	Class	I	II	III		
Original (cross-validated)	I	30	7	0	37	81.1
	II	6	19	0	25	76.0
	III	1	0	7	8	87.5
Total		37	26	7	70	
Producer's accuracy (%)		81.1	73.1	100.0		
Correctly classified group classes					70	80.0%

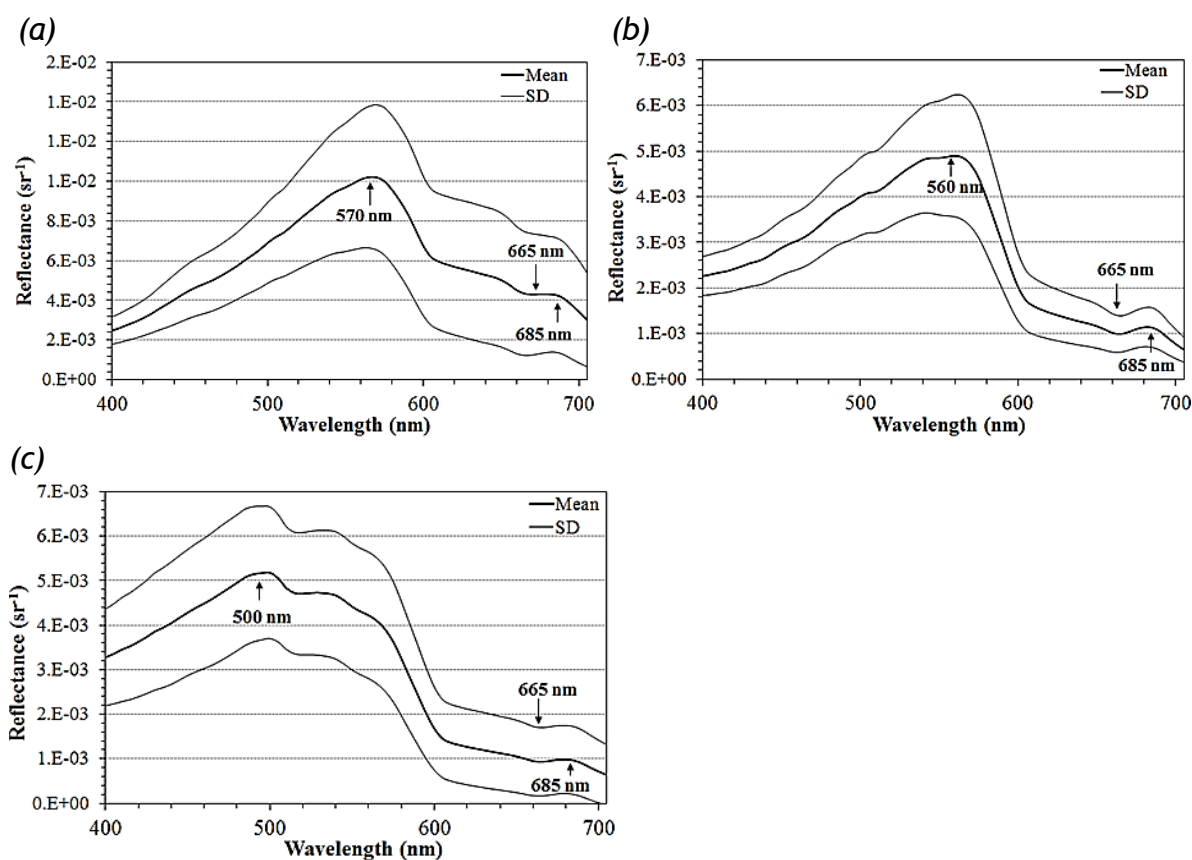


Figure 3.3. Spectral signatures (average and standard deviation) for the three types of surface water masses identified: (a) Type I, (b) Type II, and (c) Type III (see text).

The spectral signatures for each water type, as defined by the cluster analysis, show peaks at different wavelengths between 400 and 705 nm (Figure 3.3); this is probably related to the different water constituents. The average reflectance spectrum of water Type I (estuarine or river water) has its main peak located at around 570 nm, with Type II (the river-influenced water mass) being around 560 nm and Type III (oceanic water, not influenced by the river runoff) around 500 nm. The three curves show a change of slope at around 605 nm, a slight depression around 665 nm and a small peak at 685nm; these could correspond to chl-*a* absorption. The highest deviations are observed between 550 nm and 705 nm for Type I; 550 nm and 600 nm for Type II; and, 400 and 600 for Type III.

3.4. Phytoplankton groups and pigments

Two types of phytoplankton pigments were analysed: chlorophylls and carotenoids (the most abundant, Diadinoxanthin, 19'-Hexanoyloxyfucoxanthin (19' HFU) and Fucoxanthin, are shown in Figure 3.4). Tables A3 and A4 in the appendix, present a complete listing of the phytoplankton pigment concentrations. Most of the samples had a chl-*a* contribution of above 50% of the total pigments, except for 7 stations located within the Adour river-influenced marine waters. At these stations, chl-*b* accounted for more than 40% of the total pigment composition, while chl-*c* was the next most important contributing pigment. The highest concentration of chl-*a* determined using HPLC ($4.6 \text{ mg}\cdot\text{m}^{-3}$), was found at a station located in the St-Jean-de-Luz embayment (Station D8, Figure 3.1). The next most abundant pigment was Fucoxanthin ($0.57\pm 0.3 \text{ mg}\cdot\text{m}^{-3}$), followed by 19'-Hexanoyloxyfucoxanthin and Diadinoxanthin (0.24 ± 0.19 and $0.21\pm 0.12 \text{ mg}\cdot\text{m}^{-3}$, respectively). No particular differences could be identified between reflectance spectral signatures, for different pigment concentrations; hence no relationship could be established.

The complete listing of the phytoplankton taxa identified is presented in the supplementary material. Some 56 species were identified, while 8 additional morphospecies were counted for the 16 samples collected during the Batel-2 survey. The most abundant species was the diatom *Chaetoceros salsugineum*, with a total abundance of $8.7 \cdot 10^6 \text{ cells}\cdot\text{l}^{-1}$ for 8 stations; all of these were sampled in June. The highest concentration was found at a station located close to the Bidasoa river mouth (at an offshore distance of 600 m) during the June survey (Batel-2). The second most abundant species

was *Leptocylindrus danicus* with $7.5 \cdot 10^6$ cells.l⁻¹ for 8 stations: the highest abundance was found to the north (2.5 km offshore) of the Adour river mouth. This species was found only during the June 2009 survey (Batel-2); it was the most abundant species at all of the stations located close to the Adour river mouth.

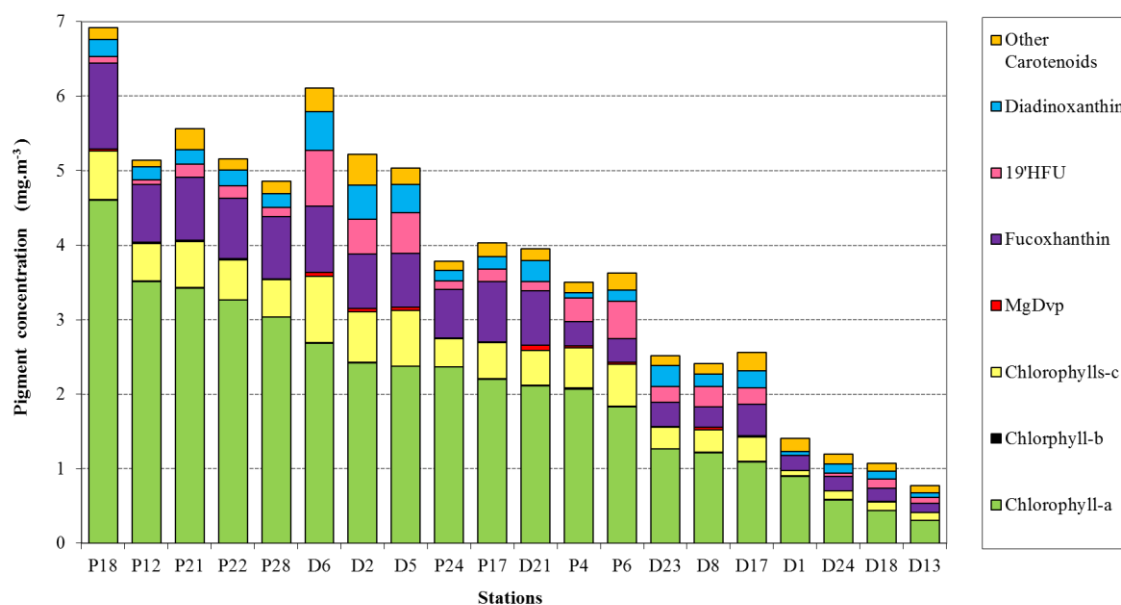


Figure 3.4. Pigment concentration for representative stations, estimated with HPLC for the Batel-2 survey.

3.5. Chlorophyll-a estimation and mapping

The algorithm obtained for estimating chl-a (i.e. local) encompasses three band ratios, selected by step-wise procedure:

Local MERIS Algorithm II:

$$\text{chl-a} = 10 \left[1.66 - 1.09 \times R_{rs} \left(\frac{510}{560} \right) - 2.39 \times R_{rs} \left(\frac{708}{681} \right) + 1.69 \times R_{rs} \left(\frac{708}{665} \right) \right]$$

Figure 3.5 shows the log-transformed linear regression between the chl-a determined *in situ* and the predicted chl-a, with the jackknife validation; this resulted in a coefficient of determination (r^2) for the local algorithm of 0.67 and a jackknife coefficient of determination (r^2_{jac}) of 0.68.

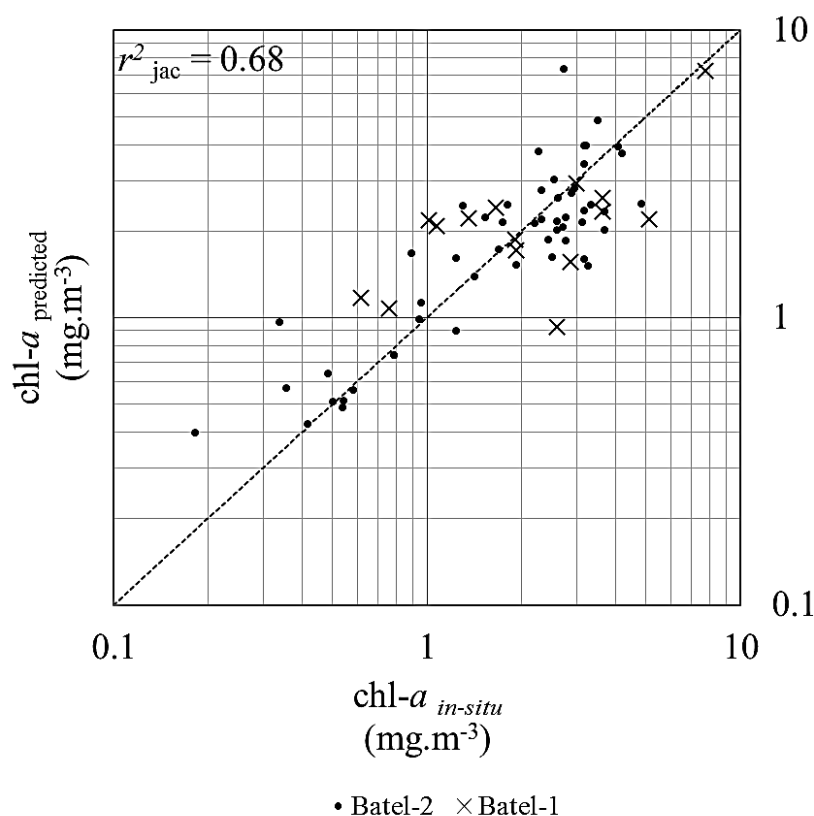


Figure 3.5. Linear regression between the predicted chl-*a* by the local algorithm and the *in situ* measured chl-*a* for Batel-1 (×) and Batel-2 (●) data.

The performance of the algorithm developed with reference to TSM was tested for 3 different ranges, which were not significantly different from each other, according to the Kruskal-Wallis test performed (Figure 3.6; p -value=0.062). Therefore, the changes in TSM below 6.6 g.m^{-3} affected, to the same magnitude, the retrieval of chl-*a* by the algorithm (Figure 3.6). The TSM range of 0 to 6.6 g.m^{-3} corresponds to general conditions within the Spanish Basque coastal waters, as calculated from the Basque water quality monitoring data (Garmendia et al. 2011), within the period 1993-2006 (i.e. 96% out of 787 of stations sampled, showed concentrations within that range). Also, when 5 stations with the highest TSM (5.0 - 27.7 g.m^{-3}) were removed from the dataset ($n=65$), the r^2_{jac} value for relationship between the log-transformed predicted chl-*a* and the chl-*a* measured *in situ*, increased by 0.04 (from 0.68 to 0.72); this suggests that TSM above 5.0 g.m^{-3} affected the estimation of chl-*a* using the algorithm. When all of the stations with TSM above 2.0 g.m^{-3} were removed from the dataset ($n=53$), the r^2_{jac} slightly increased (from 0.72 to 0.73).

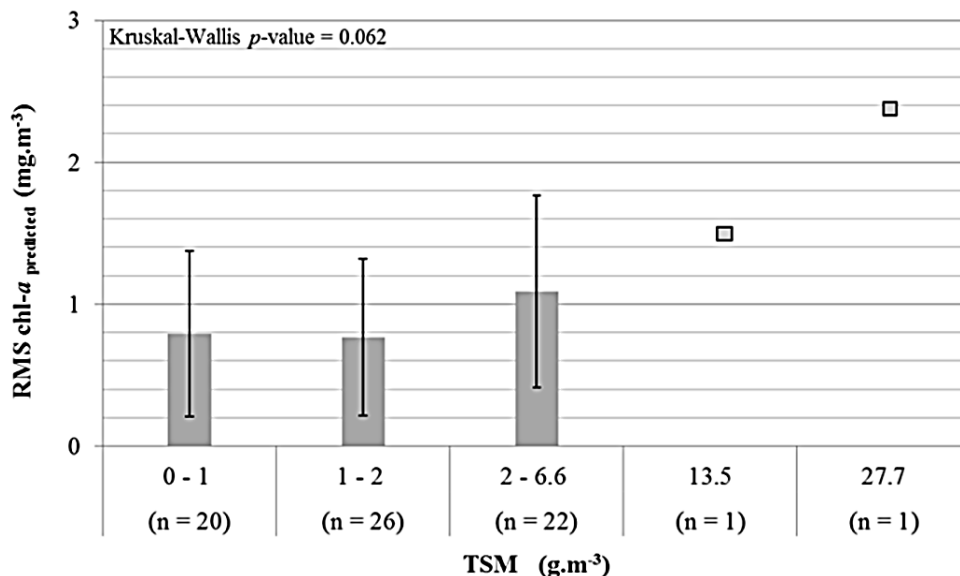


Figure 3.6. Root-Mean-Square difference (RMS) between the chl-a observed and predicted with the local algorithm in relation to Total Suspended Matter (TSM) concentration. Key: n = number of samples.

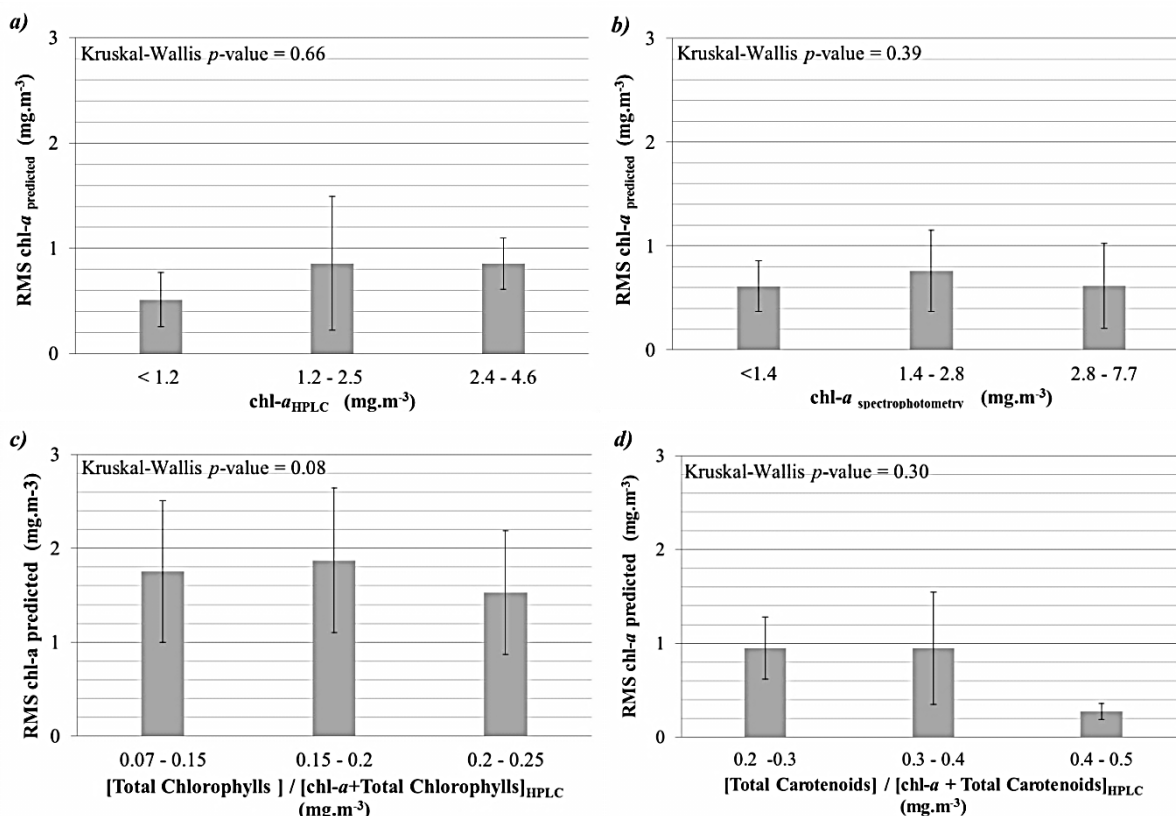


Figure 3.7. RMS difference for the chl-a predicted with the local algorithm, plotted against the chl-a estimated *in situ*: (a) using HPLC (n=20); (b) using spectrophotometry (n=70); (c) total chlorophylls (without considering chl-a), derived from HPLC (n=20); and (d) total carotenoids derived using HPLC (n=20).

Figure 3.7 (a) shows an increase in RMS, with increasing chl-a estimated *in situ* for the samples analysed with HPLC (n=20). Figure 3.7 (b) shows a slight increase and then

a decrease of RMS calculated for the complete dataset ($n=70$), where chl-*a* was measured using spectrophotometry. However, the Kruskal-Wallis test indicated no significant difference between the groups of chl-*a*, predicted for the total dataset and for the HPLC samples. With increasing relative concentration of total chlorophylls (except chl-*a*), there is a slight decrease in the RMS. In this case too, the Kruskal-Wallis test showed no significant differences between the concentration groups (Figure 3.7 (c)). No significant differences were found on the effect of the relative concentrations of these pigments, on the prediction of chl-*a* by the algorithm. In summary, the results indicate that the presence of relative concentrations (concentrations of pigments with respect to chl-*a*) of accessory pigments (i.e. other than chl-*a*) does not affect the estimation of chl-*a* by the local algorithm.

3.6. Comparison of chlorophyll-*a* algorithms

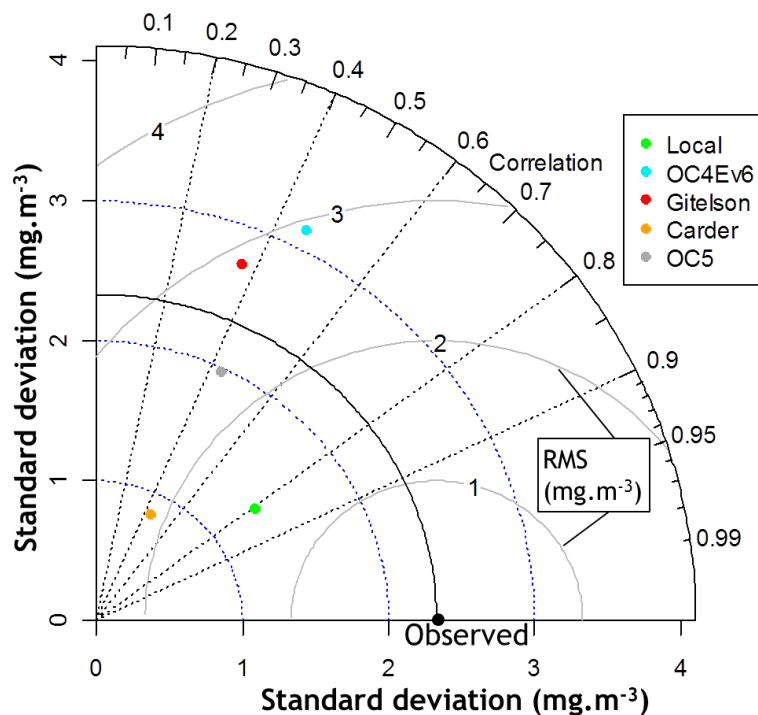


Figure 3.8. Taylor Diagram showing the correlation coefficient (R), the Root-mean square difference (RMS), and the standard deviation of the observed chl-*a* measured *in situ* (observed) and the chl-*a* predicted by 4 algorithms derived from reflectances measured *in situ*, with a TriOS spectrometer. The algorithms represented are the OC4v6, Gitelson's 3 band MERIS algorithm, Carder's empirical algorithm, the OC5 and the local empirical algorithm (as developed in this study).

The Taylor Diagram (Figure 3.8) summarises the statistics related to the four algorithms being compared. The local algorithm shows the best correlation between the observed and the predicted chl-*a* ($R= 0.8$) and the lowest centred RMS (1.7 mg.m^{-3}),

while the standard deviation of the chl-*a* estimation by this algorithm ($\sigma_f = 1.2 \text{ mg.m}^{-3}$) is lower than the observed standard deviation (2.3 mg.m^{-3}); this is indicated by the black solid arc. The OC5 shows the closest standard deviation ($\sigma_f = 1.9 \text{ mg.m}^{-3}$) to the observed standard deviation of all the models, but the correlation ($R = 0.46$) is lower and the RMS is higher ($\text{RMS} = 2.4 \text{ mg.m}^{-3}$) than those of the local algorithm.

Table 3.4. Algorithm performance indices for chl-*a* validation with Batel-1 dataset: mean, standard deviation (Std), Root mean square difference (RMS), the slope and intercept of the linear regression between *in situ* and predicted chl-*a*, and the correlation coefficient (*R*). Chl-*a* concentration is predicted with R_{rs} measured *in situ* and compared to chl-*a* measured *in situ*.

Algorithm	Mean	Std	Correlation Coefficient (<i>R</i>)	RMS (mg.m^{-3})	Slope	Intercept
Local	1.8	1.5	0.8	1.7	0.5	0.6
OC4Ev6	4.5	3.1	0.4	3.5	0.6	2.9
Gitelson	1.7	2.7	0.4	3.0	0.4	0.6
Carder	0.7	2.1	0.4	2.8	0.2	0.3
OC5	3.1	1.9	0.5	2.4	0.4	2.2
<i>In situ</i>	2.6	2.3				

The OC4v6, Carder and Gitelson algorithms show similar RMS values and similar correlations between the predicted chl-*a* and the reference chl-*a* ($R = 0.4$). However, the standard deviation of the Carder predicted chl-*a* (2.1 mg.m^{-3}) is closer to the observed standard deviation. Table 3.4 shows the statistics related to Figure 3.8, in addition to the intercept and the slope values of the predicted chl-*a* values obtained from the regression between *in situ* chl-*a* obtained from reflectances values of the validation data. The local algorithm's slope (0.6) and intercept (0.5) values are the closest combination that meets the criteria described by Campbell and O'Reilly (2006) for an algorithm to be acceptable: a slope of 1 and an intercept of 0.

3.7. Application to MERIS imagery

One MERIS image was acquired with low cloud coverage during the Batel-1 survey, while there were not cloud and flag free images for the Batel-2 survey. A comparison of chl-*a* estimated by the local algorithm and the OC5 is presented in Figure 3.9. This fig-

ure shows that in areas away from the coast, the OC5 algorithm provides, in general, higher chl-*a* concentrations than those described from the local algorithm at reduced resolution. The application of the algorithm to the full resolution image, provides more information and detail on the concentration of chl-*a*. In general a good accordance is observed between both images (RR and FR), but slightly higher concentrations of chl-*a* are observed in certain areas of the FR chl-*a* map. The FR map shows more similarities with the OC5 map than the RR map. Unfortunately, the best performing chl-*a* algorithm could not be determined from only a single image. The satellite-*in situ* match-up scatterplot (Figure 3.10) shows a good correspondence between the chl-*a* concentrations measured *in situ* and the concentrations derived from reflectance bands of the FR product ($r^2=0.9$). The ratio between the satellite and the *in situ* R_{rs} at wavelengths 442 nm, 490 nm, 510 nm and 560 nm were of 1.6, 1.0, 0.93 and 1.4 respectively, showing a general overestimation of the satellite with respect to *in situ* R_{rs} . The match-up scatterplots of the R_{rs} measurements are shown in the appendix.

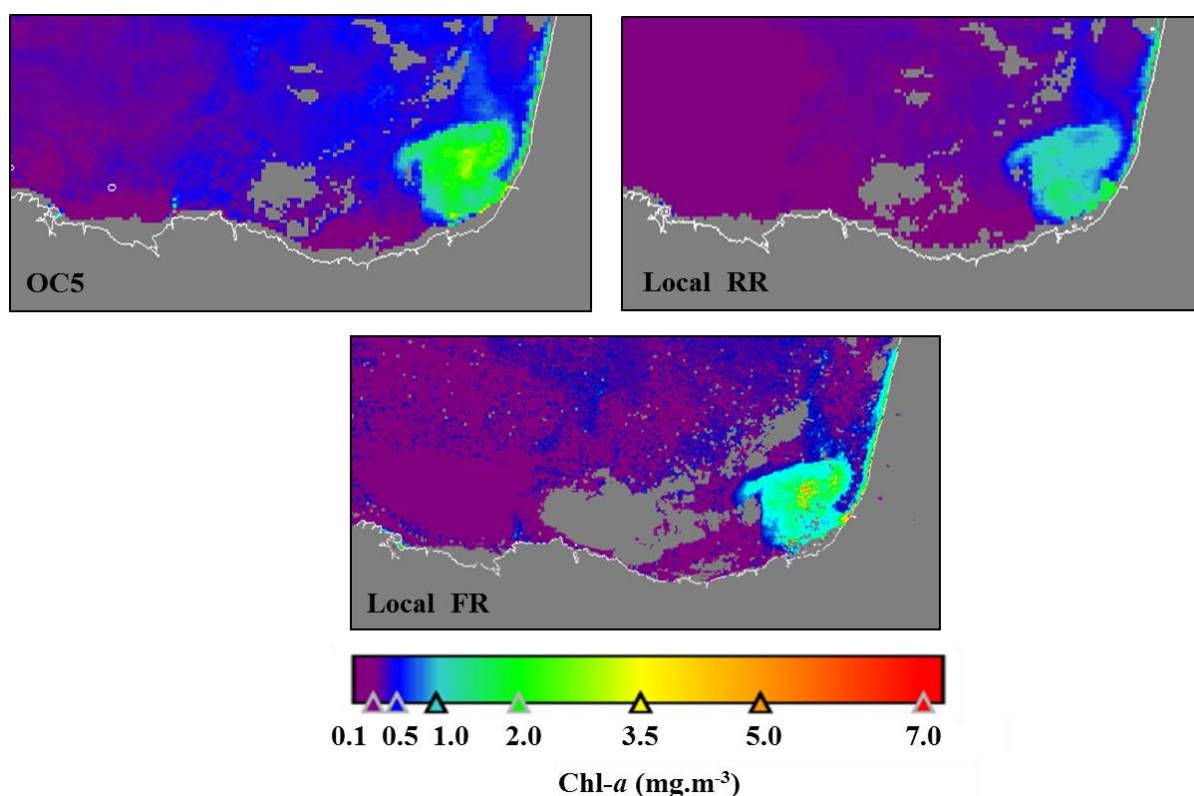


Figure 3.9. Chl-*a* maps generated with the OC5 and the local algorithm, at reduced (RR) and full resolution (FR) for the second. The local algorithm map was generated with the RR Level 2 product image, belonging to the 3rd MERIS reprocessing release; this was acquired at reduce resolution on the 5th June 2007. The FR image was acquired before the reprocessing.

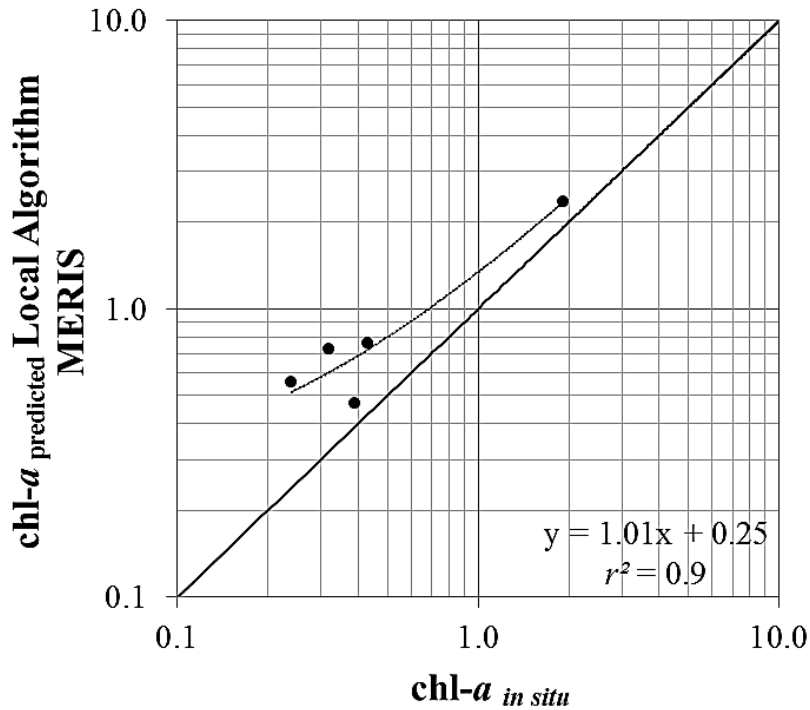


Figure 3.10. *In situ*-Satellite match-up scatterplot. Chl-*a* was derived with the Local MERIS Algorithm II. *In situ* chl-*a* was measured using CTD fluorescence.



Figure 3.11. K-means cluster classification of the Basque coastal water bodies using reflectance bands of the MERIS FR products acquired on the 5th of June 2007. Class I corresponds to the red colour, class II to the green colour and class III to the blue colour. Station B2 was sampled on that date and included in the classification analysis of the biogeochemical and optical data.

The classification map (Figure 3.11) showed three distinct surface water classes in the region of study that generally coincide with previous classifications of the water masses (Sections 3.2, 3.3). Thus, type I would correspond to the red area (class I), type II to the green area (class II) and type III to blue area (class III). Class I would correspond to estuarine or highly river influence waters, class II to moderately river-influenced waters and class III to oceanic waters. There was only one station (B2) that could be classified using the biogeochemical and the radiometric data, and the MERIS FR reflectance

bands. The three types of analysis classified the station as type II or river influenced area. The chl-*a* concentration at this station was of 1.6 mg.m⁻³, TSM of 1.1 g.m⁻³ and the stratification index of 0.1.

4. DISCUSSION

4.1. Water mass classification

Three types of coastal surface water masses were defined according to biogeochemical parameters, which could be discriminated on the basis of optical measurements. Water Type I has considerably higher TSM than the other two types, with higher variability in average chl-*a*, in comparison with the other two types. The reason for this variability is a higher content in TSM, which restricts the irradiance penetration into the water column, diminishing phytoplankton photosynthesis. As relatively turbid river waters mix with clearer marine waters, moderate proliferation of the phytoplankton takes place; this is favoured by the nutrients present in the river freshwater (e.g. Petus et al. (2010)), permitting also an increase in the phytoplankton photosynthetic pigment, chl-*a* (water Type II). As river runoff becomes diluted with marine waters, the nutrient concentration decreases and a lower chl-*a* is measured (water Type III). Such characteristics are in agreement with other results (Revilla et al. 2009) obtained for this region. The linear correlation between TSM and salinity suggests that the TSM input is related to river discharge. The good correlation existing between turbidity and TSM ($r^2 = 0.9$) confirms that the degree of transparency in the water could be caused, mainly, by the suspended matter; this is confirmed by Petus (2009), using Secchi disc depth of disappearance and attenuation coefficient (K_d) measurements. The discriminant analysis resulted in 80% of the groups being selected by the cluster analysis, classified and cross-validated correctly with the reflectance spectra; hence water constituents in these river systems alter the colour of the water. As such, the spectra acquired during these surveys could be used to classify different types of coastal water masses in the study area. In addition, the classification map shows that three types of water masses, from river- influenced to oceanic, can be identified using the atmospherically-corrected MERIS FR reflectance product. Further satellite-*in situ* measurements match-ups would be necessary to confirm that the classes identified using the three methods coincide.

4.2. Chlorophyll-*a* estimation

The ratios selected as contributing significantly to the estimation of chl-*a*, in the dataset presented here, consisted of: (i) bands within the blue-green part of the spectrum (510 and 560 nm); and (ii) bands which incorporated the peaks and depressions around the fluorescence wavelengths i.e. 665, 681 and 708 nm. The fluorescence bands selected match those of Gitelson et al.'s 2008 findings, which showed that the optimal wavelengths their algorithm for chl-*a* retrieval in turbid waters, were around 660-670 nm and 700-730 nm. Also, Härmä et al. (2001) have highlighted the importance of MERIS Band 9, centred at 708.75 nm, which is included in their algorithm, for the detection of chl-*a* in Finnish coastal surface waters. A combination of these ratios performed well for the area i.e. Basque coastal waters. The validation of the developed algorithm, with chl-*a* measurements performed with the Batel-1 survey and the LQM data set in coastal areas obtained between February and October, resulted also in a lower error compared to the use of the OC4Ev6, Gitelson's, Carder and OC5 algorithms. Empirical algorithms using bands with similar wavelengths and developed for turbid waters provided higher coefficients of determination (Gons et al. 2008). However, they were determined with a higher number of measurements and performed for different areas. No empirical algorithms for chl-*a* have been developed previously for the study area, and *in situ* chl-*a* measurements are few.

When mapping phytoplankton biomass with empirical algorithms, those based on blue-to-green ratios function well in clear waters (IOCCG 1998), while algorithms using green to Near Infra-Red (NIR) ratios perform better in turbid coastal and inland waters (Gitelson 1992, 1993; Gitelson et al. 2007). Taking into account the three water mass types defined in this investigation, the empirical algorithm developed in Chapter II, for the continental shelf of the Bay of Biscay, could be applied to the more clear or off-shore water masses (e.g. $TSM < 2 \text{ g.m}^{-3}$, water Type III). In contrast, the algorithm presented in this contribution could be more suitable for waters influenced by river runoff (e.g. $TSM > 2 \text{ g.m}^{-3}$, water Types I and II). Thus, an algorithm for clear waters (e.g. OC4Ev6) could be used when the concentrations of TSM estimated with the remote sensor are below 2.0 g.m^{-3} . Subsequently, with an increase in the TSM concentration, there would be a switch to a Case 2 chl-*a* algorithm, such as the local algorithm developed in this study.

Another source of error in coastal areas is the presence of colour dissolved organic matter (CDOM). Algorithms considering blue and green bands of the spectrum, where CDOM absorbance is at a maximum, can overestimate chl-*a* due to the presence of this component (Darecki and Stramski 2004). It is likely that this parameter had an influence on the 510/560 ratio of the algorithm developed here, since previously, CDOM concentration, influenced negatively the accuracy of chl-*a* retrieval for the continental shelf waters of the Bay of Biscay (with the algorithm developed in Chapter II). Unfortunately, the number of CDOM measurements (in this case DOC) was not sufficient to derive any conclusions about the effects of this water constituent on the algorithms.

4.3. Evaluation of algorithm performance

The averaged spectra obtained for the surveys shows a shift towards longer wavelengths, with increasing TSM. Also, the magnitude of reflectance increases throughout the entire spectrum with increasing TSM; showing higher reflectance values throughout the entire spectrum ($1 \times 10^{-1} \text{ sr}^{-1}$, compared to $\sim 5 \times 10^{-3} \text{ sr}^{-1}$), as demonstrated by Doxaran et al. (2002); Morel and Bélanger (2006), Hunter et al. (2008), Petus et al. (2010). Morel and Bélanger (2006) showed that there is an increase in reflectance, which affected the magnitude of the entire spectrum with increasing suspended matter concentrations. Likewise, Bricaud and Morel (1987) demonstrated that the green part of the spectrum (510-570 nm) was heightened, when compared to the same part of the spectrum for oceanic waters with the same chl-*a*. Gitelson et al. (2007) showed that chl-*a* was responsible for only 2% of the peak magnitude variation, suggesting that scattering by inorganic and non-living organic suspended matter controlled, mainly, reflectance within this part of the spectrum. Such an effect of suspended and dissolved matter on the colour of the water masks the chl-*a* signal. For this reason, researchers have focused upon reducing the inaccuracies, by selecting wavelengths less affected by these elements, such as the fluorescence peak. The three water types identified in the present study have shown a depression around 665 nm and a low magnitude peak around 685 nm; this could correspond to the fluorescence produced by the chl-*a* (Morel and Prieur 1977). However, the interpretation of fluorescence, in terms of phytoplanktonic biomass, is difficult; this is because the fluorescence signal depends not only upon the chl-*a* itself, but also upon the intensity of the excitation, and on the fluorescence

quantum yield, whose predictability is still questionable (Morel 2006). Despite the aforementioned problems, algorithms using fluorescence bands have been used successfully in the retrieval of chl-*a* values for the open ocean (Borstad et al. 1985; Gower and Borstad 1987), e.g. MODIS product 20 (Letelier and Abbott 1996). Gower and King (2007) found that the fluorescence signal from MERIS correlated well with surface chl-*a* measured *in situ*. On the other hand, R_{rs} can be highly variable in coastal areas, due partly to coastal hydrodynamics, driven by wind and terrestrial run-off; these result, often, in considerable spatial heterogeneity in very small areas (Ferrer et al. 2009). Furthermore, the fluorescence signal can be affected by the complex and variable aerosol composition of the transition zone, between the land and sea (Zielinski 2004). Here, chlorophyll fluorescence overlaps with a strong NIR scattering peak (Gitelson et al. 2007). Gower and Borstad (1987) have suggested the use of a combination of the blue/green ratio approach and fluorescence, which could help in the accurate retrieval of chl-*a*, provided that a good atmospheric correction is available.

The phytoplankton pigments analysed with the HPLC showed that the stations influenced by the Adour river discharges (D2, D5, D6, D13) have a higher concentration of accessory pigments, in relation to chl-*a*, than stations located farther offshore or closer to the other rivers (P12, P22). Two carotenoids, Fucoxanthin and Diadinoxanthin, were present in higher concentrations in areas lying close to the Adour river mouth and inside the estuary; these are indicator pigments for the algal class Bacillariophyta (diatoms) (Jeffrey and Vesk 1997). The presence of this particular group is confirmed by the phytoplankton counts at these stations, where diatoms were the most abundant algae present. These types of pigments have absorption peaks within the blue area of the spectrum (445-478 nm), which correspond with the absorption spectra of chl-*a*. For this reason, it was assumed originally that higher concentrations of these pigments would affect negatively the estimation of chl-*a*. However, the results have shown that they do not have an effect on the performance of the algorithm (Figure 3.7, (d)), since the differences in RMS with increasing accessory pigment concentration are not significant. Therefore, on the basis of the RMS results, it can be inferred that accessory pigments, at the range of concentrations (0.04-11.30 mg.m⁻³) found during the surveys, do not affect the accuracy of chl-*a* retrieval by the local algorithm. However, the calculation of spectral derivatives could be used in future studies, as a technique to reduce

background signals and to resolve overlapping spectral features (Lahet et al. 2001). Several authors have demonstrated that phytoplankton discrimination, at group level (Sathyendranath et al. 2004; Alvain et al. 2005) and even at species level, is possible with remote sensing of accessory pigments in certain circumstances (Kutser et al. 2006; Cannizzaro et al. 2008). In the case of cyanobacteria, but only if the algal concentration is high enough to form a bloom (Smayda 1997), the reflectance signal can be used to separate this group from other phytoplankton groups using satellite remote sensing imagery (Simis et al. 2005, 2007; Kutser et al. 2006; Kahru et al. 2007). However, separating blooms of species or groups based solely upon optical signatures, is highly problematic (Kutser 2009). Local knowledge of the area's hydrodynamics, the ecological requirements of algal groups or water masses characteristics are necessary, to be able to discriminate phytoplankton groups from each other and from those of the river plumes. The latter can affect the accuracy of biomarker pigments, when associated with inorganic and organic material (Hunter et al. 2008).

The most abundant identified species varied with the period of sampling and the type of water mass. *Leptocylindrus danicus* was the most abundant species at all of the stations sampled in June, and located close to the Adour river mouth. This diatom is associated with coastal waters, and has been reported to cause occasional discoloration of seawater, to yellowish-brown, when present in high concentrations (Lagos 2002; Salbatier et al. 2008). This phenomenon could be affecting also the shape of the spectra acquired along the Adour river plume, as 5 out of the 6 stations where this species is the most abundant, correspond with river-influenced stations defined by the cluster analysis. In turn, this species was not found at the Spanish Basque coastal stations sampled during the surveys. The presence of this species only during the June survey coincides with Casas et al. (1999) findings, where this species was found to be dominant during summer stratification periods, within coastal water areas of northern Spain. The diatom *Cerataulina pelagica* was the most abundant species in 88% of the samples collected during the April survey; and it was found in lower abundances during June. This species has been found to bloom in nutrient-enriched waters (Gamble et al. 1977). It was present in concentrations which reached almost 10^6 cells.l⁻¹ at some stations, suggesting that these particular locations may be subjected to nutrient enrichment, although no sampling for nutrient concentration was performed. Certainly, the station

with the highest abundance of this species (9.5×10^5) was located near to St-Jean-de-Luz (Station D8, Figure 3.1), an urban embayment likely to be affected by nutrient enrichment. This station is associated with the highest chl-*a* of the entire dataset. The total species abundances are shown in the appendix (Table A3). In general, the species identified during the Batel-2 survey are typical of the study area (Revilla et al. 2009). Sarmiento and Descy (2008) proved that a combination of inverted microscopy, together with HPLC, are a useful approach for monitoring phytoplankton assemblages, in large monitoring programmes such as the Water Framework Directive (WFD) or the Marine Strategy Framework Directive (MSFD). Hence, these methodologies combined with satellite imagery could help to fulfil the requirements of these Directives, to assess phytoplankton biomass, abundance and community composition, as recommended by some authors (Ferreira et al. 2011).

4.4. Application to MERIS imagery

The main advantages of the products provided by the MERIS sensor are: (i) the higher number of bands (15) located within the visible and NIR parts of the spectrum (412.5-900 nm), appropriate for the parameterization of the empirical algorithms for the estimation of biophysical parameters; and (ii) the products provide a higher spatial resolution for these bands, with a pixel size that is appropriate for coastal studies and monitoring (300 x 300 m, per pixel). These advantages are an improvement over products provided by other sensors, such as MODIS and SeaWiFS. On the other hand, the temporal resolution is lower than that provided by latter sensors, as an image for the Bay of Biscay can be obtained only every 2-3 days. The atmospheric correction provided with the Level 2 products can be also a cause for a decrease in algorithm accuracy (IOCCG 2010).

During the Batel-1 survey, the river discharge was slightly higher than the mean annual recorded for the month of June ($385 \pm 67 \text{ m}^3 \cdot \text{s}^{-1}$), and, for this reason, a higher concentration of chl-*a* is observed around the Adour river mouth corresponding to the river plume. However, chl-*a* over the adjacent Spanish Basque coastal area shows low concentrations. This pattern could be due to the different river hydrologic regimes, the Adour is of pluvio-nival regime and, as such, dependent on the snowmelt and rainfall.

In contrast, the regime of the Spanish Basque Country Rivers is torrential and related to rainfall.

Measured chl-*a in situ* during the Batel-1 and LQM surveys corresponded satisfactorily with the predicted chl-*a* concentration derived on the basis of the local algorithm. Further validation, with additional *in situ* data, matched with FR MERIS images (300 x 300 m), would be necessary to better improve the chl-*a* estimation provided by the local algorithm. The 5 match-ups obtained on the 5th of June 2007, with the chl-*a* and the R_{rs} data are not enough to derive definite conclusions on the performance of the algorithm, nor on the correspondence between the *in situ* and satellite reflectance data (for atmospheric correction validations). The difference in standard deviation, between the chl-*a* predicted by the local algorithm and the chl-*a* measured *in situ*, implies that more *in situ* measurements in the area are required to validate and perhaps adjust the algorithm coefficients. However, the frequently overcast skies (70% of annual cloud cover) over the Bay of Biscay make it difficult to obtain coincidence with *in situ* measurements; this is the reason why only a single image was acquired without error flags during both of the surveys.

Chapter IV

Water quality assessment using MODIS satellite-derived chlorophyll-*a* within the European directives, in the southeastern Bay of Biscay

1. INTRODUCTION

The implementation of the Water Framework Directive (WFD, 2000/60/EC) and the Marine Strategy Framework Directive (MSFD, 2008/56/EC), entails a densification and an increase in frequency of water quality monitoring in areas along the coast and within the limits of the Exclusive Economic Zone (EEZ) (200 nautical miles). According to the WFD and the MSFD, “good” surface water status should be achieved for all European waters by 2020. In order to reach this objective, the ecological and chemical status of the surface water bodies need to be assessed and the quality conditions reported using a classification scheme. Phytoplankton biomass has been selected by the WFD and MSFD (Borja et al. 2011; Ferreira et al. 2011) as one of the parameters for quality assessment, as it can respond to nutrient enrichment that causes water eutrophication (Nixon 1995; Halpern et al. 2008; Conley et al. 2009). However, some authors (Domingues et al. 2008) have stressed the constraints on the use of this element within the European Directives, related to the sampling frequency, the overlooking of blooms, etc. In this way, remote sensing technologies provide the most effective means for frequent, synoptic, water-quality observations over large areas (Lee et al. 2005). Therefore, satellite imagery can be used to complement traditional monitoring techniques (Gohin et al. 2008; Domingues et al. 2008), offering a substantial improvement in terms of spatial and temporal coverage for the upper layers of the water column, especially when a densification of sampling effort is necessary for monitoring purposes.

Along the Basque coast (southeastern Bay of Biscay), *in situ* coastal monitoring network surveys have been carried out since 1994 (Borja et al. 2009, 2011), to accomplish the WFD and MSFD requirements. However, the researchers performing these studies have highlighted the need to obtain more extensive (spatial) and intensive (temporal) data coverage to produce more accurate assessments of phytoplankton status, as recommended by Ferreira et al. (2011).

1.1 Objectives

Chapter III revealed that the estimation of chl-*a* concentration can be improved with the development of regionally parameterised algorithms, but also that they need to be validated with a large number of data. It is therefore necessary to employ a great

amount of satellite and *in situ* measurements to determine the best performing algorithm for a particular region.

Hence, the aim of this study is to evaluate the potential of satellite data estimations of chl-*a*, as a tool for the assessment of both the phytoplankton status within the WFD, and the anthropogenic eutrophication within the MSFD, for Basque coastal and offshore water bodies. For this purpose: (i) an algorithm to predict chl-*a* with suitable accuracy in coastal areas had to be selected; (ii) chl-*a* estimations predicted by three different algorithms developed for MODIS (Moderate Resolution Imaging Spectroradiometer) were compared to chl-*a* measured *in situ* obtained from historical data (WFD monitoring surveys) and *ad hoc* oceanographic surveys, using satellite *in situ* comparisons and 90th percentile (P90) monthly values for the 2005-2010 period. Further, P90 chl-*a* maps were generated with the selected algorithm; and then, (iii) an ecological status assessment was performed, based upon a phytoplankton biomass metric. Finally, the results were compared with the present assessment undertaken only with chl-*a* *in situ* measurements.

2. MATERIALS AND METHODS

2.1. Basque Littoral Monitoring Network

The Littoral Water Quality Monitoring and Control Network (LQM) of the Basque Country (southeastern corner of the Bay of Biscay) started in 1994 (Borja et al. 2004). At present, in the coastal waters, the LQM is composed of 16 *in situ* sampling stations (Borja et al. 2009); 3 additional stations are surveyed in offshore waters for the implementation of the MSFD (Borja et al. 2011). The monitored coastal water bodies lie within the Northeast Atlantic eco-region and belong to the type NEA-1 (North-East Atlantic), following the WFD typology system. This type is characterised by euhaline fully-mixed waters, in exposed and shallow (30 m) coastal areas subject to a mesotidal regime (Borja et al. 2007). The coastal stations were selected based on the following criteria: (i) the depth of the water bodies had to be appropriate to reduce the variability caused by coastal features such as bathymetry, waves or currents, so all the coastal stations are located within the 1 nautical mile limit, established by WFD over waters of 25-35 metres in depth; (ii) they needed to be situated at a suitable distance from land

to be influenced by anthropogenic discharges, and most stations were therefore located near the most important river mouths of the region, whereas (iii) the offshore stations are considered to be reference stations because they are not impacted *a priori* by anthropogenic influence due to their distance from the main land-based pollution sources (10-15 km), over water depths of approx. 100 m. The stations are allocated in 5 different water bodies, which are classified is based on the geographical characteristics of the area, such as the orientation of the coast, the presence of a submarine outfall, and the geographical limits established by the European Water Framework (from the coastline to 1 nautical mile offshore of the baseline) and Marine Strategy Directives (from the baseline to 200 nautical miles) (Borja et al. 2009, 2011), see Figure 4.1. The 1 nautical mile is measured from the 3 main capes of the Spanish Basque Country (Matxitxako, Getaria, Higer), and the water bodies are delimited by linking nautical points off the capes. Four water bodies are considered as coastal (See Figure 4.1), while one corresponds to ‘oceanic waters’, located beyond the coastal waters (MSFD area).

Development of the methods used to evaluate the quality of coastal waters in relation to the WFD began in 2000. The first method used to assess the quality status of the WFD phytoplankton element in the Basque marine environment (Borja et al. 2004) was based upon a method developed at Ifremer (Vincent et al. 2002). This method utilised phytoplankton biomass (derived from chl-*a* concentration) and phytoplankton abundance and composition, to calculate an integrated index that classified the quality status into five distinct categories (from “High” to “Poor”), matching the WFD typology classification. However, this method did not provide any information on reference conditions and ecological quality ratios, which is a requisite of the WFD. Therefore, a new method for phytoplankton quality assessment was developed for the eastern Cantabrian coast, which includes the Basque coastal waters (Revilla et al. 2009). This new method involves integrating, for the water body, the results of two metrics that are calculated on the basis of a 6-year period: (i) the biomass metric (calculated as P90 of the chl-*a* concentrations); and (ii) the bloom metric (calculated as frequency of cell counts above a threshold, for any single taxa). The values for the high/good and good/moderate boundaries had been established during the first phase of the WFD intercalibration exercises (Carletti and Heiskanen 2009). The boundary values of the chl-*a* metric for the moderate, poor and bad status classes along the Basque coast were proposed previously

by Revilla et al. (2009). Thus, at present, in the Basque offshore and coastal waters, the range of P90 concentrations corresponding to the high, good, moderate, poor and bad classes are: <3.5 , $3.5-7.0$, $7.0-10.5$, $10.5-14.5$, ≥ 14.5 $\text{mg} \cdot \text{m}^{-3}$, respectively.

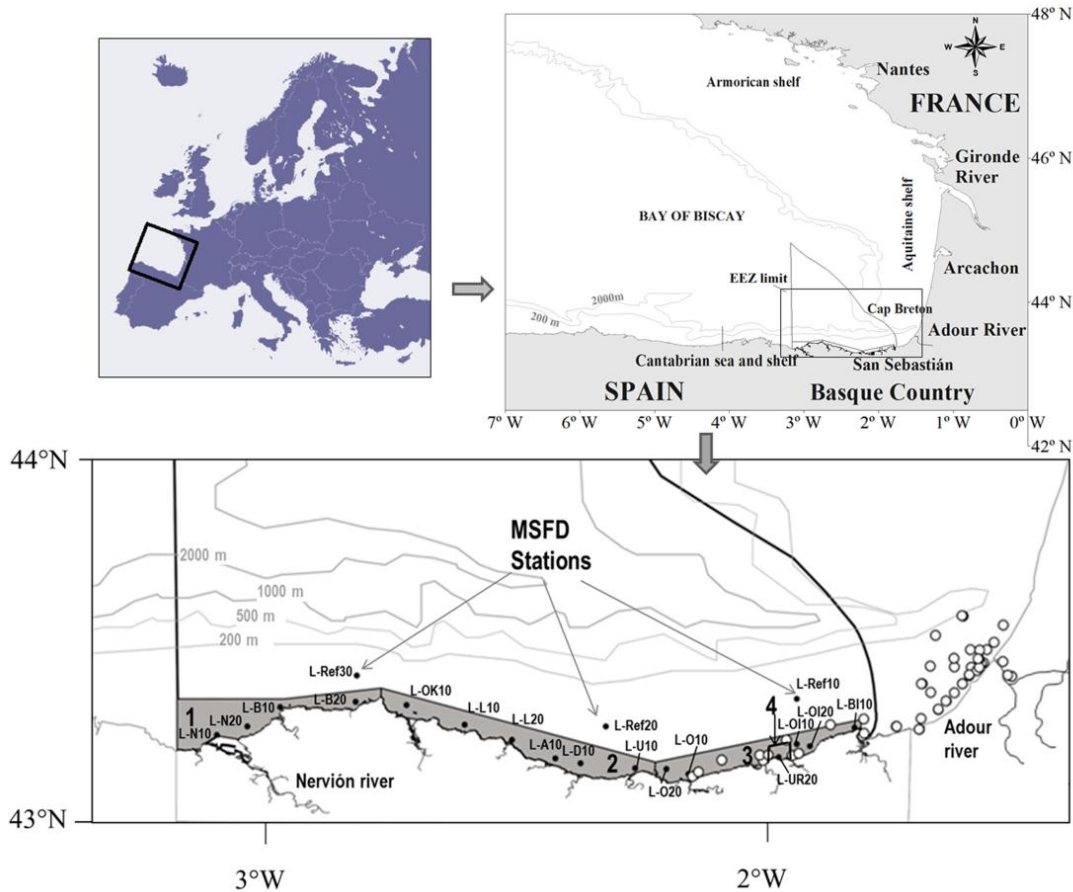


Figure 4.1. Sampling stations of the Framework Directive monitoring network within the Basque Littoral Monitoring Network (dark circles with labels), which are distributed among 4 coastal water bodies and an offshore water body, as well as *ad hoc* oceanographic surveys stations (white circles). Key to water bodies: (1) Cantabria-matxitxako; (2) Matxitxako-Getaria; (3) Getaria-Higer; (4) Mompás Outfall, (5) Oceanic waters. EEZ: Exclusive Economic Zone.

2.2. In situ dataset

The main dataset used for this study was obtained from the Basque LQM between 2005 and 2010. Measurements were performed every three months, from February to November, to collect data representative of winter, spring, summer and autumn conditions. At each station, chl-*a* was estimated based on CTD fluorescence in continuous vertical profiles with a SeaBird 25 CTD. Fluorescence units were calibrated regularly against spectrophotometer measurements of chl-*a* in natural water samples. The spectrophotometric analyses involved the filtration of water samples through Whatman GF/C filters, pigment extraction in acetone, and the use of the equations developed by

Jeffrey and Humphrey (1975) without correction for phaeopigments. The chl-*a* data used for this study were those corresponding to the CTD measurements at 1m below the water surface, in natural water samples (referred to as chl-*a in situ*).

In addition, simultaneous chl-*a* concentration measurements were performed using methods, CTD fluorescence and spectrophotometric analysis, during two *ad hoc* oceanographic surveys (n=64), in June 2007 and April and June 2009, undertaken over the study area. The collected water samples were filtered in the field and the spectrophotometric measurements were performed in the laboratory some 72 hours after their collection (Figure 4.1). Simultaneous measurements with both methods were performed also monthly, at a coastal station near the Mompás submarine Outfall (Station L-UR20; Figure 4.1) for a complete year (2009-2010). The comparison between the measurements obtained using both methods was performed to test their correlation and to account for the possible inaccuracies related to *in situ* measurements.

2.3. MODIS Imagery

The images selected for this study were provided by MODIS. The high frequency of synoptic images (daily) obtained by MODIS as well as their ready availability, number of spectral bands, and resolution (1 km x 1 km) make these images suitable for the estimation of chl-*a* and water quality monitoring. MODIS Level 1 (Top-of-the-atmosphere Radiances, Calibrated and Geolocated) products were downloaded from the MODIS ftp site (<ftp://ladsweb.nascom.nasa.gov/>) and converted to Level 2 reflectance bands and chl-*a* products, through the SeaDAS (<http://oceancolor.gsfc.nasa.gov/seadas/>) processing chain. The SeaDAS operational atmospheric correction from Gordon and Wang (1994) with NIR iteration was applied in that process. The bands applied were numbers 11 (531 nm), 12 (547 nm), 13 (667 nm), 14 (678 nm), 15 (748 nm), all with a resolution of 1 x 1 km.

A total of 962 images corresponding to the Basque coast (Fig. 1) acquired between 2005 and 2010 that were free of clouds were downloaded. MODIS imagery was selected due to its multiple advantages with respect to the aims of this study compared to images provided by other recently launched remote sensors, such as MERIS (Medium Resolution Imaging Spectrometer Instrument; <http://www.envisat.esa.int/>). The

advantages of MODIS include a higher frequency of images since 2000 compared to the MERIS frequency of 2-3 days since 2002 and the ready image access provided by NASA.

2.4. Chlorophyll-*a* algorithms

The chl-*a* products generated by three algorithms were compared in this study. These algorithms were (i) OC3M, developed by O'Reilly et al. (1998) and adapted for MODIS; (ii) OC5, developed by Gohin et al. (2002); and (iii) a local empirical algorithm developed specifically for the study area during two surveys (named MODIS Local Algorithm II).

The standard chl-*a* images provided by NASA's Ocean Color Group are based on the global OC3M empirical algorithm, which is statistically-derived based on chl-*a* concentrations ranging from 0.0008 to 90 mg.m⁻³. However, most measurements were performed between 0.08 and 3 mg.m⁻³. The OC3M algorithm is defined as follows:

$$\text{chl-}a = 10^{0.283+2.753R+1.457R^2+0.659R^3-1.403R^4} \quad (\text{eq. 4.1})$$

$$R = \log_{10} \left[\frac{\max(R_{rs443}, R_{rs489})}{R_{rs555}} \right]$$

where *max* denotes the greater of the two values and $R_{rs}(\lambda)$ is the above-water remote-sensing reflectance. This algorithm was applied to MODIS imagery through SeaDAS and IDL programming.

OC5 is an empirical algorithm developed to retrieve chl-*a* concentration in Case 2 coastal waters, based upon a Look-up Table (Gohin et al. 2002). This method is derived from OC4 algorithm developed by O'Reilly et al. (1998) and is based on the same band ratios, but the 412 band is used as an indicator of atmospheric overcorrection. This band is used to detect signal overextraction in coastal environments in the case of high concentrations of suspended matter in the water and/or continental aero-sols in the atmosphere. A more detailed description can be found in Druon et al. (2005). In the case of MODIS, 4 channels are used to derive chl-*a* concentration from Level 2 reflectance products, which need have been processed previously with SeaDAS. This algorithm has been validated largely over coastal stations located in the Bay of Biscay, the

North Sea and the northern Mediterranean Sea (Gohin 2011). MODIS chl-*a* composites, calculated using the OC5 algorithm (Gohin et al. 2002), were downloaded from the Ifremer ftp site (ftp://ftp.ifremer.fr/ifremer/cersat/products/gridded/ocean-color/) for the Bay of Biscay.

A specific empirical algorithm (Local MODIS Algorithm II) was developed for the Basque coastal area with *in situ* spectral and biogeochemical measurements (chl-*a*, Total suspended matter, Turbidity, Secchi disc depth) performed during two *ad hoc* surveys, carried out in June 2007 and April and June 2009. The algorithm was developed by linearly regressing the log-transformed chl-*a* concentrations estimated by spectrophotometry and the reflectance measurements acquired *in situ* during those surveys; these were validated with additional data, obtaining a Root Mean Square Error (RMSE) of +/- 0.49 mg. m⁻³. The resulting algorithm (Eq. 2) described and validated in Chapter III, was adapted to MODIS imagery and applied to Level 2 reflectance bands.

Local MODIS algorithm II:

$$\text{chl-}a = 10^{\left[-0.18 - \left(5.85 \times \log_{10} \left(R_{rs} \left(\frac{531}{547} \right) \right) \right) - \left(5.56 \times \log_{10} \left(R_{rs} \left(\frac{678}{667} \right) \right) \right) + \left(0.442 \times \log_{10} \left(R_{rs} \left(\frac{748}{678} \right) \right) \right) \right]} \quad (\text{eq.4.2})$$

This algorithm is referred to in this section as the "local" algorithm.

Table 4.1. Reflectance ranges (in sr⁻¹) measured *in situ* with the field spectroradiometer for the local algorithm bands.

Band wavelength (nm)	Minimum Reflectance (sr ⁻¹)	Maximum Reflectance (sr ⁻¹)
531	2.3 × 10 ⁻³	9.7 × 10 ⁻³
547	2.1 × 10 ⁻³	1.2 × 10 ⁻²
667	2.7 × 10 ⁻⁴	1.2 × 10 ⁻²
678	3.1 × 10 ⁻⁵	1.2 × 10 ⁻²
748	3.8 × 10 ⁻⁵	2.3 × 10 ⁻³

The algorithm was applied only to the range of spectral reflectance values measured *in situ*, during the oceanographic surveys (see Table 4.1). Inclusion of values out-

side of this range could lead to erroneous chl-*a* values. Hence, only the range between the maximum and minimum spectral values measured in the field for each band selected were considered for each image. Thus, pixels with high reflectance values due to the presence of continental aerosols, coastal processes, such as haze, or other artificial artefacts could be discarded, because the standard SeaDAS fails to correct these features in some images.

2.5. 90th Percentile Calculation

The P90 was calculated both for the satellite-derived and the *in situ* chl-*a* concentration. For the satellite image calculations, the IDL function “Quantile” (Type 7) was used (Becker et al. 1988; Hyndman and Fan 1996). Chl-*a* P90 maps were produced for the 2005-2010 period by initially selecting all of the cloud-free images available during the 2005-2010 period for the study area. Subsequently, the P90 value was calculated for each pixel in all of the images selected for that period using IDL programming. As such, the IDL program calculated the value that 90% of the observations were equal to or below for each pixel. This approach resulted in two types of products: (i) one final image including the P90 value for each individual pixel for the 2005-2010 period (Total P90 map); and (ii) 12 monthly images (January-December) of the P90 values for the period and area studied. In this case, the P90 was calculated for all of the images selected for each month. The chl-*a* concentration values resulting from these 12 images were used for comparison with the chl-*a* annual cycle. In addition, a Total Suspended Matter (TSM) P90 map was created for the complete 2005-2010 period. The algorithm used to estimate the TSM concentration was developed by Petus et al. (2010) specifically for the study area.

2.6. Algorithm evaluation

The performance of the algorithms was evaluated by three means: (i) two methods used previously by Gohin et al. (2008, 2011), e.i. *in situ* match-ups and P90 of the chl-*a* annual cycles; and (ii) a method that utilises root mean square error percentages.

Firstly, the images with low cloud coverage were matched-up with *in situ* measurements. As such, the images were acquired on the same day as the *in situ* measure-

ments were performed. The chl-*a* concentrations determined by the satellite product were compared with the *in situ* measurements acquired at the same location.

Secondly, the P90 chl-*a* annual cycle estimated with the local and the OC5 algorithm, were compared to P90 values estimated with *in situ* measurements to validate the algorithms. Conversely, both algorithms were compared to P90 annual cycle estimates provided by the OC3M algorithm, to confirm their improvement regarding the estimation of chl-*a* concentrations for coastal waters.

Finally, the percent root mean square error (RMSE) was calculated between the *in situ* data and the algorithm-derived chl-*a* concentration to estimate the uncertainty related with the algorithms. The following formula was used:

$$\text{RMSE (\%)} = \sqrt{\frac{\sum_{i=1}^n (V_{est,i} - V_{in\ situ,i})^2}{N}} \times 100 \quad (\text{eq. 4.3})$$

where, V_{est} is the predicted variable, $V_{in\ situ}$ is the *in situ* measurement, and N is the number of stations.

The RSM Error was calculated for the P90 monthly products for each water body. The resulting values were averaged in three ways, (i) for the complete year; (ii) for the high chlorophyll months, October to March; and (iii) for the low chlorophyll months, April to September.

The mean chl-*a* concentration and standard deviation for each station and water body were also calculated for both the *in situ* and satellite methods. The standard deviation was used to estimate the uncertainty related to the difference in the number of measurements acquired using the two methods.

2.7. Quality status classification

The range of P90 concentrations corresponding to the High/ Good/ Moderate/ Poor/ Bad classification were established (Borja et al. 2009; Revilla et al. 2010b) during the intercalibration exercise, as noted above. Each station of the WFD surveys was assigned

a quality status according to its *in situ* P90 value. For the satellite data, each pixel of the resulting Total P90 chl-*a* map for the complete study period 2005-2010 (i.e. all the images selected for all the months and years) was treated as a station and assigned an ecological quality status according to its chl-*a* concentration. As a result, a quality status map was obtained showing the quality status for each pixel. The quality status of the WFD surveys' stations were assigned with P90 values determined using *in situ* measurements.

3. RESULTS

3.1. Spectrophotometry versus CTD fluorescence

The correlation between the chl-*a* concentrations estimated using CTD and spectrophotometric measurements in surface waters (0-1 m) during the oceanographic surveys was lower than expected ($r^2 = 0.44$; Fig. 4.2).

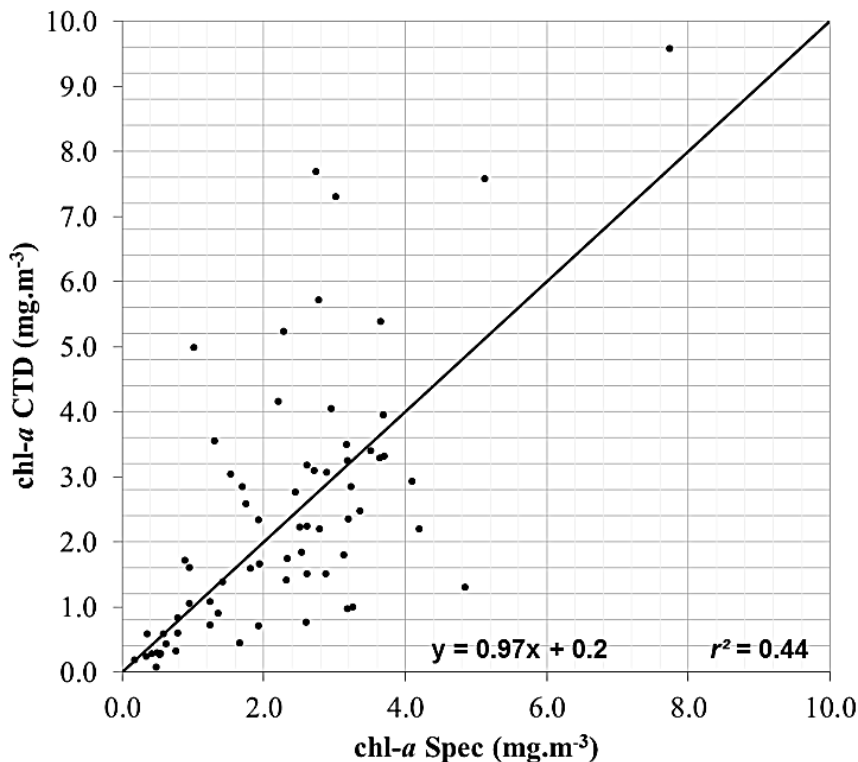


Figure 4.2. Chl-*a* concentration estimated with a spectrophotometry (Spec) and CTD during the oceanographic surveys.

Additionally, the CTD measurements performed simultaneously with both methods at the coastal station near the outfall for a complete year (2009-2010) did not capture

the March chl-*a* peak with the same intensity as the spectrophotometry measurements, because the latter method indicated a chl-*a* concentration of 8.86 mg m⁻³, while the CTD method indicated a value of only 3.31 mg.m⁻³ (Fig. 4.3).

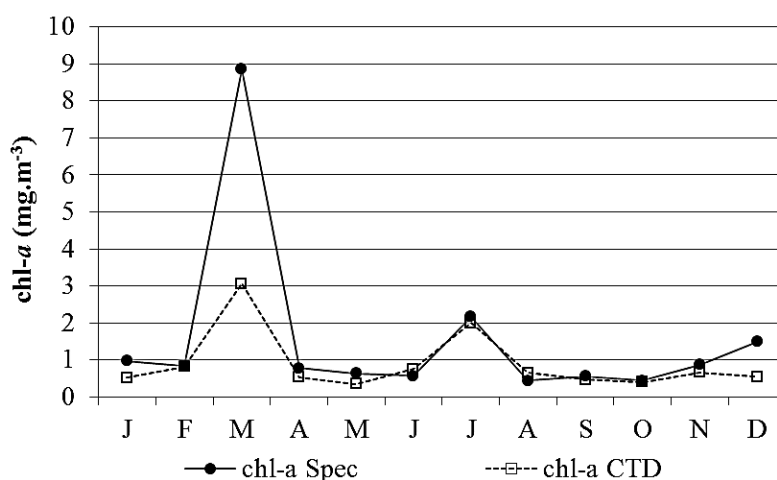


Figure 4.3. Monthly chl-*a* measurements at sea surface obtained simultaneously with a CTD and spectrophotometry (Spec), for the year 2010 at the Outfall station (L-UR20).

3.2. Satellite versus *in situ* data

Ninety five comparisons between *in situ* measurements and chl-*a* composites were generated with the local algorithm, 100 with the OC5 algorithm and 130 with the OC3M algorithm. The difference in the number is due to the limitations applied to the reflectance bands used by the local algorithm and to the erroneous pixel flags detected by the OC5 algorithm.

Figures 4.4 (b) and (c) show that the correlation between *in situ* and predicted chl-*a* concentrations is similar for both the OC5 and the local, because they generally overestimate this parameter at concentrations below 1 mg.m⁻³. While the correlation is unbiased between 1 and 4 mg.m⁻³ for the local algorithm, there is an overestimation by the OC5 algorithm within that range. Conversely, at concentrations greater than 4 mg.m⁻³, there is an underestimation by the local algorithm, while the OC5 adjustment seems accurate. The OC3M clearly overestimates chl-*a* in coastal waters, reaching almost a 10-fold overestimation at some points (Figure 4.4 (a)).

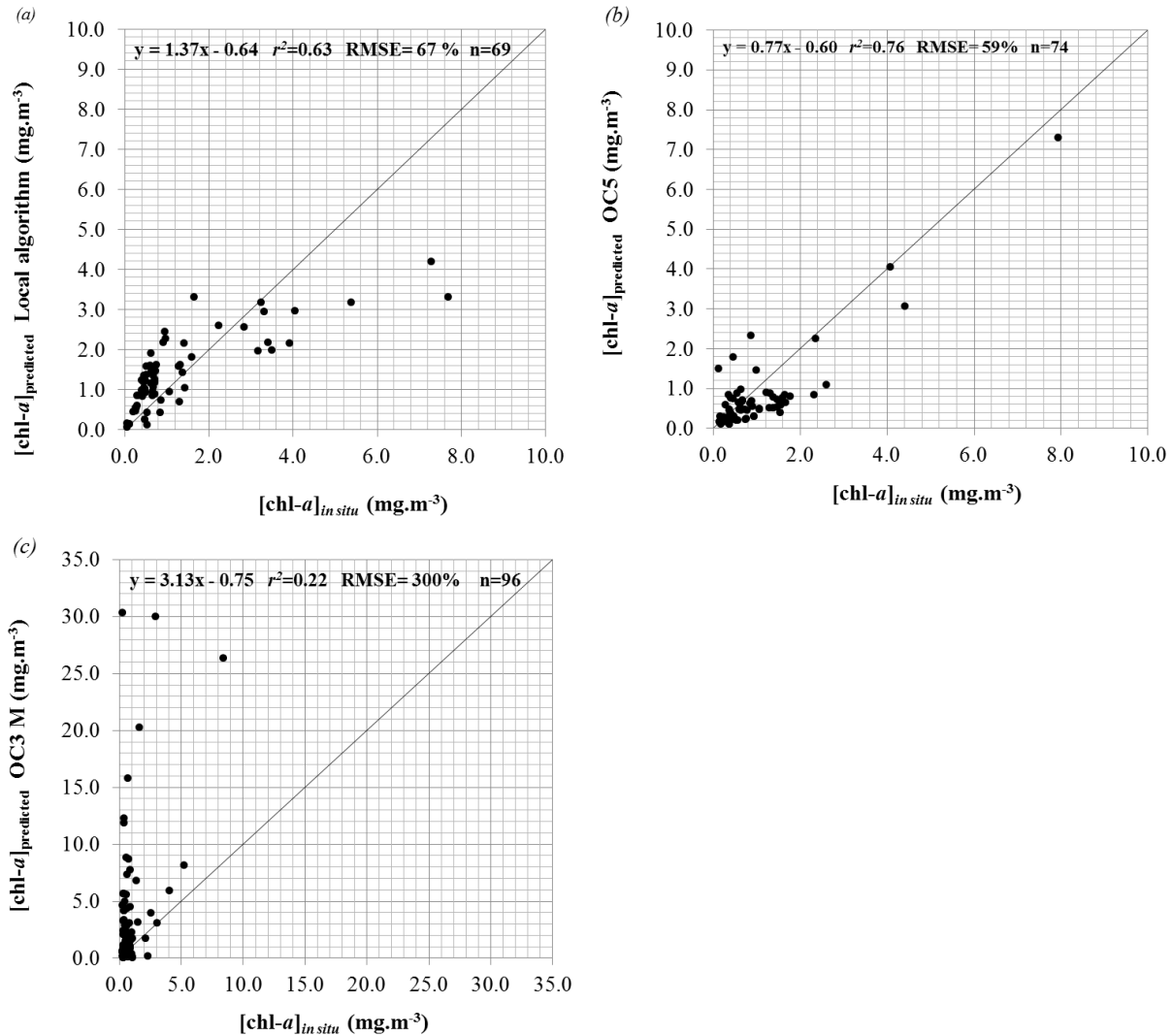


Figure 4.4. *In situ*-Satellite match-up scatterplots: (a) Local; (b) OC5; and (c) OC3M algorithm.

3.3. Chlorophyll-*a* annual cycle

Figures 4.5 (a)-(e) show the comparison between the P90 chl-*a* values derived quarterly from the *in situ* measurements and the P90 chl-*a* values estimated monthly with the OC3M, OC5 and local empirical algorithms. The OC3M considerably overestimates the chl-*a* concentration, with respect to *in situ* measurements. Both the OC5 and the local algorithms reproduce a similar annual cycle than the one observed with the *in situ* data; as they show a spring peak in March, followed by a decrease between April and October, and an increasing again during October. However, the OC5 algorithm provides slightly higher chl-*a* concentration values during the autumn months, compared to those shown by the *in situ* and local algorithms. One exception to this pattern is ob-

served for oceanic waters, where the fit between *in situ* and OC5 values is somewhat accurate.

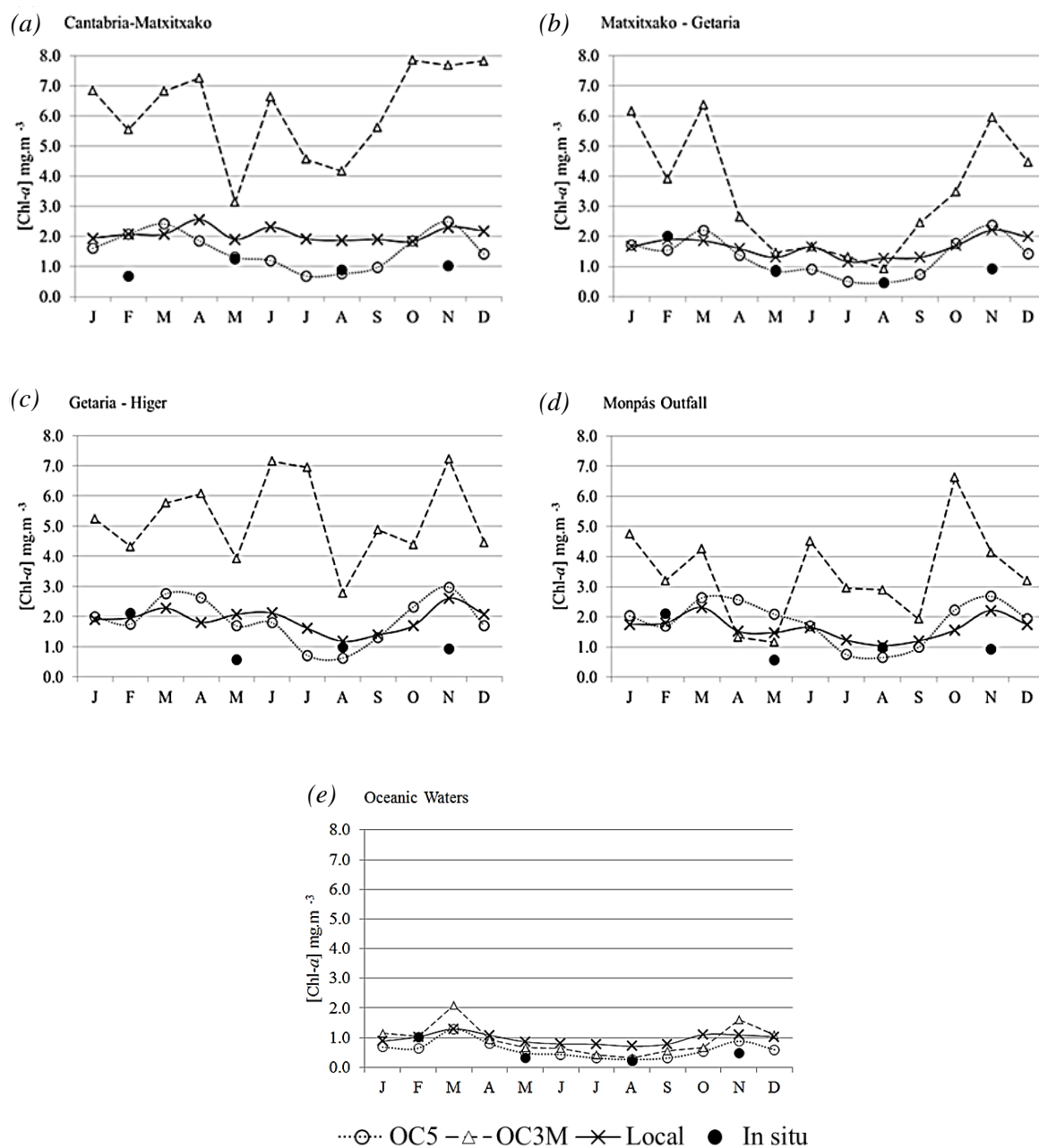


Figure 4.5. Annual cycle of the chl-a concentration P90 observed *in situ* (trimestral) and by satellite (monthly) for the 5 water bodies of the Water Framework Directive monitoring network: (a) Cantabria-Matxitxako; (b) Matxitxako-Getaria; (c) Getaria-Higer; (d) Mompás Outfall; and (e) Oceanic waters.

The OC5 and the local algorithm improve considerably the estimation of chl-a in coastal waters compared with OC3M, as the chl-a concentration values produced by the

former two methods show higher correspondence with *in situ* estimates. As expected, in the case of oceanic waters, the difference between the P90 values estimated *in situ* and predicted by the OC3M algorithm decreases.

The local algorithm shows a general overestimation of chl-*a* concentration for the chl-*a* annual cycle, for the two more western water bodies (Cantabria-Matxitxako and Matxitxako-Getaria), which during the months with the lowest surface chl-*a* concentration (April-September). OC5 predicts more accurately the chl-*a* concentration during these months (April-September) but overestimates the concentration during the period of highest surface chl-*a* concentration (October-March). OC5 provides a wider range of average chl-*a* concentration values (min=0.24; max=3.02), while the range of the chl-*a* concentrations provided by the local algorithm is smaller (min=0.59; max=1.91). The minimum value observed in the *in situ* data (0.19) is similar to the minimum predicted by the OC5 algorithm, while the maximum (1.5) is closer to that predicted by the local empirical algorithm (Appendix). The P90 results are similar; the OC5 algorithm shows a wider range of chl-*a* concentration (max=5.23, min=0.36) than the local empirical algorithm (max=2.65, min=0.7) and the *in situ* data (max=3.57, min=0.25).

Table 4.2 presents the RMS Error (%) calculated for the three algorithms, with respect to *in situ* measurements in surface waters. In general, the local algorithm shows a slightly higher error in comparison with the OC5, an exception is the low chl-*a* months, where the error is substantially higher (P90: 73% vs. 54%). The error associated with OC3M is considerably higher (4 times higher in some cases) than that produced by the other two algorithms.

Table 4.2. Root Mean Square Error (%) (RMSE) between *in situ* measurements and chl-*a* predicted by three algorithms OC3M, OC5 and local, for the complete year, the high chl-*a* months (October-March) and the low chl-*a* months (April-September), averaged for the five water bodies.

RMSE (%)	OC3M		OC5		Local	
	Mean	P90	Mean	P90	Mean	P90
Complete Year	168	388.7	53.7	82.5	60.7	83.7
High chl- <i>a</i> period	218	430.5	62.3	99.1	62.3	81.5
Low chl- <i>a</i> period	87.3	381.6	36.6	54.8	54.6	73.6

A Kruskal-Wallis test showed that the chl-*a* concentration values predicted by the 3 algorithms were significantly different (i.e. all *p*-values < 0.05).

3.4. Ecological quality classification using satellite images

Two total P90 chl-a maps were generated: using the local algorithm and the other the OC5 algorithm. In general, the P90 values were higher with the OC5 algorithm, reaching chl-a concentrations between 5 and 7.5 mg.m⁻³ near the Adour river discharge area. The maximum obtained for the same area with the local algorithm was on the order of approx. 5 mg.m⁻³. (Figure 4.6). Figure 4.7 shows that the highest TSM concentrations overlap the highest chl-a concentrations.

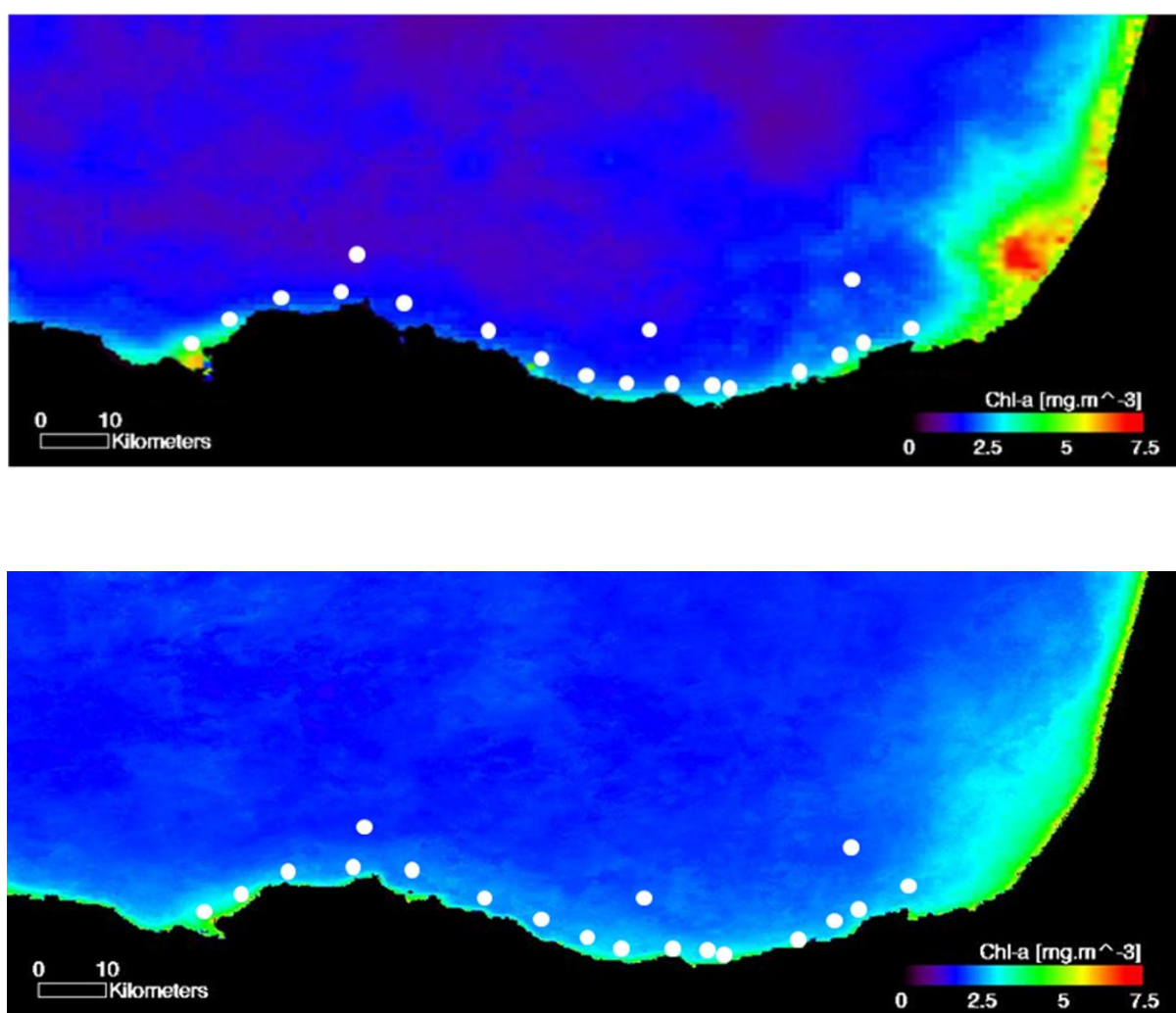


Figure 4.6. Chl-a concentration 90th percentile maps developed with the OC5 (a) and the local (b) algorithms, for the period 2005-2010, and monitoring network stations.

Taking into consideration the algorithm validation results, the OC5 P90 map was selected as the best option for applying the ecological quality classification because the annual cycle maps adjusted slightly better and the total RMSE was lower in general. Each pixel of the resulting P90 image was assigned an ecological quality status class,

according to its chl-*a* concentration. The assessment performed based on *in situ* sampling indicates a high quality status, for all the stations.

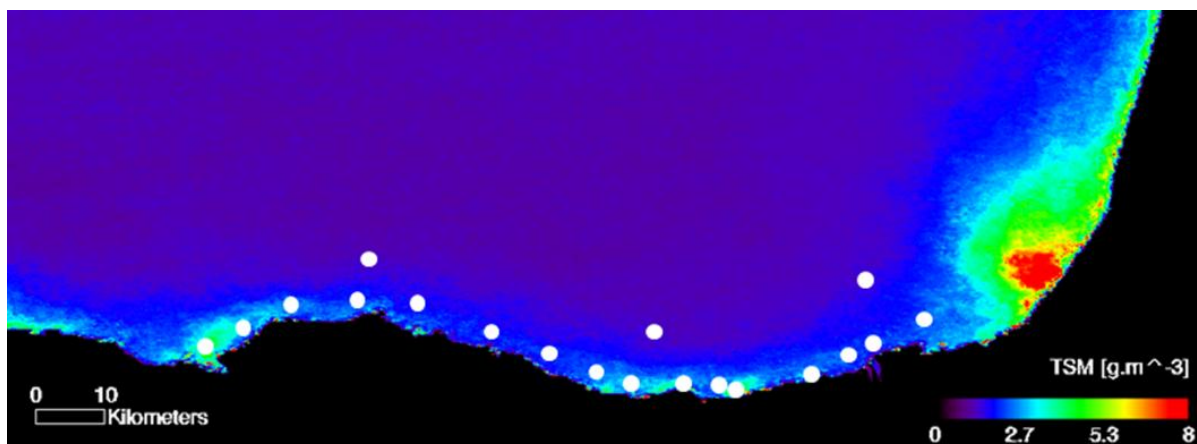


Figure 4.7. Percentile 90th map of Total Suspended Matter for the 2005-2010 period, and monitoring network stations.

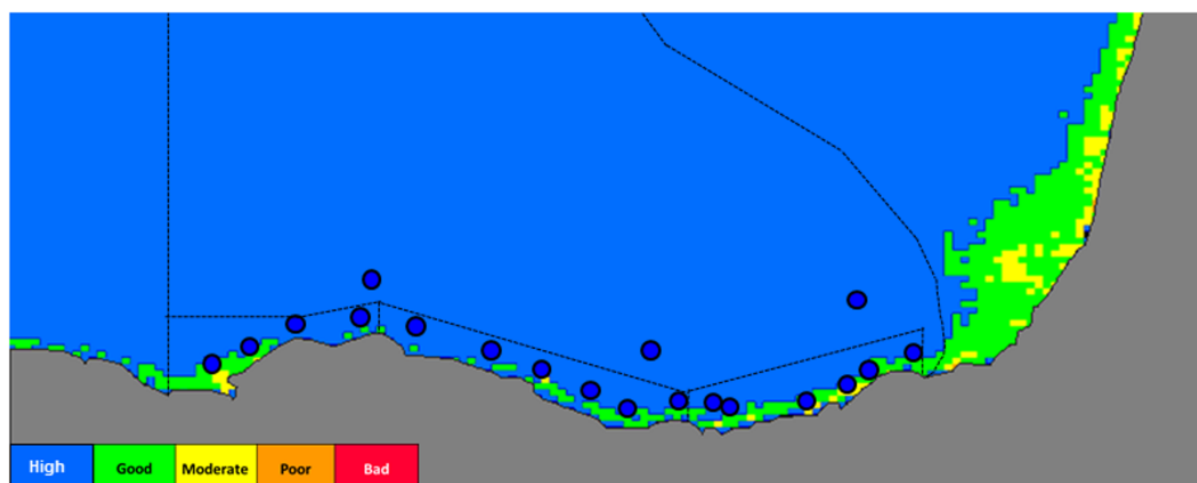


Figure 4.8. Ecological quality status map for chl-*a*, obtained using the OC5 algorithm. The circles represent the quality status estimated by *in situ* sampling and follow the same colour classification. The limits of the water bodies are also represented.

The map obtained with the OC5 algorithm showed a correspondence of 70% (13 out of 19 had “high” status) with the *in situ* quality assessment; while the rest showed “Good” quality statuses (Figures 4.8 and 4.9). Nevertheless, all of the water bodies classified using the remote sensing composite showed a 100% correspondence with the field classification (Figure 4.8) and they all showed ‘High’ quality status, as can be seen in Table 4.3. Additionally, the standard deviations obtained using the satellite images are lower than those obtained with *in situ* estimates of chl-*a* concentration. The 5 water masses comprise a total of 7457 points of information (pixels).

Table 4.3. Mean, standard deviation (Std), 90th percentile of chl-a concentration, and ecological status for each water body and method (*in situ* and satellite with OC5 algorithm).

Zone	Mean chl-a	Std	P90 chl-a	Ecological	Mean chl-a	Std chl-a	P90 chl-a	Ecological
	<i>In situ</i> (mg.m ⁻³)	<i>In situ</i> (mg.m ⁻³)	<i>In situ</i> (mg.m ⁻³)	Status <i>In situ</i>	Satellite OC5 (mg.m ⁻³)	Satellite OC5 (mg.m ⁻³)	Satellite OC5 (mg.m ⁻³)	Status Satellite OC5
Cantabria-Matxitxako	0.65	0.58	0.96	High	0.89	0.33	2.37	High
Matxitxako-Getaria	0.61	0.62	1.09	High	0.80	0.30	2.08	High
Getaria-Higer	0.75	0.58	1.18	High	1.01	0.38	2.81	High
Monpás Outfall	0.69	0.50	1.14	High	1.01	0.35	2.61	High
Oceanic (MSFD)	0.58	0.85	1.00	High	0.40	0.29	1.34	High

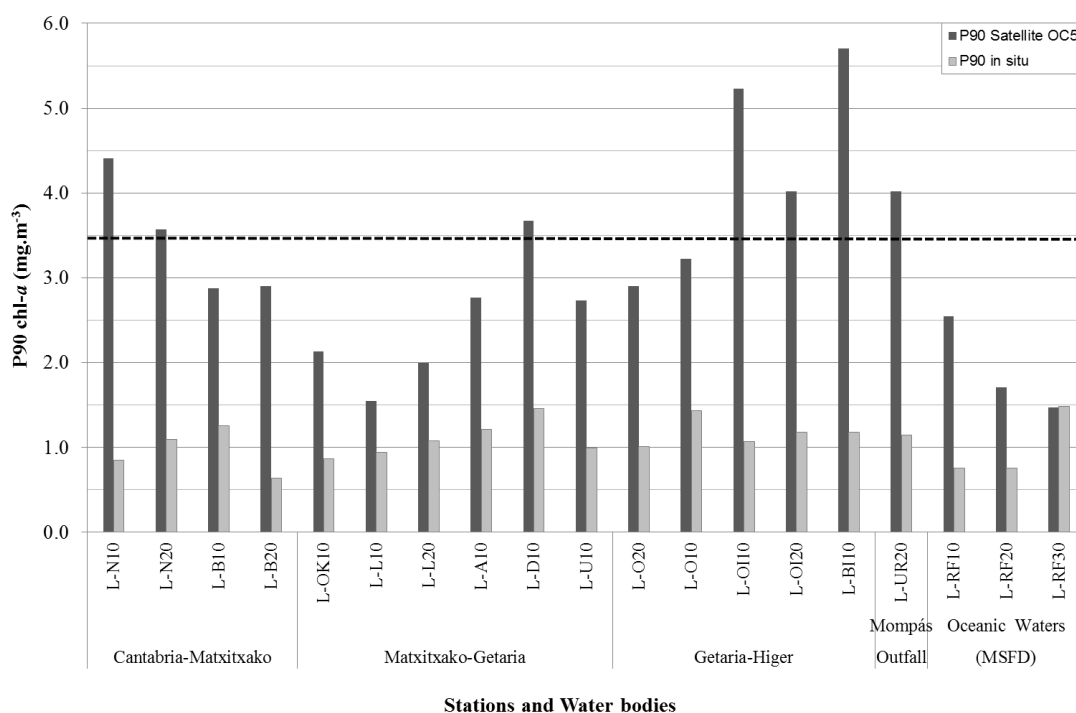


Figure 4.9. 90th Percentile chl-a concentration values for the 2005-2010 period, for each station, estimated with the OC5 algorithm and with *in situ* measurements. The striped line is the P90 chl-a concentration limit between “High” and “Good” ecological quality status (P90 = 3.5 mg.m⁻³).

4. DISCUSSION

The OC5 and local algorithms represent an important improvement in relation to the OC3M algorithm, which highly overestimates chl-a in coastal area. Although both OC5 and local algorithms predict the chl-a with a similar accuracy it can be stated that the OC5 generally offers a better correspondence with *in situ* data, and as they are both significantly different, it is more accurate to use it for the quality assessment.

4.1. *In situ*-Satellite match-ups

The *in situ* match-ups over the 2005-2010 period show that the OC5 provides an advantage in terms of frequency of images compared to the local algorithm, as the bands used by the local algorithm were limited. However, OC5 can overestimate chl-*a* concentration at some coastal stations, whereas the local algorithm can underestimate the chl-*a* in other areas.

The RMS Error observed between *in situ* and predicted chl-*a* concentration could be due to the temporal lag existing between the time when *in situ* measurements were performed and the time that satellite images were captured (a maximum of a 3 hour time-lag was considered), which could have introduced inaccuracies (Chang and Gould 2006). Such differences can lead to inconsistencies when comparing the results provided by both methods (satellite and *in situ*), as observed in Figure 4.4. In addition, even when the pixels located closest to land were not considered in the assessment, the proximity of some stations to the coast can introduce artefacts, or inaccuracies due to the influence of land pixels over the water pixels (Binding et al. 2011). A bias can also appear when there are methodological differences in estimating chl-*a* (Sørensen 2002). In this case, local empirical algorithms are developed with *in situ* data that estimated based on spectrophotometry, as this method is considered to be more accurate for this purpose (Doerffer 2002), and validated using *in situ* data estimated based on CTD fluorescence during the LQM. This technical difference could cause inaccuracies during validation of the algorithm with the *in situ* measurements from the surveys. As such, it has been observed in this study that CTD fluorescence can underestimate slightly the chl-*a* concentration in the water (Figures 4.2 and 4.3). Such an underestimation was also reported in the study performed by Mignot et al. (2011), addressing the derivation of chl-*a* concentration based on CTD fluorescence profiles.

In addition, uncertainties related to the comparison of *in situ* water samples, with image pixels, can also be an issue. Differences in water volume and the spatial variability presented by chl-*a* at a small, local scale can also cause differences in absolute values. This particular issue was explained by Gohin et al. (2008), who described it as the “support effect” stating that in coastal areas, small scale chl-*a* patchiness is caused by local bathymetry and hydrographical features, such as currents, which enhance the support effect. Consequently, this effect has a direct influence on the estimation of

P90, which is associated with the variance. For this reason, none of the methods can be considered to be more representative of the “real” chl-*a* concentration present in the environment based on the dataset presented in this study. The *in situ* measurements are more spatially restricted than those predicted by the satellite algorithms and differences in absolute values are expected.

4.2. Chlorophyll-a annual cycle

With respect to the annual cycle of the surface chl-*a* concentration, the overestimation of chl-*a* with the OC5, during the autumn-winter season (October-March), could be explained to some extent by the low frequency of *in situ* measurements, as this frequency may not be sufficient to capture the autumn-winter and winter- spring bloom (throughout all of the years). During the colder months, one *in situ* survey is performed usually in October, with the next taking place in February or March. Therefore, the increase in phytoplankton abundance may not always coincide with any of these (one-day) *in situ* surveys.

Another reason for the chl-*a* overestimation could be the increases in suspended particulate matter, caused by increases in rainfall that characterise the cold season. During the 2005-2010 period, a 5-fold rainfall increase was observed for the Basque coastal rivers (eastern), between the months of July-August and October-November (approx. 2 mm.day⁻¹ to 10 mm.day⁻¹; information available at the Diputación Foral de Guipúzcoa" webpage*). The 90th percentile of suspended material maps showed a 3-fold increase within the coastal water bodies (approx. 0.3 g.m⁻³ in August, to approx. 1 g.m⁻³ in November on average; see appendix Figure A10). This augmentation of optically-active suspended inorganic material and dissolved organic matter in coastal waters influences the signal retrieved by remote sensors; it can cause algorithms to overestimate chlorophyll levels (Gordon and Morel 1983; Carder et al. 1991; IOCCG 2000). Alternatively, it could be caused simply by phytoplankton blooms produced by the same phenomenon (increase in rainfall, river runoff and nutrients) that exist for too short of a period (7-9 days as reported by Alvarez et al. (2009); in Cantabrian waters) to be captured by *in situ* monitoring (one measurement every three months). Even if the magnitude of the peaks is higher for the satellite than the *in situ* data, there is generally a peak in surface chl-*a* during early spring, a decrease approximately between April-May

and September, and a further increase during autumn. This cycle corresponds with the description of Fernández and Bode (1991), who defined the phytoplankton cycle of the area as typically temperate. At the offshore station L-REF10, previous studies have shown that there is an increase in the monthly average chl-*a* concentration in the surface waters during the cold season, with a decrease during the warm season (Revilla et al. 2010a). In the present study, the seasonal pattern of chl-*a* slightly different in oceanic waters, in comparison to the coastal waters. In the coastal waters, the period of low chl-*a* is usually shorter because these levels can present some small peaks from spring to summer. The seasonal variability of chl-*a* of the Basque offshore waters is affected, considerably by the availability of nutrients, which responds to the mixing/stratification processes of the water column, associated to the thermal cycle (Valencia et al. 2004; Borja et al. 2009). The existence of additional sources of nutrients in the coastal water bodies (i.e. river runoff, resulting from summer storms or anthropogenic inputs, such as the outfall), could explain their higher productivity during the warm season.

Furthermore, the field monitoring surveys were carried out only 4 times a year, between February and November during the 2005-2010 period (providing a total of 6 measurements *in situ* per season, for the entire period). In comparison, the P90 results have utilised 80 images, on average, per month for the same period (2005-2010; 962 images in total), which makes it difficult to consider the *in situ* data as the most representative information of the chl-*a* annual cycle. Additionally, the greater magnitude of the standard deviation obtained through *in situ* sampling indicates a possible increase in error, which is due to the lower number of measurements performed using this method.

4.3. Ecological quality classification using satellite images

Despite the technical differences between the *in situ* and satellite methods, the P90 values and the status classification of stations and water bodies are very similar when compared. The satellite approach has provided high-frequency measurements, supporting findings of previous studies using *in situ* CTD data that indicated low risk of eutrophication in the Basque coastal and offshore waters (e.g. (Revilla et al. 2009; Borja et al. 2011)). Within the NEA region, the Basque coast located within the north of

Spain belongs to the Eastern Cantabrian Coast subregion, which is characterised by various small-river plumes and low upwelling intensity (Carletti and Heiskanen 2009). These natural features, together with a high flushing and dilution capacity related to anthropogenic inputs that result from the geomorphology and hydro-meteorological regimen, can explain the low chl-*a* concentration in this area in comparison with other European coastal waters (Revilla et al. 2010a). The alternative of using satellite imagery for chl-*a* data acquisition would involve a more exigent evaluation (fulfilling the precautionary principle) of water quality in relation with eutrophication, as the values obtained for the phytoplankton biomass metric (P90) are slightly higher using the satellite imagery. Although both methods present a degree of uncertainty, the differences in the P90 values are probably due to the different sampling frequencies employed. In this regard, other authors have warned about the risk of water quality misclassification, when employing a low frequency of data acquisition for phytoplankton because these organisms represent a biological element that is subjected to a high temporal variability in the marine environment (Domingues et al. 2008).

4.4. Combination of *in situ* and satellite data for water quality assessment

Valid *in situ* measurements are necessary to check and validate, on a regular basis, the satellite data. Additionally, *in situ* surveys are essential for the acquisition of water samples for the analyses of phytoplankton composition and abundance to meet the requirements of the WFD and MSFD. Regarding the chl-*a* concentration estimated from satellite images, an option for improving the accuracy of phytoplankton quality assessments could be to use the OC5 algorithm for the offshore waters and in coastal water bodies during the months presenting the lowest surface chl-*a*, and to use the local algorithm for the coastal water bodies during high chl-*a* months. However, the basis for shifting between algorithms may be difficult to establish and could be another source of inaccuracies. Hence, the use of the OC5 algorithm would be the most pragmatic option. Another alternative would be to use the same basis of the OC5 “Look-up Table” but adjusted via to the local algorithm, thus incorporating the data obtained through *in situ* measurements during the field surveys into the OC5 Look-up Table. The OC5 algorithm has been validated using a large number of field measurements obtained in water bodies adjacent to the Basque coastal area (Gohin et al. 2008; Saulquin et al. 2010). In addition, it is able to provide a wider range of chl-*a* concentrations, a higher image

frequency, and more accurate estimates of this parameter in oceanic waters. In this regard, the extensive validation work performed for this algorithm, the lower RMSE it provides, and its more accurate correspondence with the *in situ* chl-*a* annual cycle and match-ups overcome the slightly higher accuracy obtained via the local algorithm during the months with higher surface chl-*a* levels. Also, the RMSE values obtained are lower to the levels of accuracy found other studies undertaken in the Bay of Biscay (Morozov et al. 2010) and similar to the levels obtained other in case 2 water bodies (Gitelson et al. 2009).

Additionally, the P90 maps produced with the OC5 algorithm can be used to identify areas more vulnerable to anthropogenic discharges that were not recorded with previous field surveys, hence new field monitoring stations could be established in such areas. According to the data presented in Figure 4.8, the satellite imagery provides a lower classification for some stations than the *in situ* data, which could be due to an overestimation of chl-*a* by the algorithms or to an underestimation of the *in situ* measurements. However, the maximum P90 values for the water bodies do not overcome the “High-Good” class boundary chl-*a* concentration (Table 4.3), which was established at 3.5 mg.m^{-3} (Figure 4.5). Hence, this overestimation could be neglected for the assessment of the water bodies, throughout the period of the study. The RMSE values obtained for the estimation of chl-*a* with the OC5, were sufficient to apply the classification scheme, since, taking them into account did not cause a change of status of the 4 water bodies selected.

As stated by Gohin et al. (2008), satellites may incorrectly chl-*a* concentration of near shore pixels, but the *in situ* sampling could be misrepresenting the entire water body. Nevertheless, in the present study the remote sensing methods provided realistic estimates of chl-*a*, based on the comparisons. Likewise, the observed overestimations did not result in a lower quality status being indicated for the water bodies. The overestimation was not sufficiently high to establish a change in the status of the majority of the pixels, only those closest to the shore or those most influenced by river runoff. Therefore, along the coast of the Bay of Biscay, as well as in other NEA waters satellite imagery is a potential tool for the acquisition of surface chl-*a* data and for the subsequent assessment of the phytoplankton quality status (WFD) and marine environmental status (MSFD). Additionally, this tool could allow a comparable assessment of water

quality across different water types and Member States, counteracting the difficulties that arise in making comparisons when different methodologies are utilised regionally. The OC5 algorithm has been shown to be suitable for the French coast (Gohin et al. 2008) and, as demonstrated in the present study, for the Basque continental shelf in the north of Spain. MODIS imagery was considered to be appropriate for use in this study, due to its high image frequency (two passes a day), and because these images are available through an ftp server that is easy to access. A total of 962 images were used in this study, whereas this number would be reduced to 624 if MERIS images were used. MERIS images can also be downloaded (free of charge) for reduced resolution images (1 km x 1 km), although MERIS can also provide images at full resolution (300 m x 300 m), at an extra cost. Even if these full resolution images would have been appropriate for this study, MODIS imagery presented more operational advantages. A large number of images were necessary to perform the comparison with *in situ* data, while the cost and the lower frequency of the MERIS images represented restrictions.

Chapter V

Chlorophyll-*a* variability within Basque coastal waters and the Bay of Biscay

1. INTRODUCTION

Primary productivity in temperate areas is subjected to a high spatio-temporal variability (Cebrián and Valiela, 1999). Phytoplankton blooms are events of rapid production and accumulation of phytoplankton biomass that are usually responses to changing physical forcings originating in the ocean (e.g., upwelling), the atmosphere (wind), or on the land surface (precipitation and river runoff). These drivers have different time-scales of variability; thus, phytoplankton blooms can be short-term episodic events, recurrent seasonal phenomena, or sporadic events associated with extraordinary climatic or hydrologic conditions (Cloern 1996). Several studies have reported the high variability present in oceanic, continental shelf and coastal areas of the Bay of Biscay (Tréguer et al. 1979; García-Soto and Pingree 1998; Lampert 2001; Gohin et al. 2003; Loyer et al. 2006).

River discharges into coastal waters are an important element in the dynamics of the continental shelf in the Bay of Biscay (Puillat 2004; Guillaud et al. 2008; Prego et al. 2008). The plume regions off the river mouths play an important role in the shelf's physical, biogeochemical and ecological functioning, as the river discharge includes nutrient, sediments, pollutants and other constituents in addition to freshwater (Arnau et al., 2004; Wysocki et al., 2006; Weston et al., 2008; Petus et al., 2010). In the presence of a river plume, light and circulation patterns, stratification, nutrient pathways are significantly altered. Hence, the ecological processes taking place in the plume area are influenced by this exchange between the continental shelf and the river water (Sierra et al. 2002). The extent of the influence of the river discharge depends mainly on the river flow regime and on the volume of the discharges (Cravo et al. 2006), at seasonal and annual scales (Signoret et al. 2006). Additionally, the exchange dynamics between river discharges and coastal waters is affected by wind (turbulence) and waves (bottom shear stress) (Stumpf et al. 1993; Gonzalez et al. 2004). Hydrological features related to river plumes, and light availability, seem to be the two major factors regulating the winter to spring phytoplankton production in the Bay of Biscay (Morin et al. 1991; Labry et al. 2001; Gohin et al. 2003). Nutrients brought by river runoff play an important role on the in primary production (Lavín et al. 2006) and the presence of non-living particulate and dissolved matter decreases water clarity (increases the coefficient of light attenuation), limiting phytoplankton growth (Huret et al. 2007; Rivier et al. 2011).

Furthermore, the WFD requires member states to assess the quality status of water bodies based on the hydromorphological elements, such as freshwater inputs, in relation to reference conditions. Therefore, knowledge of the dynamics taking place on the coast is critical in the assessment of eutrophication and water quality.

1.1. Objectives

Former chapters have exposed the variability of chl-*a* algorithms' performance in relation to regions (Chapters II and III), seasons (Chapter IV) and the presence of other water constituents (Chapters II-IV). Hence, it seems important to study the spatio-temporal variability of chl-*a* in relation to river inputs, one of the main factors affecting this variability. The first objective of this chapter was to examine and describe the variability of chlorophyll-*a* concentration in surface waters of the Basque coastal area, using satellite imagery, and its possible relationship with river discharge. The hypothesis is that rain events and river discharge act as fertilization factors, enhancing phytoplankton growth and leading to increased biomass (i.e. chlorophyll-*a*) in the Basque coast. To perform this study, three approaches to analyse rainfall, river discharges and chlorophyll-*a* patterns were followed: (i) daily, (ii) seasonal, and (iii) inter-annual variability. The second objective was to offer a synoptic description of chlorophyll-*a* spatio-temporal variability in the entire Bay of Biscay, using multivariate statistical methods.

2. MATERIALS AND METHODS

2.1. *In situ* dataset

A time series of daily data at inland stations of two rivers, the Adour (France) and the Nervión (Spain) were acquired for the 2005-2010 period. In the case of the Nervión River, rainfall (mm), river discharge ($\text{m}^3 \cdot \text{s}^{-1}$), turbidity (NTU) and suspended and dissolved matter ($\text{mg} \cdot \text{m}^{-3}$) were measured at a station located on the river. The station selected was the nearest station to the river mouth without influence of the marine tides; its name is Abusu. The data was downloaded from the "Diputación Foral de Bizkaia" web site (www.bizkaia.net/). In the case of the Adour, only daily river discharge data was available and the data was downloaded from the DIREN web site (Direc-

tions Régionales de l'Environnement; www.hydro.eaufrance.fr/). The total river discharge was computed by combining the contributions from the 6 main streams of the Adour basin (Figure 1; Petus, 2009).

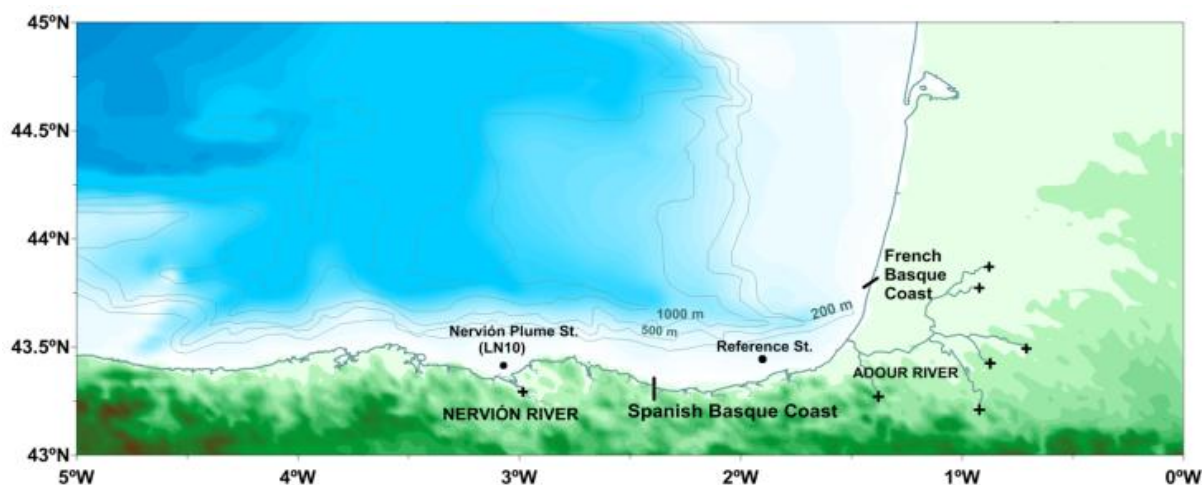


Figure 5.1. Study area in the southeastern corner of the Bay of Biscay. The crosses (+) represent river stations, the black circles (●) represent the marine stations.

2.2. Satellite data

A total of 1672 OC5 products for the 2005-2010 period were downloaded from Ifremer's ftp server*. The OC5 is an empirical algorithm, developed and validated by Gohin et al. (2002, 2008) and Gohin (2011). This algorithm derives chl-*a*, turbidity and suspended matter products with Look-up tables applied to Standard MODIS/Aqua Level-2 reflectance products (processed with SeaDAS).

2.3. Daily data analysis

First, two OC5 chl-*a* products corresponding to two days before and one day after a rainfall event were downloaded. The rainfall event occurred on the 13th of January 2009 (a time of the year with high precipitation levels), but no images were available on that day due to the cloud cover, hence, chl-*a* products corresponding to the 11th and the 14th of January 2009 are presented here. Satellite chl-*a* concentrations extracted from a 3 x 3 pixel window near the river mouth was compared to river discharge data. Then, to obtain information on the effect that rainfall had on coastal waters, a sequential diagram was created with an average of 13 rainfall events, selected during the 2005-2010 period for the Nervión River. The *in situ* variables measured (rainfall, river discharge, turbidity and organic matter) were averaged, between days -1 and 7, being -

*<ftp://ftp.ifremer.fr/ifremer/cersat/products/gridded/ocean-color>

1, one day before the rainfall event, 0 the day of the event, 1 the day after the event, and so on. Chl-*a*, turbidity and suspended matter data, within surface waters of the river plume area, were acquired using satellite imagery. Values of the three variables were extracted using the averaged 3 x 3 pixel window located near the river mouths. The distance from the river mouth was approximately 1.5 pixels (or 0.9 nautical miles); this distance was necessary to avoid the effect of the land pixels. The analysis could not be performed for the Adour due to the lack of rainfall data.

Then, cross-correlation analyses with daily lags were performed with the different *in situ* variables obtained for the Nervión River, i.e. rainfall *versus* river discharge, organic matter and turbidity.

2.4. Seasonal analysis

Chl-*a* 90th percentile (P90) and average maps were produced for the 2005-2010 period (see Chapter IV, for more details). This was performed by initially selecting all cloud-free images available for the study area during the 2005-2010 period. Subsequently, the P90 and average values were calculated for each pixel of all images selected for that period, with IDL programming. As such, the IDL program calculated for each pixel, the average chl-*a* value and, for P90 maps, the value where 90% of the observations were equal or below. This approach resulted in two types of products, monthly P90 and mean chl-*a* maps for the 2005-2010 period. A comparison was also performed between chl-*a* concentration values extracted using a 3 x3 pixel window positioned near the Adour and Nervión river mouths and at the offshore reference station.

2.5. Inter-annual analysis

The long-term trends (years 2005-2010) of sea surface (0-1 m) chl-*a*, suspended particulate matter and turbidity in river plume areas, were analysed along with the variability of rainfall and river discharge of the rivers at the inland stations. *In situ* data from the Littoral Water Quality Monitoring and Control Network (LQM) of the Basque Country, managed by the Basque Water Agency, used previously in Revilla et al. (2009) and in Chapter IV, was used to perform a time series analysis of the 2005- 2010 period, and was compared to the same analysis performed with satellite data. The locations of the

Nervi3n (LN10) and the reference stations are shown in Figure 1. The 3 x 3 pixel window positioned at those locations was used to extract the chl-*a* concentrations.

In the case of the satellite-derived variables, 2-week means were used to avoid missing values. In the case of *in situ* data, daily measurements of river discharge and rainfall were employed for the analysis, while chl-*a* *in situ* measurements used in this analysis were performed once per trimester. The variability of each variable was examined by means of the “*decompose*” procedure in R language, which extracts the seasonal component of the time series, and outputs the trend followed by each variable without this component. Subsequently, the trend values were linearly regressed against the years, and the significance of the trend-line was measured with the *p*-value returned by the regression. A permutation resampling method was performed to test the significance of the trend-lines. The time series was permuted 1000 times, and the observed slope from the regression between the trend and the time series was then compared to the permuted slopes. The null hypothesis established that the observed slope did not show a significant change over the years. If the observed value is found to be outside 95% quantile range of the histogram, then the null hypothesis is refuted. For more information on this procedure see Davison and Hinkley (1997).

2.6. Spatial analysis

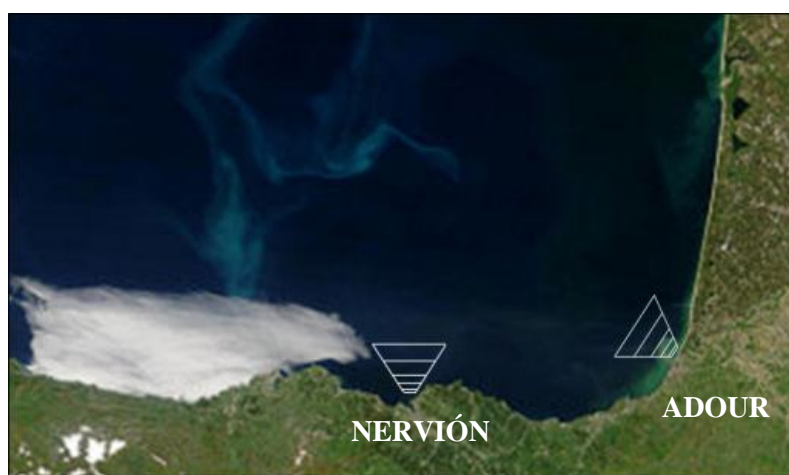


Figure 5.2. Polygons used to extract mean chl-*a* concentrations at different distances from the river Nervi3n and Adour mouths (MODIS Terra, 17/05/2004).

The evolution of chl-*a* concentration in the river plume areas with increasing distance from the coast, was examined using the monthly P90 chl-*a* maps calculated with

images downloaded between 2005 and 2010. As such, mean values of chl-*a* at different distances from the coast were extracted in the form of polygons, as shown in Figure 5.2.

2.7. Cluster and Principal Component Analysis

Two multivariate statistical analyses were performed over the entire Bay of Biscay, an unsupervised classification and a Principal Component Analysis (PCA), to synoptically describe the variability of chl-*a* concentration throughout the seasons and from coasts to open waters. The entire bay was considered for these analyses to examine the spatial variability of the Basque coast area in relation to the entire bay.

The unsupervised cluster classification of the chl-*a* OC5 products was performed with the k-means routine from the ENVI program. All the products available for the 2005-2010 period were included in this analysis. This routine initially computes class means evenly distributed in the data space. Three classes were selected for this classification. Then, it iteratively clusters the pixels into the nearest class using a minimum distance technique. Every single iteration recalculates class means and reclassifies pixels with respect to the new means. This process continues until the maximum number of iterations is reached. For more information see Tou and Gonzalez (1974).

The PCA was performed using the ENVI program as well. All the OC5 chl-*a* products available for the 2005-2010 period for the entire Bay of Biscay were used for this purpose. The PCA produces uncorrelated output bands, to segregate noise components, and to reduce the dimensionality of data sets. This routine finds several sets of orthogonal axes that have their origin at the data mean and that are rotated so the data variance is maximized. It produces principal component bands that are linear combinations of the original spectral bands and are uncorrelated. The first PC band contains the largest percentage of data variance and the second PC band contains the second largest data variance, and so on. The percent of total variance can be determined from the eigenvalues, which are the measure of variance in a PCA. The set of weights applied to band values to obtain a principal component are called eigenvectors. To obtain more information on this procedure see Richards and Jia (2006).

In this study, the results provided by the PCA offer a visualization of the similarities and differences among pixels in relation to the temporal evolution of the chl-*a* concentration averages. This analysis also provides a visualization of the global connections between the chl-*a* pixels of the entire Bay of Biscay. In this case, the PCA variables are the averaged chl-*a* months, which are 70 in total and the number of observations used in the analysis are the total number of pixels in the area of study, hence 244097 points of observation (the land is not included). Monthly composites were chosen for this analysis because the PCA principles state that missing values should be avoided. Some areas show missing values during large periods of time (more than 10 days in some cases), due to clouds or image artifacts. The 70 monthly averaged composites rarely provided missing values for the Bay of Biscay area.

3. RESULTS

3.1. Daily variability

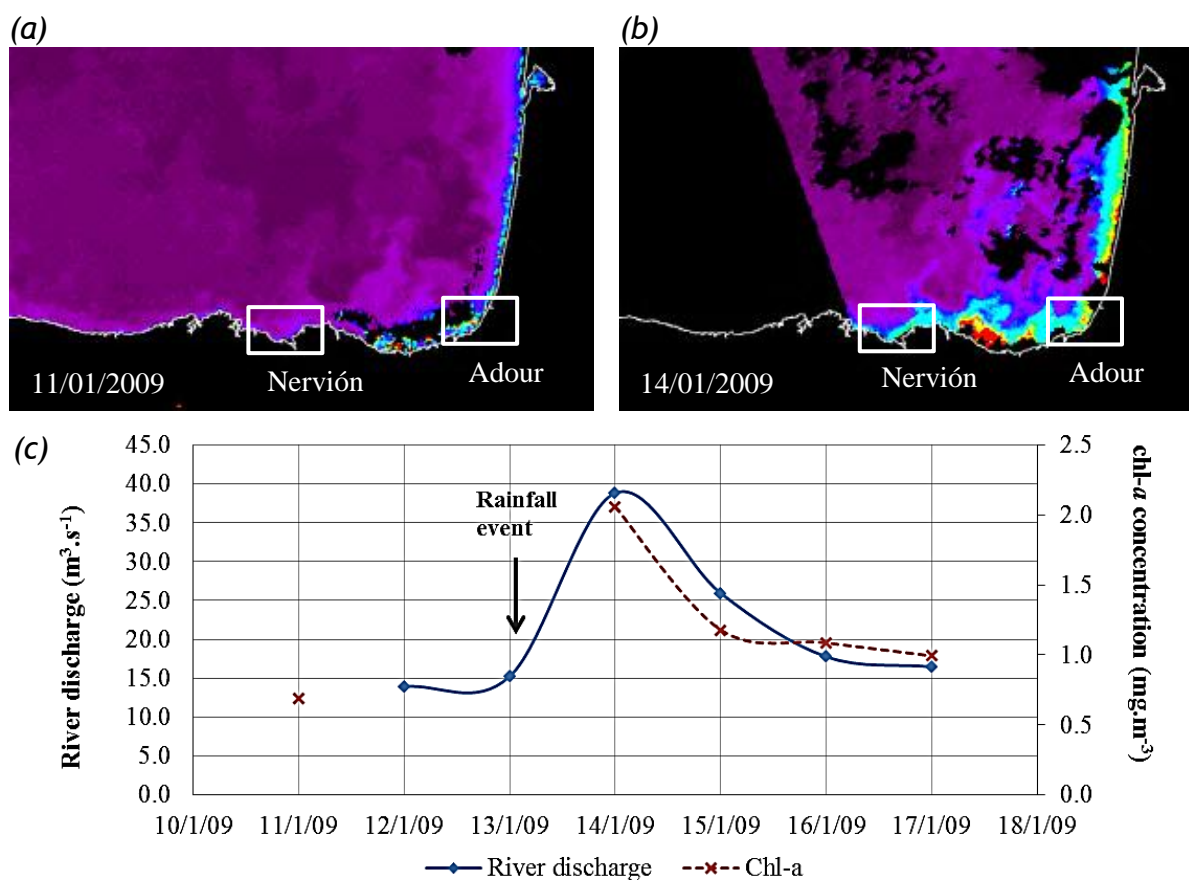


Figure 5.3. MODIS daily image showing chl-*a* distribution (estimated with the OC5 algorithm) before (a) and after (b) a rainfall and discharge event occurred on the 13th of January 2009. (c) High chl-*a* concentration (dashed lines) was observed one day after the rainfall event, and on the same day of the river discharge increase was recorded in the river station.

Images before and after the rainfall event, which occurred on the 13th of January 2009, showed an increase of chl-*a* in the coastal area one day after the event (Figure 5.3). In the case of the Nervión River, there was an increase of river discharge on the same day of the rainfall event and the maximum river discharge was reached after one day (Figure 5.3).

Figure 5.4 shows that, in the case of the Nervión river, the averaged turbidity and organic matter measured *in situ*, present a maximum increase one day after the event. The cross-correlation analysis showed that chl-*a*, suspended matter and turbidity estimated with satellite imagery reached a maximum concentration 2 days (on average) after a rainfall event i.e. average of 13 rainfall events (Figure 5.4).

The cross-correlation between rainfall and river discharge is significant on the same day of the event and on the seven following days. Rainfall and turbidity measured *in situ* are also significantly correlated at day lags between 0 and 7, while organic matter is significantly correlated with rainfall only on the day of the event (Figure 5.5).

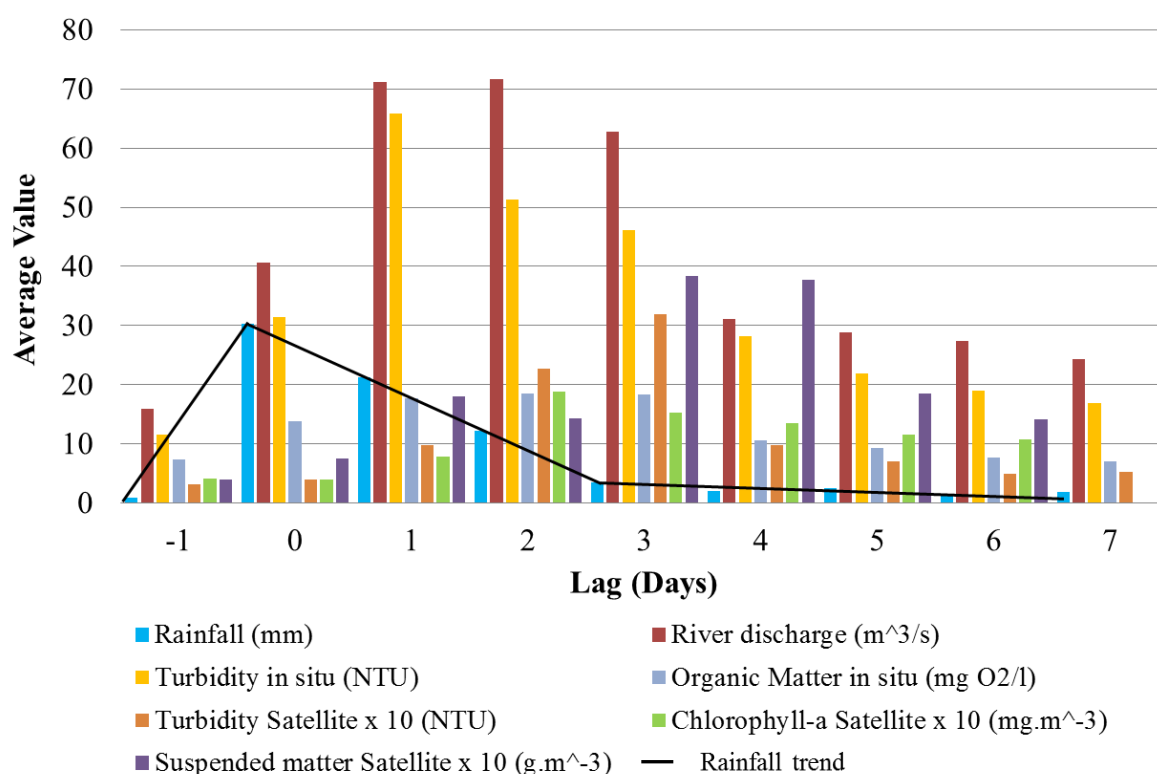


Figure 5.4. Diagram showing the evolution of the different variables measured *in situ* (rainfall, river discharge, organic matter, and turbidity) at the river Nervión station and with satellite imagery at the river plume (chl-*a*, suspended matter and turbidity). The values shown are an average of 13 rainfall events. Some parameter values are transformed for display purposes.

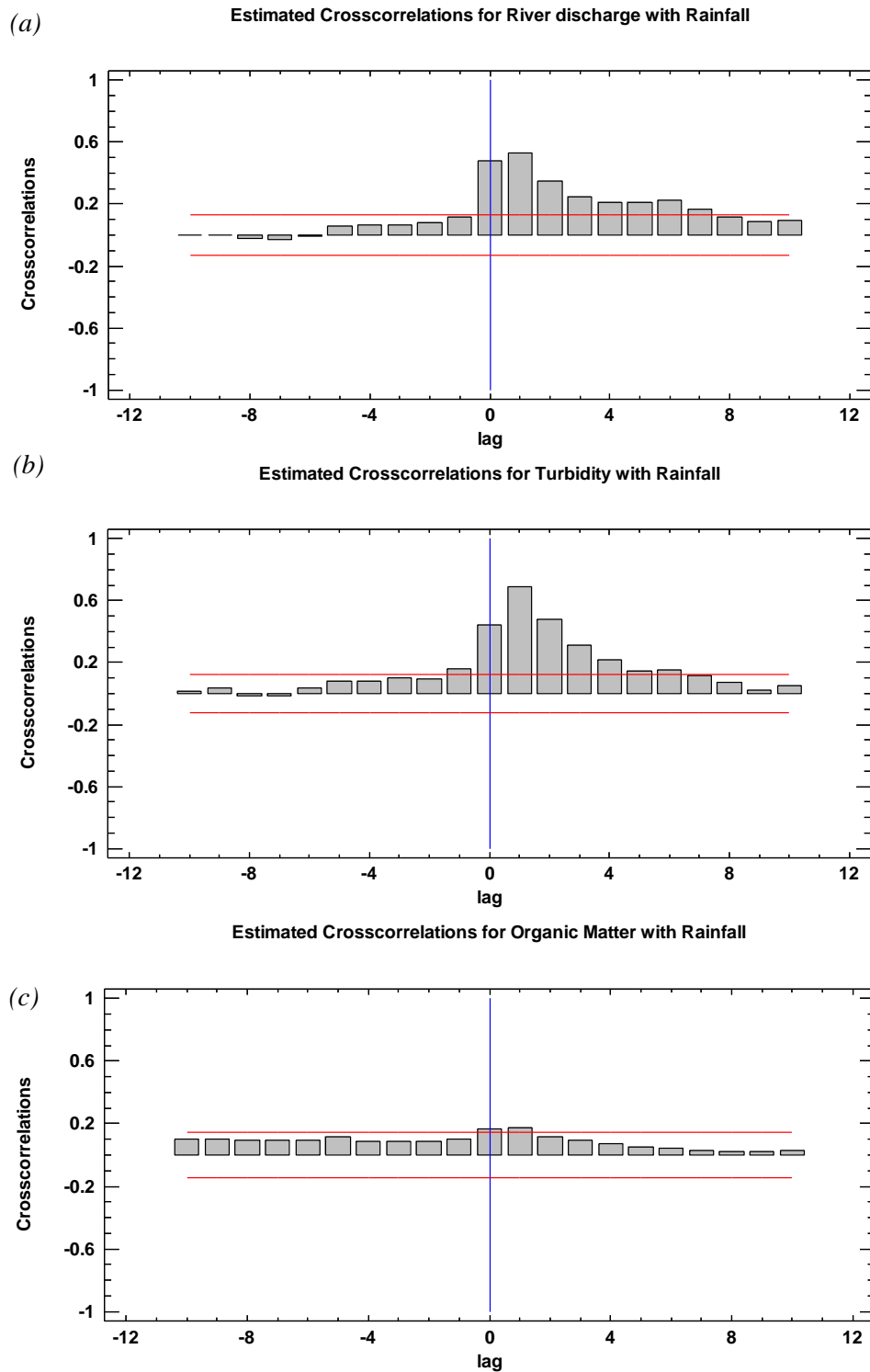


Figure 5.5 Cross-correlations between *in situ* parameters. (a) River discharge with rainfall, (b) Turbidity with rainfall and (c) Organic matter with rainfall.

3.2. Seasonal variability

The monthly P90 and mean images for the 2005-2010 period showed similar seasonal patterns for both the offshore and the coastal areas, with some exceptions (Figure

5.6, 5.7, 5.8). In offshore waters, two main chl-*a* concentration peaks are observed, one of them is observed during spring (March-April) and the other in November. However, the P90 and the mean values extracted from the images show different magnitudes. The P90 chl-*a* levels are greater in November than in March, while the mean data shows the opposite, higher chl-*a* concentrations in March compared to November (Figure 5.8). The summer months in offshore areas show the lowest levels of chl-*a* concentration.

In coastal waters, seasonal differences are observed in different areas (Figures 5.6 and 5.7). In the area of the Adour river plume, the maximum chl-*a* concentration is observed in May, for both the P90 and the mean products (Figures 5.6, 5.7, 5.8). A peak is observed with the P90 chl-*a* values in February that is observed with less magnitude on the chl-*a* mean figure (Figure 5.8). In the area of the Nervión plume (Figure 5.8), there are two major chl-*a* peaks, one in March and one in November. Both the P90 and the mean values of the pixels located at the Nervión plume show this pattern and the chl-*a* concentrations are higher in November than in March. The patterns of the Nervión river discharges and chl-*a* levels observed in the river plume area coincide, except for the chl-*a* concentration increase observed in June (Figure 5.9). The variability of the river discharges is also greater during the spring and the autumn months. In the case of the Adour, the patterns are slightly different, as the highest river discharges occurred in April-May, and the highest mean chl-*a* concentration values at the Adour river plume area are observed in May (Figure 5.9). These are also the periods of greatest river discharge variability (Figure 5.9).

The chl-*a* seasonal pattern slightly changes with distance from the coast (Figure 5.10). Chl-*a* 90th percentile between 1.2 and 11 nautical miles from the Nervión river mouth, exhibits two major peaks, one in spring and another in November. The magnitude of the chl-*a* concentration decreases with increasing distance. However, two particularities can be observed. First, at 1.2 miles from the coast, there is a peak in June that is not observed at a farther distance. Second, the peak occurring in November is of greater magnitude compared to the peak occurring in March at 1.2 miles, but this is not observed at larger distances. In the case of the Adour, the month with the highest chl-*a* concentration is May, up until a distance of 11 nautical miles; at this distance, March is the month with the highest chl-*a* concentration.

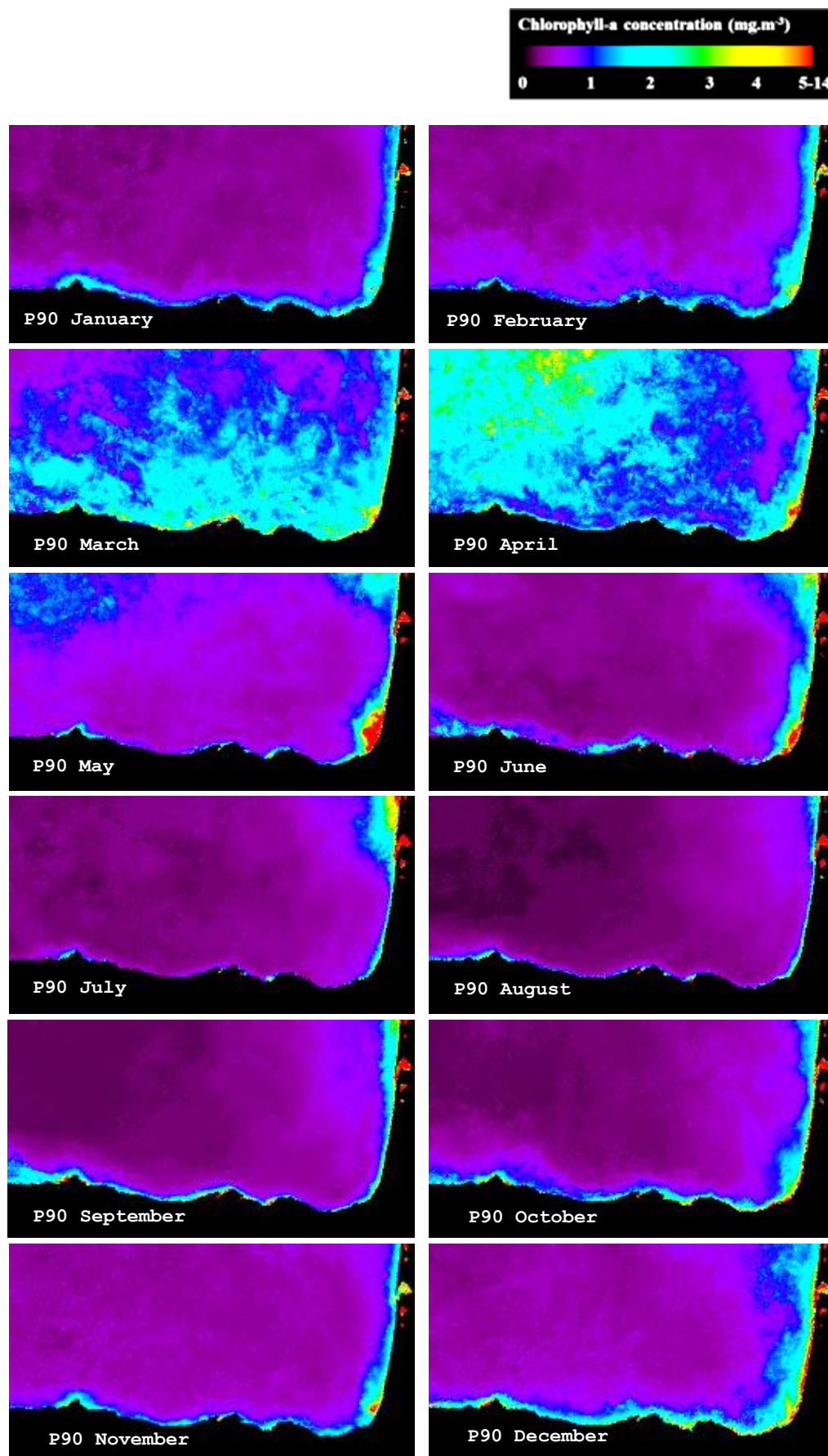


Figure 5.6. Monthly P90 chl-a maps for the 2005-2010 period.

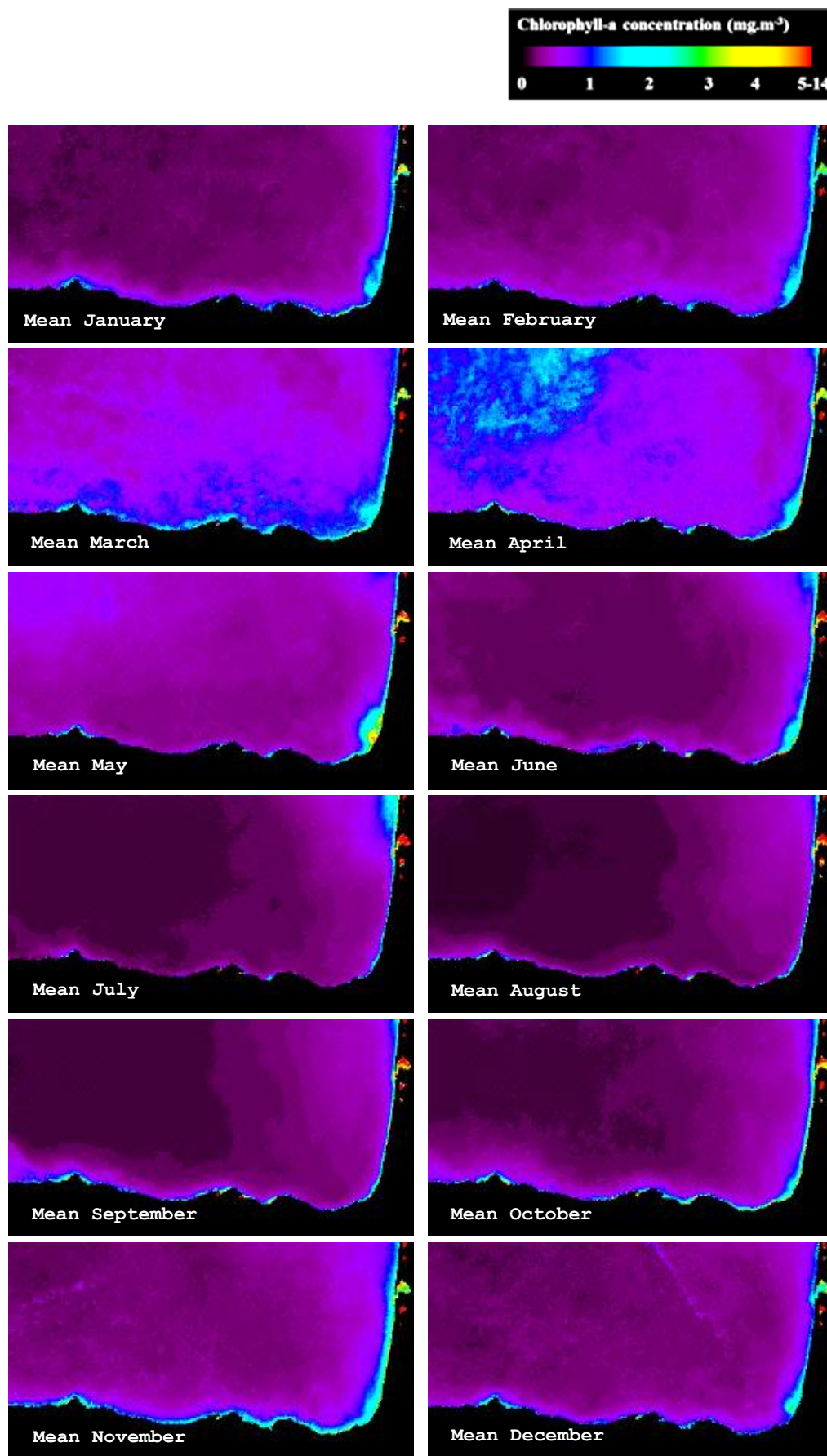


Figure 5.7. Monthly mean chl-a maps for the 2005-2010 period.

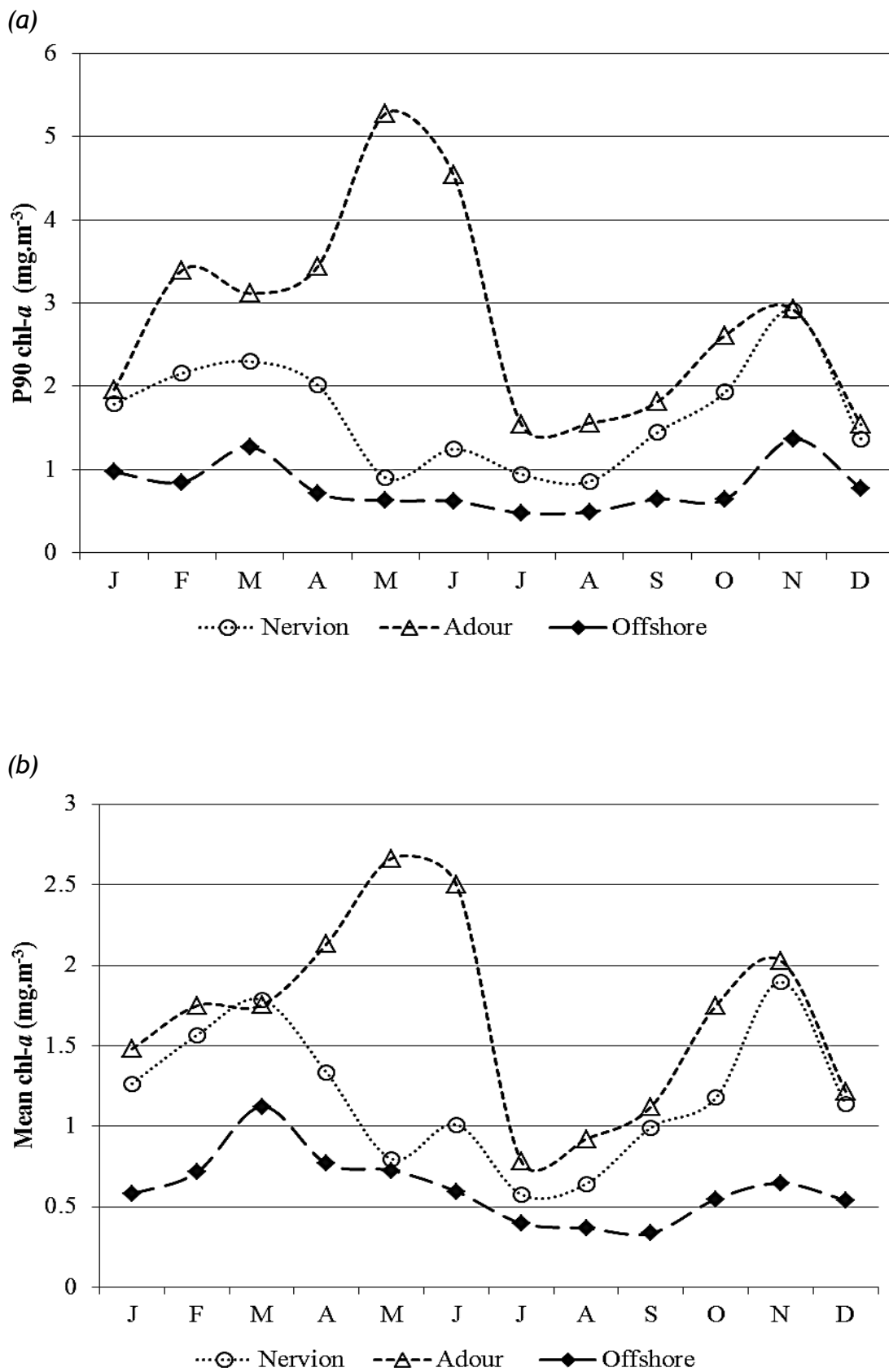


Figure 5.8. P90 Chl-*a* monthly values (a) and means (b) for the 2005-2010 period at 3 different locations: The Nervión river plume, the Adour river plume and the offshore reference station.

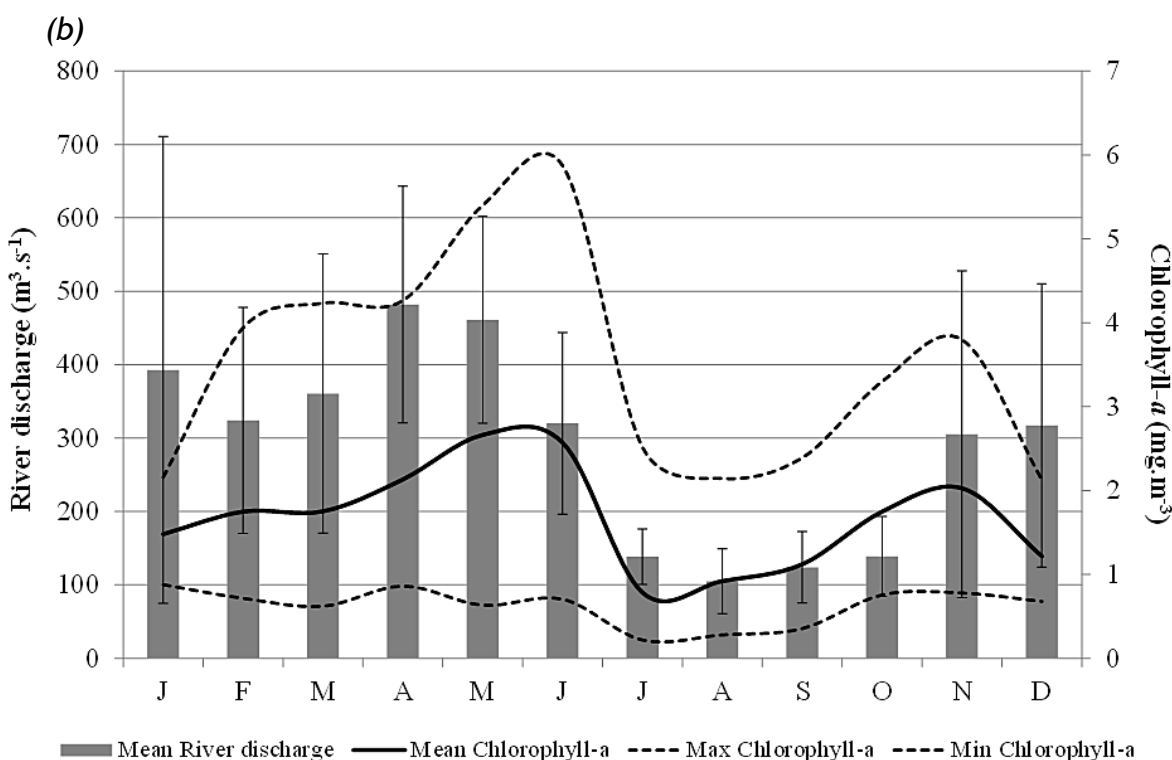
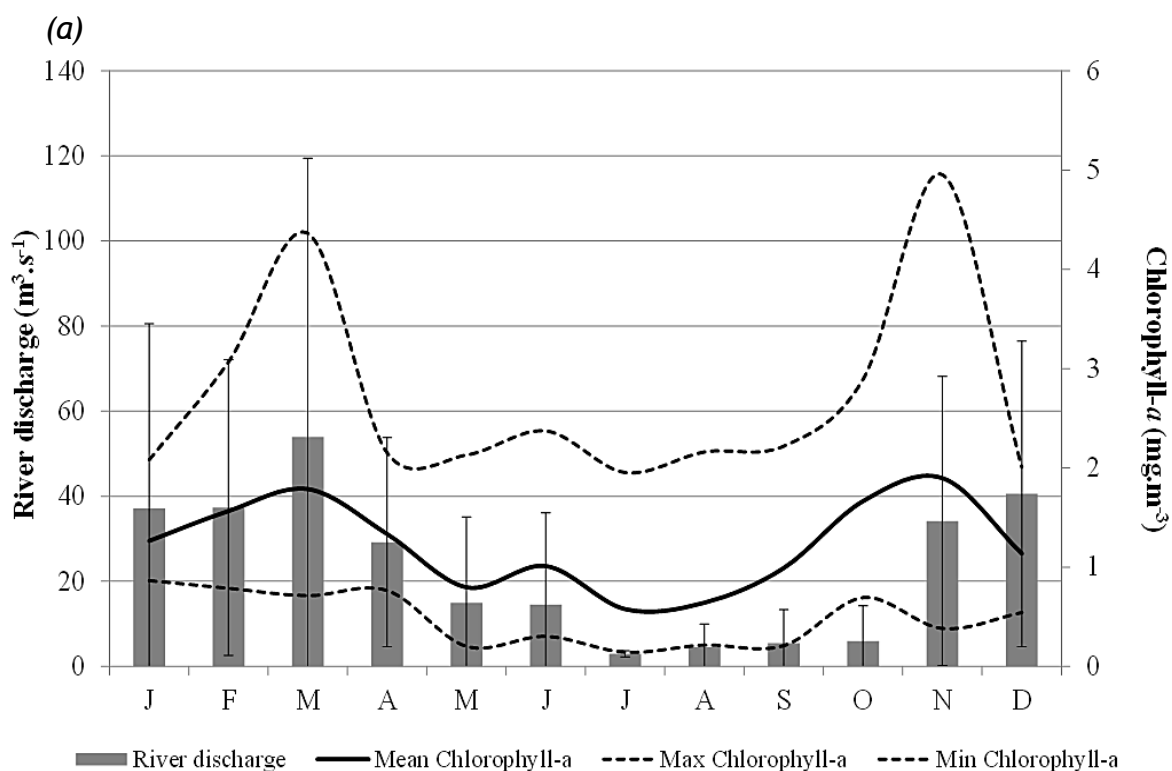


Figure 5.9. Monthly mean, maximum and minimum chl-a concentrations, and monthly mean river discharge and standard deviations, at the Nervión (a) and Adour (b) rivers, for the 2005-2010 period.

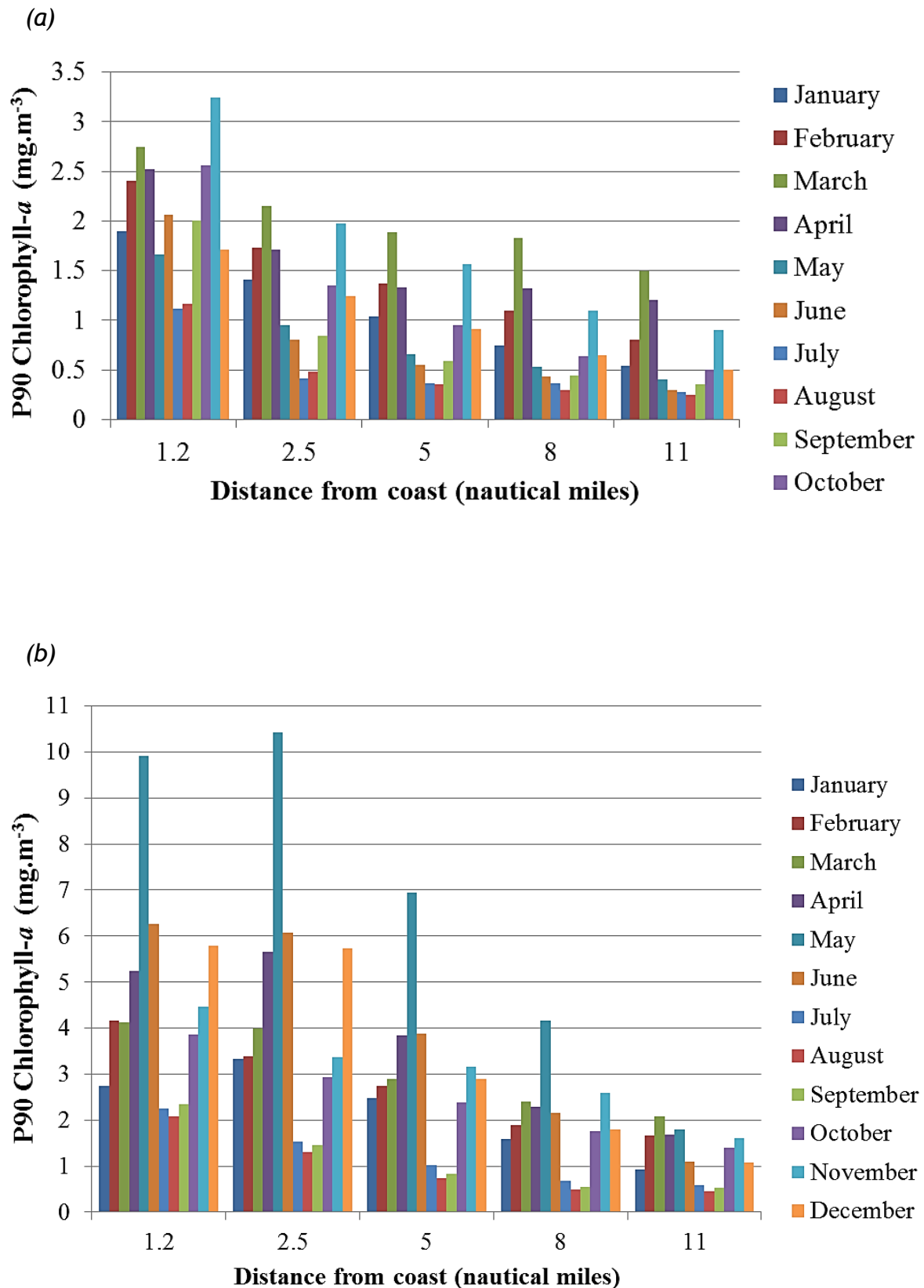


Figure 5.10. P90 Seasonal variation of chlorophyll-a with increasing distance from the coast, from 1.2 nautical miles until 11 nautical miles, at the Nervión (a) and the Adour (b) river plumes

3.3. Inter-annual variability

Chl-*a* concentration calculated from monthly means show considerable inter-annual variation in magnitude and duration of peak events. In general, the chl-*a* variability coincided with the river discharge events during the 2005-2010 period. A peak in spring, followed by another peak of lower magnitude in autumn was observed, while the lowest values were observed during the summer months. Chl-*a* concentration is generally higher in plume waters than at the offshore station, which is not usually influenced by river discharges (Figure 5.11).

The variation of chl-*a* concentration in coastal water usually coincides with the long duration of river discharges (Figures 5.11, 5.12), and do not necessarily coincide with their magnitude. The highest mean chl-*a* concentration in the Adour plume area was 6.5 mg.m⁻³ (June, 2007), followed by 4.6 mg.m⁻³ (May, 2009). The lowest mean chl-*a* concentration in the Adour river plume was 0.5 mg.m⁻³ and occurred in August 2008. The mean annual chl-*a* concentration reached 2.4 mg.m⁻³ in 2007 and 1.3 mg.m⁻³ in 2008. The levels of the other years varied between those two values.

The highest mean chl-*a* concentration in the Nervión plume area was 3.0 mg.m⁻³ (November, 2008), followed by 2.9 mg.m⁻³ (October, 2009). The lowest monthly mean chl-*a* concentration was 0.3 mg.m⁻³ and occurred in July 2009. The annual mean chl-*a* concentration was the highest in 2005, with 1.3 mg.m⁻³, while the lowest annual mean chl-*a* concentration was 1.0 mg.m⁻³ and was observed in 2008. In general, the variability of river discharges coincided with the rainfall variability at the Nervión inland station (Figures 5.12 and 5.13).

The highest monthly mean chl-*a* concentration found at the offshore location was 1.5 mg.m⁻³ (March, 2006), followed by 1.3 mg.m⁻³ (April, 2008). The lowest mean chl-*a* concentration at the offshore location was of 0.2 and occurred in September 2006. The maximum annual chlorophyll mean value was reached in 2007 as well, and was of 0.7 mg.m⁻³; the minimum mean value was observed in 2008, and was of 0.5 mg.m⁻³.

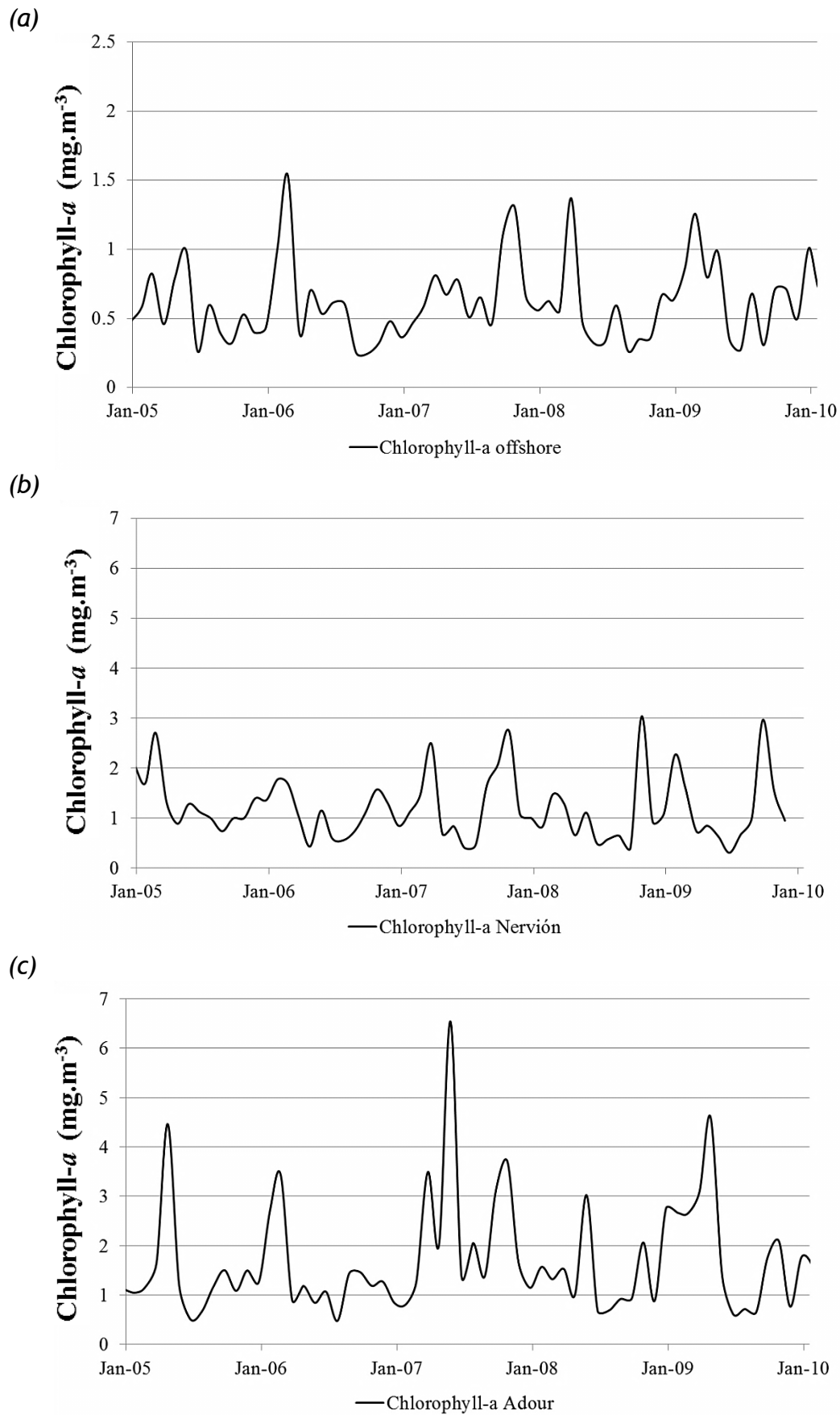
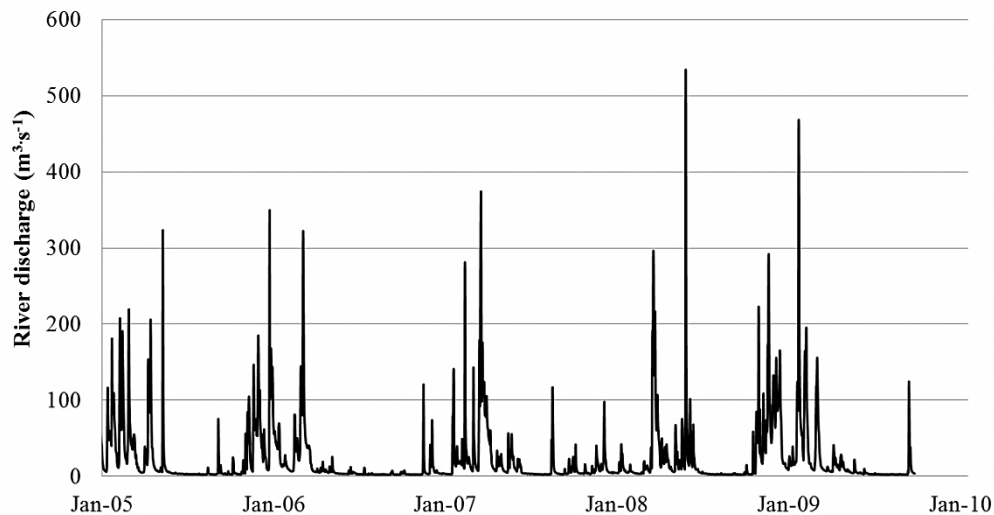


Figure 5.11. Time series of two-week mean chl-*a* concentration, at the offshore station (a), the Nervión (b) and the Adour (c) river plumes.

(a)



(b)

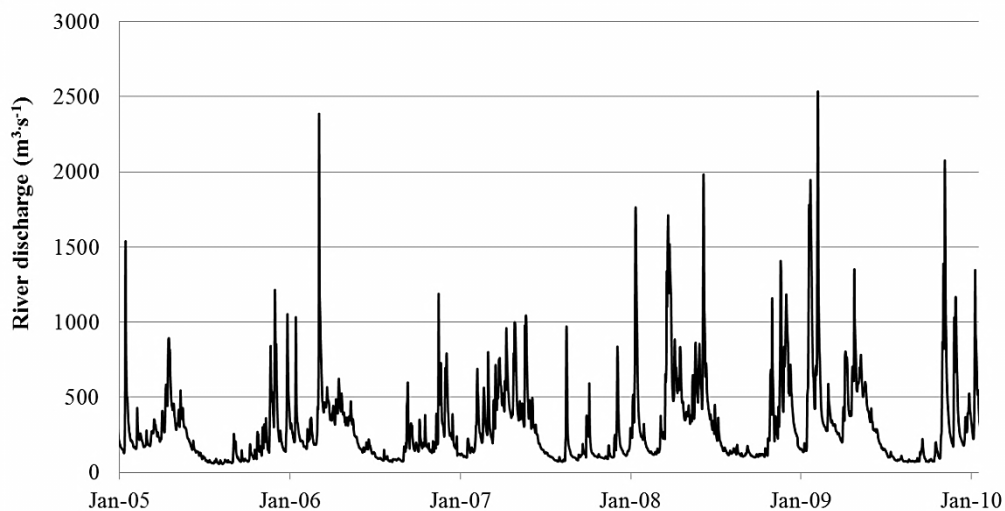


Figure 5.12. Time series of daily river discharges at the Nervión (a) and the Adour (b) river stations.

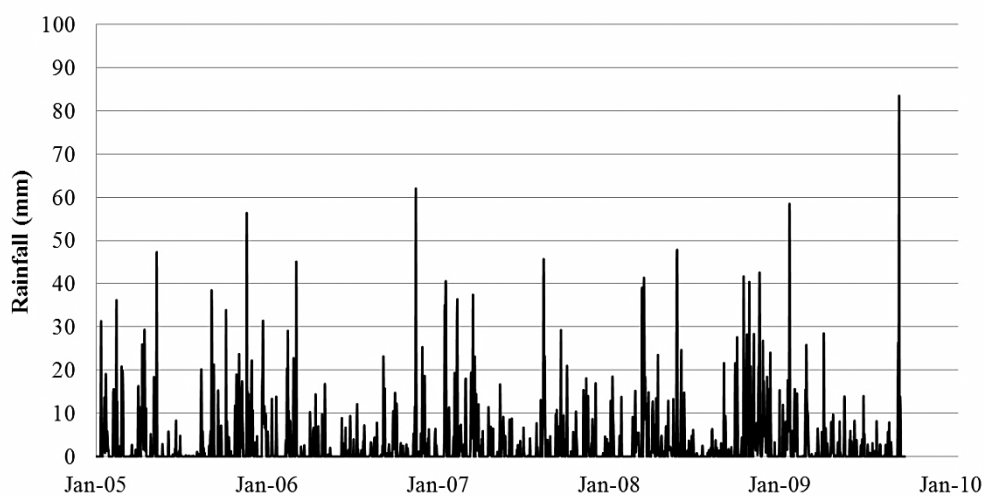


Figure 5.13. Time series of daily precipitation (rainfall) values at the Nervión river station.

Table 5.1. Time series analysis of several variables measured in situ and with satellite imagery. The values provided are the slopes of trend analysis. The asterisk (*) means that the bootstrap analysis proved the trend is significant.

slope	chl- <i>a</i> (<i>in situ</i>)	chl- <i>a</i> (satellite)	River discharge	Rainfall	Turbidity (satellite)
Nervi3n	-0.0220*	-0.0027*	0.0012*	0.0002*	0.0086*
Adour		-0.0020*	0.067*		0.0103
Offshore	-0.0010*	0.0017*			0.0141

The bootstrap analysis revealed a significant decrease in chl-*a* at the Nervi3n river plume region, measured with satellite and *in situ* data between 2005 and 2009 (Table 5.1). The *in situ* data resulted in a steeper slope than the satellite data (-0.0220 vs. -0.0027). The chl-*a* concentration measured in the Adour river plume showed as well, a significant decrease during the same period. The river discharge and rainfall measured at the inland river stations, increased significantly. The turbidity measured with satellite imagery significantly increased over the same period of time in plume and offshore waters.

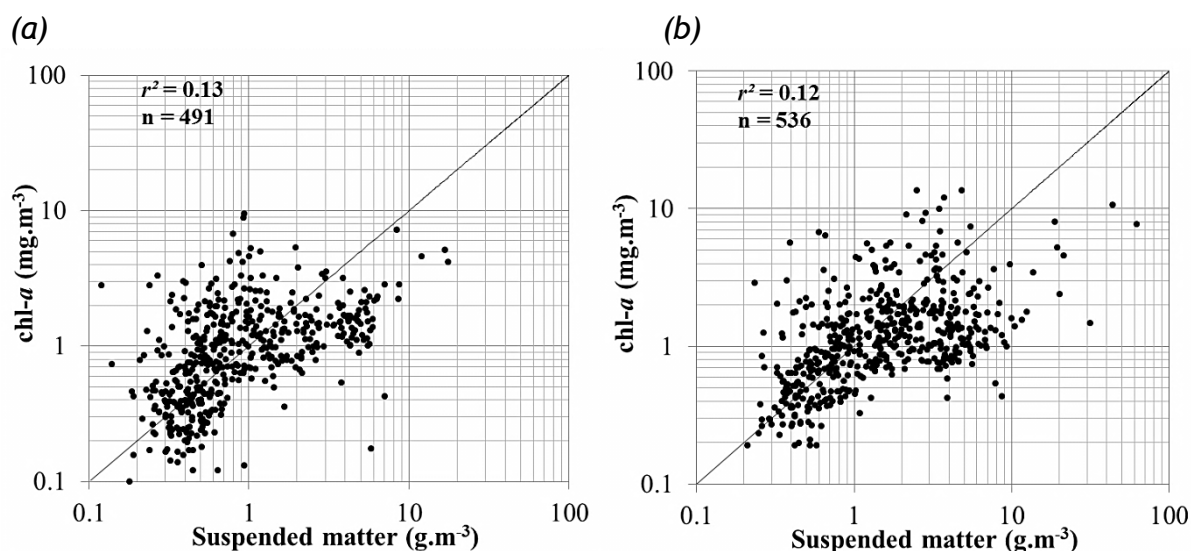


Figure 5.14. Linear regression between suspended matter and chl-*a* estimated with satellite imagery, for the Nervi3n (a) and the Adour (b) river plumes. The data are shown on a logarithmic scale for display purposes.

The logarithmic regression between the suspended matter and the chl-*a* concentrations (Figure 5.15) did not show a very high determination coefficients in both river plumes (Nervión $r^2=0.13$; Adour $r^2=0.12$).

3.4. Unsupervised classification and principal component analysis

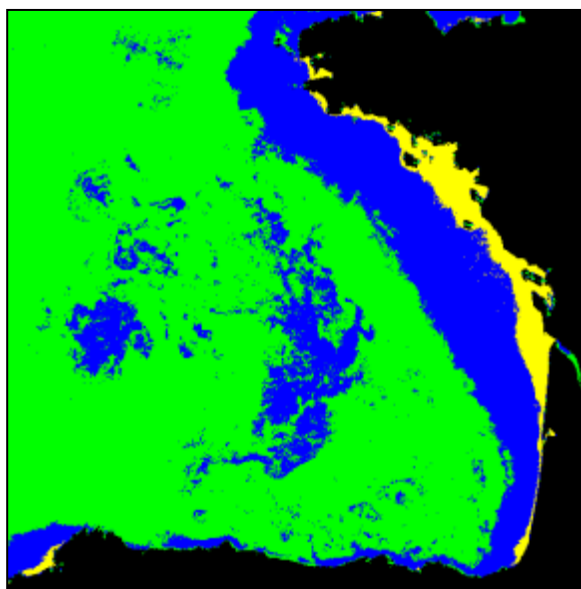


Figure 5.15 Unsupervised K-means classification performed with 1672 chl-*a* OC5 products. The black area is the land and was not considered in the classification. Class 1 is shown in yellow, class 2 in blue and class 3 in green.

The classification map showed three distinct surface water classes in the Bay of Biscay according to chl-*a* concentration (Figure 5.15). The first class (in yellow) includes the French part of the continental shelf influenced by river discharges, where chl-*a* concentrations are the highest. The Adour river plume area is included in this class. The second class (in blue) corresponds to an area of transition between river influenced areas and oceanic waters. This class has probably lower chl-*a* concentrations than the first class and it includes the region inside the continental shelf beyond the influenced areas by the French rivers. Northern Spain's coastal waters belong to the second classes well except for Galician waters. The third class (in green) would correspond to oceanic waters, where chl-*a* concentration is lower in general. This class includes the area beyond the continental shelf. However, some regions in the centre of the Bay located over deep water (>2000 m) and beyond the shelf, belong to class 2, indicated similar chl-*a* levels than transitional waters (Class 2, in blue). These higher concentrations are probably reached during bloom periods.

The first PCA band explained 57.3% of the total variance of the data and shows prevalent positive values in coastal areas, which are characterised by higher chl-*a* concentration (Figure 5.16).

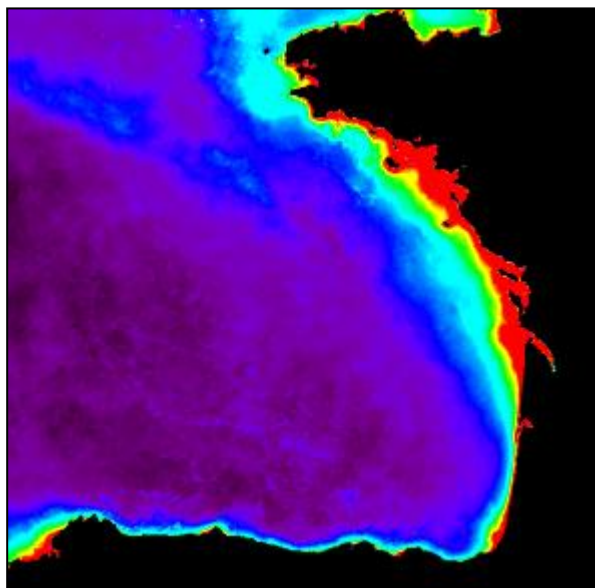


Figure 5.16. Spatial projection of the first Principal Component band. The lowest eigenvalues are shown in dark purple and the highest in red; the blue, green and yellow colours are used for the eigenvalues in between.

4. DISCUSSION

MODIS imagery provides a comprehensive spatio-temporal quantification of the variability of chl-*a* concentration in the Basque coastal area and the Bay of Biscay. This variability was examined by approaching the temporal and spatial dimensions.

4.1. Daily variability

This study has shown that the primary production increases in the Basque coastal area are very closely influenced by rainfall events and consequent river discharges, also reported by Valencia and Franco (2004). In general, an increase of chl-*a* concentration was observed 1 or 2 days after a rainfall event in Basque coastal areas near the Adour and the Nervión river plumes. Such a rapid phytoplankton growth after an input of nutrients has not been reported previously in the area, where other studies found longer reactive periods. In particular, García-Soto et al. (1990) reported an increase of primary productivity 4-5 days after a rainfall event in a coastal embayment near the Nervión estuary, and Alvarez et al., (2009) suggested a delay of 7 to 9 to detect primary

productivity after an increase in nutrient concentrations from upwelling nutrients in the Cantabrian coast. The increase in chl-*a* concentration observed with satellite images shortly after the rainfall event is not produced by phytoplankton proliferation caused by nutrient inputs, but to an effect of the storms. Winds (turbulence) and waves (bottom shear stress), usually more intense during winter storms, have major effects on the particles in suspension and on the dynamics of coastal waters and the river plumes (Huret et al. 2007). These disturbances are producing a resuspension and an advection of particulate material (e.g. microalgae and sediments) of marine, benthic, or estuarine origin (Abreu et al. 2009). In fact, benthic diatoms were found in some water samples collected in coastal areas during the LQM survey (Borja et al, 2010). Furthermore, the presence of higher levels of dissolved and suspended particulate inorganic material, due to resuspension or to river plume advection, could be also causing an overestimation of chlorophyll-*a* concentration by satellite imagery (Lahet et al. 2001; Bowers et al. 2009). However, the low correlation observed between suspended matter and chl-*a* in coastal areas extracted from the images ($r^2 = \sim 0.12$) for the entire 2005-2009 period does not confirm an overestimation by the OC5 algorithm (Figure 14). However, an *ad hoc* survey during runoff events and stormy weather, with associated satellite images and a study of the sediment dynamics using biogeochemical and statistical models (Huret et al. 2007; Rivier et al. 2011), would be useful to understand the causes of chl-*a* variability and provide more accurate estimates of chl-*a* in coastal waters. This would help determine if there is an overestimation by satellite imagery.

4.2. Seasonal variability

In ocean areas, the main annual bloom was observed in spring (February-March) while low concentrations predominated most of the year. Near the coast, bloom events appeared several times a year and chlorophyll concentrations were higher in general than those in the nearby ocean. These observations coincide with those reported by Bode et al. (2011) for the Cantabrian sea.

In the case of the Adour, the highest chl-*a* concentration levels are observed during late autumn and spring, but mainly between April and June, the months of the greatest river floods, driven by its pluvio-nival regime (Brière 2005). In the case of the Nervión, the cycle is similar to offshore waters, where blooms are observed in spring (February-

March) and late autumn-early winter (Fernández and Bode 1991; Revilla et al. 2010a; Bode et al. 2011), except for a secondary peak detected in June. These recurrent phytoplankton proliferations observed in June could be caused by favourable conditions encountered at that time of the year: abundance of nutrients, longer daylight and calm conditions (low river discharges). The high phytoplankton cell abundance that has been reported in that area at the end of May (Borja et al., Agencia Vasca del Agua 2007-2011), confirms it is not an inaccuracy produced by satellite data. Additionally, Loyer et al. (2006) findings also revealed peaks of chl-*a* concentration in June in river influenced areas by the Gironde and the Loire rivers.

Although the spatial influence of Nervión river is rather constrained (1.2 nautical miles from estuary), the Adour discharge has an influence up to 8 nm from coast. This can be noticed because the seasonal cycle is different at 11 nautical miles than at shorter distances from the coast; the highest chl-*a* peaks are observed in March and November, instead of observing a high peak in May. The influence of river discharge on the distribution and growth of phytoplankton has been demonstrated elsewhere (Retailleau et al. 2009). No studies describing the seasonal variability of phytoplankton in coastal waters influenced specifically by Adour plume waters have been found. However, Lampert et al. (2002) described a similar pattern observed near river influenced areas of the Bay of Biscay.

Seasonal patterns exhibit some differences when analysed using the P90 or the mean values as, for example, a peak observed in February with the P90 values (Figure 8 (a)) that is barely revealed with the mean values (Figure 8 (b)). The 90th percentile represented a statistic that covers the extent of data for chlorophyll biomass, avoiding highly skewed values, which can occur during bloom periods (Devlin et al. 2007). It has been reported that mean chl-*a* does not provide a good overview of the chlorophyll measurement (Clarke and Warwick 1994), since they can mask the irregularity of the data. Phytoplankton chlorophyll presents periodicity and episodic change and, as a result, tends to be asymmetrically distributed with few high values and many low values. Therefore, the 90th percentile metric has been recognised as an appropriate statistical approach to measure phytoplankton biomass (Atchinson 1986; Clarke and Warwick 1994). Accordingly, the P90 values were considered more appropriate for this study.

4.3. Inter-annual variability

The inter-annual analysis also shows a significant decrease of chl-*a* concentration (estimated with satellite data) between 2005 and 2010 in coastal areas near the Nervión and Adour river mouths, and a significant increase in offshore waters. The negative tendency in coastal waters, detected both by satellite and *in situ* data, could be related to the pollution control programmes set up in Nervión river in 1993 (García-Barcina et al. 2006), and from 1975 in the Adour river (Tudesque et al. 2008) that have considerably improved the water quality of these estuaries. At its lower reaches, the phytoplankton classification improved from good to high status (Revilla et al., 2011b) according to the chl-*a* metric that is employed in the European directive classification scheme (Revilla et al. 2009). The improvement of the water quality could be explaining the decrease of chl-*a* concentration over time in these areas.

Nevertheless, in offshore waters the time series analysis performed with *in situ* and satellite chl-*a* estimates are contradictory: *in situ* measurements show a significant decrease of surface chl-*a* between 2005 and 2010, while satellite data estimate a significant increase, in the same location. Interestingly, although a negative chl-*a* tendency was found by Revilla et al. (2010a) in surface waters with *in situ* measurements over the 1986-2008 period, they also reported (Revilla et al. 2011) an increase in chl-*a* concentration at higher depths in the photic layer. Thus, a possible explanation of this contradiction could lay on the fact than under clear water conditions, which is the case for this reference station, satellite estimates are integrating the part of the water column (Miller et al. 2005), where an increase in chl-*a* occurs. In this case chl-*a* satellite estimates would coincide with chl-*a* *in situ* estimates.

Additionally, the difference in the number of samples could have caused as well the inconsistency between *in situ* superficial and satellite chl-*a* estimates. As such, approximately one *in situ* sample was acquired per month, whereas monthly means of 20 images (on average), were used to analyse the tendency with satellite imagery. Hence, the results presented in this section, although interesting, cannot be considered as completely conclusive. Further analysis should be performed to confirm these findings.

4.4. Unsupervised classification and principal component analysis

The cluster analysis has resulted in three types of water bodies (Adour, Nervión and Oceanic) that converge in a relatively small area. Interestingly, the station used as a reference of offshore waters, not affected by river discharges (Revilla et al. 2010a; b), belongs to the same class as the coastal areas of the Spanish Basque coastal waters. Therefore, this confirms that, at present, phytoplankton is at good status and eutrophication risk is low in the Basque coastal waters (Revilla et al., 2009; Garmendia et al., 2011).

The first PCA band, explaining 57% of the total variance, indicates that the highest levels of chl-*a* in the Bay of Biscay are located near coastal areas (Figure 5.16). This is related to both the morphology of the continental shelf and the nutrient enrichment of these coastal areas by continental waters. The high levels of phytoplankton growth near river plumes has been previously reported in the Bay of Biscay (Labry et al. 2001, 2002; Lampert et al. 2002; Gohin et al. 2003; Guillaud et al. 2008) and elsewhere (Cruzado and Velasquez 1990; Cravo et al. 2006; Wysocki et al. 2006; Chen and Chen 2006; Lihan et al. 2011).

GENERAL DISCUSSION

GENERAL DISCUSSION

As described in the introduction of this thesis, one of the main issues encountered in relation to the accurate estimation of chl-*a* concentration with satellite remote sensing, is the inaccuracies obtained with global algorithms in marine coastal areas. Estimation errors are produced in these areas due to the presence of region-specific suspended and dissolved matters, which do not covary with chl-*a* (IOCCG, 2000), and affect the accurate estimation of this pigment. Until a global case II algorithm is developed, the adjustment of existing global and regional chl-*a* algorithms or the development of new ones for a specific area, are usually performed to improve the chl-*a* estimation and the assessment of water quality in regional coastal areas (IOCCG, 2000).

In this sense, this thesis provides a validation of already existing algorithms (i.e. OC4, OC3, OC5, Carder MODIS) with *in situ* reflectance and chl-*a* data, in addition to regionally-parameterised empirical algorithms developed with *in situ* optical data (Chapters II-IV). The *in situ* radiometric measurements performed at sea, were carried out in part with a protocol and a platform developed specifically for this study (Chapter I-II). The algorithms developed were also compared to well-established global and regional chl-*a* algorithms and were validated with *in situ* chl-*a* data (Chapter II-IV). Also, the effects of suspended matter and phytoplanktonic pigments on the accurate retrieval of chl-*a* was studied (Chapters II-III). In general, an improvement in the estimation of chl-*a* with respect to other chl-*a* products was obtained with the local algorithms developed for MERIS and MODIS images. Despite this improvement, the OC5 algorithm (Gohin et al. 2002) was considered more suitable, from an operational point of view, to assess the ecological water quality assessment of the Basque coastal waters (Chapter IV) and to study the variability of chl-*a* in the area (Chapter V). In order to apply operationally the algorithms developed in this thesis, additional calibration and validation work should be performed with supplementary *in situ* optical and biogeochemical data. The ecological water quality assessment performed with satellite imagery (with the OC5 algorithm) resulted in a similar classification of the Basque coastal water masses than the obtained with traditional *in situ* sampling. Hence, it was demonstrated that remote sensing is suited for the quality assessment and water body classification of Basque coastal waters, when a densification of the monitoring network is needed to comply with European Maritime policies. Finally, the analysis of chl-*a* products derived

with the OC5 algorithm and MODIS images acquired between 2005 and 2010, provided an improved characterisation of the variability of chl-*a* in the region. Thus, the effect of river discharges on the spatial and temporal variability of chl-*a* in the Bay of Biscay demonstrated elsewhere (Lampert et al. 2002; Gohin et al. 2003; Guillaud et al. 2008), was revealed as well in this study (Chapter V). It has been shown that in the case of strong river discharges, inaccuracies in the retrieval of chl-*a* in coastal areas with satellite imagery were still detected, due to presence of non-algal matter.

Below are discussed in more detailed the results presented in this thesis, as well as the prospective research and new challenges related to the estimation of chl-*a* with satellite imagery as a tool to assess water quality in the marine environment.

1. Radiometric measurements

Due to the absence of optical information in the area of study, radiometric measurements were necessary. For that purpose, the development of the protocol to perform measurements at sea was approached in Chapter I. The challenge was to carry out high quality optical measurements *in situ* dealing with adverse maritime conditions (i.e. oscillating movement of the vessel in wave-exposed areas), the corrosiveness of the salty water on instruments, and most importantly, at a reasonable cost. Field spectrometers have been used successfully in the retrieval of chl-*a* from reflectance spectra with Bio-optical algorithms (O'Reilly et al. 1998; Gitelson et al. 1999; Tzortziou et al. 2007), and the validation of remote sensing data products (Werdell and Bailey 2005).

Different protocols for the acquisition of radiometric measurements have been published and several spectrometers and measuring platforms haven been used for that purpose including above and below water measuring platforms and freefalling radiometers (see chapter 18 in Barale et al. 2010). The protocol published by NASA and developed by Mueller et al. (2000, 2003a; b) was the most widely employed and the one applied in the SeaWiFS and MODIS calibrations. In our study, the economically affordable HR4000CG ocean optics was first selected to develop a protocol and a platform, based on the one established by Froidefond and Ouillon (2005). The previous model to the HR4000CG ocean optics spectrometer, the Ocean Optics USB2000, was already used by Dall'Olmo and Gitelson (2005), Dall'Olmo et al. (2003, 2005) and Gitelson et al. (2007, 2008) to obtain reflectance spectra, with a similar methodology, and evaluate the ex-

tent to which reflectance ratios could be applied to remote sensors to estimate chl-*a* in turbid waters. Similar results to the exposed by these authors were obtained in Chapter II. Hence, since the HR4000CG spectrometer, the platform developed and the protocol established, provided coherent reflectance spectra when compared to those found in the literature (e.g. Schalles 2006) and to measurements performed with the TriOS spectrometer (Chapter I), we used those spectra to develop an empirical chl-*a* algorithm (Algorithm I, Chapter II).

During the Batel 2 survey (Chapter III), it was possible to perform a calibration exercise between the TriOS and the HR4000CG spectroradiometers. Even though the spectra mainly corresponded in shape and magnitude, the radiometric data produced by the HR4000CG was noisier than data produced by TriOS. Higher correlations were obtained between chl-*a* concentration (measured *in situ*) and ratios of reflectance values estimated with TriOS measurements, than those estimated with HR4000CG measurements. The TriOS instrument was considered to be better suited for the measurements in coastal waters, where the sea water surface (e.g. Coastal bathymetry, waves) and constituents' variability (concentration TSM, CDOM) is higher, because the measurements of the downwelling and upwelling radiances are simultaneous. In the case of the HR4000CG an approximate 10 minute lag exists between the two measurements, which could increase the measurement error. Therefore, the HR4000CG was found less adequate to develop chl-*a* algorithms for the coastal waters influenced by Adour river and the algorithm II was developed with spectra measured with the TriOS spectrometer (Chapter III).

In this study, it was easier to perform measurements of AOPs than IOPs, since additional costly instrumentation would have been necessary; thus, the protocol presented here could be used by those who need to carry out this type of research, at a reasonable cost and effort (Chapter I).

2. Chlorophyll-*a* algorithms

When successful algorithms estimating chl-*a* in open waters are applied to complex case 2 coastal waters, they generally fail and lead to large overestimates of chl-*a* (Carder et al. 1991; Gordon and Morel 1983; Hu et al. 2000; IOCCG, 2000). No global case 2 chl-*a* algorithm has been established yet, therefore, locally-adapted algorithms,

which are still being developed, are useful for such coastal waters (IOCCG, 2000). Several approaches are used to cope with the difficulties related with the estimation of chl-*a* in these case 2 waters (IOCCG 2000), for instance, there is a general tendency to develop algorithms with modelling techniques that are based on inherent optical properties (Gons 2002; Gitelson et al. 2008) or the use of neural networks (Schiller and Doerffer 1999; Tanaka et al. 2006; Doerffer and Schiller 2007).

In this thesis, the empirical approach was selected to develop regional algorithms because of its easy application and simplicity compared to other approaches (IOCCG 2000). No measurements of inherent optical properties have ever been performed in coastal waters of the Basque Country and there was no equipment available for the measurement of IOPs. Additionally, the knowledge of the range of concentrations of suspended material, chl-*a* and CDOM in the area are not very well known, hence there were too many unknown variables to apply a semi-empirical approach. The empirical approach was the most sensible option, since the study is performed in a specific area, where the variability of the types of phytoplankton, suspended and dissolved material is limited by the region itself. Even with the seasonality characterizing the area that can affect the application of the algorithms during some periods of the year, the empirical approach provided good results with the data available. Also, the fact that Gohin et al. (2002, 2008) had shown that an empirical algorithm combined with Look-up tables provided accurate chl-*a* estimates in the Bay of Biscay, motivated the development of an empirical algorithm for the area. The RMS error values obtained are lower than the levels of accuracy found by other studies undertaken in the Bay of Biscay (Morozov et al. 2010) and similar to the levels obtained in other case 2 water bodies (Gitelson et al. 2009, Kratzer et al. 2008). The improvement obtained with the regional algorithms (OC5 and Local) indicates that the regional parameterization is suited for Basque Coastal waters.

3. MERIS and MODIS imagery

Algorithm II was developed for both MERIS and MODIS reflectance bands due to the advantages presented by these two sensors for the purpose of this thesis.

They were selected based on the frequency of images, the spatial resolution and coverage and the number of bands sensitive to water quality indicators (Chl-*a*, TSM and

CDOM); and from an operational point of view, the availability of long time series (at least for the last 5 years), as well as products that are easy to treat and use, at low cost.

MERIS high resolution images (300 x 300 m) were especially important for the validation of MERIS Algorithm II, since the measurements performed during the surveys were at stations located near the coast. The MERIS Algorithm II provided better results with MERIS the Batel-1 validation data than the other algorithms tested, but there were not sufficient satellite-*in situ* match-ups to determine which algorithm was more accurate (Chapter III). The processing of all MERIS images available between 2005 and 2010 would have been useful to validate the MERIS algorithm II, in the same way as the MODIS algorithm II was compared to *in situ* measurements in chapter IV, with the 90th percentile chl-*a* annual cycle. However, the automatic processing of large series of images could not be adapted for the Beam software. In addition, the extra cost required for full resolution images would have exceeded the budget for this project. The reduced resolution images (1,040 m × 1,160 m) could have been used for that type of validation (90th percentile annual cycle); however, since MODIS image resolution (1,000 m) was better for the bands employed and provided a higher frequency of images than MERIS, it was considered more suitable for that purpose.

4. Variability of water constituents.

Knowledge of the spatio-temporal variability of chl-*a* in relation to river discharges is crucial to assess water quality accurately (Chapter V). Non-algal suspended particulate and dissolved matter coming from river runoff, controls water clarity in coastal areas. Water clarity determines the amount of light available in the water column for primary production and, thus, plays a key role in coastal ecosystem functioning. In coastal European waters, this influence on photosynthesis is observed during light limiting periods, in winter and at the beginning of spring (Huret et al. 2007). In winter, the "background" levels of particles can be particularly high after a storm, and during a few weeks after, independently of river runoff. The bottom shear stress and turbulence due to wind-generated surface-gravity waves, affect surface waters and the quantity of particles in suspension. This has a major effect on water clarity of surface waters, limiting phytoplankton growth, but also affecting the accurate retrieval of chl-*a* concen-

tration. As demonstrated in chapters II and III, the presence of suspended and dissolved inorganic material in water surface can increase the inaccuracies related to chl-*a* estimation with satellite algorithms (Lahet et al. 2001). Therefore, when deriving chl-*a* with satellite imagery, it is important to study the variability of water constituents, to adapt the algorithms to that area, but also to fulfil the WFD requirements in relation to the assessment of hydromorphological features (Devlin et al. 2007). For example, the estimation of chl-*a* could be improved by applying the best performing algorithm for each season or adjusting algorithm parameters for different seasons (Devred et al. 2005).

5. Sources of error

5.1. Influences of optical water constituents on algorithms

In some cases, it is difficult to determine to which case a water body belongs in near-shore coastal waters, ocean fronts or in the presence of eddies. In these areas, the merging of water masses of very different biogeochemical composition and different bio-optical properties can produce complex spatial and temporal patterns of near-surface optical properties. This is the case of Basque coastal waters, where the narrowness of the continental shelf, wave and wind action, and tidal and density currents cause small-scale patchiness and dynamic spatial and temporal variability (Valencia et al. 2004). For that reason, when it comes to remote sensing of ocean colour over those areas, it is important to sample for both the “required” and the “highly desired” variables, established in NASA’s ocean optics protocol (Volume I, chapter 3), such as downwelling irradiance and upwelling radiance, TSM, fluorescence, CDOM absorption, or complete pigment composition of important blooming phytoplankton such as diatoms, cyanobacteria, dinoflagellates, coccolithophores or *Trichodesmium*. In this manner, the effect of these water constituents on the algorithms developed can be taken into account. The influence of CDOM and suspended matter on the local MERIS Algorithm I was analysed in Chapter II, and the impact of TSM and phytoplankton species on the local MERIS algorithm II was analysed in Chapter III. The employment of fluorescence bands in algorithm II with respect to algorithm I (Chapter III), improved the estimation of chl-*a* in coastal waters, as it has been reported in the literature (Gitelson 1992, 1993; Gower et al. 1999; IOCCG 2000; Dall’Olmo and Gitelson 2005; Dall’Olmo et al. 2005;

Gitelson et al. 2007, 2009). Shafique et al. (2002) also used the 705/675 nm reflectance ratio to quantify chl-*a* and reported similar results ($r = 0.71$ and 0.72) in case 2 waters. The effect of suspended matter, CDOM and phytoplankton species on the retrieval of chl-*a* has been extensively demonstrated (IOCCG 2000) and still causes errors when estimating chl-*a*, but until the functioning of inherent properties of in water constituents is fully understood, the regional parameterisation is useful to cope with the inaccuracies (see Chapter 20 in Barale et al. 2010).

5.2. Atmospheric correction

The atmospheric correction is an important step in the processing of satellite imagery since errors in this stage can lead to erroneous estimations of water constituents (Kratzer et al. 2008). Over 89-90% of the total visible radiance received by a satellite sensor pointing at the ocean is due to atmospheric scattering of solar radiation (i.e. aerosols) or specular reflection (the mirror-like reflection of light) by ocean's surface; only 10-20% of the signal comes from the ocean. This contamination needs to be removed, since it can be a source of error when the remote sensing surface radiance or reflectance values are used to quantify water constituents (e.g. chl-*a* concentration as well as suspended and dissolved particles). Atmospheric correction procedures have to assess these atmospheric optical properties accurately and precisely in order to compute what would have been the ocean-colour signal in the absence of the atmosphere. The standard atmospheric corrections over case 1 waters assume that the water-leaving radiance at the near-infrared wavelengths (NIR, $\lambda > 700$ nm) is equal to zero (Siegel 1999), so the atmospheric properties at the NIR are then derived and extrapolated to the visible part of the spectrum using pre-computed Look-up tables (Gordon and Morel, 1983, Chavez et al. 1988; Gordon et al. 1997). However, in case 2 waters the NIR water-leaving radiance is not equal to zero due to the presence of suspended materials that cause light backscattering in the red and NIR (Siegel et al. 2000; Ruddick et al. 2003; Lavender et al. 2005). This causes an overcorrection in the visible spectral region, which often results in negative water-leaving radiances. Different methods have been studied by several authors to deal with this issue. For instance, Wang and Shi (2005) used the black pixel assumption with the SWIR (Short wave infrared) bands instead of the NIR bands to atmospherically correct MODIS images over coastal waters. MERIS employs inverse modelling of radiative transfer calculations by using artificial

neural network techniques (Doerffer and Schiller 2007). The neural network methodology is used to achieve a mapping between the measurements performed at top-of-atmosphere measurements and reflectance or geophysical parameters obtained bottom-of-atmosphere (inverse modelling). Despite the remarkable progress already made in atmospheric correction of ocean-colour data, it remains a major obstacle in the accurate retrieval of water quality indicators. The validation of the MERIS product with *in situ* reflectance measurements was aimed in Chapter II; however, the low number of match-ups was not enough to derive any definite conclusions. In this thesis, the atmospheric corrections applied are the standard provided by the products, to facilitate the operational application of the algorithms. In the case of MODIS, the "standard algorithm" (Gordon and Wang, 1994) was applied and in the case of MERIS the default case 1 and case 2 corrections were applied (Doerffer, 2008). Although the aim of these study was not the validation of the atmospheric corrections, the reflectance data acquired *in situ* was compared to the satellite data, with the intention of evaluating the inaccuracies related to atmospheric corrections and *in situ* radiometric measurements (Chapter II and III). Even if the number of match-ups was not sufficient to be able to assess the uncertainties, generally an overestimation by satellite imagery was observed.

5.3. *In situ* vs. satellite measurements

One source of error encountered in chapters II, III, and IV, which has been discussed by Sathyendranath and Platt in "Oceanography from space" (Barale et al. 2010), is the consideration of *in situ* observation as "truth" in satellite validation exercises. These authors argue that satellite observations are "true" in the sense that only remote sensors are able to sample an entire area in an instant, and this may be more representative of the reality. In Chapter IV, this issue was discussed when comparing satellite imagery and estimates of chl-*a* with CTD fluorescence, which had been reported to underestimate chl-*a*. However, the issue of whether the satellite or the *in situ* samples are the true estimate of a water constituent is hard to resolve. Sathyendranath and Platt mentioned as well that until the incompatibility existent between the scale of the sample compared is not solved, it would be difficult to accurately estimate chl-*a*. Likewise, Gohin et al. (2008) discussed the effect of the difference in sampling size when validating the OC5 algorithm in coastal waters. Due to this effect, named "support effect", the distributions of chl-*a* concentrations observed *in situ* through a small volume

unit, or by satellite through a greater volume unit, could be different. This effect is especially noticed in coastal areas, where currents and bathymetry create small scale chl-*a* features. The incompatibility of scales in the comparisons could attribute errors to algorithms that do not exist in reality. Until a novel approach to validate algorithms is developed, *in situ* and satellite imagery should be complimentary to each other, especially in water quality management purposes.

6. Further research

Some of the results exposed in this thesis could be used in the future to improve the estimation of chl-*a* concentration in the area of study and, consequently, the assessment of water quality. Following are discussed some possibilities for an operational use of the results obtained in this work:

6.1. Combination of Algorithms I and II

The variability of biogeochemical and optical properties of the water bodies assessed in the study area can depend upon the meteorological conditions. In particular, during high precipitation periods, and because of the torrential character of Basque rivers, the surface conditions of coastal waters can vary rapidly in a short period of time due to river runoff; hence, a water body can rapidly change from Case 1 to Case 2. In this case, establishing a geographical separation between case I and case II waters in the area of study would be complicated due to this variability. An alternative to estimate chl-*a* in these areas is to switch between algorithms I and II, depending on the CDOM and TSM concentrations. As such, if there is an interest in using these algorithms operationally for the estimation of chl-*a*, a model designed specifically for the area of study, applied with computer programming would detect the concentrations of TSM and CDOM of a water body and apply the Algorithm I to the more clear or Case 1 water masses (e.g. $TSM < 2 \text{ g.m}^{-3}$, $CDOM < 0.4 \text{ m}^{-1}$, water Type III), and algorithm II to waters influenced by river runoff or Case 2 (e.g. $TSM > 2 \text{ g.m}^{-3}$, $CDOM > 0.4 \text{ m}^{-1}$, water Types I and II). MERIS products do this in a way by flagging the case II water areas, warning about the necessity of applying the chl-*a* algorithm for case II waters (Aiken and Moore 2000).

6.2. Algorithm adjustment

Since inaccuracies in the estimation of chl-*a* concentration were still detected with the OC5 algorithm and the Algorithm II performed well in the area (Chapter IV), it would be interesting to use the biogeochemical and radiometric data acquired to adjust the OC5 algorithm. The OC5 extracts chl-*a* by applying a Look-up table that relates certain bands to chl-*a* concentration. Therefore, the next step would be to use the data acquired during the Batel surveys and add it to the OC5 Look-up table, connecting optical measurements to chl-*a* concentrations as explained by Gohin et al. (2002). The acquisition of additional radiometric and biogeochemical simultaneous measurements in Basque coastal waters would be useful to complete that Look-up table, but also to develop more robust and accurate regional empirical algorithms. It would also be of great interest to perform *in situ* measurements of inherent optical properties such as backscattering and absorption, to develop a semi-analytical algorithm with inverse modeling, and to test if it performs better than the empirical.

6.3. Merging images

To combine the advantages of both MODIS and MERIS products, an interesting approach would be the one followed by Gohin (2011). This author indicated that instead of choosing one remote sensing imagery provider or one product, the best option is to merge and interpolate the products (suspended matter or turbidity for example, in addition to chl-*a*), as they can help fulfill many requirements of the European directives for the surveillance and the monitoring of coastal water bodies. These types of products are already been developed by IFREMER (Gohin 2011). Previous studies have exposed that merging images from multiple satellite sensors can significantly improve the daily coverage of the global ocean (e.g., Gregg and Woodward, 1994; Gregg et al. 1998). However, Sathyendranath stated in the IOCCG (2007) report that data merging is a great technical and political challenge. The ocean-colour sensors are very complex, the signal they received is very small in relation to the noise, and require an extensive amount of work to obtain high-quality products. Also, international collaboration between the spatial agencies can be complicated. Problems and solutions for combining coincident data from several satellite sensors is extensively discussed in the IOCCG report number 6 (2007).

6.4. Data applications

The radiometric and biogeochemical data collected and analysed in this study could be used in the future for the validation and calibration of other remote sensors, in addition to the validation and development of algorithms to derived chl-*a*, SPM or CDOM. Furthermore, the field and satellite measurements could be used as forcing data into biogeochemical models. This would provide better knowledge on the dynamics of water constituents and improve the assessment of water quality of surface waters of the southeastern Bay of Biscay

7. Towards a better assessment of water quality with satellite imagery

7.1. Phytoplankton discrimination

New trends in remote sensing of ocean colour are being directed towards the discrimination of chlorophyll into different phytoplankton groups, in part to identify the species causing harmful blooms (HABs). Traditional monitoring of HABs involved the collection of sea water samples for species identification of toxicity analysis. However, *in situ* monitoring has its limitations when extensive monitoring is required, hence, there is considerable interest among the scientific community in using satellites to provide synoptic discriminations of phytoplankton groups (Shutler et al. 2005a; b; Miller et al. 2006). In oceanic waters, Alvain et al. (2005, 2008) were able to identify different groups from their spectral characteristics with an empirical approach and Aiken et al. (2007) used MERIS data to distinguish between different phytoplankton types in the Benguela ecosystem, proving the potential of this particular area of phytoplankton research. Additionally, the retrieval of inherent optical properties (IOPs) of the water from ocean colour data (IOCCG, 2006) is also offering a promising step towards the goal of distinguishing functional groups. Interesting results have been reached with the use of satellite data in the study of coccolithophore blooms (Groom and Holligan 1987), diatoms (Sathyendranath et al. 2004) and cyanobacteria (Subramaniam et al. 2002). A detailed review on the different bio-optical models used to discriminate between phytoplankton groups from satellite remote sensing can be found in Brewin et al. (2011). However, the development of discriminating algorithms in coastal waters is still questionable according to Kutser (2009), due to the high resolution necessary for this pur-

pose. Nevertheless, he presented some particular cases where algorithms for medium resolution remote sensors recognized phytoplankton blooms species. Still, phytoplankton discrimination in coastal waters remains complicated. In Chapter III of this thesis, HPLC pigment analysis and phytoplankton counts were performed with the primary intention of determining the effect of different phytoplankton pigments or species on the algorithm II developed; but also, to see if a relation could be established between reflectances acquired *in situ* and pigment absorption of different phytoplankton groups, as found in the literature (Hirata et al. 2008), for a later application to MERIS imagery. Unfortunately, no successful results in establishing significant relationships were reached in the present study, probably due to the interference of suspended and dissolved matter, as reported by Hunter et al. (2008), or the inappropriate quality of the reflectance spectra. Information on the phytoplankton pigments and species analysed during the Batel II survey can be found in the appendix.

7.2. Collaboration projects

This work has shown that considerable effort is necessary to acquire radiometric measurements at sea and to process those measurements to develop algorithms that would accurately estimate chl-*a*. The need of fast and synoptic assessment of water quality indicators as well as the technical and processing requirements necessary to parameterise regional algorithms, has pushed institutions to collaborate and provide services to facilitate this purpose through different international programs.

For example, the COASTCOLOUR project was launched by the European Space Agency to fully exploit the potential of the MERIS instrument for remote sensing of the coastal zone. Their activities include development, demonstration, validation and comparison of different Case 2 algorithms over a global range of coastal water types, identifying best practices, and promoting discussion of the results in an open, public form. A wide range of case 2 algorithms have been developed within the international community, so the COASTCOLOUR multi-sensor Round Robin task has emerged as a way to find a consensus on how to select the optimal algorithms and to determine which algorithms should be applied in different circumstances. This task provides a forum for the scientific community to compare coastal algorithms and obtain a detailed report on the comparison of the water products derived with the participant's algorithms and the

coastcolour products. The Round Robin project report was published in December 2011. More information on this project can be found in (<http://www.coastcolour.org/>).

7.3. New challenges

Even though significant advances have been performed in the estimation of bio-optical properties of the ocean for many coastal studies applications, the satellite products are not enough to make operational assessments (Arnone and Parsons 2004). Daily images are not enough to assess the evolution of some processes occurring in the coast, such as the dissipation of river plumes and tidal fluctuations. New challenges in remote sensing of bio-optical properties include the acquisition of several images per day. This objective could be reached with the coupling of different ocean colour products or with the combination of bio-optical products with ocean circulation models (see chapter 19, Barale et al. 2010; Rivier et al. 2011).

CONCLUSIONS

CONCLUSIONS

Below are listed the main conclusions of this thesis.

A protocol for radiometric measurements

1. The platforms developed make *in situ* radiometric sampling to be carried out fast and in a consistent manner, as the sensor is easily adjusted to the correct position and its stability is guaranteed by the design. The advantages of the upwelling-radiance measuring platform (a stainless steel flotation device) developed include: its relative lightness (it can be easily released overboard), its stability (the sensor is maintained at a fairly constant distance just below the water surface, approx. 1-2 cm), and the fact that measurements can be performed at nadir (perpendicular to the water surface). The advantages of the downwelling radiance measuring platform are also that it allows performing the measurements at a fixed distance from the Spectralon® target and at nadir. To reduce measurement errors at sea, it is recommended to carry out the measurements under clear sky and calm sea conditions, and during the central hours of the day. Still, further optimisation of the measuring protocol and platforms would be useful to improve measurement accuracy.
2. Spectral signatures acquired during the field survey (Chapter II) with the HR4000cg OceanOptics spectrometer, were consistent with published spectra in the literature (Gitelson et al. 1999; Morel 2006). In phytoplankton dominated water bodies, a depression in the blue part of the spectra and a red peak near 675 nm with increasing chl-*a* was noticeable. In water bodies with high suspended matter content, the signatures showed a shift of the highest spectral peak (around 570 nm) towards higher wavelengths, with increasing influence of sediment loaded river water. Additionally, a spectral classification of different water bodies influenced by river freshwater was possible, and these corresponded with reported findings (Schalles 2006).
3. A comparison with simultaneous measurements performed with the TriOS spectrometer during the Batel 2 survey, resulted in similarly shaped spectra but with a

higher signal noise in the case of the HR4000CG. Therefore, the TriOS spectra resulted more suitable for the development of algorithms for case 2 waters.

4. The radiometric data acquired during this study are valuable to adjust or develop algorithms for future remote sensors, or for future studies of the water optical properties of the area.

Development of chlorophyll-a algorithms

5. Two types of bio-optical algorithms were developed for the estimation of chlorophyll-a concentration, one for the continental shelf waters of the Bay of Biscay (Algorithm I, Chapter II), and Basque coastal waters (Local Algorithm II, Chapter III). The first type was derived from optical data acquired with the HR4000CG spectrometer over the continental shelf. The second type was developed with the radiometric data acquired with the TriOS spectrometer during oceanographic surveys over Basque coastal waters.
6. For continental shelf waters, correlations between reflectance ratios of MODIS and MERIS sensors and chl-*a* concentration measured *in situ* were established and were validated with the jackknife resampling procedure. The two best statistically significant correlations obtained with MODIS and MERIS simulated bands, was obtained with two ratios: the R_{rs510}/R_{rs560} ratio ($r^2_{jac}=0.68$), and R_{rs488}/R_{rs551} ($r^2_{jac}=0.67$). These ratios were used to develop two algorithms for satellite imagery:

MERIS Algorithm I: $chl-a = 10^{-1.432R+0.388}$, where $R = \log_{10}(R_{rs510}/R_{rs560})$

MODIS Algorithm I: $chl-a = 10^{-1.32R + 0.501}$; where $R = \log_{10}(R_{rs488}/R_{rs551})$

7. The effect of additional water constituents on the estimation of chlorophyll-*a* concentration by the Algorithm I was evaluated. High content in CDOM ($> 0.4 \text{ m}^{-1}$) and TSM ($> 2.80 \text{ g.m}^{-3}$) influenced the estimation of chlorophyll-*a*, although CDOM could be noted to have a stronger effect ($r^2_{jac}(\text{CDOM} < 0.4 \text{ m}^{-1}) = 0.82$, $r^2_{jac}(\text{TSM} < 2.8 \text{ mg l}^{-1}) = 0.74$).

8. The measurements acquired during the Basque Littoral Monitoring Program (LQM), Batel I and II surveys were used to develop and validate two algorithms of local algorithms for Basque coastal waters, one with MERIS bands and the other with MODIS bands (simulated bands):

MERIS Algorithm II:

$$\text{chl-}a = 10 \left[1.66 - 1.09 \times R_{rs} \left(\frac{510}{560} \right) - 2.39 \times R_{rs} \left(\frac{708}{681} \right) + 1.69 \times R_{rs} \left(\frac{708}{665} \right) \right]$$

MODIS Algorithm II:

$$\text{chl-}a = 10 \left[-0.18 - \left(5.85 \times \log_{10} \left(R_{rs} \left(\frac{531}{547} \right) \right) \right) - \left(5.56 \times \log_{10} \left(R_{rs} \left(\frac{678}{667} \right) \right) \right) + \left(0.442 \times \log_{10} \left(R_{rs} \left(\frac{748}{678} \right) \right) \right) \right]$$

9. The MERIS algorithm II was not affected by different concentrations of suspended matter in surface waters within the range from 0 to 6.6 g.m⁻³; this is consistent with prevailing conditions over the study area. There was no significant effect of 23 accessory pigments (corresponding to 56 different phytoplankton species) found in the area on the retrieval of chl-*a* by the developed algorithm, which confirms the good performance of the algorithm as a proxy of phytoplankton biomass. Therefore, these algorithms are valid for water bodies with chl-*a* concentrations between 0.1 and 9.57 mg.m⁻³, TSM concentrations between 0 and 6.6 g.m⁻³ and DOC values between 0.1 and 10 mg.m⁻³.
10. The MERIS Algorithm II showed a higher reliability than the global algorithm OC4v4, the Gitelson and the MERIS OC5 regional algorithms with the existing data for the analysis and when applied to MERIS bands.
11. Two out of three MODIS satellite-based algorithms tested, the OC5 and the MODIS algorithm II, represent a significant improvement with respect to the global algorithm OC3M to estimate sea surface chl-*a* within the Basque coastal waters; however, the MODIS OC5 provides the best estimates in general.

12. When proper atmospheric and radiometric corrections are applied, there is an advantage of using 300-m resolution MERIS images, with respect to MODIS, as they provide a pixel size suited for coastal investigations and provide more accurate estimates. MODIS provides a higher image frequency than MERIS, which more appropriate for operational applications.

Application to water quality assessment

13. Satellite imagery from MODIS sensor enabled to estimate sea surface chl-*a* within the Basque coastal waters with 40 times higher frequency than the field-based water quality monitoring, and 7457 grid points of information for the 5 water masses, compared to 19 *in situ* stations.
14. A considerable deviation between the field and satellite-derived estimates is still present, and the origin could be due to a difference in the sampling number between both methods, the difference of *in situ*-pixel scale, the “support effect”, the methodology employed or a combination of these factors. Still, the errors are lower than the obtained by other regional algorithms in the area of study.
15. The water quality status assessment obtained using satellite images resulted in a lower status for some stations than the *in situ* assessment, although when the comparison is performed at a water body level, the results are the same: all water bodies show a high quality status. A complementary use of both methodologies would be best to provide an efficient assessment of the water quality within the WFD and the MSFD. *In situ* sampling could be adequate for the monitoring of coastal stations, covered by the WFD, where the satellite could be overestimating chl-*a* in some areas near the coastline, while the satellite-based approach would be necessary to cover the monitoring of 200 nautical miles required by the MSFD.

Chlorophyll-a variability

16. Knowledge of the dynamics of water constituents in the area of study is crucial to provide accurate estimations of water quality constituents. This investigation has

shown that river discharges partially affect the variability of chlorophyll-*a* concentration levels in coastal areas at a daily, seasonal and inter-annual scale.

17. In general, an increase of chl-*a* concentration was observed 1 or 2 days after a rainfall event, in Basque coastal areas near the Adour and the Nervión river plumes. This increase is caused by the effect of storms (wind and waves that covariate with rainfall events) on the quantity of particles in suspension (e.g. microalgae and sediments), and by river discharges. Thus, there is an increase of phytoplankton of estuarine, marine or benthic origin, producing a chl-*a* increase, and an increase of non-algal suspended material, which could be producing an overestimation of chl-*a* by satellite imagery.
18. The seasonal variability patterns of chlorophyll-*a* concentration are different for the Adour and the Nervión river plumes, and differ as well from the pattern observed in offshore waters. In the case of the Adour, the highest chlorophyll-*a* concentrations are observed during late autumn and spring, but mainly between April and June, the months of the greatest river discharges. In the case of the Nervión, the cycle is similar to offshore waters, where blooms are observed in spring and late autumn-early winter, except for a peak that was detected in June.
19. The inter-annual analysis shows a slight decrease of chlorophyll-*a* concentration levels (estimated with satellite data) between 2005 and 2010 at the Adour and Nervión river plume areas and a slight increase at the offshore station.
20. An unsupervised classification showed the distribution of 3 different classes of water bodies in the Bay of Biscay, in relation to chlorophyll-*a* concentration levels, the Spanish and French Basque coastal waters belong to two different classes. This is due to the difference in the chl-*a* concentrations levels reached in both areas, the different river regimes and to the morphology of the continental shelf. This analysis also confirms that, at present, phytoplankton is at good status and eutrophication risk is low in the Basque coastal waters.

In summary, the results presented in this thesis provide important scientific knowledge on the use of satellite remote sensing to derive chlorophyll-*a* concentration, using MERIS and MODIS imagery, within the Basque coast and offshore areas of the Bay of Biscay. The quality assessment method developed, combining *in situ* measurements and satellite imagery, represents a powerful approach towards the efficient evaluation of the water quality over the areas covered by the WFD and the MSFD. Moreover, this thesis provides substantial information on the spatial and temporal variability of chlorophyll-*a* in the areas of study between 2005 and 2010, using MODIS satellite imagery. It also provides optical and biogeochemical information on the water bodies of the area that can be valuable for future studies. The next step would be to analyse in further depth the processes and factors affecting the variability of chlorophyll-*a* in the area of study by means of satellite remote sensing and biogeochemical models, and continue to improve the estimation of chlorophyll-*a* in coastal areas with satellite imagery.

REFERENCES

- Abadie, S., R. Butel, S. Mauriet, D. Morichon, and H. Dupuis. 2006. Wave climate and longshore drift on the South Aquitaine coast. *Continental Shelf Research* **26**: 1924-1939.
- Abril, G., M. Nogueira, H. Etcheber, G. Cabeçadas, E. Lemaire, and M. J. Borgueira. 2002. Behaviour of Organic Carbon in Nine Contrasting European Estuaries. *Estuarine, Coastal and Shelf Science* **54**: 241-262.
- Ahn, Y. H., A. Bricaud, and A. Morel. 1992. Light backscattering efficiency and related properties of some phytoplankters. *Deep-Sea Research* **39**: 1835-1855.
- Aiken, J., J. R. Fishwick, S. J. Lavender, R. Barlow, G. Moore, and H. Sessions. 2007. Validation of MERIS reflectance and chlorophyll during the BENCAL cruise October, 2002: Preliminary validation of new products for phytoplankton functional types and photosynthetic parameters. *International Journal of Remote Sensing* **28**: 497-516.
- Aiken, J., and G. Moore. 2000. Case 2 Turbid water flag. ATBD 2.5. Algorithm Theoretical Basis Document.
- Alvain, S., C. Moulin, Y. Dandonneau, and F. Breon. 2005. Remote sensing of phytoplankton groups in case 1 waters from global SeaWiFS imagery. *Deep Sea Research Part I Oceanographic Research Papers* **52**: 1989-2004.
- Alvain, S., C. Moulin, Y. Dandonneau, and H. Loisel. 2008. Seasonal distribution and succession of dominant phytoplankton groups in the global ocean: A satellite view. *Global Biogeochemical Cycles* **22**: GB3001.
- Alvarez, E., E. Nogueira, J. L. Acuna, M. Lopez-Alvarez, and J. A. Sostres, 2009. Short-term dynamics of late-winter phytoplankton blooms in a temperate ecosystem (Central Cantabrian Sea, Southern Bay of Biscay). *Journal of Plankton Research* **31**: 601-617.
- Antoine D. and A. Morel, 2011. Atmospheric correction of the MERIS observations over ocean case 1 waters. MERIS ATBD 2.7. (<http://envisat.esa.int/instruments/MERIS/ATBD>; March 2012)
- Antoine, D. and A. Morel, 1999. A multiple scattering algorithm for atmospheric correction of remotely-sensed ocean colour (MERIS instrument) principle and implementation for atmospheres carrying various aerosols including absorbing ones, *International Journal of Remote Sensing*, **20**, 1875-1916.
- Arnone, R. A., and A. R. Parsons. 2004. Real-time use of ocean color remote sensing for coastal monitoring, *In* R.L. Miller, C.E. DelCastillo, and B.A. McKee [eds.], *Remote Sensing of the Coastal Environments*.
- Atchinson, J. 1986. *The statistical analysis of compositional data*, Chapman and Hall.
- Arnau, P., C. Liqueste and M. Canals. 2004. River mouth plume events and their dispersal in the northwestern Mediterranean Sea. *Oceanography*, **17**: 22-31.
- Babin, M., D. Stramski, G. M. Ferrari, H. Claustre, A. Bricaud, G. Obolensky, and N. Hoepffner. 2003a. Variations in the light absorption coefficients of phytoplankton, nonalgal particles, and dissolved organic matter in coastal waters around Europe. *J. Geophys. Res.* **108(C7)** 3211.
- Babin, M., V. Fournier, P. Montard, and F. Fell. 2003b. Light scattering properties of marine particles in coastal and open ocean waters as related to the particle mass concentration. *Filtration* **48**: 843-859.
- Bailey, S. W., S. B. Hooker, D. Antoine, B. A. Franz, and J. Werdell. 2008. Sources and assumptions for the vicarious calibration of ocean color satellite observations. *Applied Optics* **47**: 2035-2045.

- Barale, V., J. F. R. Gower and L. Alberotanza. 2010. *Oceanography from Space, revisited*. Springer
- Barnes, R. a, and E. F. Zalewski. 2003. Reflectance-based calibration of SeaWiFS. II. Conversion to radiance. *Applied optics* 42: 1648-60.
- Becker, R. A., J. M. Chambers, and A. R. Wilks. 1988. *The New S Language*, Chapman & Hall.
- Bidigare, R. R., M. E. Ondrusek, J. H. Morrow, and D. A. Kiefer. 1990. In vivo absorption properties of algal pigments. *SPIE Ocean Optics X* 1302: 209-302.
- Binding, C E., T. A., Greenberg, R.P Bukata. 2011. Time series analysis of algal blooms in Lake of the Woods using the MERIS maximum chlorophyll index. *Journal of Plankton Research* 33(12): 1847-1852.
- Bode, A., R. Anadón, X.A. G. Morán, E. Nogueira, E.Teira, and M.Varela. 2011. Decadal variability in chlorophyll and primary production off NW Spain. *Climate Research* 48: 293-305
- Borja, A., and V. Valencia. 1993. Campaña 1992 de medición de variables biológicas para los estudios de implantación y seguimiento medioambiental de los emisarios submarinos de San Sebastián y de Pasajes (Guipúzcoa). Ministerio de Obras Públicas, Transportes y Medio Ambiente.
- Borja, A., J. Franco, V. Valencia, J. Bald, I. Muxika, M. J. Belzunce, and O. Solaun. 2004. Implementation of the European water framework directive from the Basque country (northern Spain): a methodological approach. *Marine Pollution Bulletin* 48: 209-218.
- Borja, A. 2005. The European water framework directive: A challenge for nearshore, coastal and continental shelf research. *Continental Shelf Research* 25: 1768-1783.
- Borja, A. 2006. The new European Marine Strategy Directive: difficulties, opportunities, and challenges. *Marine pollution bulletin* 52: 239-42.
- Borja, A., A. B. Josefson, A. Miles, I. Muxika, F. Olsgard, G. Phillips, J. G. Rodríguez, and B. Rygg. 2007. An approach to the intercalibration of benthic ecological status assessment in the North Atlantic ecoregion, according to the European Water Framework Directive. *Marine Pollution Bulletin* 55: 42-52.
- Borja, A., J. Bald, J. Franco, J. Larreta, I. Muxika, M. Revilla, J. G. Rodríguez, O. Solaun, A. Uriarte, and V. Valencia. 2009. Using multiple ecosystem components, in assessing ecological status in Spanish (Basque Country) Atlantic marine waters. *Marine pollution bulletin* 59: 54-64.
- Borja, A., I. Galparsoro, X. Irigoien, A. Iriondo, I. Menchaca, I. Muxika, M. Pascual, I. Quincoces, M. Revilla, J. G. Rodríguez, M. Santurtún, O. Solaun, A. Uriarte, V. Valencia, and I. Zorita. 2011. Implementation of the European Marine Strategy Framework Directive: a methodological approach for the assessment of environmental status, from the Basque Country (Bay of Biscay). *Marine Pollution Bulletin* 62: 889-904.
- Borja A., J. Bald, M.J. Belzunce, J. Franco, J.M. Garmendia, J. Larreta, I. Muxika, M. Revilla, G. Rodríguez, O. Solaun, A. Uriarte, and V. Valencia. 2007. Agencia Vasca del agua. Red de seguimiento del estado ecológico de las aguas de transición y costeras de la comunidad del País Vasco: masa de agua costera Matxitxako-Getaria. (www.uragentzia.euskadi.net).
- Borja A., J. Bald, M.J. Belzunce, J. Franco, J.M. Garmendia, J. Larreta, I. Muxika, M. Revilla, G. Rodríguez, O. Solaun, A. Uriarte, I. Zorita, and V. Valencia. 2008. Agencia Vasca del agua. Red de seguimiento del estado ecológico de las aguas de transición y costeras de la comunidad del País Vasco: masa de agua costera Matxitxako-Getaria. (www.uragentzia.euskadi.net).
- Borja A., J. Bald, M.J. Belzunce, J. Franco, J.M. Garmendia, J. Larreta, I. Muxika, M. Revilla, G. Rodríguez, O. Solaun, A. Uriarte, and I. Zorita, 2009. Agencia Vasca del agua. Red de seguimiento del esta-

- do ecológico de las aguas de transición y costeras de la comunidad del País Vasco: masa de agua costera Matxitxako-Getaria. (www.uragentzia.euskadi.net).
- Borja, A., J. Bald, M.J. Belzunce, J. Franco, J.M. Garmendia, J. Larreta, I. Muxika, M. Revilla, J.G. Rodríguez, O. Solaun, A. Uriarte, V. Valencia, I. Zorita, I. Adarraga, F. Aguirrezabala, I. Cruz, A. Laza, M.A. Marquiegui, J. Martínez, E. Orive, J.M^a Ruiz, S. Seoane, J.C. Sola, and A. Manzanos. 2010. Agencia Vasca del agua. Red de seguimiento del estado ecológico de las aguas de transición y costeras de la comunidad del País Vasco: masa de agua costera Matxitxako-Getaria. (www.uragentzia.euskadi.net).
- Borstal, G. A., H. R. Eel, J. F. R. Gower, and A. B. Hollinger. 1985. Analysis of test and flight data from the Fluorescence Line Imager. Canadian Special Publication of Fisheries and Aquatic Science, pp. 38.
- Brando, V. E., and A. G. Dekker. 2003. Satellite Hyperspectral Remote Sensing for Estimating Estuarine and Coastal Water Quality. *41*: 1378-1387.
- Brewin, R. J. W., N. J. Hardman-Mountford, S. J. Lavender, D. E. Raitsos, T. Hirata, J. Uitz, E. Devred, A. Bricaud, A. Ciotti, and B. Gentili. 2011. An intercomparison of bio-optical techniques for detecting dominant phytoplankton size class from satellite remote sensing. *Remote Sensing of Environment* **115**: 325-339.
- Bricaud, A., and A. Morel. 1987. Atmospheric corrections and interpretation of marine radiances in CZCS imagery: use of a reflectance model. *Oceanologica Acta* 33-50.
- Bricaud, A., and D. Stramski. 1990. Bricaud 1990 - Spectral absorption coefficients of living phytoplankton & nonalgal bio matter.pdf. *Limnology And Oceanography* **35**: 562-582.
- Bricaud, A., M. Babin, A. Morel, and H. Claustre. 1995. Variability in the chlorophyll-specific absorption coefficients of natural phytoplankton: Analysis and parameterization. *Journal of Geophysical Research* **100**: 13321-13332.
- Brière, C. 2005. Étude de l'hydrodynamique d'une zone côtière anthropisée : l'embouchure de l'Adour et les plages adjacentes d' Anglet. PhD thesis. Université de Pau et des Pays de l'Adour.
- Burnham, K. P., and D. R. Anderson. 2002. Model selection and multimodel inference: a practical information-theoretic approach, p. 488. *In Ecological Modelling*. Springer, The Netherlands.
- Bøgestrand, J., P. Kristensen, and B. Kronvang. 2005. Source apportionment of nitrogen and phosphorus inputs into the aquatic environment.
- Campbell, J. W., and J. E. O'Reilly. 2006. Metrics for Quantifying the Uncertainty in a Chlorophyll Algorithm: Explicit equations and examples using the OC4.v4 algorithm and NOMAD data. *Ocean Color Bio-optical Algorithm Mini Workshop* **4**: 1-15.
- Cannizzaro, J. P., K. L. Carder, F. R. Chen, C. A. Heil, and G. A. Vargo. 2008. A novel technique for detection of the toxic dinoflagellate *Karenia brevis* in the Gulf of Mexico from remotely sensed ocean color data. *Continental Shelf Research* **28**: 137-158.
- Cannizzaro, J. P., C. Hu, D. C. English, K. L. Carder, C. A. Heil, and F. E. Müller-Karger. 2009. Detection of *Karenia brevis* blooms on the west Florida shelf using *in situ* backscattering and fluorescence data. *Harmful Algae* **8**: 898-909.
- Carder, K. 2004. Performance of the MODIS semi-analytical ocean color algorithm for chlorophyll-*a*. *Advances in Space Research* **33**: 1152-1159.
- Carder, K. L., F. R. Chen, Z. P. Lee, S. K. Hawes, and D. Kamykowski. 1999. Semi-analytic Moderate-Resolution Imaging Spectrometer algorithms for chlorophyll *a* and absorption with bio-optical domains based on nitrate-depletion temperatures. *Journal of Geophysical Research* **104**: 5403-5421.

- Carder, K. L., S. K. Hawes, R. G. Steward, K. A. Baker, R. C. Smith, and B. G. Mitchell. 1991. Reflectance model for quantifying chlorophyll a in the presence of productivity degradation products. *Journal of Geophysical Research* **96**: 20599-20611.
- Carder, K. L., F. R. Chen, Z. Lee, S. K. Hawes, and J. P. Cannizzaro. 2003. ATBD 19: Case 2 Chlorophyll-*a*. MODIS Ocean Science Team Algorithm Theoretical Basis. Algorithm Theoretical Basis Document 1-67.
- Carletti, A. and A. Heiskanen. 2009. Reports Water Framework Directive intercalibration technical report. Part 3: Coastal and Transitional waters. JRC Scientific and Technical.
- Casas, B., M. Varela, and A. Bode. 1999. Seasonal succession of phytoplankton species on the coast of A Coruña (Galicia, northwest Spain). *Boletín del Instituto Español de Oceanografía* **15**: 413-429.
- Castaing, P. and G. P. Allen. 1981. Mechanisms controlling seaward escape of suspended sediment from the Gironde: a macrotidal estuary in France. *Marine Geology* **40**: 101-118.
- Cebrián, J. and I. Valiela. 1999. Seasonal patterns in phytoplankton biomass in coastal ecosystems. *J. Plankton Res.* **21**:429-444
- Chang, G. C. and R. W. Gould. 2006. Comparisons of optical properties of the coastal ocean derived from satellite ocean color and *in situ* measurements. *Optics Express* **14**: 10149-10163.
- Chust, G. and Y. Sagarminaga. 2007. The multi-angle view of MISR detects oil slicks under sun glitter conditions. *Remote Sensing of Environment* **107**: 232-239, doi:10.1016/j.rse.2006.09.024
- Clarke, G.L., G. C. Ewing, and C. J. Lorenzen. 1970. Spectra of backscattered light from the sea obtained from aircraft as a measure of chlorophyll concentration. *Science* **167**: 11-19.
- Clarke, K.R. and R. M Warwick,. 1994. Change in marine communities: an approach to statistical analysis and interpretation. Natural Environmental Research Council, UK, pp. 144.
- Conley, D. J., H. W. Paerl, R. W. Howarth, D. F. Boesch, S. P. Seitzinger, K. E. Havens, C. Lancelot, and G. E. Likens. 2009. Controlling Eutrophication : Nitrogen and Phosphorus. *Science* **323**: 1014-1015.
- Corbet, C. A. 2007. Colored Dissolved Organic matter (CDOM) workshop summary. Technical Document 07-3. Charlotte Harbor National Estuary Program pp. 90.
- Dall'Olmo, G., A. A. Gitelson, D. C. Rundquist, B. Leavitt, T. Barrow, and J. C. Holz. 2005. Assessing the potential of SeaWiFS and MODIS for estimating chlorophyll concentration in turbid productive waters using red and near-infrared bands. *Remote Sensing of Environment* **96**: 176 - 187.
- Dall'Olmo, G., A. A. Gitelson, and D. Rundquist. 2003. Towards a unified approach for remote estimation of chlorophyll-*a* in both terrestrial vegetation and turbid productive waters. *Geophysical Research Letters* **30**: 8-11.
- Dall'Olmo, G., and A. A. Gitelson. 2005. Effect of bio-optical parameter variability on the remote estimation of chlorophyll-*a* concentration in turbid productive waters: Experimental results. *Applied Optics* **44**(3): 412-422.
- Darecki, M. and D. Stramski. 2004. An evaluation of MODIS and SeaWiFS bio-optical algorithms in the Baltic Sea. *Remote Sensing of Environment* **89**: 326 - 350.
- Del Castillo, C.E. 2005. Remote sensing of organic matter in coastal waters 157-177, *In* Miller, L., C.E. Del Castillo and B.A. McKee [eds.], *Remote sensing of coastal waters: technologies, techniques and applications*. Springer, The Netherlands.

- Devlin, M., M. Best, D. Coates, E. Bresnan, S. O'Boyle, R. Park, J. Silke, C. Cusack, and J. Skeats. 2007. Establishing boundary classes for the classification of UK marine waters using phytoplankton communities. *Marine pollution bulletin* **55**: 91-103.
- Devred, E., S. Sathyendranath, C. Caverhill, H. Maass, and V Stuart. 2005. A semi-analytic seasonal algorithm to retrieve chlorophyll-*a* concentration in the Northwest Atlantic Ocean from SeaWiFS data. *Indian Journal of Marine Sciences*, 34(December), 356-367.
- Doerffer, R. 2002. Protocols for the validation of MERIS water products. Doc. No. PO-TN-MEL-GS-0043. European Space Agency.
- Doerffer, R., and H. Schiller. 2007. The MERIS Case 2 water algorithm. *International Journal of Remote Sensing* **28**: 517-535.
- Doerffer, R. 2008. Algorithm Theoretical Basis Document (ATBD) MERIS Regional Coastal and Lake Case 2 Water Project Atmospheric Correction ATBD. Version 1: 1-42.
- Domingues, R. B., A. Barbosa, and H. Galvão. 2008. Constraints on the use of phytoplankton as a biological quality element within the Water Framework Directive in Portuguese waters. *Marine pollution bulletin* **56**: 1389-95.
- Doxaran, D. 2002. Télédétection et Modélisation numérique des flux sédimentaires dans l'estuaire de la Gironde. PhD thesis. Université de Bordeaux 1.
- Doxaran, D., J.M Froidefond, S. Lavender, and P. Castaing. 2002. Spectral signature of highly turbid waters Application with SPOT data to quantify suspended particulate matter concentrations. *Remote Sensing of Environment* **81**: 149 - 161.
- Doxaran, D., N. C. Cherukuru, S. J. Lavender, and G. F. Moore, 2004: Use of a Spectralon panel to measure the downwelling irradiance signal: case studies and recommendations. *Applied optics*, **43**, 5981-5986.
- Doxaran, D., N. Cherukuru, and S. J. Lavender. 2006. Apparent and inherent optical properties of turbid estuarine waters: measurements, empirical quantification relationships, and modelling. *Applied optics* **45**: 2310-24.
- Duron, J.-N., S. Loyer, and F. Gohin. 2005. Scaling of coastal phytoplankton features by optical remote sensors: comparison with a regional ecosystem model. *International Journal of Remote Sensing* **26**: 4421-4444.
- Durrieu de Madron, X., P. Castaing, F. Nyffeler, and T. Courp. 1999. Slope transport of suspended particulate matter on the Aquitanian margin of Bay of Biscay. *Deep-Sea Research II* **46**: 2003-2027.
- Díez, I., A. Secilla, A. Santolaria, and J. M. Gorostiaga. 2000. The North coast of Spain. Seas at the Millennium an environmental evaluation. Pergamon Press, Amsterdam, I: 135-150.
- Etcheber, H., A. Taillez, G. Abril, J. Garnier, P. Servais, F. Moatar, and M.V. Commarieu. 2007. Particulate organic carbon in the estuarine turbidity maxima of the Gironde, Loire and Seine estuaries: origin and liability. *Hydrobiologia* **588**: 245-259.
- Fernández, E. and A. Bode. 1991. Seasonal patterns of primary production in the Central Cantabrian Sea (Bay of Biscay). *Scientia Marina* **55**: 629-636.
- Ferreira, J. G., J. H. Andersen, A. Borja, S. B. Bricker, and J. Camp. 2011. Overview of eutrophication indicators to assess environmental status within the European Marine Strategy Framework Directive. *Estuarine, Coastal and Shelf Science* **93**: 117-131.

- Ferrer, L., A. Fontán, J. Mader, G. Chust, M. González, V. Valencia, A. Uriarte, and M. B. Collins. 2009. Low-salinity plumes in the oceanic region of the Basque Country. *Continental Shelf Research* **29**: 970-984.
- Fontán, A., M. González, N. Wells, M. Collins, J. Mader, L. Ferrer, G. Esnaola, and A. Uriarte. 2009. Tidal and wind-induced circulation within the Southeastern limit of the Bay of Biscay: Pasaia Bay, Basque Coast. *Continental Shelf Research* **29**: 998-1007.
- Froidefond, J. M. and S. Ouillon. 2005. Introducing a mini-catamaran to perform reflectance measurements above and below the water surface. *Optics Express* **13**: 926-936.
- Gamble, J. C., J. M. Davies, and J. H. Steele. 1977. Loch Ewe bag experiment, 1974. *Bulletin of Marine Science* **27**: 146-175.
- García-Soto, C. and R. D. Pingree. 2009. Spring and summer blooms of phytoplankton (SeaWiFS/MODIS) along a ferry line in the Bay of Biscay and western English Channel. *Continental Shelf Research* **29**: 1111-1122.
- Garmendia, M., Revilla M., Bald, J., Franco, J., Laza-Martínez, A., Orive, E., Seoane, S., Valencia, V. and Á. Borja. 2011. Phytoplankton communities and biomass size structure (fractionated chlorophyll "a"), along trophic gradients of the Basque coast (northern Spain). *Biogeochemistry* **106**(2): 243-263.
- Gilerson, A. A., J. Zhou, S. Hlaing, I. Ioannou, J. Schalles, B. Gross, F. Moshary, and S. Ahmed. 2007. Fluorescence component in the reflectance spectra from coastal waters. Dependence on water composition. *Optics Express* **15**: 15702-15721.
- Gitelson, A. A. 1992. The peak near 700 nm on radiance spectra of algae and water: relationships of its magnitude and position with chlorophyll concentration. *International Journal of Remote Sensing* **13**: 3367-3373.
- Gitelson, A. A. 1993. Algorithms for remote sensing of phytoplankton pigments in inland waters. *Advances in Space Research* **13**: 197-201.
- Gitelson, A. A., J. F. Schalles, D. C. Rundquist, F. R. Schiebe, and Y. Z. 1999. Comparative reflectance properties of algal cultures with manipulated densities. *Journal of Applied Phycology* **345**-354.
- Gitelson, A. A., J. Schalles, and C. Hladik. 2007. Remote chlorophyll-*a* retrieval in turbid, productive estuaries: Chesapeake Bay case study. *Remote Sensing of Environment* **109**: 464-472.
- Gitelson, A. A., G. Dall'Olmo, W. Moses, D. Rundquist, T. Barrow, T. Fisher, D. Gurlin, and J. Holz. 2008. A simple semi-analytical model for remote estimation of chlorophyll-*a* in turbid waters: Validation. *Remote Sensing of Environment* **112**: 3582-3593.
- Gitelson, A. A., D. Gurlin, W. J. Moses, and T. Barrow. 2009. A bio-optical algorithm for the remote estimation of the chlorophyll- *a* concentration in case 2 waters. *Environmental Research Letters* **4**: 045003.
- Goddijn-Murphy, L., D. Dailoux, M. White, and D. Bowers. 2009. Fundamentals of *in situ* Digital Camera Methodology for Water Quality Monitoring of Coast and Ocean. *Sensors* **9**: 5825-5843.
- Gohin, F. 2011. Joint use of satellite and in-situ data for coastal monitoring. *Ocean Science Discussions* **8**: 955-998.
- Gohin, F., J.N. Druon, and L. Lampert. 2002. A five channel chlorophyll concentration algorithm applied to SeaWiFS data processed by SeaDAS in coastal waters. *International Journal of Remote Sensing* **23**: 1639-1661.

- Gohin, F., L. Lampert, J. F. Guillaud, A. Herbland, and E. Nézan. 2003. Satellite and *in situ* observations of a late winter phytoplankton bloom in the northern Bay of Biscay. *Continental Shelf Research* **23**: 1117-1141.
- Gohin, F., S. Loyer, M. Lunven, C. Labry, J. Froidefond, D. Delmas, M. Huret, and A. Herbland. 2005. Satellite-derived parameters for biological modelling in coastal waters: Illustration over the eastern continental shelf of the Bay of Biscay. *Remote Sensing of Environment* **95**: 29-46.
- Gohin, F., B. Saulquin, H. Oger-Jeanneret, L. Lozac'h, L. Lampert, A. Lefebvre, P. Riou, and F. Bruchon. 2008. Towards a better assessment of the ecological status of coastal waters using satellite-derived chlorophyll-*a* concentrations. *Remote Sensing of Environment* **112**: 3329-3340.
- Gons, H. J. 2002. A chlorophyll-retrieval algorithm for satellite imagery (Medium Resolution Imaging Spectrometer) of inland and coastal waters. *Journal of Plankton Research* **24**: 947-951.
- Gons, H., M. Auer, and S. Effler. 2008. MERIS satellite chlorophyll mapping of oligotrophic and eutrophic waters in the Laurentian Great Lakes. *Remote Sensing of Environment* **112**: 4098-4106.
- Gonzalez, M., A. Uriarte, A. Fontán, J. Mader, and P. Gyssels. 2004. Marine dynamics, *In* A. Borja and M. Collins [eds.], *Oceanography and Marine Environment of the Basque Country*. Elsevier Oceanography Series.
- Gordon, H. R., O. B. Brown, R. H. Evans, J. W. Brown, R. C. Smith, K. S. Baker, and D. K. Clark. 1988. A semi-analytic radiance model of ocean colour. *Journal of Geophysical Research* **93**: 10909-10924.
- Gordon, H. R., and A. Y. Morel. 1983. Remote assessment of ocean color for interpretation of satellite visible imagery: A review. *Lecture Notes on Coastal and Estuarine Study* **4**: 1-114.
- Gordon, H. R., O. B. Brown, R. H. Evans, J. W. Brown, R. C. Smith, K. S. Baker, and D. K. Clark. 1988. A semi-analytic radiance model of ocean colour. *Journal of Geophysical Research* **93**: 10909-10924.
- Gordon, H. R., O. B. Brown, and M. M. Jacobs. 1975. Computed relationships between the inherent and apparent optical properties of a flat homogeneous ocean. *Applied Optics* **14**: 417-427.
- Gordon, H. R., and K. Ding, 1992: Self-shading of in-water optical instruments. *Limnol. Oceanogr.*, **37**, 491-500.
- Gordon, H.R., and M. Wang, 1994. Retrieval of water-leaving radiance and aerosol optical thickness over the oceans with SeaWiFS: A preliminary algorithm, *Appl. Opt.*, **33**: 443-452.
- Gower, J. F. R., and G. A. Borstad. 1987. On the use of the solar-stimulated fluorescence signal from chlorophyll *a* for airborne and satellite mapping of phytoplankton. *Advances in Space Research* **7**: 101-106.
- Gower, J. F. R., R. Doerffer, and G. A. Borstad. 1999. Interpretation of the 685nm peak in water-leaving radiance spectra in terms of fluorescence, absorption and scattering, and its observation by MERIS. *International Journal of Remote Sensing* **20**: 1771-1786.
- Gower, J. and S. King. 2007. Validation of chlorophyll fluorescence derived from MERIS on the west coast of Canada. *International Journal of Remote Sensing* **28**: 625-635.
- Gregg, W. W., W. E. Esaias, G. C. Feldman, R. Frouin, S. B. Hooker, and R. H. McClain, C. R., Woodward. 1998. Coverage opportunities for global ocean color in a multimission era. *IEEE Transactions on Geoscience and Remote Sensing* **36**: 1620-1627.
- Gregg, W. and R. H. Woodward. 1994. The simulated SeaWiFS data set, Version 2. In S. B. pp. 42. *In* E. Hooker and Firestone R [eds.], *NASA Technical Memorandum 104566* Vol. 15.

- Grelie, J. 1933. La Charente, étude de fleuve. *Annales de Géographie* **42**: 44-60.
- Groom, S. B., and P. M. Holligan. 1987. Remote sensing of coccolithophorid blooms. *Advances in Space Research* **7**: 73-78.
- Guillaud, J. F., A. Aminot, D. Delmas, F. Gohin, M. Lunven, C. Labry, and A. Herbland. 2008. Seasonal variation of riverine nutrient inputs in the northern Bay of Biscay (France), and patterns of marine phytoplankton response. *Journal of Marine Systems* **72**: 309 - 319.
- Halpern, B. S., S. Walbridge, K. A. Selkoe, C. V. Kappel, F. Micheli, C. D'Agrosa, J. F. Bruno, K. S. Casey, C. Ebert, H. E. Fox, R. Fujita, D. Heinemann, H. S. Lenihan, E. M. P. Madin, M. T. Perry, E. R. Selig, M. Spalding, R. Steneck, and R. Watson. 2008. A Global Map of Human Impact on Marine Ecosystems. *Science* **319**: 948-952.
- Härmä, P., J. Vepsäläinen, T. Hannonen, T. Pyhälähti, J. Kämäri, K. Kallio, K. Eloheimo and S. Koponen. 2001. Detection of water quality using simulated satellite data and semi-empirical algorithms in Finland. *The Science of the total environment* **268**: 107-21.
- Harvey, J. 1982. Theta-S relationships and water masses in the eastern North Atlantic. *Deep-Sea Research* **29**: 1021-1033.
- Hellweger, L., P. Schlosser, U. Lall and K. Weisel. 2004. Use of satellite imagery for water quality studies in New York Harbor. *World Trade* **61**: 437-448.
- Hirata, T., J. Aiken, N. Hardman-Mountford, T. J. Smyth, and R. G. Barlow. 2008. Remote Sensing of Environment An absorption model to determine phytoplankton size classes from satellite ocean colour. *Remote Sensing of Environment* **112**: 3153-3159.
- Hoge, F. E., C. W. Wright, P. E. Lyon, R. N. Swift and J. K. Yungel. 2003. Validation of satellite-retrieved oceanic inherent optical properties: proposed two-color elastic backscatter lidar and retrieval theory. *Applied Optics* **42**: 7197-7201.
- Hoge, F. E., and R. N. Swift. 1986. Chlorophyll pigment concentration using spectral curvature algorithms: an evaluation of present and proposed satellite ocean color sensor bands. *Applied Optics* **25**: 3677.
- Holmhanen, O., M. Kahru, C. Hewes, S. Kawaguchi, T. Kameda, V. Sushin, I. Krasovski, J. Priddle, R. Korb and R. Hewitt. 2004. Temporal and spatial distribution of chlorophyll- in surface waters of the Scotia Sea as determined by both shipboard measurements and satellite data. *Deep Sea Research Part II: Topical Studies in Oceanography* **51**: 1323-1331.
- Hooker, S. B. and C. R. McClain. 2000. The calibration and validation of SeaWiFS data. *Progress in Oceanography* **45**: 427-465.
- Hunter, P. D., A. N. Tyler, and T. Preston. 2008. Spectral discrimination of phytoplankton colour groups: The effect of suspended particulate matter and sensor spectral resolution. *Remote Sensing of Environment* **112**: 1527 - 1544.
- Huret, M., Gohin, F., Delmas, D., Lunven, M., & Garçon, V. (2007). Use of SeaWiFS data for light availability and parameter estimation of a phytoplankton production model of the Bay of Biscay. *Journal of Marine Systems*, *65*(1-4), 509-531
- Hyndman, R. J., and Y. Fan. 1996. Sample quantiles in statistical packages. *American Statistician* **50**: 361-365.
- IOCCG. 1998. Minimum requirements for an Operational Ocean Colour Sensor for the Open Ocean, pp. 46. *In Reports of the International Ocean Colour Coordinating Group.*

- IOCCG. 2000. Remote Sensing of Ocean Colour in Coastal, and Other Optically-Complex, Waters, pp. 144. *In* S. Sathyendranath [ed.], Reports of the International Ocean Colour Coordinating Group 3.
- IOCCG. 2006. Remote Sensing of Inherent Optical Properties : Fundamentals, Tests of Algorithms , and Applications, p. 126. *In* R. Arnone, M. Babin, A.H. Barnard, E. Boss, J.P. Cannizzaro, K.L. Carder, F.R. Chen, E. Devred, R. Doerffer, K. Du, F. Hoge, O.V. Kopelevich, T. Platt, A. Poteau, C. Roesler, and S. Sathyendranath [eds.], Reports of the International Ocean Colour Coordinating Group 5.
- IOCCG. 2007. Ocean-Colour Data Merging, pp. 68. *In* W.W. Gregg [ed.], Reports of the International Ocean colour Coordinating Group 6.
- IOCCG. 2009. Atmospheric Correction for Remotely-Sensed Ocean- Colour Products, p. 76. *In* M. Wang [ed.], Reports of the International Ocean Colour Coordinating, 10.
- Ibañez, M. 1979. Hydrological studies and surface currents in the coastal area of the Bay of Biscay. *Lurralde* 2: 37-75.
- Jeffrey, S. W., and G. F. Humphrey. 1975. New spectrophotometric equations for determining chlorophylls a, b, c1 and c2 in higher plants, algae and natural phytoplankton. *Biochemie und Physiologie der Pflanzen* 167: 191-194.
- Jeffrey, S. W. and M. Vest. 1997. Introduction to marine phytoplankton and their pigment signatures, *In* S.W. Jeffrey, R.F.C. Mantoura, and S.W. Wright [eds.], *Phytoplankton pigments in oceanography guidelines to modern methods*. United Nations Educational Scientific and Cultural Organization (UNESCO).
- Kirk, O. 1994. *Light and photosynthesis in aquatic ecosystems*, Cambridge University Press.
- Jouanneau, J., O. Weber, M. Cremer, and P. Castaing. 1999. Fine-grained sediment budget on the continental margin of the Bay of Biscay. *Deep Sea Research Part II: Topical Studies in Oceanography* 46: 2205-2220.
- Jouanneau, J.M, O. Weber, N. Champilou, P. Cirac, I. Muxika, A. Borja, A. Pascual, J. Rodríguez-Lázaro, and O. Donard. 2008. Recent sedimentary study of the shelf of the Basque country. *Journal of Marine Systems* 72: 397-406.
- Kahru, M., O. P. Savchuk, and R. Elmgren. 2007. Satellite measurements of cyanobacterial bloom frequency in the Baltic Sea : interannual and spatial variability. *Marine Ecology Progress Series* 343: 15-23.
- Koutsikopoulos, C., and B. L. E. Cann. 1996. Physical processes and hydrological structures related to the Bay of Biscay anchovy. *Scientia Marina* 60: 9-19.
- Kratzer, S., C. Brockmann, and G. Moore. 2008. Using MERIS full resolution data to monitor coastal waters – A case study from Himmerfjärden, a fjord-like bay in the northwestern Baltic Sea. *Remote Sensing of Environment* 112: 2284-2300.
- Kruskal, W. H., and W. A. Wallis. 1952. Use of Ranks in One-Criterion Variance Analysis. *Journal of the American Statistical Association* 47: 583-621.
- Kutser, T. 2009. Passive optical remote sensing of cyanobacteria and other intense phytoplankton blooms in coastal and inland waters. *International Journal of Remote Sensing* 30: 4401-4425.
- Kutser, T., L. Metsamaa, N. Strömbeck, and E. Vahtmäe. 2006. Monitoring cyanobacterial blooms by satellite remote sensing. *Estuarine, Coastal and Shelf Science* 67: 303–312.

- Laborde, P., J. Urrutia, and V. Valencia. 1999. Seasonal variability of primary production in the Cap-Ferret Canyon area (Bay of Biscay) during the ECOFER cruises. *Deep Sea Research Part II: Topical Studies in Oceanography* **46**: 2057-2079.
- Labry, C., A. Herbland, D. Delmas, P. Laborde, P. Lazure, J. M. Froidefond, A. M. Jegou, and B. Sautour. 2001. Initiation of winter phytoplankton blooms within the Gironde plume waters in the Bay of Biscay. *Marine Ecology Progress Series* **212**: 117-130.
- Lagos, N. 2002. Floraciones algales nocivas en el Cono Sur Americano, pp. 55-77. *In* E. Sar, M. Ferrairo, and B. Reguera [eds.]. Instituto Español de Oceanografía.
- Lahet, F., S. Ouillon, and P. Forget. 2001. Colour classification of coastal waters of the Ebro river plume from spectral reflectances. *International Journal of Remote Sensing* **22**: 1639-1664.
- Lampert, L., B. Quéguiner, T. Labasque, A. Pichon, and N. Lebreton. 2002. Spatial variability of phytoplankton composition and biomass on the eastern continental shelf of the Bay of Biscay (north-east Atlantic Ocean). Evidence for a bloom of *Emiliana huxleyi* (Prymnesiophyceae) in spring 1998. *Continental Shelf Research* **22**: 1225-1247.
- Lavender, S., M. H. Pinkerton, G. F. Moore, and J. Aiken. 2005. Modification to the atmospheric correction of SeaWiFS ocean colour images over turbid waters. *Continental Shelf Research* **25**: 539-555.
- Lavín, A., L. Valdés, F. Sánchez, P. Abaunza, A. Forest, J. Boucher, P. Lazure, and A. M. Jegou. 2006. The Bay of Biscay: The encountering of the ocean and the shelf, p. 935-1003. *In* A.R. Robinson and K. Brink [eds.], *The Sea 14*. Harward Press.
- Le Bris, H., and M. Glémarec. 1996. Marine and brackish ecosystems of South Brittany (Lorient and Vilaine Bays) with particular reference to the effect of the turbidity maxima. *Estuarine, Coastal and Shelf Science* **42**: 737-753.
- Le Cann, B. 1990. Barotropic tidal dynamics of the Bay of Biscay shelf: observations, numerical modelling and physical interpretation. *Continental Shelf Research* **10**: 723-758.
- Leathers, R. A., V. Downes, and C. D. Mobley, 2001: Self-shading correction for upwelling sea-surface radiance measurements made with buoyed instruments. *Optics Express*, **8**, 561-570.
- Leathers, R. A., T. V. Downes, and C. D. Mobley, 2004: Self-shading correction for oceanographic upwelling radiometers. *Opt. Express*, **12**, 4709-4718.
- Lee, Z., K. L. Carder, S. Florida, and S. Petersburg. 2005. Hyperspectral remote sensing, pp. 181-204. *In* *Remote Sensing of Coastal Aquatic Environments: Technologies, Techniques and Applications*.
- Lee, Z., and C. Hu. 2006. Global distribution of case-1 waters: An analysis from SeaWiFS measurements. *Remote Sensing of Environment* **101**: 270-276.
- Letelier, R. M., and M. R. Abbott. 1996. An analysis of chlorophyll fluorescence algorithms for the moderate resolution imaging spectrometer (MODIS). *Remote Sensing of Environment* **58**: 215-223.
- Longhurst, A. 1998. *Ecological geography of the sea*, Academic Press.
- Lohrenz, S. E., G. L. Fahnenstiel, D. G. Redalje, G. A. Lang, X. Chen, and M. J. Dagg. 1997. Variations in primary production of northern Gulf of Mexico continental shelf waters linked to nutrient inputs from the Mississippi River. *Marine Ecology Progress Series* **155**: 45-54.
- Maffione, R. A., J. M. Voss, and C. D. Mobley. 1998. Theory and measurements of the complete beam spread function of sea ice. *Limnology and Oceanography* **43**: 34-43.

- Maneux, E., J. Dumas, O. Clement, H. Etcheber, X. Charriton, E. J. V. E, and R. P. 1999. Assessment of suspended matter input into the oceans by small mountainous coastal rivers: the case of the Bay of Biscay. *C. R. Acad. Sci., Ser. II* **329**: 413-420.
- McCave, I. N., I. R. Hall, A. N. Antia, L. Chou, F. Dehairs, R. S. Lampitt, L. Thomsen, T. C. E. Van Weering, and R. Wollast. 2001. Distribution, composition and flux of particulate material over the European margin at 47°-50°N. *Deep-Sea Research II: Topical Studies in Oceanography* **48**: 3107-3139.
- Mignot, A., H. Claustre, F. D'Ortenzio, X. Xing, a. Poteau, and J. Ras. 2011. From the shape of the vertical profile of in vivo fluorescence to Chlorophyll-*a* concentration. *Biogeosciences* **8**: 2391-2406.
- Miller, P., J. Shutler, G. Moore, and S. Groom. 2006. SeaWiFS discrimination of harmful algal bloom evolution. *International Journal of Remote Sensing* **27**: 2287-2301.
- Miller, R. L., C. E. Del Castillo, and B. A. McKee. 2005. *Remote Sensing of Coastal Aquatic Environments. Technologies, Techniques and Applications*, Springer, The Netherlands.
- Mobley, C. D. 1994. *Light and Water: Radiative Transfer in Natural Waters*, Academic Press.
- Mobley, C. D. 1995. *Hydrolight 3.0 Users' Guide*, SRI International, Menlo Park, California.
- Mobley, C. D. 1999. Estimation of the remote-sensing reflectance from above-surface measurements. *Applied Optics* **38**: p7442-7455.
- Mobley, C. D., B. Gentili, H. R. Gordon, Z. Jin, G. W. Kattawar, A. Morel, P. Reinersman, K. Stamnes, and R. H. Stavn. 1993. Comparison of numerical models for computing underwater light fields. *Applied Optics* **32**: 7484-7504.
- Mobley, C. D. 1994. *Light and Water: Radiative Transfer in Natural Waters*, Academic Press.
- Mobley, C. D., and R. A. Maffione. 1997. Effects of absorption and boundary conditions on the utility of diffusion theory. *Ocean Optics XII SPIE* **2963**: 16-20.
- Mobley, C. D., and D. Stramski. 2004. Coastal ocean optics dynamics. *Optical Modelling of Ocean Water. Is the Case 1- Case 2 Classification Still Useful? Oceanography* **17**.
- Morel, A. 1974. Optical properties of pure water and pure sea water, chapter 1, p. 1-24. *In Optical Aspects of oceanography*.
- Morel, A. 2006. Meeting the Challenge of Monitoring Chlorophyll in the Ocean from Outer Space, pp. 521-534. *In Chlorophylls and bacteriochlorophylls Biochemistry biophysics function and applications*. Springer, the Netherlands.
- Morel, A. 1988. Optical Modelling of the Upper Ocean in Relation to Its Biogenous Matter Content (Case I Waters). *Journal of Geophysical Research* **93**: 10749-10768.
- Morel, A., and L. Prieur. 1977. Analysis of variations in ocean color. *Limnology and Oceanography* **22**: 709-722.
- Morel, A., and B. Gentili. 1991. Diffuse reflectance of oceanic waters: its dependence on Sun angle as influenced by the molecular scattering contribution. *Applied Optics* **30**: 4427-4438.
- Morel, A., and B. Gentili. 1993. Diffuse reflectance of oceanic waters. II Bidirectional aspects *Applied Optics* **32(33)**: 6864-6879

- Morel, A., and S. Belanger. 2006. Improved detection of turbid waters from ocean color sensors information. *Remote Sensing of Environment* **102**: 237-249.
- Morel, A., and S. Maritorena. 2001. Bio-optical properties of oceanic waters: A reappraisal. *Journal of Geophysical Research* **106**: 7163-7180.
- Morichon, D., and D. Dailloux. 2006. River plume monitoring using two combined remote sensing techniques: satellite (MODIS) and video (ARGUS) images. Application to the Adour River plume (France). *Proceedings of the 30th International Conference on Coastal Engineering, San Diego.*, 2095-2105
- Morin, P., P. Lecorre, Y. Marty, and S. Lhelguen. 1991. Spring Evolution of Nutrients and Phytoplankton on the Armorican Shelf (North-West European Shelf). *Oceanologica Acta* **14**: 263-279.
- Morozov, E., A. Korosov, D. Pozdnyakov, L. Pettersson, and V. Sychev. 2010. A new area-specific bio-optical algorithm for the Bay of Biscay and assessment of its potential for SeaWiFS and MODIS/Aqua data merging. *International Journal of Remote Sensing* **31**: 6541-6565.
- Moses, W. J., A. A. Gitelson, S. Berdnikov, and V. Povazhny. 2009. Estimation of chlorophyll- a concentration in case II waters using MODIS and MERIS data—successes and challenges. *Environmental Research Letters* **4**: 045005.
- Mueller, J. L., C. Davis, R. Amone, R. Frouin, K. Carder, Z. P. Lee, R. G. Steward, S. Hooker, C. D. Mobley, and S. McLean. 2000. Above-water radiance and remote sensing reflectance measurement and analysis protocols, p. 98-107. *In* G.S. Fargion and J.L. Mueller [ed.], *Ocean Optics for Satellite Ocean color sensor validation*, rev. 2. NASA.
- Mueller, J. L., G. S. Fargion, C. R. McClain, J. L. Mueller, R. R. Bidigare, C. Trees, W. M. Balch, J. Dore, D. T. Drapeau, and D. Karl. 2003a. NASA / TM-2003- Ocean Optics Protocols For Satellite Ocean Color Sensor Validation , Revision 5 , Volume V: Biogeochemical and Bio-Optical Measurements and Data Analysis Protocols NASA / TM-2003- Ocean Optics Protocols For Satellite Ocean Color Sensor Va. Revision V.
- Mueller, J. L., G. S. Fargion, C. R. McClain, J. L. Mueller, A. Morel, R. Frouin, C. Davis, R. Arnone, K. Carder, R. G. Steward, S. Hooker, C. D. Mobley, S. Mclean, B. Holben, C. Pietras, K. D. Knobelspiesse, and J. Porter. 2003b. NASA / TM-2003-Ocean Optics Protocols For Satellite Ocean Color Sensor Validation, Revision 4 , Volume III : Radiometric Measurements and Data Analysis Protocols,.
- Muller-Karger, F. E., C. Hu, S. Andréfouët, R. Varela, and R. Thunell. 2005. The Color of the Coastal Ocean and Applications in the Solution of Research and Management Problems, p. 101-127. *In* R.L. Miller [ed.], *Remote Sensing of Coastal Aquatic Environments Remote Sensing and Digital Image Processing 7*. Springer, the Netherlands.
- Muller-Karger, F. E., C. Hu, S. Andréfouët, R. Varela, and R. Thunell. 2005. The color of the coastal ocean and applications in the solution of research management problems, p. 101-127. *In* *Remote Sensing of Coastal Aquatic Environments Remote Sensing and Digital Image Processing 7*.
- Navarro, G., and J. Ruiz. 2006. Gabriel. *Deep Sea Research Part II: Topical Studies in Oceanography* **53**: 1241-1260.
- Nixon, S. W. 1995. Coastal marine eutrophication--A definition, social causes, and future concerns. *Ophelia* **41**: 199-219.
- Ocean Optics Inc., 2001-2006. High-Resolution Fibre Optic Spectrometers HR4000 / HR4000CG-UV-NIR. Installation and Operation Manual: 1-40. (Document Number 210-00000-000-02-1006).
- Ocean Optics Inc., 1999-2007. Spectrasuite manual. Spectrometer Operating Software Installation and Operation Manual: 1-154. (Document Number 000-20000-300-02-0307).

- Ohde, T., and H. Siegel. 2003. Derivation of immersion factors for the hyperspectral TriOS radiance sensor. *Journal of Pure and Applied Optics* **5**: L12-L14.
- Orive, E., J. Franco, I. de Madariaga, and M. Revilla. 2004. Bacterioplankton and phytoplankton communities, p. 367-388. In A. Borja and M.B. Collins [eds.], *Oceanography and Marine Environment of the Basque Country*. Elsevier Oceanography Series.
- O'Reilly, J. E., S. Maritorena, B. G. Mitchell, D. A. Siegel, K. L. Carder, S. A. Garver, M. Kahru, and C. McClain. 1998. Ocean color chlorophyll algorithms for SeaWiFS. *Journal of Geophysical Research* **103**.
- O'Reilly, J. E., S. Maritorena, D. A. Siegel, M. C. O. Brien, D. Toole, B. G. Mitchell, M. Kahru, G. F. Cota, K. L. Carder, F. Muller-Karger, L. Harding, A. Magnuson, D. Phinney, G. F. Moore, J. Aiken, K. R. Arriago, R. Letelier, and M. Culver. 2000. Ocean Color Chlorophyll a Algorithms for SeaWiFS, OC2 and OC4: Version 4. *SeaWiFS Postlaunch Calibration and Validation Analyses, Part 3*: 8-22.
- Petus, C. 2009. Qualité des eaux côtières du sud du Golfe de Gascogne par télédétection spatiale. Méthodologie de détermination et de quantification de substances particulaires et dissoutes. PhD thesis. Université de Bordeaux 1.
- Petus, C., G. Chust, F. Gohin, D. Doxaran, J.-M. Froidefond, and Y. Sagarminaga. 2010. Estimating turbidity and total suspended matter in the Adour River plume (South Bay of Biscay) using MODIS 250-m imagery. *Continental Shelf Research* **30**: 379-392.
- Patti, B., C. Guisande, A. R. Vergara, I. Riveiro, I. Maneiro, A. Barreiro, A. Bonanno, G. Buscaino, A. Cuttitta, G. Basilone, and S. Mazzola. 2008. Factors responsible for the differences in satellite-based chlorophyll a concentration between the major global upwelling areas. *World* **76**, doi:10.1016/j.ecss.2007.08.005
- Pingree, R. D. 1973. A Component of Labrador Sea Water in the Bay of Biscay. *Limnology and Oceanography* **18**: 711-718.
- Pingree, R. D., and B. Le Cann. 1989. Celtic and Armorican slope and shelf residual currents. *Progress in Oceanography* **23**: 303-338.
- Plass, G., and G. Kattawa. 1968. Monte Carlo Calculations of Light Scattering from Clouds. *Applied Optics* **7**: 415-419.
- Platt, T., S. Sathyendranath, C. M. Caverhill, and M. R. Lewis. 1988. Ocean primary production and available light: further algorithms for remote sensing. *Deep Sea Research Part A. Oceanographic Research Papers* **35**: 855-879.
- Prego, R., P. Boi, and A. Cobelo-garcía. 2008. The contribution of total suspended solids to the Bay of Biscay by Cantabrian Rivers (northern coast of the Iberian Peninsula). *Journal of Marine Systems* **72**: 342-349.
- Prego, R., D. Guzmán-Zuñiga, M. Varela, M. de Castro, and M. Gómez-Gesteira. 2007. Consequences of winter upwelling events on biogeochemical and phytoplankton patterns in a western Galician ría (NW Iberian peninsula). *Estuarine, Coastal and Shelf Science* **73**: 409-422.
- Prego, R., and J. Vergara. 1998. Nutrient fluxes to the Bay of Biscay from Cantabrian rivers (Spain). *Oceanologica Acta* **21**: 271-278.
- Prieur, L., and S. Sathyendranath. 1981. An optical classification of coastal and oceanic waters based on the specific spectral absorption curves of phytoplankton pigments, dissolved organic matter, and other particulate materials. *Limnology and Oceanography* **26**: 671-689.

- Proust, J.L. 1986. Dissolved and suspended matter transported by the Giroux River (France): mechanical and chemical erosion rates in a calcareous molasse basin. *Hydrological Sciences Journal* **31**: 61-79.
- Puillat, I., P. Lazure, A.-M. Jegou, L. Lampert, and P. Miller. 2006. Mesoscale hydrological variability induced by northwesterly wind on the French continental shelf of the Bay of Biscay. *Scientia Marina* **70**: 15-26.
- Pérez Puebla, F. 2009. El riesgo de tormenta (The Storm risk), Asociación Española de Meteorología.
- Radiata, I. N., and S.I. Saitoh. 2008. Satellite-derived measurements of spatial and temporal chlorophyll-*a* variability in Funka Bay, southwestern Hokkaido, Japan. *Estuarine, Coastal and Shelf Science* **79**: 400-408, doi:10.1016/j.ecss.2008.04.017
- Rochelle-Newall, T. R., T. R. Fisher, C. Fan, and P. M. Glibert. 1999. Dynamics of chromophoric dissolved organic matter and dissolved organic carbon in experimental mesocosms. *International Journal of Remote Sensing* **20**: 627-641.
- Revilla, M., J. Franco, J. Bald, Á. Borja, A. Laza, S. Seoane, and V. Valencia. 2009. Assessment of the phytoplankton ecological status in the Basque coast (northern Spain) according to the European Water Framework Directive. *Journal of Sea Research* **61**: 60-67.
- Revilla, M., Á. Borja, A. Fontán, J. Franco, M. González, and V. Valencia. 2010a. A two-decade record of surface chlorophyll "a" and temperature in offshore waters of the Basque country (southeastern Bay of Biscay) Marta. *Revista de Investigación Marina* **17**: 20.
- Revilla, M., J. Franco, M. Garmendia, and Á. Borja. 2010b. A new method for phytoplankton quality assessment in the Basque estuaries (northern Spain), within the European Water Framework Directive. *Revista de Investigación Marina* **17**: 149-164.
- Rivier, A., Gohin, F., Bryère, P., Petus, C., Guillou, N., Chapalain, G. 2011. Observed vs. predicted variability in non-algal suspended particulate matter concentration in the English Channel in relation to tides and waves. *Geo-Marine Letters*.
- Rios, A., F. Pérez, and F. Fraga. 1992. Water masses in the upper and middle North Atlantic Ocean east of the Azores. *Deep Sea Research Part A. Oceanographic Research Papers* **39**: 645-658.
- Ruddick, K., V. D. Cauwer, Y. Park, G. Becu, E. D. Vreker, B. Nechad, A. Pollentier, P. Roose, D. Saudemont, and D. V. Tuyckom. 2003. Preliminary validation of MERIS water products for Belgian Coastal waters. *North* **2002**: 9 - 13.
- Salbatier, M., S. Osorio, W. Fajardo, F. Roncal, and V. Olivares. 2008. Phytoplanktonic characterisation from coastal area of Callao, Peru Polluted wastewater. *Biologist* **6**: 135-145.
- Sarmiento, H., and J.-P. Descy. 2008. Use of marker pigments and functional groups for assessing the status of phytoplankton assemblages in lakes. *Journal of Applied Phycology* **20**: 1001-1011.
- Sathyendranath, S., L. Watts, E. Devred, T. Platt, C. Caverhill, and H. Maass. 2004. Discrimination of diatoms from other phytoplankton using ocean-colour data. *Marine Ecology Progress Series* **272**: 59-68.
- Sathyendranath, S., L. Lazzara, and L. Prieur. 1987. Variations in the spectral values of specific absorption of phytoplankton. *Limnol. Oceanogr* **32**: 403-415.
- Sathyendranath, S., A. Longhurst, C. M. Caverhill, and T. Platt. 1995. Regionally and seasonally differentiated primary production in the North Atlantic. *Deep-Sea Research I* **42**: 1773-1802.
- Sathyendranath, S., and T. Platt. 1997. Analytic model of ocean color. *Applied Optics* **36**: 2620-2629.

- Sathyendranath, S., and T. Platt. 1998. Ocean-Color Model Incorporating Transpectral Processes. *Applied Optics* **37**: 2216-2227.
- Saulquin, B., F. Gohin, and R. Garrello. 2010. Regional Objective Analysis for Merging and SeaWiFS Chlorophyll-*a* Data From 1998 to 2008 on the European Atlantic Shelf. *IEEE Transactions on Geoscience and Remote Sensing* 1-12.
- Schalles, J. F. 2006. Chapter 3. Optical remote sensing techniques to estimate phytoplankton chlorophyll-*a* concentrations in coastal waters with varying suspended matter and CDOM, *In* L.L. Richardson and E.F. LeDrew [eds], *Remote Sensing of Aquatic Coastal Ecosystem Processes: Science and Management Applications*, 27-79. Springer. The Netherlands.
- Schiller, H., and R. Doerffer. 1999. Neural network for emulation of an inverse model operational derivation of Case II water properties from MERIS data. *International Journal of Remote Sensing* **20**: 1735-1746.
- Schott, J. R. 1997. *Remote Sensing: The Image Chain Approach* States, Oxford University Press.
- Schroeder, T., I. Behnert, M. Schaale, J. Fischer, and R. Doerffer. 2007. Atmospheric correction algorithm for MERIS above case-2 waters. *International Journal of Remote Sensing* **28**: 1469-1486.
- Shafique, N. A., F. Fulk, B. C. Autrey, and J. Flotemersch. 2002. Hyperspectral Remote Sensing of Water Quality Parameters for Large Rivers in the Ohio River Basin.
- Sharp, J. H., L. A. Cifuentes, R. B. Coffin, J. R. Pennock, and K. H. Wong. 1986. The Influence of River Variability on the Circulation, Chemistry, and Microbiology of the Delaware Estuary. *Estuaries* **9**: 261-269.
- Shutler, J. D., M. G. Grant, and P. I. Miller. 2005a. Towards spatial localisation of harmful algal blooms: statistics-based spatial anomaly detection. *SPIE proc. Image and Signal Processing for Remote Sensing XI* **5982**: 218-228.
- Shutler, J. D., P. I. Miller, S. B. Groom, and J. Aiken. 2005b. Automatic near-real time MERIS data as input to a phytoplankton classifier. *European Space Agency MERIS and (A) ATSR Workshop*. Frascati, Italy.
- Siegel, D. A., M. Wang, S. Maritorena, and W. Robinson. 2000. Atmospheric correction of satellite ocean color imagery: the black pixel assumption. *Applied Optics* **39**: 3582-3591.
- Siegel, H., T. Ohde, M. Gerth, G. Lavik, and T. Leipe. 2007. Identification of coccolithophore blooms in the SE Atlantic Ocean off Namibia by satellites and in-situ methods. *Continental Shelf Research* **27**: 258-274, doi:10.1016/j.csr.2006.10.003
- Siegel, M. G. T. N. R. D. H. 1999. Case studies on phytoplankton blooms in coastal and open waters of the Baltic Sea using Coastal Zone Color Scanner data. *International Journal of Remote Sensing* **20**: 1249-1264.
- Simis, S. G. H., S. W. M. Peters, and H. J. Gons. 2005. Remote sensing of the cyanobacterial pigment phycocyanin in turbid inland water. *Limnology And Oceanography* **50**: 237-245.
- Simis, S., A. Ruizverdu, J. Dominguez-Gomez, R. Peña-Martinez, S. Peters, and H. Gons. 2007. Influence of phytoplankton pigment composition on remote sensing of cyanobacterial biomass. *Remote Sensing of Environment* **106**: 414-427, doi:10.1016/j.rse.2006.09.008
- Smayda, T. J. 1997. What is a bloom? A commentary. *Limnology And Oceanography* **42**: 1132-1136.

- Schalles, J. F., F. R. Schiebe, P. J. Starks, and W. W. Troeger. 1997. Estimation of algal and suspended sediment loads (singly and combined) using hyperspectral sensors and experiments. *Proceedings of the Fourth International Conf. on Remote Sensing of Marine and Coastal Environments* 1: 247-258.
- Signoret, M., M. Monreal-Gómez, J. Aldeco, and D. Salasdeleon. 2006. Hydrography, oxygen saturation, suspended particulate matter, and chlorophyll-*a* fluorescence in an oceanic region under freshwater influence. *Estuarine, Coastal and Shelf Science* 69: 153-164, doi:10.1016/j.ecss.2006.04.011
- Smith, R. C., and K. S. Baker. 1981. Optical properties of the clearest natural waters (200-800 nm). *Applied optics* 20: 177-84.
- Stoichev, T. D., D. Amouroux, J. C. Wasserman, D. Point, A. Diego, G. Bareille, and O. F. X. Donard. 2004. Dynamics of mercury species in surface sediments of a macrotidal estuarine-coastal system (Adour River, Bay of Biscay). *Estuarine, Coastal and Shelf Science* 59: 511-521.
- Stumpf, R. P., and M. C. Tomlinson. 2005. Remote Sensing of Harmful Algal Blooms, p. 277-296. *In* R.L. Miller, C.E. Del Castillo, and B.A. Mckee [eds.], *Remote Sensing of Coastal Aquatic Environments*. Springer, The Netherlands.
- Subramaniam, A., C. W. Brown, R. R. Hood, E. J. Carpenter, and D. G. Capone. 2002. Detecting *Trichodesmium* blooms in SeaWiFS imagery. *Deep-Sea Research II* 49: 107-121.
- Suzuki, R., and H. Shimodaira. 2006. Pvcust: an R package for assessing the uncertainty in hierarchical clustering. *Bioinformatics (Oxford, England)* 22: 1540-2.
- Sørensen, K. 2002. Report on the Use of Ferrybox Data for Validation Purposes of Satellite Data. Deliverable for the European Commission. Fifth Framework Programme of the European Commission 1998-2002 48.
- Tanaka, A., H. Sasaki, and J. Ishizaka. 2006. Alternative measuring method for water-leaving radiance using a radiance sensor with a domed cover. *Optics Express* 14: 160-166.
- Taylor, K. E. 2001. Summarizing multiple aspects of model performance in a single diagram. *Journal of Geophysical Research* 106: 7183-7192.
- Tréguer, P., P. Le Corre, and J. R. Grall. 1979. The seasonal variations of nutrients in the upper waters of the Bay of Biscay region and their relation to phytoplankton growth. *Deep Sea Research Part A. Oceanographic Research Papers* 26: 1121-1152.
- Tzortziou, M., a Subramaniam, J. Herman, C. Gallegos, P. Neale, and L. Hardingjr. 2007. Remote sensing reflectance and inherent optical properties in the mid Chesapeake Bay. *Estuarine, Coastal and Shelf Science* 72: 16-32.
- Uriarte, A., M. Collins, A. Cearreta, J. Bald, and G. Evans. 2004a. Sediment supply, transport and deposition: contemporary and Late Quaternary evolution, pp. 98-131. *In* Á. Borja and M. Collins [eds.], *Oceanography and Marine Environment of the Basque Country*. Elsevier Oceanography Series.
- Valencia, V., A. Borja, and J. Franco. 1996. Estudio de las variaciones, a corto y largo término, de varios parámetros oceanográficos y meteorológicos de interés para las pesquerías del Golfo de Bizkaia. *Informes Técnicos (Departamento de Agricultura y Pesca, Gobierno Vasco)*, pp. 75
- Valencia, V., J. Franco, A. Borja, and A. Fontán. 2004. Hydrography of the southeastern Bay of Biscay, p. 159-194. *In* *Oceanography and Marine Environment of the Basque Country*. Á. Borja and M. Collins [eds.], Elsevier Oceanography Series.

- Valencia, V., and J. Franco. 2004. Main characteristics of the water masses, pp. 197-232. In Á. Borja and M. Collins [eds.], *Oceanography and Marine Environment of the Basque Country*. Elsevier Oceanography Series.
- Varela, M. 1996. Phytoplankton ecology in the Bay of Biscay. *Scientia Marina* **60**: 45-53.
- Venables, W. N., and B. D. Ripley. 2002. Modern Applied Statistics with S, pp. 86. In *American Statistician*. Springer, The Netherlands.
- Venables, W. N., and D. M. Smith. 2008. An Introduction to R. Notes on R: A Programming Environment for Data Analysis and Graphics, R Development Core Team.
- Vincent, C., H. Heinrich, A. Edwards, K. Nygaard, and J. Haythornthwaite. 2002. Guidance on typology, reference conditions and classification systems for transitional and coastal waters. Produced by: CIS Working Group 2.4 (Coast), Common Implementation Strategy of the Water Framework Directive, European Commission, pp. 119.
- Wang, M., and W. Shi. 2005. Estimation of ocean contribution at the MODIS near-infrared wavelengths along the east coast of the U.S.: Two case studies. *Geophysical Research Letters* **32**: L13606.
- Werdell, P. J., and S. W. Bailey. 2005. An improved *in situ* bio-optical dataset for ocean color algorithm development and satellite data product validation. *Remote Sensing of Environment* **98**: 122-140.
- Werdell, P. J., S. W. Bailey, B. a. Franz, L. W. Harding Jr., G. C. Feldman, and C. R. McClain. 2009. Regional and seasonal variability of chlorophyll-*a* in Chesapeake Bay as observed by SeaWiFS and MODIS-Aqua. *Remote Sensing of Environment* **113**: 1319-1330.
- Weston, K., N. Greenwood, L. Fernand, D. J. Pearce, D. B. Sivyer, 2008. Environmental controls on phytoplankton community composition in the Thames plume, U.K. *Journal of Sea Research*, **60**: 262-270.
- Wysocki, L. A., T. S. Bianchi, R. T. Powell, and N. Reuss. 2006. Spatial variability in the coupling of organic carbon, nutrients, and phytoplankton pigments in surface waters and sediments of the Mississippi River plume. *Estuarine, Coastal and Shelf Science* **69**: 47-63.
- Woodruff, D. L., R. P. Stumpf, J. A. Scope, and H. W. Paerl. 1999. Remote Estimation of Water Clarity in Optically Complex Estuarine Waters. *Remote Sensing of Environment* **68**: 41-52.
- Zainuddin, M., H. Kiyofuji, K. Saitoh, and S. I. Saitoh. 2006. Using multi-sensor satellite remote sensing and catch data to detect ocean hot spots for albacore (*Thunnus alalunga*) in the northwestern North Pacific. *Deep-Sea Research II* **53**: 419-431.
- Zapata, M., F. Rodríguez, and J. Garrido. 2000. Separation of chlorophylls and carotenoids from marine phytoplankton: a new HPLC method using a reversed phase C8 column and pyridine-containing mobile phases. *Marine Ecology Progress Series* **195**: 29-45.
- Zielinski, T. 2004. Studies of Aerosol Physical Properties in Coastal Areas. *Aerosol Science and Technology* **38**: 513-524.
- Yang, W., B. Matsushita, J. Chen, and T. Fukushima. 2011. Estimating constituent concentrations in case II waters from MERIS satellite data by semi-analytical model optimizing and look-up tables. *Remote Sensing of Environment* **115**: 1247-1259.

APPENDIX

Table A1. Examples of equations used to derive absorption and back-scattering coefficients.

Component	Absorption coefficients (a)	Back-scattering coefficients (b_b)
Water		$b_w = 0.00288 \left(\frac{\lambda}{500} \right)^{-4.3}$ Where $b_w = 0.5b_{bw}(\lambda)$ (Morel 1974; Smith and Baker 1981) b_w : scattering coefficient b_{bw} : backscattering coefficient
Phytoplankton	$a_{ph} = a_{ph}^*(\lambda) \cdot chl$ (Lahet et al. 2000) $a_{ph} = Aa_{ph}^*(\lambda) \cdot chl^{-B}$ (Bricaud et al. 1995) a_{ph}^* : specific absorbance coefficient of phytoplankton; chl : chl- a concentration	$b_{bph} = b_{bph}^*(\lambda) \cdot chl$ (Ahn et al. 1992) b_{bph}^* specific backscattering coefficient
Suspended Matter	$a_s = a_s(\lambda_0) \cdot \exp(-k_s(\lambda - \lambda_0))$ (Bricaud and Stramski 1990) λ_0 reference wavelength k slope of the exponential curve that depends on the type of particles.	$b_{bs}(\lambda) = TSM b_s^*(550) \cdot \left(\frac{\lambda}{550} \right)^{-\gamma}$ (Babin et al. 2003b) $b_{bs}(\lambda) = 0.019 b_s^*(\lambda)$ (Doxaran et al. 2006) b_s^* : specific scattering coefficient of suspended material b_{bs} : backscattering coefficient
CDOM	$a_y = a_y(\lambda_0) \cdot \exp(-S_y(\lambda - \lambda_0))$ (Babin et al. 2003a) λ_0 reference wavelength (440 nm) S_y slope of the exponential curve	

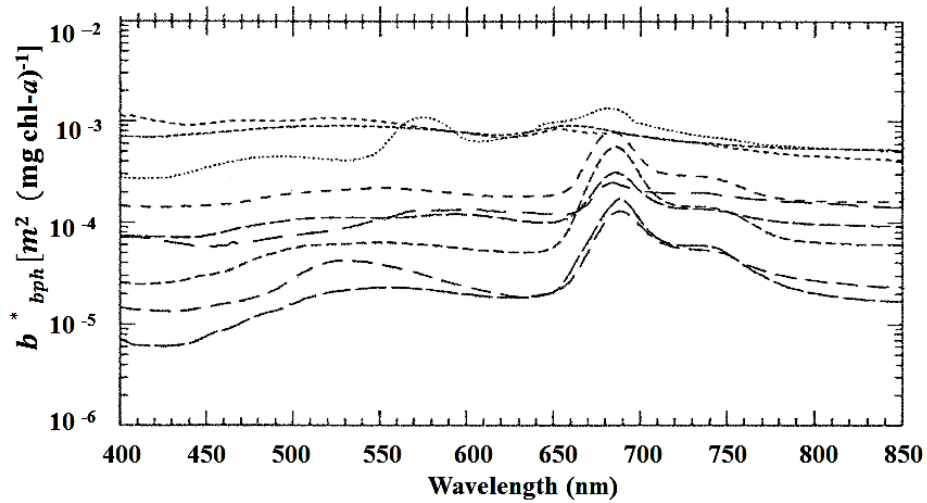


Figure A1. Chlorophyll-*a* backscattering specific coefficient for different phytoplankton species, extracted from Ahn et al. (1992).

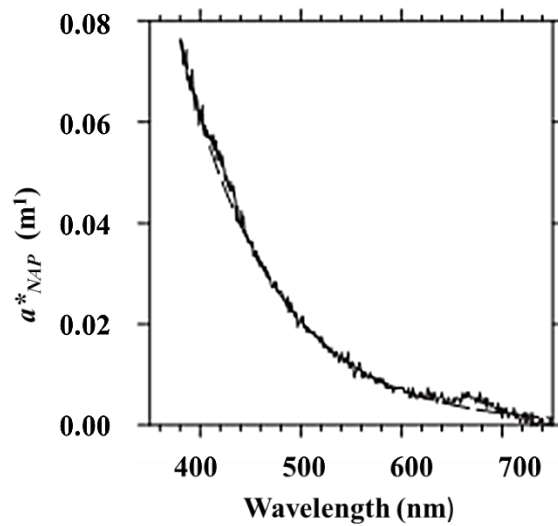


Figure A2. Example of non-algal particles (NAP) absorption spectrum from the Atlantic region. This figure was extracted from Babin et al. (2003a); NAP corresponds to the total suspended matter without the algal particles.

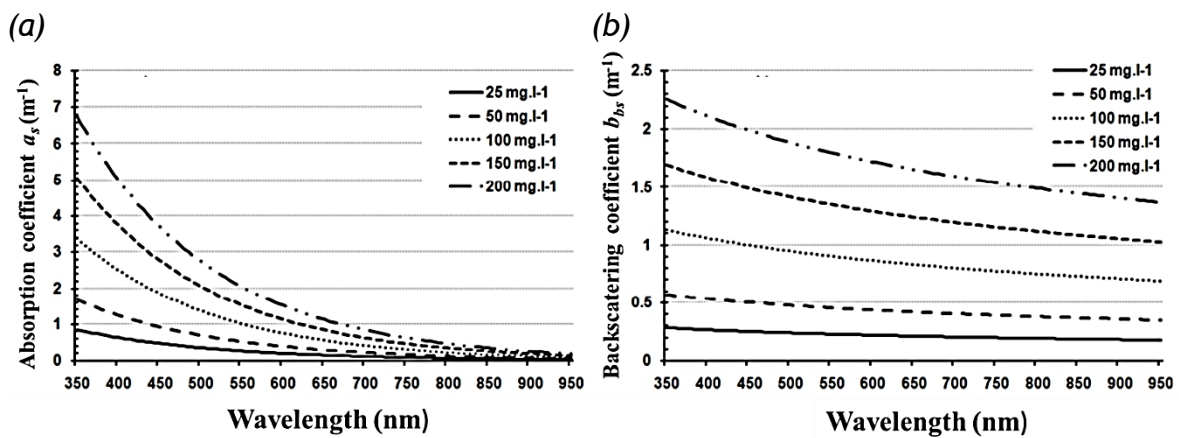


Figure A3. Absorption (a) and backscattering (b) coefficients of sediments according to different TSM concentrations. Extracted from Petus (2009). Calculated with equations in table 4: $k=0.006 \text{ m}^{-1}$; $\gamma = 0.5 \text{ m}$ and $b_{bs}^* (550) = 0.09 \text{ m}^2 \cdot \text{g}^{-1}$.

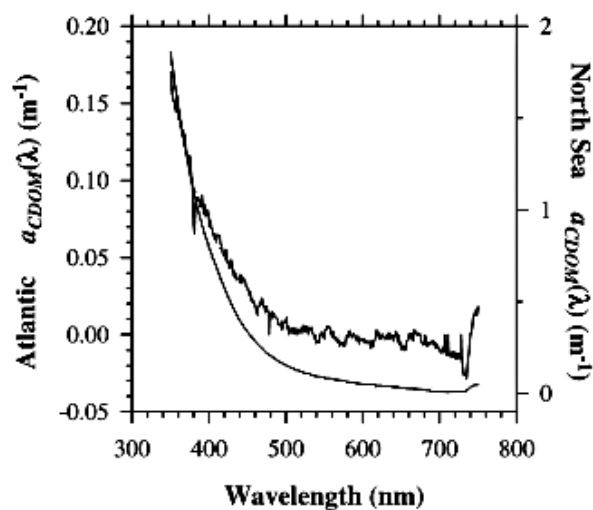


Figure A4. Examples of measured CDOM absorption spectra for the Atlantic (upper curves, y axis on the left) and North Sea (lower curves, y axis on the right). Extracted from Babin et al. (2003a).

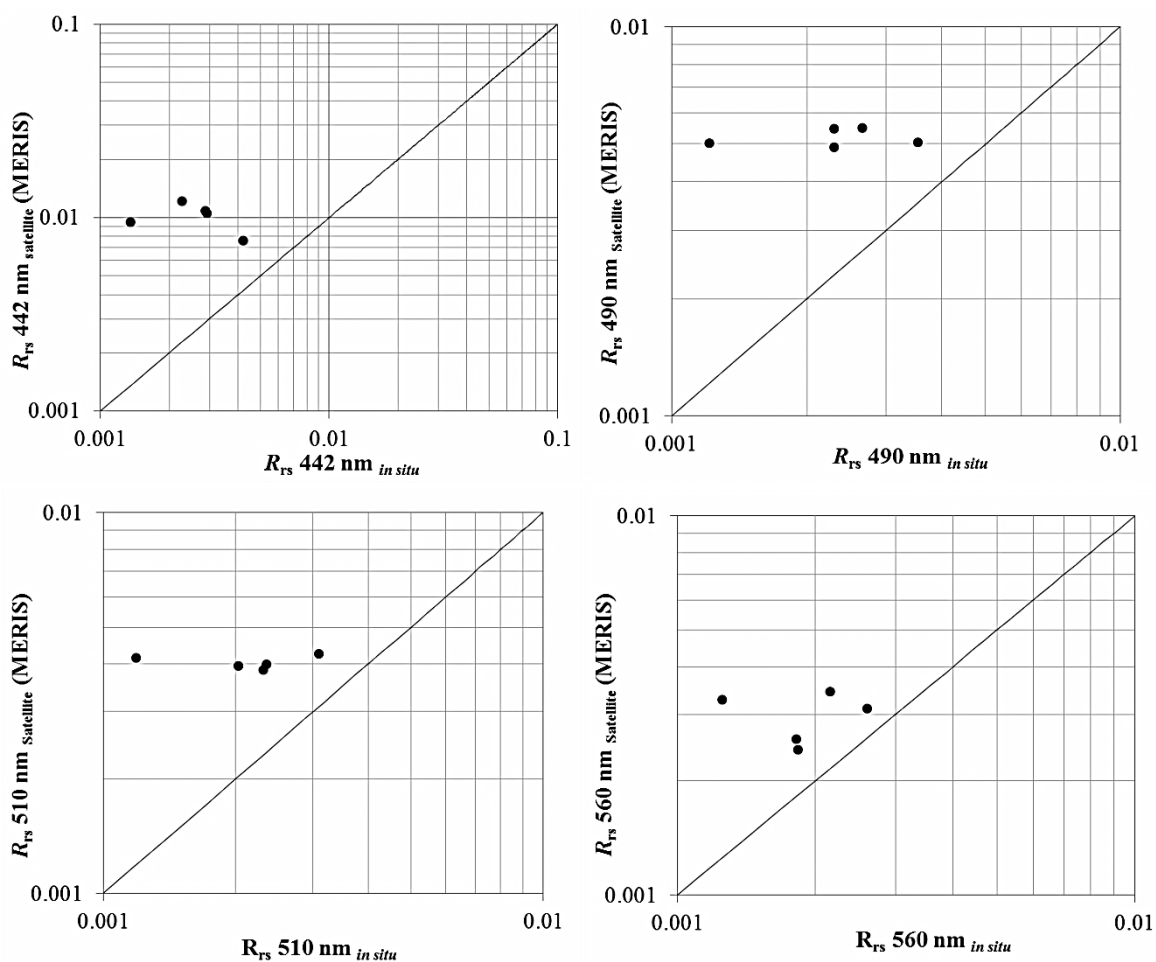


Figure A6: *In situ*-satellite reflectance match-ups for the image acquired on the 20th of May 2008 (Chapter II) with MERIS (FR).

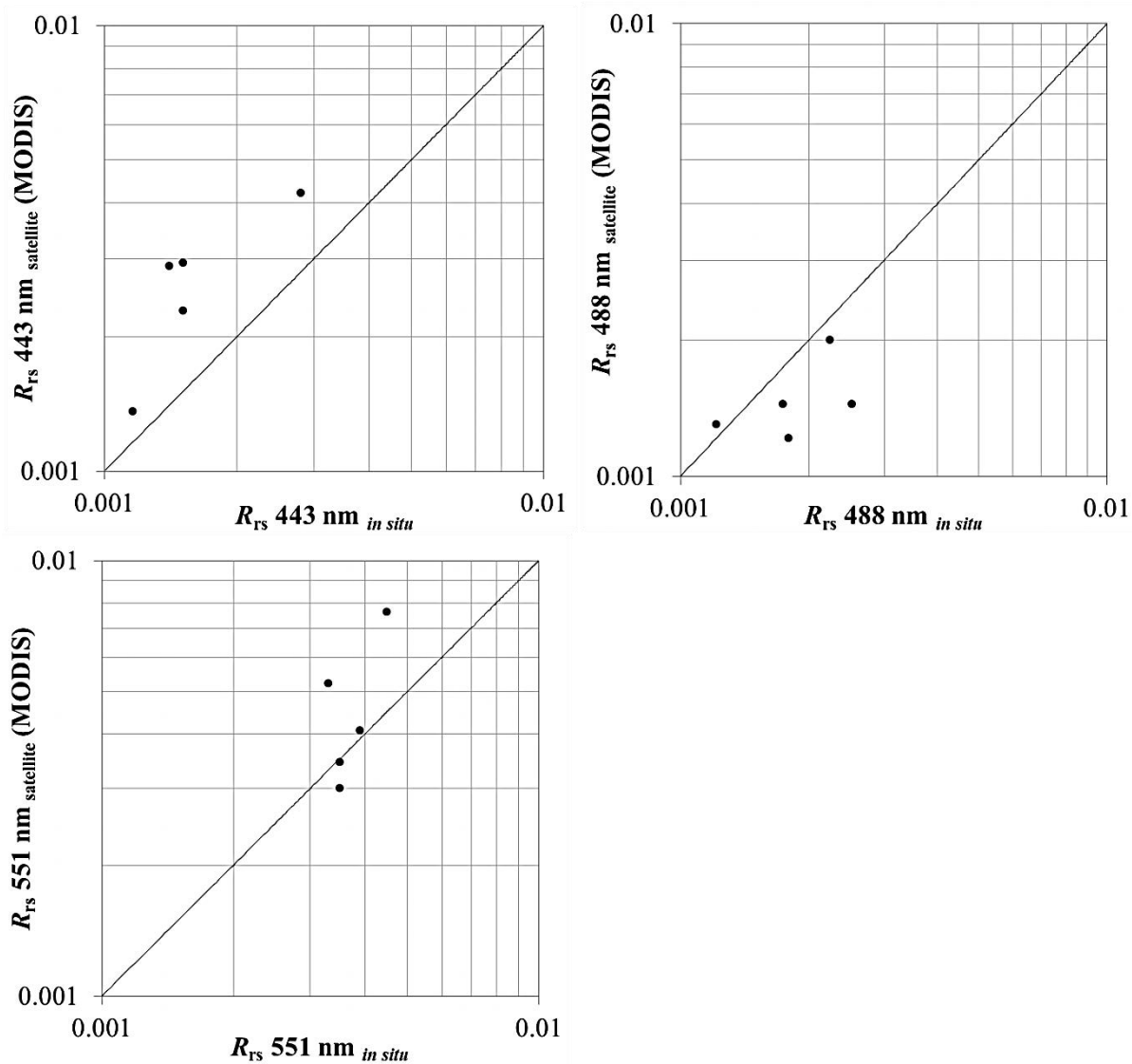


Figure A7. *In situ*-satellite reflectance match-ups for the image acquired on the 20th of May 2008 (Chapter II) with MODIS

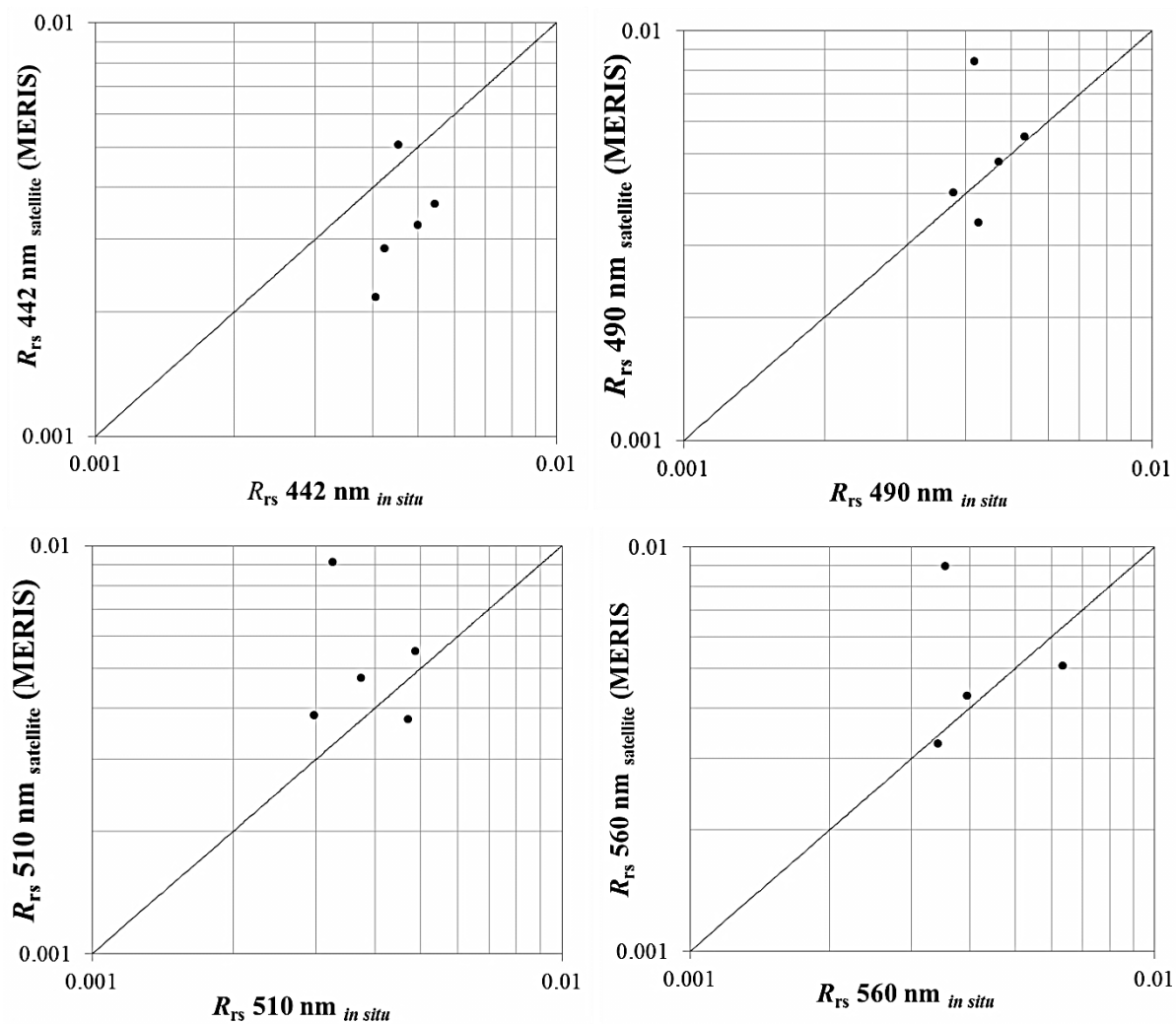


Figure A8: *In situ*-satellite reflectance match-ups for the image acquired on the 5th of June 2007 (Chapter III)

Table A2. Chlorophyll pigment concentrations per station in $\text{mg}\cdot\text{m}^{-3}$ ("chl" means chlorophyll).

STATIONS	Chl- <i>a</i>	Chl-c3	MgDvp	Chl-c2	Chl-c1	Chl-b	Non polar Chl-c2 <i>E. huxleyi</i>	Non polar Chl c2 <i>C.</i> <i>polylepis</i>	Total Chlorophylls (No chl- <i>a</i>)
<i>P6</i>	4.6	0.04	0.03	0.48	0.13	0.01	--	--	0.68
<i>P4</i>	3.51	0.03	0.02	0.38	0.1	0	--	--	0.53
<i>P28</i>	3.42	0.07	0.02	0.43	0.07	0.01	0.02	0.03	0.65
<i>P24</i>	3.26	0.06	0.02	0.39	0.08	0.01	--	0.02	0.58
<i>P22</i>	3.03	0.06	0.01	0.38	0.06	0.01	--	0.01	0.53
<i>P21</i>	2.68	0.14	0.02	0.54	0.06	0.01	0.07	0.08	0.91
<i>P18</i>	2.42	0.1	0.02	0.45	0.05	0.01	0.03	0.05	0.71
<i>P17</i>	2.37	0.14	0.01	0.42	0.04	0.01	0.07	0.07	0.76
<i>P12</i>	2.37	0.05	0.01	0.27	0.06	0.01	--	0.02	0.41
<i>D1</i>	2.2	0.06	0.01	0.35	0.07	0.01	0.01	--	0.51
<i>D8</i>	2.11	0.04	0.03	0.36	0.07	0.01	--	0.01	0.51
<i>D6</i>	2.07	0.13	0.02	0.29	0.03	0.01	0.02	0.08	0.58
<i>D5</i>	1.83	0.14	0.02	0.3	0.02	0.01	0.03	0.07	0.59
<i>D24</i>	1.27	0.05	0.01	0.19	0.01	0	0.01	0.01	0.3
<i>D23</i>	1.21	0.05	0.02	0.19	0.02	0.01	0.02	0.02	0.33
<i>D21</i>	1.09	0.07	--	0.19	0.03	0	0.02	0.02	0.33
<i>D2</i>	0.9	--	--	0.03	0.03	0.01	--	--	0.08
<i>D18</i>	0.58	0.02	0	0.09	0.01	0	--	--	0.12
<i>D17</i>	0.44	0.03	0	0.09	--	0	0.01	0.01	0.14
<i>D13</i>	0.3	0.02	0	0.07	0	0	0	0	0.11
<i>Total</i>	41.67	1.29	0.26	5.91	0.95	0.13	0.3	0.5	9.35
<i>Average</i>	2.08	0.07	0.01	0.3	0.05	0.01	0.03	0.03	0.47
<i>St. dev.</i>	1.15	0.04	0.01	0.15	0.03	0	0.02	0.03	0.24

Table A3. Carotenoid pigment concentrations per station in $\text{mg}\cdot\text{m}^{-3}$.

STATIONS	Peridinine	19'BFU	Fucoxanthin	Neoxanthin	Prasincoxanthin	4-Keto-HFU	Violaxanthin	19'HFU	Diadinoxanthin	Dinoxanthin	Aloxanthin	Diatoxanthin	Zeaxanthin	Lutein	B-Carotene	Total carotenoids
P6	0.04	0.02	1.15	0.01	--	0.01	0.01	0.09	0.23	--	0.02	0.02	--	--	0.05	1.67
P4	--	--	0.77	0.01	--	0	--	0.06	0.18	--	0.02	0.04	--	--	0.03	1.1
P28	0.15	--	0.85	0.01	--	0.02	--	0.17	0.19	0.01	0.02	0.03	--	--	0.03	1.5
P24	0.05	--	0.81	0.01	--	0.02	--	0.17	0.21	--	0.03	0.01	--	--	0.04	1.34
P22	0.05	--	0.83	--	--	0.02	--	0.12	0.19	--	0.02	0.04	--	--	0.03	1.31
P21	0.1	0.08	0.89	0.01	--	0.02	--	0.75	0.52	0.01	0.04	0.07	0.02	--	0.03	2.56
P18	0.14	0.07	0.72	0.01	--	0	--	0.47	0.46	0.01	0.06	0.13	0.02	--	0.04	2.13
P17	0.04	0.05	0.72	--	--	0.03	--	0.55	0.38	0.05	0	0.05	0.02	--	0.03	1.92
P12	0.04	--	0.65	0.01	--	0.01	--	0.11	0.14	--	0.01	0.03	0	--	0.03	1.03
D1	0.02	0.03	0.81	0.01	0.01	0.02	--	0.17	0.17	--	0.02	0.06	0	--	0.03	1.36
D8	0.02	--	0.73	0.01	0.01	0	--	0.13	0.28	--	0.04	0.03	0.01	--	0.05	1.3
D6	0.04	0.04	0.33	0.01	0.01	0.03	--	0.31	0.07	--	0.02	0.01	0.01	0	0.01	0.9
D5	0.03	0.06	0.32	0.02	0.01	0.05	--	0.5	0.15	--	0.06	0.03	0.01	0	0.02	1.26
D24	0.08	0.05	0.33	0	--	--	0.01	0.21	0.28	0.01	0.02	--	0.01	--	0.02	1.01
D23	0.04	--	0.27	0.01	0.01	--	0.01	0.27	0.17	--	0.03	0.02	0.01	0	0.03	0.87
D21	0.06	0.02	0.42	0	--	0.01	0.01	0.22	0.23	0.01	0.01	0.1	0.02	--	0.02	1.14
D2	--	--	0.21	--	--	--	0.02	--	0.05	--	0.04	--	0.04	0.07	0.04	0.45
D18	0.06	0.01	0.19	--	--	--	0.01	0.04	0.12	0.01	0.01	0.02	0.01	0.01	0.01	0.5
D17	0.03	0.02	0.18	--	--	--	0	0.13	0.11	0	0.01	0.04	0.01	0	0.01	0.54
D13	0.03	0.01	0.13	0	--	--	0	0.07	0.06	0	0.01	0.04	0.01	0	0.01	0.38
Total	1.02	0.47	11.31	0.13	0.04	0.24	0.07	4.54	4.2	0.1	0.49	0.78	0.21	0.09	0.57	1.02
Average	0.06	0.04	0.57	0.01	0.01	0.02	0.01	0.24	0.21	0.01	0.02	0.04	0.01	0.01	0.03	0.06
St. dev.	0.04	0.02	0.3	0	0	0.01	0.01	0.19	0.12	0.01	0.02	0.03	0.01	0.02	0.01	0.04

Table A4. Total abundance of the phytoplankton species.

Phylum	Class/family	Taxon	Abundance (cells.l ⁻¹)
Chlorophyta	Prasinophyceae	Flagellated chlorophyte	15930
		Flagellated chlorophyte 15 µm	5310
		<i>Cymbomonas</i> sp.	1
		<i>Mamiella</i> spp.	5310
		<i>Pachysphaera</i> spp.	127442
		Cf. <i>Pseudoscorfeldia marina</i>	5310
		<i>Pyramimonas</i> spp.	180541
		<i>Scenedesmus</i> sp.	1
		<i>Tetraselmis</i> spp.	233643
Ochrophyta	Bacillariophyceae	<i>Centrica</i> 5 µm	15930
		<i>Centrica</i> 10 µm	5310
		<i>Cerataulina pelagica</i>	4646253
		<i>Chaetoceros curvisetus</i>	1
		<i>Chaetoceros decipiens</i>	63722
		<i>Chaetoceros lorenzianus</i>	1
		<i>Chaetoceros salsugineum</i>	8729640
		<i>Chaetoceros</i> spp.	382322
		<i>Cylindrotheca closterium</i>	26553
		<i>Dactyliosolen fragilissimus</i>	15930
		<i>Leptocylindrus danicus</i>	7476480
		<i>Pennada</i> sin identificar	90271
		<i>Proboscia alata</i>	642510
		<i>Pseudonitzschia</i> <3µm	122133
		<i>Pseudonitzschia</i> spp.	276121
		<i>Rhizosolenia</i> spp.	2
		<i>Thalassionema nitzschioides</i>	21241
		<i>Thalassiosira</i> spp.	1
		<i>Thalassiotrix longissima</i>	42481
			Chrysophyceae
	Dyctiochophyceae	<i>Apedinella spinifera</i>	26550
Cryptophyta	Cryptophyceae	<i>Plagioselmis</i> spp.	297363
		<i>Teleaulax</i> spp.	801810
Dinophyta	Dinophyceae	<i>Amphidinium acuttisimum</i>	21240
		<i>Ceratium furca</i>	301
		<i>Ceratium fusus</i>	200
		<i>Ceratium lineatum</i>	100
		<i>Ceratium macroceros</i>	100
		<i>Ceratium tripos</i>	300
		<i>Gonyaulax</i> sp.	5311
		<i>Gyrodinium</i> cf. <i>flagellare</i>	5310
		<i>Gyrodinium spirale</i>	10620
		<i>Heterocapsa</i> spp.	977040
		<i>Kriptoperidinium foliaceum</i>	5310
		<i>Oblea</i> spp.	21241
		<i>Pronoctiluca pelagica</i>	5310
		<i>Prorocentrum micans</i>	95582
		<i>Prorocentrum minimum</i>	63723
		<i>Prorocentrum</i> spp.	5311
		<i>Protoperidinium diabolum</i>	5313
		<i>Protoperidinium</i> spp.	3
		<i>Scrippsiella</i> spp.	95585
		Unidentified dinoflagellate >20 µm	15930
		Unidentified dinoflagellate <20 µm	175231
		Naked dinoflagellate >20 µm	5310

		Naked dinoflagellate <20 μm	122131
Euglenophyta	Euglenophyceae	<i>Eutreptiella</i> sp. (fagotr.)	5310
		<i>Eutreptiella</i> spp.	10623
Haptophyta	Prymnesiophyceae	<i>Chrysochromulina</i> spp.	2161170
		<i>Chrysochromulina</i> - <i>Phaeoc</i>	430110
		Coccolithophore	392941
		<i>Emiliana huxleyi</i>	238953
		<i>Syracospahera</i> spp.	318602
Unidentified		Coccolith forms	541620
		Flagelated forms	3717000

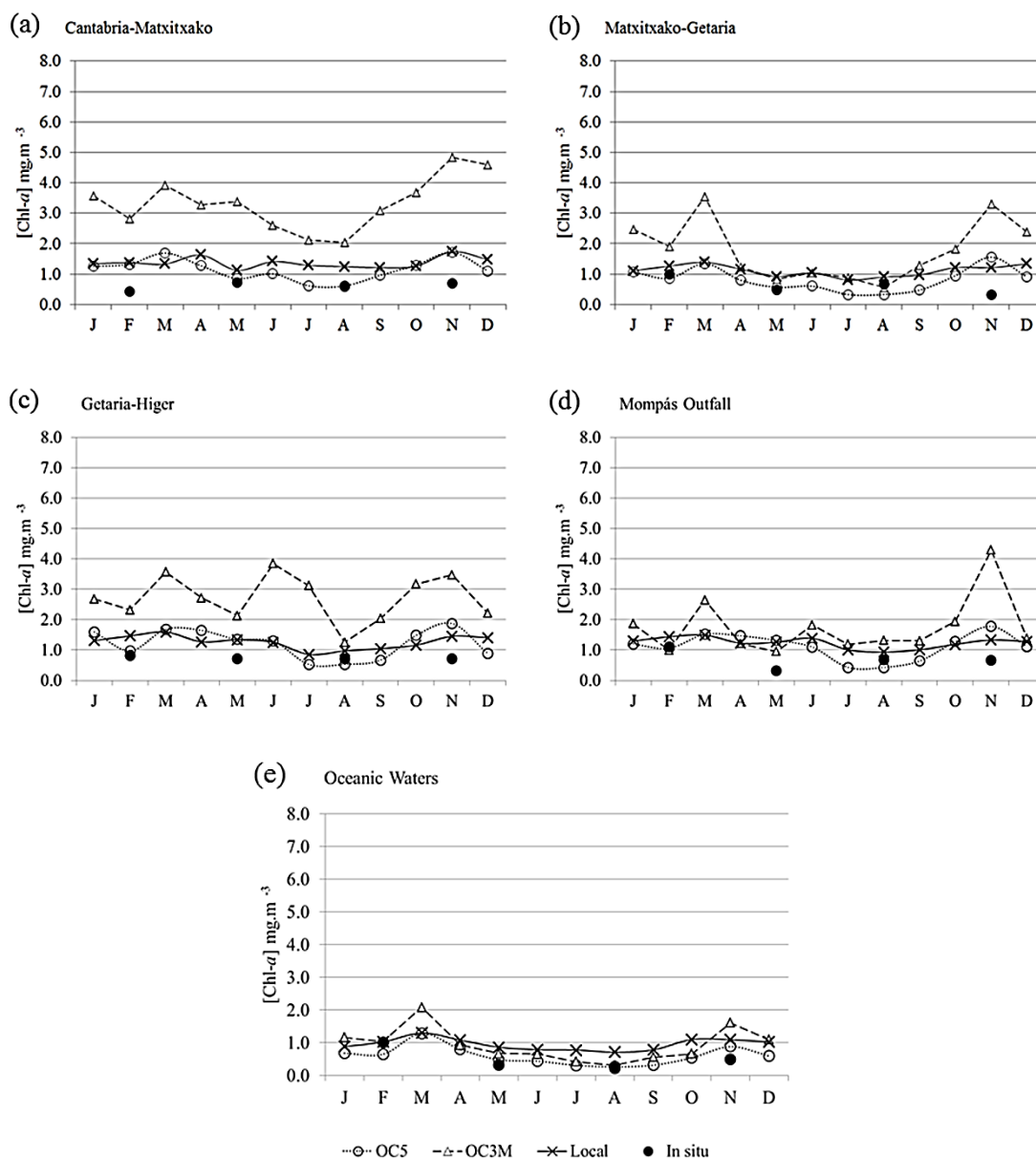


Figure A9. Annual cycle of the mean chl-*a* concentration observed *in situ* (trimestral) and by satellite (monthly) for the 5 water bodies of the Water Framework Directive monitoring network: (a) Cantabria-Matxitxako; (b) Matxitxako-Getaria; (c) Getaria-Higer; (d) Mompás Outfall; and (e) Oceanic waters.

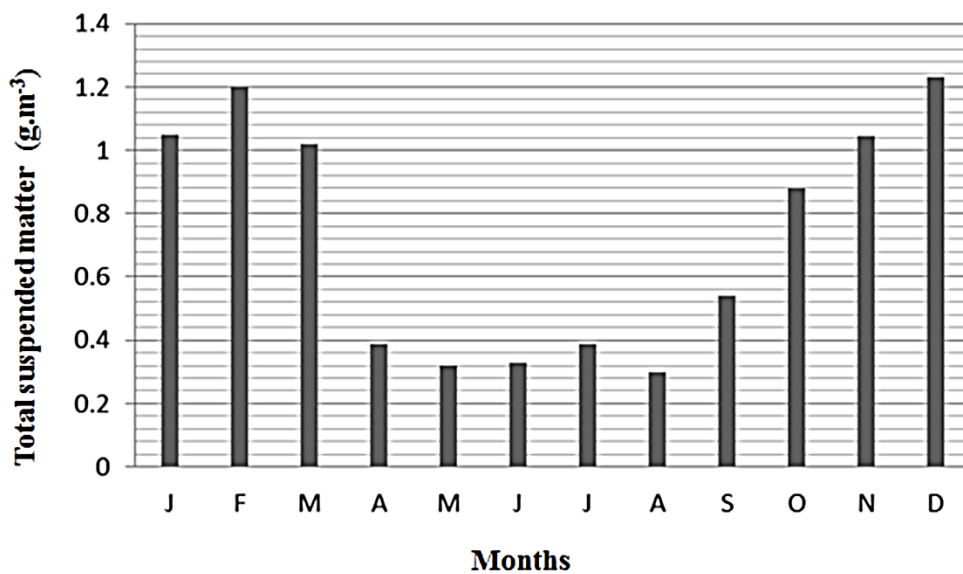


Figure A10. Annual 90th percentile for the total suspended matter concentration (TSM) averaged for the four coastal water bodies (1-4, see Chapter IV).

Summary

The implementation of water quality European Water Framework (WFD) and Marine Strategy Directives (MSFD) requires an intensification of water quality monitoring, within the limits of the Exclusive Economic Zone. Remote sensing technologies can provide a valuable tool for frequent, synoptic, water-quality observations, over large areas. Hence, ocean colour data is used increasingly as a tool to assess water quality, by estimating the concentration of the water constituents, such as chlorophyll-*a* (a proxy of the eutrophication risk). Both MODIS and MERIS, the satellite sensors selected for this study, provide global and daily ocean information and satellite-derived chlorophyll-*a* maps at a medium resolution. However, algorithms designed for assessments at global scales for these sensors are less accurate locally, due to the variability of optically-active in-water constituents. Hence, regionally parameterized empirical algorithms are useful to cope with the inaccuracies produced. Additionally, to improve the water quality assessment in Basque coastal waters, the effect of river discharges needs to be studied, as it is one of the major factors affecting phytoplankton growth in this region.

The main objectives of this thesis are: 1) to select the most suitable chlorophyll-*a* algorithms applied to MERIS and MODIS satellite images to assess the water quality in the Basque coastal and offshore waters (southeastern corner of the Bay of Biscay); and 2) to study the variability of chlorophyll-*a* with respect to river discharges into the same area, between 2005 and 2010.

To address these objectives, four regional empirical algorithms for MERIS and MODIS were developed with optical and biogeochemical data acquired *in situ*. Two were developed for the entire Bay of Biscay with biogeochemical data and radiometric measurements acquired using the OceanOptics spectrometer. A protocol and a specific platform were developed in this study especially for this spectrometer. Another two algorithms were developed for Basque coastal waters using biogeochemical and radiometric data obtained during oceanographic surveys in the region of study. The optical data during these surveys was acquired using the TriOS spectrometer, as it provided improved results for the coastal waters than the Ocean Optics spectrometer. The influence of suspended matter, phytoplankton species and pigment content on the algorithms developed was explored. These algorithms were validated with *in situ* data and were compared to well-established global and regional chlorophyll-*a* algorithms. The algorithms developed in this study generally improved the estimation of chlorophyll-*a* in Basque coastal waters. However, the OC5 algorithm was considered more suitable for the ecological water quality assessment of the study area, as it corresponded most accurately with *in situ* measurements. A 90th percentile chlorophyll-*a* map was generated with this algorithm to apply the classification scheme required by the Directives. The water quality status assessment obtained using both, *in situ* and satellite data, resulted in high quality status for all the water bodies. Hence, remote sensing is suited for the quality assessment and water body classification, when a densification of the monitoring network is needed to comply with European marine policies. A complementary use of both methodologies provides an efficient assessment of the water quality, within European Directives. Finally, daily MODIS imagery permitted the characterisation of the variability of chlorophyll-*a* in the Basque coast and the Bay of Biscay at a daily, seasonal and inter-annual scale. The seasonal chlorophyll-*a* cycle differs slightly in coastal waters, compared to the offshore waters, especially those areas affected by high river discharges (such as the Adour). The spring chlorophyll-*a* peak in March, in the offshore waters, is shifted to May in the nearby area influenced by the Adour. The unsupervised classification performed confirms that, at present, phytoplankton is at good status and eutrophication risk is low in the Basque coastal waters.

This thesis is the first study that provides scientific knowledge on the assessment of water quality, using remote sensing and chlorophyll-*a*, in Basque coastal and offshore water bodies. It provides also important optical and biogeochemical information on the water bodies of the area, which will be valuable in future studies.



Universidad
del País Vasco

Euskal Herriko
Unibertsitatea

